TECHNISCHE UNIVERSTÄT MÜNCHEN

Lehrstuhl für Biologische Chemie

Protein design of hapten-specific Anticalins as therapeutic antidotes and biochemical reagents

M.Sc. Biol. Mikhail Barkovskiy

Vollständiger Abdruck der von der Fakultät Wissenschaftszentrum Weihenstephan für Ernährung, Landnutzung und Umwelt der Technischen Universität München zur Erlangung des akademischen Grades eines

Doktors der Naturwissenschaften

genehmigten Dissertation.

Vorsitzender: Prof. Dr. Wolfgang Liebl

Prüfer der Dissertation:

1. Prof. Dr. Arne Skerra
2. Prof. Dr. Kay H. Schneitz

Die Dissertation wurde am 30.01.2020 bei der Technischen Universität München eingereicht und durch die Fakultät Wissenschaftszentrum Weihenstephan für Ernährung, Landnutzung und Umwelt am 16.06.2020 angenommen.

Acknowledgements

I would like to thank Prof. Dr. Arne Skerra for allowing me to dive into the world of protein engineering and for teaching to be precise.

I am very grateful to Antonia Richter, Uli Binder, Martin Dauner, Lars Friedrich and Joscha Breibeck for the warm welcome in the lab; to Fabian Rodewald for sharing the office and to Tony Schmidt for not letting us starve to death; to Volker Morath for the philosophical discussions and for keeping me company no matter how late it was; to Elena Ilyukhina for the possibility to communicate in my mother tongue and for continuing the Colchicalin project. I am thankful to our whole team including Christian Deuschle, Julia Martin and Emanuel Peplau for making every lunch desired not just because of the meal.

I would like to thank our cooperation partners from the Klinikum rechts der Isar in Munich: Dr. med. Jochen Stenzel, Dr. med. vet. Nicole Jung, Heidemarie Neuberger and Prof. Dr. Florian Eyer for making the preclinical studies possible and for the pleasant work atmosphere.

This work would have been much harder without the support of Klaus Wachinger, Irmgard Neumaier, Ina Theobald, Stefan Achatz; I thank Dr. Andreas Eichinger for the measurement of the X-ray datasets and the help with the preparation of the 3D protein models.

I am grateful to Stephan Dickgießer and Dominik Hinz for starting the Catacalin project, as well as to my students Erich Stefan and Johannes Krumm for bringing it forward.

I also want to specially thank Elena Ilyukhina, Martin Dauner, Christian Deuschle, and Volker Morath for reviewing and proofreading this dissertation.

Я благодарен своим родителям за то, что они поддерживали меня в моих начинаниях и за то, что терпели моё долгое отсутсвие дома – эта работа посвящается им. Также я благодарен моей жене Ксюше за то, что она мирилась с моим отлучением от семейной жизни вечерами, когда я писал эту диссертацию.

Table of contents

1. Introduction

1.1 Poisons and antidotes

1.1.1 Colchicine and its role in science and healthcare

Colchicine is a plant alkaloid found in several species of the *Colchicaceae* family (order *Liliales*) including *Colchicum autumnale, Gloriosa superba* and *Androcymbium gramineum*, the first two being the most common sources (Figure 1.1; see also Figure 1.2, **1**). The visual resemblance of *C. autumnale* with some members of the genus *Crocus* (family *Iridaceae*) led to a long-lived confusion of their terms in various languages (Hartung, 1954). The modern scientific name, eventually fixed by Karl Linnaeus, was mentioned by various authors starting from Ancient Greece (e.g. by Nicander around 150 B.C. in his 'Alexipharmaca') and originates from the region of Colchis on the Eastern coast of the Black Sea – a district that Greeks associated with sorcery of all kinds (Hartung, 1954).

The first evidence of colchicine use as a medicinal agent can be traced to the ancient Egypt, where a remedy with very similar properties was mentioned in the Ebers papyrus – one of the oldest collections of medicinal facts dating to 1550 B.C. The first certain evidence of the use of colchicum against gout can be found in the accounts of Alexander of Tralles; Hypocrates also appreciated its anti-gout potency and believed that "the best natural relief for this disease is an attack of dysentery" (Garrod, 1859). In Middle Age Europe it was almost completely forgotten as an anti-gout drug mainly because of its purgative action, especially after the influential Abbes Hildegard von Bingen (1098–1179) had declared it "a deadly poison and not a health giving drug" (Copeman, 1964). The latest wide-spread use of colchicum was initiated by Baron Anton von Störck from the city of Vienna (von Störck, 1763). After a series of experiments (which he also performed on himself), he found the root extract of *C. autumnale* to act as a good diuretic, and used it to treat dropsy, ascites and anasarca (von Störck, 1764).

The modern history of colchicine use to treat gout started with a drug patented in 1783 by the French officer Nicholas Husson – 'Eau Médicinale d'Husson'. While Husson advertised it as a universal remedy and recommended it nearly for any sickness, the tincture – virtually by chance – turned out to be a potent remedy against acute gout (Moore, 1811). Soon it gained enormous popularity in continental Europe, England, and it was even introduced in the USA, where Benjamin Franklin used it to treat his gout (Jones, 1810; Nuki, 2008). However, the composition of 'Eau Médicinale' was deliberately kept secret, even though Husson stated that it was "a simple extract of a plant whose properties were before unknown" (Moore, 1811). The pursuit of the true active component lasted more than three decades and filled the London Medical and Physical Journal with harsh polemics, which stopped only several years after John

Want stated that his infusion of *C. autumnale* roots exerted the same effect and possessed identical properties with the Eau Médicinale d'Husson (Want, 1811; Sutton, 1814).

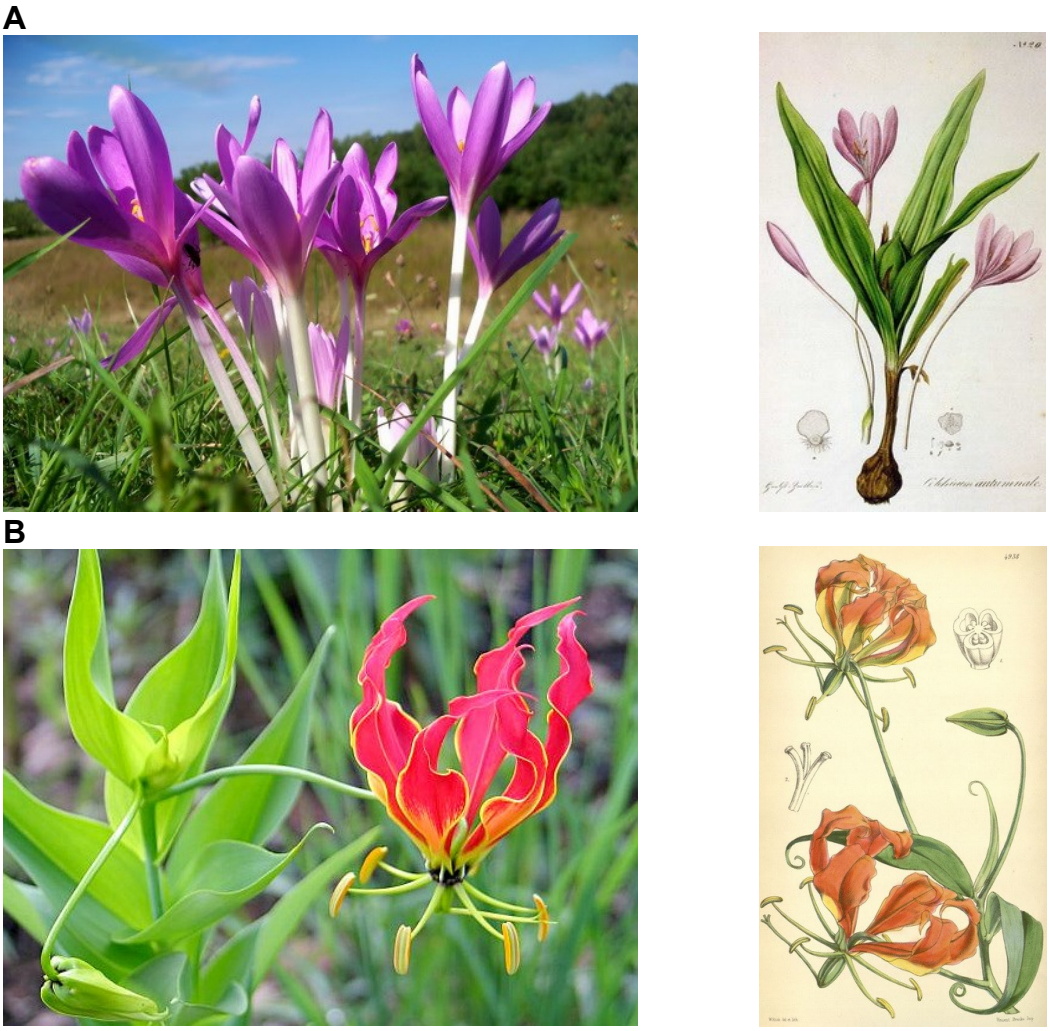

Figure 1.1. Plants with high colchicine content. **A:** *Colchicum autumnale* (autumn crocus, meadow saffron, naked lady). **B:** *Gloriosa superba* (glory lily, flame lily, fire lily).

The active substance – colchicine – was first identified by the French chemists Pelletier and Caventon in 1820, after which it became widely exploited for the treatment of gout attacks on both sides of the globe (Pelletier *et al.*, 1820; Nuki, 2008). Much knowledge about the effect of colchicine on gout was gathered by Alfred Garrod in his fundamental work in 1859 (Garrod, 1859). While it was known that gout is associated with elevated amount of urate in blood, he noticed that colchicum released the symptoms of gout but had no effect on the concentration of urates or their excretion. Since then, the mechanism of the medicinal action of colchicine remained obscure for over a century.

Colchicine remained the most effective drug against acute gout flares until the 1960's when its leading position was slowly substituted by nonsteroidal anti-inflammatory drugs (NSAID)

providing a better benefit-to-risk ratio (Nuki, 2008). Nevertheless, colchicine is still considered the first alternative to NSAID and it seems to have reserved its place in the medical guidelines for the treatment of gout (Jordan *et al.*, 2007). For instance, Takeda Pharmaceutical Co. raised more than a $ 1 billion in revenue between 2012 and 2015 alone from marketing its colchicine drug 'Colcrys' (Langreth & Koons, 2015).

Although colchicine became famous as an anti-gout drug, it offers a much broader range of applications. Colchicine is prescribed for a range of rare inflammatory disorders: (1) Behçet's disease, immune-mediated systemic inflammation of small blood vessels with a risk of fatal outcome (Miyachi *et al.*, 1981; Yurdakul *et al.*, 2001); (2) Familial Mediterranean Fever (FMF), a rare hereditary autoinflammatory disease with higher prevalence in the people of Mediterranean origin, caused by a mutation in the immune-regulatory protein pyrin (encoded by the gene *MEFV*, for Mediterranean Fever) and characterized by periodic attacks of fever and inflammation (Goldfinger, 1972; Cerquaglia *et al.*, 2005); (3) pericarditis, an inflammation of the pericardium of viral, bacterial or autoimmune origin (Adler *et al.*, 1994); and (4) primary biliary cirrhosis, the autoimmune destruction of bile ducts in the liver, causing leakage of the bile toxins and damaging of liver tissue (Kershenobich *et al.*, 1988; Kaplan *et al.*, 1999).

1.1.1.1 Molecular mechanism of action and scientific use

The chemical constitution of colchicine was proposed in 1945 and was later confirmed experimentally (Dewar, 1945; King *et al.*, 1952). Colchicine contains a system of three annealed rings (usually designated A, B and C), ring A being a six-carbon aromatic benzene ring, ring B an aliphatic seven-carbon ring, and ring C an aromatic seven-member tropolone ring (Figure 1.2, **1**). *In vivo,* the biosynthesis of colchicine starts from the amino acids tyrosine and phenylalanine, which are coupled to form a bicyclic precursor (Leete, 1963); the central 7-carbon ring B is later formed as a result of a *para/para* phenol coupling between the two aromatic 6-carbon rings (Maier & Zenk, 1997), eventually forming colchicine via the precursors demecolcine (**2**) and deacetylcolchicine (**3**) (cf. Graening & Schmalz, 2004 for an overview).

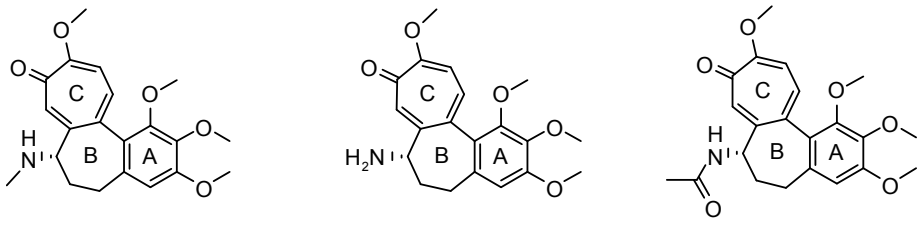

demecolcine **2** deacetylcolchicine **3** colchicine **1**

Figure 1.2. Structure of colchicine (**1**) and its direct precursors.

Colchicine acts *in vivo* via binding to tubulin – the main protein constituent of microtubules (Borisy & Taylor, 1966). Microtubules, together with actin microfilaments and intermediate filaments, are the main cytoskeletal elements of eukaryotic cells. Through their unique properties, they promote both mechanical stability and plasticity of the cells (Ganguly *et al.*, 2012), serve as a railway system for the intracellular transport of proteins and vesicles (Caviston & Holzbaur, 2006) and play a crucial role in the division of the nucleus during mitosis and meiosis by organizing the disposition and segregation of chromosomes in the absence of the nuclear membrane (Inoue, 1967). In addition, for higher eukaryotes with tissue specialization, microtubules are responsible for the transport of neuromodulator molecules along the processes of neurons (Kreutzberg, 1969; Conde & Caceres, 2009).

The nature of colchicine-tubulin interaction has been well studied. A binding site for colchicine is located at the interface between the α- and β-subunits of the tubulin heterodimer. The colchicine rings A and C interact with the β-subunit and seem to be crucial for its affinity towards tubulin, while the side chains of ring B interact with the α-subunit and play an auxiliary role (Bhattacharyya *et al.*, 2008). Colchicine can only bind to free tubulin dimers and not to an assembled microtubule, where the binding site is sterically hindered by the neighboring subunits (Wilson & Meza, 1973; Margolis & Wilson, 1977; Ravelli *et al.*, 2004). Upon colchicine binding, the tubulin dimer adopts a ‘curved’ conformation, in which α- and β-subunits are shifted versus each other by ~10°. In this conformation, the M-loop of tubulin, responsible for the lateral interactions with the neighboring protofilaments, becomes displaced (Ravelli *et al.*, 2004). The curved tubulin has a high kinetic barrier for binding normal tubulin, which results in a drastic reduction of the association rate; at the same time, the longitudinal contacts with other dimers seem to remain preserved, and tubulin-colchicine does not readily dissociate from the microtubule end (Farrell & Wilson, 1984).

Consequently, colchicine affects the microtubule polymerization in a concentration-dependent manner. At low concentration (20–50 nM), colchicine suppresses the dynamics of polymerization but has no influence on the average polymer mass, i.e. it does not cause depolymerization. Moreover, colchicine decreases the catastrophe frequency and increases the frequency of rescue events, thus stabilizing the microtubules in the attenuated state. At higher colchicine concentration (>50 nM), the microtubules depolymerize, but depolymerization does not necessarily lead to complete disassembly and can result in stable microtubules of shorter length (Panda *et al.*, 1995). This molecular behavior is explained by the nature of the colchicine-tubulin interaction. As long as the number of incorporated colchicine-tubulin complexes remains small, binding of new tubulin dimers to the plus end is suppressed, whereas the existing lateral contacts suffice to hold the protofilaments together. However, when the amount of tubulin-colchicine complexes on the plus-end reaches a critical

level, the filaments fall apart and disassemble until the increasing concentration of free tubulin dimers prevents further depolymerization and, thus, a new steady state is reached (Ravelli *et al.*, 2004).

Colchicine alters the polymerization kinetics on both ends of the microtubule, but the plus end is much more sensitive to the toxin. While dissociation rates at the plus and the minus end of native microtubules may differ only 3-fold, this kinetic gap may rise to 60-fold at a molar ratio of tubulin-colchicine to free tubulin of 4 % (Farrell & Wilson, 1984). While at suitable concentrations of free tubulin native microtubules can grow and disassemble from both ends, in the poisoned state disassembly from the plus-end is essentially blocked and association on the minus-end is further slowed down.

Due to its ability to completely inhibit mitosis and the metaphase stage already at low concentrations, colchicine has become gold standard in plant and animal karyotyping as well as for induction of polyploidy in plants; metaphase-arrested mitosis was even termed ‘colchicine-mitosis’ or ‘c-mitosis’ (Eigsti & Dustin, 1955).

1.1.1.2 Medicinal mechanism of action

Despite the extraordinary long history of medicinal use of colchicine for the treatment of gout and other diseases, the mechanism of its remarkable anti-inflammatory action remained obscure for centuries. Even after its biomolecular target had been discovered, its influence on the cellular and physiological triggers of inflammation was better understood only during the last three decades.

As we know today, the potency of colchicine as a drug is associated with its anti-inflammatory effect. In the case of gout – still the main indication of colchicine – inflammation is induced by microcrystals of sodium urate formed in the synovial fluid as a result of a long-standing elevated level of ureic acid in blood (hyperuricemia). In most cases, the elevation is due to impaired excretion of ureic acid by the kidneys, which can have a genetic origin but also depends on the diet and lifestyle. Gout affects 1–2 % of adults and represents the most prevalent inflammatory arthritis in men in the developed countries (Richette & Bardin, 2010).

Crystal-induced inflammation in acute gouty arthritis is initiated by the binding of macrophages and mast cells to the negatively charged surface of monosodium urate (MSU) microcrystals (Mandel, 1976). The binding is mediated by membrane proteins and receptors such as Toll-like receptors and integrins (Barabe *et al.*, 1998; Liu-Bryan *et al.*, 2005). Activation of macrophages leads to upregulation of the IL-1 gene and production of active interleukin IL-1β, whose processing is mediated by the caspase-1 protease and occurs in a molecular complex known as NALP3 inflammasome (Martinon *et al.*, 2002; Martinon *et al.*, 2006). The charged

microcrystals can also bind various plasma proteins, including components of the complement system C1q, C1r and C1s (Terkeltaub *et al.*, 1983). Activation of the complement system on the crystal surface leads to formation of ligands for the neutrophil receptor CR3 (CD11b/CD18) (Barabe *et al.*, 1998).

The proinflammatory cytokines IL-1β and TNF-α, secreted by monocytes or mast cells, activate vascular endothelial cells, which upregulate expression of the adhesion molecules E-selectin, intercellular adhesion molecule-1 and vascular cell adhesion molecule-1 (Chapman *et al.*, 1997; Meng *et al.*, 1995). Once the inflammation process is initiated, various types of leukocytes (mainly neutrophils, but also mononuclear phagocytes and lymphocytes) migrate through the synovial membrane and accumulate in the cavity of the joint (Agudelo & Schumacher, 1973). Neutrophils engage phagocytosis of the MSU microcrystals, which triggers release of the calgranulin heterodimer S100A8/9 and other proinflammatory mediators (e.g., IL-1β, IL-8, PGE2 and superoxide anion), thus amplifying the recruitment of neutrophils (Ryckman *et al.*, 2003; Nuki, 2008).

The suppressive effect of colchicine on the crystal-induced inflammation can be directly or indirectly attributed to its effect on the polymerization of microtubules: (1) through the impairment of cellular motility, inhibiting the chemotaxis of leukocytes, in particular neutrophils (Caner, 1965), thus disrupting their ability to migrate to the source of inflammation and to infiltrate the synovial membrane; (2) through the suppression of L-selectin expression on the surface of neutrophils and the change of E-selectin distribution on the endothelial cells, recruitment of neutrophils is additionally inhibited (Cronstein *et al.*, 1995); (3) through the impairment of vesicular transport, colchicine inhibits the excretion of lysosomal enzymes during phagocytosis and degranulation of neutrophils (Wright & Malawista, 1973); (4) due to of its effect on the lysosomes, colchicine suppresses the release of crystal-derived chemotactic factor (CCF) (McCarty, 2008) and (4) downregulates production of superoxide anions, a proinflammatory mediator capable of activating the NALP3 inflammasome (interestingly, this effect is achieved *in vivo* at 100-fold lower colchicine concentrations than those required for the inhibition of neutrophil infiltration) (Chia *et al.*, 2008). Finally, colchicine was shown to selectively inhibit tyrosine phosphorylation stimulated by leukotriene B4 and other agonists of crystal-induced inflammation (Roberge *et al.*, 1993).

At high micromolar concentrations, colchicine also inhibits NALP3-driven activation of caspase-1, which is responsible for the processing of IL-1β from its precursor (Martinon *et al.*, 2006). However, this effect in unlikely to explain the therapeutic effect of colchicine as NALP3 inhibition has only been shown for concentrations exceeding those used in the therapy (Nuki, 2008). Although the exact pathways through which colchicine exhibits all these inhibitory

effects are unclear, one can assume that it acts upstream of the NALP3 inflammasome and prevents either phagocytosis of MSU microcrystals or their presentation to the recognizing protein of the inflammasome (Martinon *et al.*, 2006).

1.1.1.3 Pharmacodynamics

The pharmacodynamics of colchicine is mainly determined by the binding to three proteins in the body. Binding to intracellular tubulin defines the large distribution volume and its plasma half-life, oxidation by intestinal and hepatic cytochrome P450 3A4 (CYP3A4) governs its catabolism, and transport via the multidrug transporter P-glycoprotein (P-gp) influences its tissue distribution and excretion via the biliary tract and the kidneys (Niel & Scherrmann, 2006).

Colchicine binds tubulin with a dissociation constant of 0.1–1 µM and a complex half-life of 10–20 h, which is in the range of its plasma half-life (Fernando Diaz & Andreu, 1991; Banerjee & Luduena, 1992; Engelborghs, 1998; Niel & Scherrmann, 2006). Thus, the slow dissociation kinetics of the tubulin-colchicine complex appears to define its pharmacokinetic behavior (see below). The ubiquity of tubulin in the body tissues explains its extremely fast absorption (especially after intravenous application) and high distribution volume (Wallace & Ertel, 1970).

Cytochrome P450 3A4 (CYP3A4) is the chief enzyme responsible for the oxidative degradation of colchicine *in vivo*, which is achieved mainly through the demethylation of two methoxy groups at the colchicine ring A (2- and 3-demethylcolchicine) and one methoxy group at ring C (10-demethylcolchicine;Tateishi *et al.*, 1997). P450 3A4 is expressed in the liver, where colchicine is supposed to be predominantly metabolized, but also in the intestinal enterocytes, where the enzyme is present at a 3-fold higher concentration than in hepatocytes (von Richter *et al.*, 2004). The high activity of CYP3A4 in the intestine implies that a considerable amount of colchicine can be demethylated already in the gut wall after ingestion, even before it reaches the liver. Activity of CYP3A4 varies across individuals, leading to the varying sensitivity to colchicine treatment. It must also be considered that simultaneous prescription of other drugs that serve as substrates for CYP3A4 can decrease the clearance rate of colchicine and, hence, influence the response to treatment (Niel & Scherrmann, 2006).

P-glycoprotein (P-gp, also known as ABCB1, MDR1 and CD243) is an ATP-dependent efflux pump expressed on the luminal side of the cells in the intestinal epithelium, liver, proximal tubules of the kidney and capillary endothelial cells (Thiebaut *et al.*, 1987; Schinkel, 1999). It possesses a high degree of substrate promiscuity (Aller *et al.*, 2009) and transports a wide range of hydrophobic molecules from the cell into the intestinal lumen, biliary or urine duct, or the capillary lumen, respectively. It also plays a role of a ‘gate-keeper’ at the blood-brain and blood-testis barrier, expelling large hydrophobic molecules (>400 Da) from the capillary

endothelium back to the blood (Schinkel, 1999). Colchicine was one of the first identified substrates of P-gp, together with another microtubule-affecting drug vinblastine (Ueda *et al.*, 1987). Because of its high relevance for the resistance to drugs in general, P-gp serves as a target for inhibition in many therapies. A lowered activity of P-gp can lead to accumulation of colchicine in the cells, causing increased pharmacological or even toxic effects (Niel & Scherrmann, 2006).

1.1.1.4 Pharmacokinetics

1.1.1.4.1 Absorption

In case of oral application, colchicine is predominantly absorbed through the jejunum and the ileum; the proportion absorbed through each of them varies across individuals. After a single oral dose of 1 mg, the peak plasma concentration is reached within 30–90 min (Wallace & Ertel, 1970). The oral bioavailability is highly variable, which is probably related to differences in the expression and activity of CYP3A4 and P-gp (Niel & Scherrmann, 2006); with a mean value of 45 %, it can vary in the range of 24–88 % (Rochdi *et al.*, 1994). Gastrointestinal side effects associated with oral colchicine administration such as nausea, vomiting and diarrhea can further affect the bioavailability (Ehrenfeld *et al.*, 1982).

Although intravenous administration of colchicine allows to avoid the typical gastrointestinal side effects, it is not recommended because of the risk of overdosing as well as vein sclerosis and necrosis. Death outcomes have been reported when a total dose of 8–18 mg was administered to humans intravenously within 3–11 days (Wallace *et al.*, 1991).

1.1.1.4.2 Distribution

Oral colchicine is distributed into the tissues with a half-life of 1–2.7 h. The hydrophobic drug easily penetrates the cell membranes, rapidly reaching its target protein tubulin. The high terminal distribution volume (V_z) of 6.7 L results from its strong affinity towards tubulin and the high abundance of tubulin in the tissues (Rochdi *et al.*, 1994). In blood, colchicine circulates not only as a free drug. According to *in vitro* experiments, around 40 % of colchicine is bound to serum albumin, and a small amount also binds to α1-glycoprotein, γ-globulins and lipoproteins (Sabouraud *et al.*, 1994b); comparable numbers of 44–65 % have been reported from *in vivo* measurements in humans (Chappey *et al.*, 1994). In addition, colchicine easily permeates blood cells, which can serve as a depository, retaining high concentration of the drug long after the peak concentration in plasma had been reached. For instance, the concentration of colchicine in erythrocytes can be 5- to 10-fold higher than in plasma (Sabouraud *et al.*, 1994b; Vehier-Mounier *et al.*, 1989). The drug is also deposited in the leukocytes, where the peak concentration is reached only after 48 h, in contrast to one hour in

plasma. As leukocytes are the main cell type responsible for the medicinal effects of colchicine, it is not surprising that the drug concentration in leukocytes correlates with the manifestation of its therapeutic action (Chappey *et al.*, 1993).

Because of its hydrophobicity and relatively small size, colchicine can at least partially cross the blood-brain barrier and accumulate in the brain, which contains a high amount of tubulin (Bennett *et al.*, 1981). Accumulation of colchicine is prevented by the active back-pumping via P-gp, whose inactivation leads to a drastic increase in the colchicine deposition in the brain (Drion *et al.*, 1996). In one case, simultaneous administration of colchicine and verapamil, an inhibitor of both CYP3A and P-gp, resulted in development of flaccid tetraparesis in a patient, most probably due to accumulation of colchicine in the nerve tissue (Troger *et al.*, 2005). The drug was also shown to cross the placental barrier and could be detected in the umbilical cord (Amoura *et al.*, 1993), but P-glycoprotein of the syncytiotrophoblasts actively pumps it back to the maternal bloodstream (Niel & Scherrmann, 2006). Despite the possible minor exposure of the fetus to colchicine, existing studies of women treated with colchicine against Familial Mediterranean Fever (FMF) suggest that this drug brings no harm to the new-born child (Rabinovitch *et al.*, 1992; Ben-Chetrit *et al.*, 2010).

Pharmacokinetics of repeated-dose colchicine has been studied as well. For instance, when 1 mg colchicine per day was given orally to healthy volunteers for 15 days, the steady state plasma concentration was reached within 5 days and maintained at 0.7–1.4 mg/mL (Chappey *et al.*, 1993). The values were in a similar range for patients treated against FMF (Katz *et al.*, 1982).

1.1.1.4.3 Metabolism and elimination

Metabolism of colchicine in mammals is governed by the oxidation via CYP3A4, as described in Chapter 1.1.1.3. No studies of colchicine metabolism have been performed in humans so far. The available data were obtained either *in vitro* from hepatocyte cultures or from animal models (Niel & Scherrmann, 2006). Initially, colchicine is similarly demethylated in human and rat microsomes (Tateishi *et al.*, 1997; Xu *et al.*, 2008). Presumably 50–70 % of the drug are excreted unchanged into the bile and urine and 30–50 % as metabolites (Jaeger *et al.*, 1989). 2- and 3-demethylcolchicine can further undergo O-glucuronidation (mainly 2-DMC) and O-sulfate conjugation (mainly 3-DMC) (Sabouraud *et al.*, 1992a; Xu *et al.*, 2008). A glutathione O-sulfate conjugate at the tropolone oxygen (ring B, position 9) has also been reported (Xu *et al.*, 2008). Interestingly, the acetyl group of colchicine seems to remain stable *in vivo*, as no compounds with a free amino group have been detected among colchicine metabolites in rats (Hunter & Klaassen, 1975; Xu *et al.*, 2008). Even more interestingly, the work by Hunter &

Klaassen (1975) has been extensively cited throughout the literature to state the opposite (Putterman *et al.*, 1991; Sullivan *et al.*, 1998; Harris *et al.*, 2000; Finkelstein *et al.*, 2010).

Colchicine is mainly excreted through the liver via the biliary route. In the liver, P-gp transports colchicine from the intrahepatocytic compartment to the bile (Ueda *et al.*, 1987; Niel & Scherrmann, 2006), finally reaching the intestine. Apart from being excreted through the feces (Eren *et al.*, 2019), the compound can be reabsorbed and undergo enterohepatic circulation (Borron *et al.*, 1996; Chen *et al.*, 2008), which may result in a delayed plasma peak within 6–8 hours after oral administration (Ferron *et al.*, 1996). Supporting the prominent role of P-gp in the biliary excretion of colchicine, ciclosporine (a potent inhibitor of P-gp) can reduce biliary colchicine clearance by up to 80 % (Speeg *et al.*, 1992a).

Excretion via the kidneys is responsible only for 5–20 % of the total drug elimination, with a renal clearance rate of 4 L/h in healthy humans (Sabouraud *et al.*, 1994a). This is achieved both via glomerular filtration of the free drug and active tubular secretion mediated by P-gp (de Lannoy *et al.*, 1994). Inhibition of P-gp in the proximal renal tubules by ciclosporine can decrease renal clearance by 50 %, further underlining its important role in the pharmacokinetics of colchicine (Speeg *et al.*, 1992b).

1.1.2 Colchicine poisoning

Cases of colchicine poisoning can be classified based on the source of the poison and the reason of ingestion. First, the poison can originate either from its natural source – plants of the *Colchicaceae* family (as described in Chapter 1.1.1) – or from pharmaceutical colchicine, usually in tablet form. Second, colchicine poisoning can be accidental or intentional. The majority of reported cases of colchicine poisoning comprise suicide attempts with a colchicine-based drug (Stapczynski *et al.*, 1981; Baud *et al.*, 1995; Folpini & Furfori, 1995; Borron *et al.*, 1996; Kintz *et al.*, 1997; Deveaux *et al.*, 2004; van Zoelen *et al.*, 2002; Abe *et al.*, 2006; Link *et al.*, 2014; Lev *et al.*, 2017) or a colchicine-containing plant (Danel *et al.*, 2001; Nagesh *et al.*, 2011; Ellwood & Robb, 1971). Accidental plant ingestion due to confusion with *Allium ursinum* or other similar plants (Gooneratne, 1966; Klintschar *et al.*, 1999; Brncić *et al.*, 2001; Brvar *et al.*, 2004b; Brvar *et al.*, 2004a; Flesch *et al.*, 2002; Sundov *et al.*, 2005; Wehner *et al.*, 2006; Amrollahi-Sharifabadi *et al.*, 2013; Sannohe *et al.*, 2002; Galland-Decker *et al.*, 2016) and accidental ingestion of colchicine tablets by children (Güven *et al.*, 2002; Atas *et al.*, 2004) is also described in the literature.

Last but not least, colchicine has also been used as a weapon for intentional poisoning. The oldest and the most famous case of homicidal colchicine poisoning is associated with Catherine Wilson, an English serial killer and the last woman publicly hanged in London, in

1862. Working as a nurse in a hospital, she persuaded her patients to bequeath her their money and subsequently poisoned them with colchicine. She was also believed to have poisoned several of her lovers as well as her husband: after a short period of marriage, he was found dead in his room, together with an empty bottle of colchicum (Court, 1862). Some spectacular poisoning cases have also been reported in the 21st century, e.g. a fatal ingestion of *C. autumnale* flowers in a hope to produce an illegal narcotic effect (van Zoelen *et al.*, 2002) or use of *G. superba* seeds in a murder attempt (Kande Vidanalage *et al.*, 2016).

Generally, however, colchicine poisonings are rare. Only 20 cases have been reported in the English scientific literature between 1947 and 1981 (Stapczynski *et al.*, 1981). The poisoning seems to be more common in Central Europe. For instance, 84 cases have been reported between 1966 and 1967 in the Hôspital Fernand-Widal in Paris (Bismuth *et al.*, 1977; Stapczynski *et al.*, 1981). While the frequency of colchicine poisoning is low, the ratio of fatalities among them is exceptionally high. For example, among all cases of poisonings with plants reported in Switzerland between 1966 and 1996, serious intoxications that required hospitalization constituted only 0.6 %, while for the poisonings with *Colchicum*, every fourth case was lethal (Jaspersen-Schib *et al.*, 1996; Klintschar *et al.*, 1999). It must also be noted that the low rate of poisoning reports concerning members of the *Colchicaceae* family may be due to the difficulty of proper diagnosis, which might have left many cases unreported (Klintschar *et al.*, 1999). The frequency of case reports notably increased in the 2000s, probably reflecting progress in the analytical methods and better hospital equipment.

Accidental poisoning by the toxic plants such as *C. autumnale* or *G. superba* usually result from their resemblance to edible plants. For instance, *C. autumnale* is often confused with *Allium ursinum*, or bear's garlic – a traditional component of the spring seasonal cuisine in many countries in Central Europe. Although the flowers of the two plants are difficult to confuse, bear's garlic is collected in the forests in the spring time when the green leaves vegetate, whereas *Colchicum* blossoms in the autumn. The leaves of *Colchicum* are similar in form to bear's garlic and often grow in the same areas, which can make them difficult to distinguish (see Figure 1.3; Wehner *et al.*, 2006). Of note, *C. autumnale* contains colchicine in all parts, with the highest content in the seeds and the flowers (0.45 % and 0.8 %, respectively; Manske *et al.*, 1950; Jaeger & Flesch, 1990).

Colchicum autumnale
autumn crocus

Allium ursinum
bear's garlic

Figure 1.3. Leaves of *C. autumnale* and *A. ursinum* during springtime.

The other colchicine-containing plant, *Gloriosa superba* (see Figure 1.1) is grown as a decorative plant throughout the world but is naturally found in tropical Africa and Asia. In the tropical areas, the tubers of *G. superba* are often confused with those of sweet potatoes (*Ipomoea patata*) or yam (*Dioscorea spp.*; Fernando & Widyaratna, 1997). Also, in tropical Africa and India the plant extract was used as a remedy against head lice, as a component of arrow poison and as a suicidal and murder poison in rural areas (Neuwinger, 1996). According to a retrospective study, 44 % of poisoning cases in Sri Lanka are linked to *G. superba*, with a fatality rate of 15 % (Fernando & Fernando, 1990).

In healthcare-related cases, colchicine poisoning can occur if the toxic drug concentration is exceeded because of a prescription error or patient incompliance. This is facilitated by the narrow therapeutic window and the absence of an exact border between the therapeutic, toxic and lethal concentrations (Finkelstein *et al.*, 2010). Based on an analysis of 22 poisoning cases, Stapczynski *et al. (1981)* noticed that all patients who digested less than 0.5 mg/kg body mass colchicine survived, while a dose of over 0.8 mg/kg resulted in a lethal outcome in all cases. Interestingly, while a lethal outcome has been registered after administration of 6 mg crystalline colchicine, an accidental ingestion of ~350 mg colchicine in form of tubers of *Gloriosa superba* was survived (Macleod & Phillips, 1947; Gooneratne, 1966).

Colchicine poisoning can even occur if the theoretical dosage guidelines are followed: liver or kidney dysfunctions slow down colchicine metabolism and excretion and may thus lead to an increase of colchicine concentration in the body up to a toxic level (Wallace *et al.*, 1991; Leighton *et al.*, 1991). Another possible reason is the physiological drug-drug interaction with inhibitors of P-gp and CYP3A4 (e.g., ciclosporine and erythromycin, see Chapter 1.1.1.4.3). Other drugs, such as cimetidine and tolbutamide, may compete with colchicine for CYP3A4

(Leighton *et al.*, 1990). Elderly patients also have higher risk of colchicine accumulation because the drug clearance and distribution volume can be 2-fold lower (Rochdi *et al.*, 1994).

1.1.2.1 Manifestation

Symptoms of colchicine poisoning are similar to those of cholera and can be divided into three stages, usually partially overlapping (see Table 1.1); (Stapczynski *et al.*, 1981; Finkelstein *et al.*, 2010). In the lethal cases, death usually occurs due to cardiovascular collapse, cardiac arrest and sudden asystole (Stapczynski *et al.*, 1981; Borron *et al.*, 1996; Brvar *et al.*, 2004a). Although being well-studied, the exact complex of symptoms of colchicine poisoning is highly case-dependent and poorly predictable, which complicates both treatment and diagnosis.

Table 1.1. Clinical stages of colchicine poisoning (adapted from Finkelstein *et al.*, 2010).

Stage	Time of onset	Features
1. Gastrointestinal phase	0–24 h post-ingestion	Nausea, vomiting, diarrhoea, abdominal discomfort Hypovolemia Leukocytosis
2. Multi-organ failure phase	1–7 days post-ingestion	Respiratory distress syndrome Cardiac arrhythmias, failure, arrest Encephalopathy, brain œdema Convulsions Renal failure Liver failure Disseminated intravascular coagulation Bone marrow suppression Pancytopenia Haemolysis Metabolic derangements: metabolic acidosis, hypokalaemia, hyponatremia, hypocalcaemia, hypoglycaemia (or hyperglycaemia), hypophosphatemia Myopathy Neuropathy Secondary sepsis
3. Recovery phase	7–21 days post-ingestion	Resolution of organ system derangements Rebound leukocytosis Alopecia

1.1.2.2 Diagnosis

Colchicine is a rare poison and not routinely tested (Klintschar *et al.*, 1999). The typical syndrome complex (toxidrome) of colchicine intoxication comprises gastroenteritis,

hypotension, lactic acidosis and prerenal azotemia (Donovan, 2007). Many symptoms of the first intoxication phase can be attributed to other systemic disorders (e.g., enterocolitis, sepsis, nonsteroidal anti-inflammatory drug or iron poisoning), but colchicine poisoning can be differentiated on the second stage by severe bone marrow suppression (Finkelstein *et al.*, 2010).

For exact diagnosis, chemical identification and quantification of colchicine in blood or other fluids (urine, bile, feces) is necessary. The analysis is complicated by the low colchicine concentration in plasma, which does not exceed 50 ng/mL (12 nM) even in severe cases of intoxication (Jaeger *et al.*, 1989). Currently, state-of-the-art colchicine detection and quantification comprises HPLC analytics coupled to mass spectrometry (Wehner *et al.*, 2006; Abe *et al.*, 2006). Such equipment is not available in every hospital facility, which complicates the analysis.

False diagnoses are common, especially if the fact of ingestion of a colchicine-containing agent is unknown. Even though the lethal intoxication phase takes at least two days to develop, correct diagnosis is often achieved only via post-mortem analysis (Weakley-Jones *et al.*, 2001; Amrollahi-Sharifabadi *et al.*, 2013). Presence of a history of gout or FMF can give clinicians a hint of colchicine poisoning (Finkelstein *et al.*, 2010), especially if combined with liver or kidney dysfunction or with administration of cytochrome P-450 and/or P-gp inhibitors (Putterman *et al.*, 1991).

1.1.3 Protein antidotes against plant toxins

Animals, plants, bacteria and fungi are specialized in the production of toxins of different chemical nature. Animal toxins are usually of protein origin, plant toxins are mainly represented by secondary metabolites and sometimes peptides or proteins (gelonin, ricin), while bacteria and fungi produce a variety of protein, peptide and small molecule toxins (Proft, 2009). The rareness of protein-based plant toxins can be well explained by the necessity of the specific application route: to cause a systemic effect, a protein toxin must reach the blood stream or at least the cytoplasm of gastrointestinal cells, for which most plants possess no specialized organs.

The scope of protein-based antidotes against plant toxins is considerably narrower than that for animal venoms. First, as mentioned above, most plant toxins are small molecules and often constitute poor haptens for animal immunization. Second, many plant and fungal toxins act on the nervous system through (in-)activation of signaling pathways, making such toxins suitable targets for physiological antidotes (compounds exhibiting an opposite physiological action to that of the toxin). However, if the latter is not possible, a specific neutralizing antidote becomes

indispensable, in particular for two potent plant toxins: digitalis (the oldest cardiac drug in medical use) and colchicine. Up to date, several antidotes against these powerful poisons have been developed or are under investigation (Table 1.2).

Table 1.2. Overview of the protein-based antidotes against plant toxins.

Name	Type*	Toxin	Source	Country	Manufacturer	Reference
DigiBind	Ab	Digoxin	Sheep	USA	GlaxoSmith Kline	(Eddleston & Persson, 2003)
DigiFab	Fab	Digoxin	Sheep	USA	Protherics	(Eddleston & Persson, 2003)
Digitalis-Antidot BM	Ab	Digoxin	Sheep	Switzer-land	Roche	(Eddleston & Persson, 2003)
DigiCal	BBP	Digoxin	Human	Germany	N/A	(Schlehuber *et al.*, 2000; Eyer *et al.*, 2012)
Anti-colchicine antibodies	Ab	Colchicine	Goat	France	N/A	(Eddleston & Persson, 2003)
Anti-colchicine antibodies	Fab	Colchicine	Ovine	France	Laboratoires SERB	(European Medicines Agency, 2010)
ColchiBIND	Fab	Colchicine	Ovine	UK	Micropharm	(Peake *et al.*, 2015; Gumm *et al.*, 2016; Eddleston *et al.*, 2018)

*Ab – full-format antibody, Fab – Fab fragment, BBP – bilin-binding protein

It should be mentioned that despite all the breakthroughs made since the invention of serotherapy, such as monoclonal antibody technology and CDR-grafting, a considerable number of protein-based antivenoms and antidotes on the market is represented by polyclonal Fab fragments. The most probable reason for this is the relative simplicity and accessibility of animal immunization, requiring a minimum of laboratory equipment and investment. As an additional factor, the habitats of most venomous animals and plants are spread through the developing countries, where low cost and ease of application play an important role.

1.1.4 Treatment of colchicine poisoning

In contrast to some neurotoxins, toxic effects of colchicine cannot be circumvented by physiological antidotes. Colchicine is hydrophobic and easily penetrates the cell membranes, rapidly reaching its target tubulin. The fast distribution into the tissues makes removal of the toxin by hemodialysis, plasma exchange or charcoal hemoperfusion ineffective (Putterman *et al.*, 1991). Gastric lavage can be useful to remove the unabsorbed toxin from the intestine but only if the poisoning has been diagnosed within the first hours after colchicine ingestion. However, in case of plant ingestion, large amounts of colchicine can be retained in the intestine for a day or more (Putterman *et al.*, 1991; Ellwood & Robb, 1971). Administration of multiple doses of activated charcoal might be effective in withdrawing colchicine from the enterohepatic circulation (Hood, 1994), although its application can be complicated by paralytic ileus,

sometimes developing as a poisoning symptom (Brvar *et al.*, 2004a). The use of charcoal is especially sensible in case of intentional suicidal drug poisoning when colchicine can be accompanied by other toxic substances (Putterman *et al.*, 1991).

Apart from generic detoxication measures, colchicine treatment remains symptomatic and mainly supportive (Putterman *et al.*, 1991). It includes correction of electrolyte and acid-base balance, vasopressive drugs, antiarrhythmic agents and blood products (Finkelstein *et al.*, 2010). The associated bone marrow suppression and leukopenia during later intoxication stages can be treated with granulocyte colony-stimulating factor (GM-CSF; Harris *et al.*, 2000). If ingestion of a high dose of colchicine is suspected, hemodynamics and respiration must be thoroughly monitored, as acute circulatory insufficiency may develop between 24 and 72 hours post-ingestion, which represents the most common cause of death after colchicine poisoning (Putterman *et al.*, 1991).

Table 1.3. Chronology of anti-colchicine antibody research and development.

Year	Source	Type		K_D	Model	Reference
1989	rabbit	(immunization)		N.A.	rabbit	(Scherrmann *et al.*, 1989)
1989	mouse	monoclonal	Ab	670 pM	CHO cells	(Rouan *et al.*, 1989)
1990	goat	polyclonal	Ab	N.A.	mouse	(Terrien *et al.*, 1990)
1991	goat	polyclonal	Fab	50 pM	mouse	(Sabouraud *et al.*, 1991)
1992	goat	polyclonal	Fab	50 pM	rat	(Sabouraud *et al.*, 1992b)
1992	goat	polyclonal	Fab	50 pM	rabbit	(Sabouraud *et al.*, 1992c)
1995	goat	polyclonal	Fab	50 pM	human	(Baud *et al.*, 1995)
2015	ovine	polyclonal	Fab	10 pM	rat	(Peake *et al.*, 2015)
2018	ovine	polyclonal	Fab	3 pM	minipig	(Eddleston *et al.*, 2018)

Immunotoxicological approach was first applied to colchicine poisoning in 1989, when it was shown that rabbits immunized with colchicine were resistant to much higher concentrations of colchicine than naïve animals (Scherrmann *et al.*, 1989; see Table 1.3). Later on, heterologous (goat) colchicine-specific antibodies were used to reverse colchicine toxicity in mice (Terrien *et al.*, 1990), followed by polyclonal Fab fragments (Sabouraud *et al.*, 1991). In addition, a monoclonal antibody has been tested *in vitro* on Chinese hamster cells (Rouan *et al.*, 1990). In a landmark paper by Baud *et al.* (1995), colchicine overdose after suicidal ingestion of colchicine-containing tablets (60 mg total, 0.96 mg/kg body mass) was treated with polyclonal anti-colchicine Fab-fragments. Although administration of the antidote was started only 40 hours after the ingestion, it instantly improved the hemodynamic parameters and may have

prevented cardiovascular collapse. Despite the development of bone marrow suppression and temporary total hair loss, which is typical for colchicine poisoning, the patient survived and recovered completely after several months.

After that work, no reports on antibody-based treatment of colchicine overdose were published for 20 years. In 2015, Peake *et al.* reported enhancement of colchicine clearance in rats using Fab fragments of an ovine polyclonal antibody (Peake *et al.*, 2015). The rats were challenged with an oral non-lethal dose of colchicine (5 mg/kg body mass, or ~1.25 mg), followed by intraperitoneal injection of 250 mg polyclonal Fab fragments (5 % of the total Fab being specific for colchicine) two hours after colchicine ingestion. Application of the Fab fragments increased colchicine concentration in serum 7-fold and boosted its excretion into the urine, evidencing affinity-driven extraction of colchicine from the tissues. These Fab-fragments were produced by Micropharm Ltd. (ColchiBIND, see Table 1.2), which has specialized in the production of sera against rare poisons and represents one of the few manufacturers of colchicine-complexing drugs. In 2018, Micropharm reported a further preclinical study with the same Fab fragment tested in a porcine model (Eddleston *et al.*, 2018). According to the manufacturer's website, a corresponding clinical trial is expected to commence in 2019 (Micropharm, 2019).

1.2 Selection of binding proteins for transition state analogs

1.2.1 Catalytic antibodies

Apart from the selection, biochemical characterization and structural elucidation of lipocalin-based on of antidotes against colchicine, the present dissertation deals with the functional and structural investigation of engineered lipocalins that bind a transition state analog (TSA) with the aim to develop lipocalin-based catalysts for a Diels-Alder cycloaddition.

Natural enzymes are incredibly efficient catalysts. Like inorganic and organic catalysts, they enhance the rates of chemical reactions with multiple turnovers but provide specificity and selectivity unachievable by simple chemical catalysts. The versatility of enzymes in terms of the broad range of reactions results from the variety of the available amino acid side chains, sometimes accompanied by co-enzymes in diverse three-dimensional arrangements, while their specificity is based on the rigidity and chirality of the surrounding protein scaffold.

The fundamental principle of enzyme catalysis and its similarity to antigen-antibody recognition was expressed by Linus Pauling. In his reflection "Chemical achievement and hope for the future" in 1948 he wrote: "*I believe that an enzyme has a structure closely similar to that found for antibodies, but with one important difference, namely, that the surface configuration of the enzyme is not so closely contemporary to its specific substrate as is that of an antibody to its homologous antigen, but is instead complementary to an unstable molecule with only transient*

existence – namely the "activated complex" for the reaction that is catalyzed by the enzyme" (Pauling, 1948). Further developing Pauling's idea, William Jencks proposed the possibility of designing catalytic antibodies: "*If complementarity between the active site and the transition state contributes significantly to enzymatic catalysis, it should be possible to synthesize an enzyme by constructing such an active site. One way to do this is to prepare an antibody to a haptenic group, which resembles the transition state of a given reaction*" (Jencks, 1969).

The first practical implementation of this concept was achieved in the mid-1980's by applying hybridoma technology for the production of monoclonal antibodies. In 1986, the groups of Richard Lerner from the Scripps Institute and Peter Schultz from the University of California simultaneously demonstrated catalytic activity in monoclonal antibodies selected against stable synthetic transition state analogs (TSA's) (Tramontano *et al.*, 1986; Pollack *et al.*, 1986). These laboratories also led the field of catalytic antibodies (later dubbed 'abzymes' for 'antibody enzymes') for the next two decades, before the general interest in this area ceased, apparently due to the lack of success in generating abzymes with practical utility. Nevertheless, antibody catalysts were obtained for many reactions that are not catalyzed by natural enzymes (Figure 1.4A). However, soon it became clear that creation of an antibody with a moderate initial level of catalytic activity constitutes a smaller problem than increasing its activity to a level comparable to that of natural enzymes.

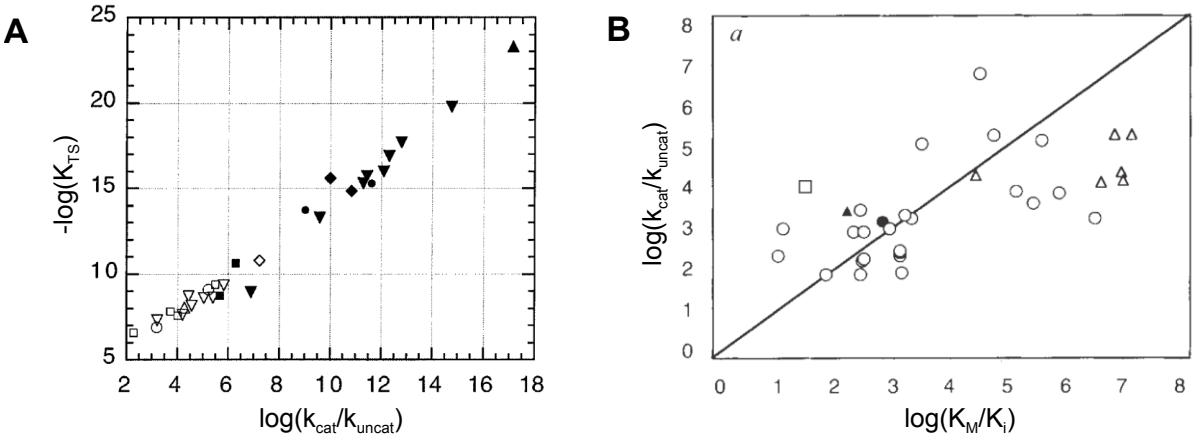

Figure 1.4. Chemical proficiency and binding energy for catalytic proteins. **A:** Comparison of chemical proficiency, $\log(K_{TS})$ (K_{TS} representing affinity to the transition state), and rate acceleration, k_{cat} / k_{uncat}, for a series of reactions catalyzed by enzymes (filled symbols) and antibodies (open symbols; from Hilvert, 2000). **B:** Comparison of binding energy (defined as $K_M/K_i = K_M/K_{TS}$) with observed acceleration rate (k_{cat}/k_{uncat}) for antibody-catalyzed unimolecular reactions (Stewart & Benkovic, 1995). ○ – hydrolysis, □ – Claisen rearrangement, Δ – decarboxylation, ● – elimination, ▲ –metallation. The diagonal line has a slope of 1 and serves as reference (not a regression line). The authors pointed out that the four of the five outliers with high positive deviation represented dephosphorylation or deacylation reactions, whose assay is prone to contamination by natural enzymatic activity.

1.2.2 Design of transition state analogs

Assuming that an enzymatic reaction proceeds through the same pathway and same transition state as the uncatalyzed reaction, the enzyme should bind the transition state more tightly than the substrate by the same factor as the catalyzed reaction rate exceeds the uncatalyzed reaction (Wolfenden, 1969). This leads to the relation $k_{cat}/k_{uncat}=K_M/K_{TS}$, or $(k_{cat}/K_M)/k_{uncat} = 1/K_{TS}$ (Kurz, 1963; Hilvert, 2000). The latter term represents the so-called catalytic proficiency – a measure by which an enzyme enhances the reaction rate compared to the uncatalyzed reaction (Radzicka & Wolfenden, 1995). Thus, theoretically, if a synthetic TSA mimics the properties of the reaction's true transition state closely enough, the search of an efficient enzyme can be reduced to finding a protein with good affinity towards the TSA (Hilvert, 2000). In favor of this assumption, Stewart and Benkovic (1995) found a weak correlation between k_{cat}/k_{uncat} and K_M/K_{TS} for a panel of 32 catalytic antibodies (Figure 1.4B).

Two aspects define the success of a selection campaign for a catalytic antibody: (1) design of a proper TSA that adequately represents the reaction transition state, and (2) application of a powerful selection strategy enabling the isolation of TSA binders from a pool of unspecific proteins and the subsequent identification of catalysts from the pool of TSA binders.

In the course of natural evolution, enzymes have developed remarkable suitability for the reactions they catalyze. Current studies show that, in accordance with the assumption of Linus Pauling, the most efficient enzymes also developed extremely high affinities towards the transition states, with dissociation constants as low as 10^{-24} M (Radzicka & Wolfenden, 1995). However, in addition to the conformational and stereochemical complementarity required for the molecular recognition of haptens by normal antibodies, recognition of the TSA by a potent catalytic antibody has to fulfil further requirements, in particular appropriate distribution of electron density and atom hybridization in the active site. For the reactions proceeding via a transition state with over-coordinated atoms, TSAs containing elements from the next group in the periodic table are often employed, since they can form stable compounds with the suitable coordination number. For instance, phosphorus compounds are often used to mimic activated transition states with penta-coordinated carbon during hydrolysis of ester bonds (Tanaka, 2002). For multisubstrate reactions, a suitable transition state analog mimics the substrates oriented similarly as in the activated complex (Hilvert, 2000).

The requirements posed on the TSA also depend on the desired mechanism of rate enhancement: for example, the catalyst might just bring the reaction counterparts together and orient them, thus acting purely entropically, it can stabilize the transition state by non-covalent interaction, thus also lowering the activation enthalpy, or it can involve covalent catalysis with participation of reactive groups. Obviously, the latter option is the trickiest and requires

sophisticated quantum modeling, application of special selection techniques as well as a piece of luck. One such technique is the so-called 'bait-and-switch' approach, in which the hapten is designed to favor selection of antibodies with negatively charged residues that later act as acid-base reactive groups. For example, a counter-charged residue in the antibody can be 'induced' by a positively charged hapten, resulting in an antibody capable of deprotonating a hydroxy group during hydrolysis of a phosphodiester bond (Wentworth *et al.*, 1998). Another approach is the so-called 'reactive immunization' (Tanaka & Barbas, 2002), which employs specially designed highly reactive haptens that conjugate with the antibody, resulting in the selection of antibodies with certain reactive groups in the binding pocket (Wagner *et al.*, 1995; Lo *et al.*, 1997). For example, a phosphonate diester hapten was used to 'induce' antibodies carrying a reactive nucleophile in the binding site, which later acted as a nucleophile for hydrolysis of the corresponding ester (Wirsching *et al.*, 1995).

Before the development of powerful *in vitro* directed evolution methods, immunogenicity of the hapten was an additional factor to consider during the TSA design. Usually the hapten was conjugated with adjuvants – high-molecular-weight proteins known to enhance induction of antibody immune response. For modern selection techniques, this is no longer a matter concern. However, the hapten still has to be immobilized and to be bulky enough to form a sufficient number of interactions with the binding protein. Finally, a good TSA also has to be chemically stable and synthesizable.

A variety of TSA haptens have been designed for different substrates and reaction types. More than 50 esterolytic antibodies were obtained using phosphonate TSAs (Hilvert, 2000; Tanaka, 2002). A range of reaction types and common TSAs is presented in Table 1.4. Published TSAs and catalytic antibodies were extensively reviewed by Thomas (1996) and Stevenson & Thomas (2000).

Table 1.4. Reaction types and some TSAs used to elicit corresponding catalytic antibodies.

Reaction type	TSA	Reference
Ester hydrolysis	Phosphonate	(Hilvert, 2000; Tanaka, 2002)
Carbamate ester hydrolysis	Phosphonamidate	(Wentworth *et al.*, 1997)
Amide bond hydrolysis	Sulfonamide/sulfinamide Boronic acid	(Moree *et al.*, 1991) (Gao *et al.*, 1998)
Phosphate diester hydrolysis	Oxorhenium (V) chelate Bait-and-switch hapten	(Weiner *et al.*, 1997) (Wentworth *et al.*, 1998)
Glycoside hydrolysis	Half-chair conformation mimic α-1,6-linkage mimic	(Suga & Tanimoto, 1994; Yu *et al.*, 1998) (Goud *et al.*, 2001)

1.2.3 Selection strategies

At the beginning of the catalytic antibody era, animal immunization was the only method of obtaining specific antibodies. Most catalytic antibodies described till 1995 were elicited with this method. This approach bears disadvantages for the selection of catalytic antibodies, since TSAs, although much more stable than true transition states, are often chemically fragile and degrade *in vivo*. Since then, the development of *in vitro* directed evolution methods such as phage display, ribosome display, cell surface display, etc. has broadened the scope of TSAs that can be utilized for generation of abzymes.

For certain chemical transformations, selection strategies were developed that allow direct selection for catalytic activity in the course of *in vitro* directed evolution. For example, if the catalytic event leads to covalent immobilization of the phage particle on a solid surface or, conversely, to detachment, phage display can be adapted for the direct selection of catalytic trait. This approach was applied for the catalytic improvement of a subtiligase mutant fused to a phage protein, which was capable of attaching biotin-labeled peptides to its own N-terminus (Atwell & Wells, 1999). In another example, it was possible to select catalytic antibodies through a covalent reaction intermediate stable at acidic pH, which hydrolyzed at basic pH and could be used for elution of the phage particles (Gao *et al.*, 1997). Eventually, a procedure called ‘covalent trapping’ was employed to select for catalytic antibodies capable of cleaving a galactopyranoside moiety from an immobilized hapten. Cleavage of the sugar conjugate led to transformation of a difluoromethylphenol moiety to a reactive quinone methide that could react with any nucleophile in the antibody binding site and thus permitted ‘trapping’ the antibody on a solid surface (Janda *et al.*, 1997).

While chemical attachment or detachment can function as a selection strategy for *ex vivo* directed evolution, *in vivo* selection approaches can be adapted for the screening for catalysis in a more diverse way. Should the reaction be able to ensure survival or provide growth advantage to fast dividing cells (e.g., bacterial or yeast), a corresponding catalyst can be improved through alternating rounds of sequence diversification and culture growth. This approach is applicable in two cases: either the enzyme may catalyze overproduction of a growth-limiting metabolite in a corresponding auxotrophic strain, or the enzyme may inactivate a substance that hinders growth, such as an antibiotic. The first approach was applied to select for the transformation of chorismate to prephenate (Tang *et al.*, 1991), orotate to uridine (Smiley & Benkovic, 1994) and, without success, to the liberation of free biotin from a p-nitrophenyl ester (Lesley *et al.*, 1993).

In cases where the chemical reaction does not allow direct selection for catalytic activity, screening for catalytic activity is facilitated if a reaction leads to an easily measurable change

of spectroscopic properties of the reaction mixture. Fluorescent properties of the products have been employed for improvement of a catalytic antibody for a retro-Diels-Alder reaction, releasing an anthracene product (Bensel *et al.*, 1999), and a pivalate-hydrolyzing antibody, releasing the fluorescent umbelliferone (Bensel *et al.*, 2001).

1.2.4 Diels-Alder reaction and the search for a Diels-Alderase

This cycloaddition reaction was first described by Otto Diels and Kurt Alder in 1928. For this discovery they received the Nobel Prize in Chemistry in 1950. The Diels-Alder cycloaddition is one of the most powerful reactions in organic synthesis as it offers one of the easiest ways to generate a carbon-carbon bond with a formation of a cyclohexene-type ring. The reaction occurs between a conjugated diene and a substituted alkene ('dienophile'). It can be classified as a $[4\pi_s + 2\pi_s]$ cycloaddition that proceeds via a single concerted cyclic transition state, representing a fundamentally concerted reaction (Dewar *et al.*, 1986). To form the transition state, the substrates must be appropriately oriented and positioned in parallel planes, whilst the diene has to adopt the *s-cis* conformation. Due to these conformational and spatial requirements, this reaction has a high activation entropy of -30 to -40 cal/(K·mol) (Wassermann, 1965).

In 'standard electron demand' DA reactions, the reaction is favored if the diene is electron-rich (e.g., quinones, maleic anhydrides or maleimides), while the dienophile possesses an electron-withdrawing group in conjugation with the double bond. The high-energy highest occupied molecular orbitals (HOMOs) of the electron-rich diene stabilize the cyclic transition state by strongly interacting with the lowest unoccupied orbitals (LUMOs) of the electron-poor dienophile. Conversely, if an electron-poor diene is used, electron-rich alkenes lead to better dienophile pairs. In that case, the interaction is guided by the HOMOs of the dienophile and LUMOs of the diene (Carey & Sundberg, 2007b). If both reactants are asymmetrically substituted, the regioselectivity of the DA reaction is explained by the Frontier orbital theory: an *'ortho'*-like product is favored if the diene has an electron-donating group at the first position, whereas a *'para'*-like product is preferred with a donor substituent at the second carbon atom of the diene (Carey & Sundberg, 2007b).

Since the reaction proceeds via a concerted mechanism, it is stereospecific with respect to the *E/Z* isomery of both the diene and dienophile, leading to the corresponding cis- or trans-products (Carey & Sundberg, 2007b). Another stereochemical feature depends on the orientation of an asymmetrical dienophile prior to the formation of transition state: the substituent on the alkene may be directed towards the newly formed double bond (leading to an *endo* transition state and product), or to the opposite side (*exo* transition state and product). This preference can be predicted by an empirical Alder rule, stating that for normal-demand

DA reactions the *endo* transition state is favored, even though it is often sterically more congested (Carey & Sundberg, 2007a).

The potency of the Diels-Alder reaction prompted the question whether this type of efficient synthetic reaction has been exploited by nature. However, the search for a natural 'Diels-Alderase' enzyme lasted for decades but evidenced a variety of false positive candidates (Klas *et al.*, 2015). In many cases, it turned out that the enzyme-catalyzed reaction proceeded via two or more steps without the formation of a concerted transition state. For instance, macrophomate synthase was claimed to be the first natural Diels-Alderase (Watanabe *et al.*, 2000) but turned out to be an aldolase (Serafimov *et al.*, 2008). The proven Diels-Alderases for which the presence of a concerted transition state was confirmed include spinosyn synthase (Kim *et al.*, 2011; Fage *et al.*, 2015) and enzymes involved in the biosynthesis of compounds of the spirotetronate/spirotetramate group (Hashimoto *et al.*, 2015; Zheng *et al.*, 2016; Byrne *et al.*, 2016) as well as the decalin cores of compounds such as equisetin and myceliothermophin (for instance, CghA, a protein with a lipocalin-like fold; Sato *et al.*, 2015).

The first antibody-based Diels-Alderases described so far and one of the most efficient abzymes is the Diels-Alderase antibody 1E9, first reported in 1989 and further developed in several steps (Hilvert & Hill, 1989; Xu *et al.*, 1999; Piatesi, 2003; Piatesi & Hilvert, 2004). 1E9 was generated by the classical immunization approach, originating from the murine germ line genes *VFM11* and V_K5.1 (Xu *et al.*, 1999). It catalyzes a [4+2] cycloaddition between the electron-poor diene tetrachlorothiophene dioxide (TCTD, **4**, Figure 1.5) and *N*-ethylmaleimide (NEM, **5**), thus representing an inverse electron demand DA reaction. This specific reaction was chosen as target for the abzyme because the cycloaddition leads to a high-energy intermediate that quickly releases sulfur dioxide and decays to dihydrotetrachloro-*N*-ethylphthalimide followed by oxidation and aromatization. The planar final product retains little resemblance to the initial transition state, thus eliminating the problem of product inhibition, which is typical for Diels-Alderase catalysts.

The antibody 1E9 was selected against the stable *endo* hexachloronorbornene derivative **9**, which mimics the unstable initial reaction product **6**. The dichloromethylene group of the TSA resembles the SO_2 group of **6**, resulting in a stable compound closely mimicking the geometry of the putative concerted transition state. 1E9 binds the TSA **9** with an affinity of 0.1 nM and catalyzes the cycloaddition with a k_{cat} of 3.7 min^{-1} (0.062 s^{-1}) and K_{NEM} = 9 mM (K_{TCTD} cannot be determined experimentally due to the low solubility of TCTD; K_M for a more soluble analog of TCTD was shown to be 2.4 mM; Xu *et al.*, 1999; Piatesi & Hilvert, 2004). Thus, 1E9 possesses an apparent catalytic efficiency k_{cat}/K_{NEM} of 410 $M^{-1}*min^{-1}$, as determined at 150 µM

TCTD concentration (Piatesi & Hilvert, 2004). This places the abzyme 1E9 among the most active catalytic antibodies selected against a TSA (Xu *et al.*, 1999).

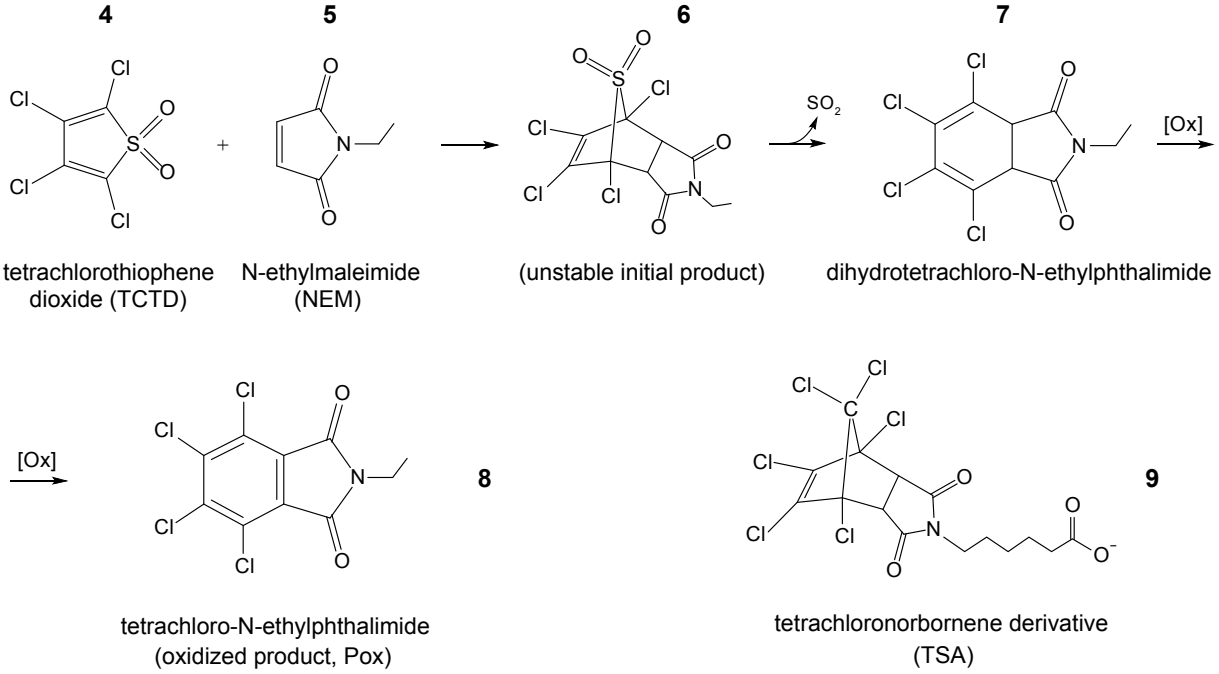

Figure 1.5. Diels-Alder cycloaddition between TCTD (**4**) and NEM (**5**). The high-energy intermediate **6** eliminates sulphur dioxide, forming the product dihydrotetrachloro-*N*-ethylphthalimide (**7**). This compound is quickly oxidized by air oxigen with formation of a phenylene ring, yielding the final product tetrachloro-*N*-ethylphthalimide (**8**). The hexachloronorbornene-based TSA **9** is shown on the right. The ethyl moiety at the succinimide nitrogen of the TSA was substituted by the caproyl moiety to provide a carboxylate group that allows regioselective conjugation for immunization and/or selection purposes.

Although one could expect such a Diels-Alderase antibody to function as an entropy trap, the temperature dependence of the catalyzed and the uncatalyzed reaction reveals that the nature of the rate enhancement by 1E9 derived entirely from a reduction of reaction enthalpy. Interestingly, the reaction entropy remained virtually the same, which might result from the restriction of the antibody flexibility upon ligand binding (Xu *et al.*, 1999). The crystal structure of 1E9 obtained by Xu *et al.* (1999) was used by Piatesi *et al.* (2003) for the structure-guided rational mutagenesis of the fab, which led an to increase in the k_{cat} by seven-fold to 25 min^{-1}. This improvement was achieved by substituting the position MetH100b at the bottom of the binding pocket against Phe, which occupies the same position in structurally related catalytic antibodies 39-A11 (selected against a bicyclo[2.2.2]octane derivative and catalyzing an unrelated Diels-Alder reaction; Braisted & Schultz, 1990; Romesberg *et al.*, 1998) and DB3 (a progesterone-binding antibody; Arevalo *et al.*, 1993), both derived from the same germ-line variable regions as 1E9 (Piatesi & Hilvert, 2004). The catalytic mechanism of 1E9 was also

investigated in a theoretical study, which showed that the transition state is bound in its *endo*-conformation. Summing up, the existing studies with 1E9 indicate that "*catalytic efficiency of antibody 1E9 is achieved by enthalpic stabilization of the transition state, near-perfect shape complementarity of the hydrophobic binding site for the transition state, and a strategically placed hydrogen-bonding interaction*" (Chen *et al.*, 2000).

1.2.5 Lipocalin-based TSA binders

The antibody scaffold was the first to host artificial enzymes based on molecular recognition of TSAs. However, a range of alternative protein scaffolds for affinity selection has been developed in the last three decades (Skerra, 2007). Many of them possess advantages over antibodies, such as higher stability, lower molecular mass and simplified production. As all these advantages are also desired for enzymatic applications, attempts to develop enzymes outside of the antibody scaffold have been made.

At the Chair of Biological Chemistry (TU Munich), the first experiments on the selection of artificial enzymes using non-antibody scaffolds were performed by Jan-Peter Mayer in his PhD thesis (Mayer, 2013). For these initial selection studies, the approach of *in vivo* complementation described in Chapter 1.2.3 was employed. Using custom-made combinatorial gene libraries based on two protein scaffolds – the bilin-binding protein (BBP) from *Pieris brassicae* and the bacterial lipocalin (Blc) from *E. coli* – catalytic activity was investigated by growing auxotrophic bacterial strains on minimal media with the addition of the precursor of a missing metabolite, e.g., proline, uracil or galactose. However, these experiments did not lead to the isolation of a catalytically active lipocalin.

The first attempts in this laboratory to select Anticalins[1] based on human lipocalin 2 (Gebauer & Skerra, 2012) against TSAs were made in 2011. In the course of his Master's thesis, Stephan Dickgießer performed a series of selection experiments with the aim of catalyzing the Diels-Alder cycloaddition between TCTD and NEM (Dickgießer, 2011). The selection was pursued using the same TSA (Figure 1.5, **9**) as employed for the generation of the catalytic antibody 1E9 (Hilvert & Hill, 1989), with the EZ-link biotin PEO-LC-amine derivative 'JG3-3' (Piatesi, 2003). A third-generation Lcn2-based combinatorial phagemid library (Gebauer *et al.*, 2013) comprising 2×10^{10} variants was first enriched via four rounds of phage display, followed by screening against this hapten via ELISA. As a result, an Anticalin designated C1G2 was isolated. Further three rounds of phage display in combination with ELISA screening allowed the isolation of a further variant, C3A5. Affinity towards the TSA **9** was studied for both lipocalin variants using fluorescence titration; C3A5 bound the TSA with single-digit nanomolar affinity,

[1] Anticalin® is a registered trademark of Pieris AG (Freising, Germany)

while the affinity of C1G2 lay in the single-digit micromolar range. The sequence of C1G2 was subsequently randomized using error-prone PCR, followed by another ELISA screening, leading to the isolation of E1G2 with 3-fold higher affinity. The three lead candidates C1G2, C3A5 and E1G2 were assayed for catalytic activity using spectrophotometry and HPLC analysis, but no differences could be observed compared with the negative controls. However, the analytical methods were not sufficiently sensitive to detect the uncatalyzed reaction, meaning that the possibility of a moderate rate enhancement was not excluded. Thus, the question whether the Anticalins previously selected against the TSA **9** exhibited catalytic activity remained open.

1.3 Objective of this work

This work consists of two projects, both involving the selection and design of binding proteins based on the human lipocalin 2 scaffold (Skerra, 2008).

The first project aimed at developing a lipocalin variant with high affinity towards the plant toxin colchicine to provide a potential antidote against acute colchicine intoxication. In the first step, a binding protein was selected from a combinatorial library using phage display and/or bacterial surface display approaches. The initial 'hit' ought to be improved for binding activity and biochemical stability to ensure efficacy in a clinical setting and simplify production upscaling and handling. Eventually, the optimized variant should be produced and purified in an amount sufficient for a pre-clinical study, its pharmacokinetics had to be fine-tuned and tested in an animal (rat) model. The selected lipocalin could also be employed as a biochemical reagent to quantify colchicine its crystallization was anticipated to obtain detailed structural information on the protein-ligand complex.

In the second project, the aim was to develop further lipocalin-based catalysts for the Diels-Alder cycloaddition between *N*-ethylmaleimide (NEM) and tetrachlorothiophene dioxide (TCTD). First of all, a fast and reliable analytical method should be established for measuring the reaction kinetics. This method had to be applied for the detection of potential catalytic activity in lipocalins that had been previously selected against a TSA. If present, the catalyzed reaction should be characterized biochemically, and the catalytic activity ought to be improved using methods of protein crystallography and rational design.

2. Materials and methods

2.1 Materials

2.1.1 Bacterial strains and bacteriophages

E. coli K12 strains:

JK321	Δ*ompT proC leu*-6 *trpE38 entA zih12::*Tn10 *dsbA::kan* (Jose *et al.*, 1996)
JM83	*ara* Δ*(lac-proAB) rpsL (= strA) φ80 lacZ*ΔM15 (Yanisch-Perron *et al.*, 1985)
KS272	F^- Δ*lacX74 galE galK thi rpsL* ΔphoA *(Pvu*II*)* (Strauch & Beckwith, 1988)
TG1-F^-	F^- *supE thi-1* Δ*(lac-proAB)* Δ*(mcrB-hsdSM)5 (r^K-m^K-)* (Gibson, 1984; Kim *et al.*, 2009)
W3110	F^- λ- IN*(rrnD-rrnE)1 rph-1* (Bachmann, 1972)
XL1-Blue	*recA1 endA1 gyrA9 (*Nal^R*) thi-1 hsdR17 glnV44 relA1 lac* F'[*$proAB^+$ $lacI^q$ lacZ*ΔM15 Tn10(Tet^R)] (Bullock *et al.*, 1987)

E. coli B strains:

BL21	F^- *fhuA2 [lon] [dcm] ompT hsdS*$_B$(r_B^- m_B^-) *gal* [*malB*$^+$]$_{K\text{-}12}$ (λ^S) (Studier & Moffatt, 1986)
Origami B	F^- *ompT hsd*S$_B$(r_B^- m_B^-) *gal dcm lacY1 ahpC gor522*::Tn*10 trxB* (Kan^R, Tet^R) (Novagen, EMD Biosciences, Darmstadt)

Bacteriophage:

VCS-M13	helper phage (Stratagene, Heidelberg)

All *E. coli* strains and bacteriophages were from the collection of Prof Dr. A. Skerra, Chair of Biological Chemistry, TU Munich.

2.1.2 Laboratory animals

Sprague-Dawley rats were provided by the Klinikum rechts der Isar, Munich.

2.1.3 Plasmids

pNGAL98	from the collection of Prof. Dr. A. Skerra (Gebauer & Skerra, 2012)
pNGAL108	from the collection of Prof. Dr. A. Skerra (Gebauer & Skerra, 2012)
pNGAL117	from the collection of Prof. Dr. A. Skerra, TU München
pNGAL124	from the collection of Prof. Dr. A. Skerra (Gebauer & Skerra, 2012)
pNGAL146	from the collection of Prof. Dr. A. Skerra (Gebauer & Skerra, 2012)
pASK-IBA4	IBA, Göttingen, Germany
pASK75-T7RBS-2	from the collection of Prof. Dr. A. Skerra, TU München

pXL2-PA#1.2(200)	XL-protein, Freising, Germany
pXL2-PA#1.2/1.3/1.2(600)	XL-protein, Freising, Germany

2.1.4 Oligodeoxynucleotides

All sequences are written left to right in the 5'- to 3'-direction. Small letters indicate mismatching or added nucleotide positions (shown not for all oligonucleotides).

Oligodeoxynucleotides for sequencing:

D20	CCACTCCCTATCAGTGAT
F83	AGACAGCTATCGCGATTGCA
PR1	CGTTTACCGCTACTGCG

Oligodeoxynucleotides for PCR and mutagenesis:

BstXI_3004-2_for	CAGGACAACCAATTCCATGGG
BstXI_3004-2_rev	GGAGGCCCAGAGATTTGG
IBA4_KasI_for	ctggtggcgccCAGGACTCCACCTCAGACCTG
IBA4_XhoI_rev	ctggtctcgagttaGCCGTCGATACACTGGTCG
IBA4_NdeI_for	CCGTAGCGcatatgGCTAGCTGGAGC
SUMO-del4-Lcn2_for	GAACAGATTGGTGGCTCAGACCTGATCCC
SUMO-del4-Lcn2_rev	GGGATCAGGTCTGAGCCACCAATCTGTTC
SUMO-del5-Lcn2_for	GAACAGATTGGTGGCGACCTGATCCCAGC
SUMO-del5-Lcn2_rev	GCTGGGATCAGGTCGCCACCAATCTGTTC

Oligodeoxynucleotides for site-directed mutagenesis of the colchicine-binding Anticalins:

D6.1_F83L_for	CATGATTGACACCTTAGTGCCGGGGAGC
D6.1_F83L_rev	GCTCCCCGGCACTAAGGTGTCAATCATG
D6.1_I55M_for	GGCAGCGACCATGTACGAGTTGAAAGAAG
D6.1_I55M_rev	CTTCTTTCAACTCGTACATGGTCGCTGCC
D6.1_I80T_for	GAAATGCCAATACATGACTGACACCTTTGTGC
D6.1_I80T_rev	GCACAAAGGTGTCAGTCATGTATTGGCATTTC
D6.1_L107F_for	CTACACATCATGGTTTGTCCGCGTCGTG
D6.1_L107F_rev	CACGACGCGGACAAACCATGATGTGTAG
D6.1_V69A_for	CATATAACGTCACCTTCGCGAAATTTCCTATGAAG
D6.1_V69A_rev	CTTCATAGGAAATTTCGCGAAGGTGACGTTATATG
D6.1_V69L_for	CATATAACGTCACCTTCCTGAAATTTCCTATGAAG

D6.1_V69L_rev	CTTCATAGGAAATTTCAGGAAGGTGACGTTATATG
D6.1_V69M_for	CATATAACGTCACCTTCATGAAATTTCCTATGAAG
D6.1_V69M_rev	CTTCATAGGAAATTTCATGAAGGTGACGTTATATG
MB101_F41Y_for	GTTGCCGGAAATGGATACCTGCGTGAGGATAAG
MB101_F41Y_rev	CTTATCCTCACGCAGGTATCCATTTCCGGCAAC
MB101_T54K_for	CAAAATGGCAGCGAAAATTTACGAGTTGAAAG
MB101_T54K_rev	CTTTCAACTCGTAAATTTTCGCTGCCATTTTG
MB101_T54Q_for	CAAAATGGCAGCGCAGATTTACGAGTTGAAAG
MB101_T54Q_rev	CTTTCAACTCGTAAATCTGCGCTGCCATTTTG
MB101_T136V_for	GAGGACTTTTTCATCGTGCTGTACGGGCGC
MB101_T136V_rev	GCGCCCGTACAGCACGATGAAAAAGTCCTC
MB101_V66I_for	GAAGATAAATCATATAACATCACCTTCATGAAATTTC
MB101_V66I_rev	GAAATTTCATGAAGGTGATGTTATATGATTTATCTTC

Oligodeoxynucleotides for site-directed mutagenesis of the catalytic Anticalins:

E1G2_Leu36Met_for	GGTATGTCGTGGGCaTGGCCGGAAATGG
E1G2_Leu36Met_rev	CCATTTCCGGCCAtGCCCACGACATACC
E1G2_Phe52Trp_for	CCGGCAAAAATGTggGCGACCATTTACG
E1G2_Phe52Trp_rev	CGTAAATGGTCGCccACATTTTTGCCGG
E1G2_Phe52Arg_for	CCGGCAAAAATGcgCGCGACCATTTACG
E1G2_Phe52Arg_rev	CGTAAATGGTCGCGcgCATTTTTGCCGG
E1G2_Arg68Trp_for	CATATAACGTCACCtGgGTGTGGTTTGGAAATAAG
E1G2_Arg68Trp_rev	CTTATTTCCAAACCACACcCaGGTGACGTTATATG
E1G2_T79Asn+W81Phe_for	GGAAATAAGAAATGCAATTACAaCATTTttACCTTTGTGCCGG
E1G2_T79Asn+W81Phe_rev	CCGGCACAAAGGTaaAAATGtTGTAATTGCATTTCTTATTTCC
E1G2_T79Phe+W81Asn_for	GGAAATAAGAAATGCAATTACttCATTaacACCTTTGTGCCGG
E1G2_T79Phe+W81Asn_rev	CCGGCACAAAGGTgttAATGaaGTAATTGCATTTCTTATTTCC
E1G2_Ile106Met_for	GGCCTGACATCAATgTTGGTCCGCGTCG
E1G2_Ile106Met_rev	CGACGCGGACCAAcATTGATGTCAGGCC
E1G2_Trp134Tyr_for	CCGCGAGCTGTTTTatATCACACTGTACG
E1G2_Trp134Tyr_rev	CGTACAGTGTGATatAAAACAGCTCGCGG

2.1.5 Antibodies and other protein reagents

Anti-A3C5 Fab	Chair of Biological Chemistry, TU Munich

Anti-polyHistidine–Peroxidase antibody clone HIS-1, produced in mice, prod. code A7058	Sigma-Aldrich, Steinheim
Alkaline phosphatase	MBI Fermentas, St. Leon-Rot
Bovine serum albumin (Fraction V, pH 7)	Applichem, Darmstadt
ExtrAvidin–alkaline phosphatase conjugate	Sigma-Aldrich, Steinheim
Lysozyme from egg white	Applichem, Darmstadt
Neutravidin-coated paramagnetic particles Sera-Mag SpeedBeads	GE Healthcare, Uppsala, Sweden
Ovalbumin	Sigma-Aldrich, Steinheim
PfuUltra II Fusion HS DNA polymerase	Agilent Genomics, Santa Clara, CA, USA
Restriction endonucleases, diverse	MBI Fermentas, St. Leon-Rot
RNase A (89 U/mg) from bovine pancreas	Sigma-Aldrich, Steinheim
StrepMAB-Immo (anti-Strep-tag II IgG, mouse)	IBA, Göttingen
Streptavidin, purity >98 % (SDS-PAGE)	Ina Theobald, Lab Prof. Dr. Skerra
Streptavidin-phycoerythrin conjugate	BD Biosciences, Heidelberg
Streptavidin-coated paramagnetic particles	Roche Diagnostics, Mannheim
Taq DNA polymerase	MBI Fermentas, St. Leon-Rot
T4 DANN ligase (1 or 5 U/µL)	MBI Fermentas, St. Leon-Rot
Proteins for the calibration of SEC:	
Carboanhydrase, from bovine erythrocytes	Sigma-Aldrich, Steinheim
Cytochrome C, from equine muscle	Sigma-Aldrich, Steinheim
Aprotinin, from bovine lung	Sigma-Aldrich, Steinheim

2.1.6 Chemicals

ABTS (tablets)	Sigma-Aldrich, Steinheim
ABTS buffer (powder)	Sigma-Aldrich, Steinheim
Acrylamide stock Rotiphorese NF-acrylamide (29 % (w/v) acrylamide and 1 % (w/v) bisacrylamide)	Carl Roth, Karlsruhe
Agarose GTQ Rotigarose	Carl Roth, Karlsruhe
Ammonium acetate	Sigma-Aldrich, Steinheim
Ammonium persulfate (APS) *BioChemica*	Applichem, Darmstadt
Ampicillin, sodium salt (Amp)	ForMedium, Hunstanton, UK
Anhydrotetracycline hydrochloride (aTc)	Acros Organics, Geel, Belgium

Antifoam Y-30-Emulsion	Sigma-Aldrich, Steinheim
Bacto Agar	Becton, Sparks, MD, USA
Bacto Tryptone	Becton, Sparks, MD, USA
Bacto Yeast Extract	Becton, Sparks, MD, USA
D-desthiobiotin	IBA, Göttingen
Dimethylaminoborane (DMAB)	Sigma-Aldrich, Steinheim
Dimethylformamide (DMF, for synthesis)	Merck, Darmstadt
dNTP-Set (dATP, dCTP, dGTP, dTTP)	MBI Fermentas, St. Leon-Rot
DY-634-*N*-hydroxysuccinimide ester	Dyomics, Jena
Ethanolamine/HCl, 1 M solution, pH 8.5	Biacore, Uppsala, Sweden
2'-(4-Hydroxyphenylazo)-benzoic acid (HABA)	Alfa Aesar, Karlsruhe
Kanamycin A monosulfate (Kan)	Sigma-Aldrich, Steinheim
p-Nitrophenylphosphate (pNPP)	Sigma-Aldrich, Steinheim
Paraformaldehyde	Sigma-Aldrich, Steinheim
Tetramethylethylenediamine (TEMED)	Carl Roth, Karlsruhe
Trifluoroacetic acid	Sigma-Aldrich, Steinheim
Thiaminhydrochloride (vitamin B_1)	Applichem, Darmstadt
tRNA from Saccharomyces cerevisiae	Roche, Karlsruhe

Other common chemicals were obtained in standard purity grades from Sigma-Aldrich (Steinheim), AppliChem (Darmstadt), Carl Roth (Karlsruhe) or Merck (Darmstadt).

2.1.7 Standards and kits

Recombinant DNA reagents:

GeneRuler 1kb-DNA ladder	MBI Fermentas, St. Leon-Rot
6x DNA Loading Dye	MBI Fermentas, St. Leon-Rot
Wizard SV Gel and PCR Clean-Up System	Promega, Madison, WI, USA
QIAprep Spin Plasmid Miniprep Kit	Qiagen, Hilden
QIAprep Plasmid Midiprep Kit	Qiagen, Hilden
QIAquick PCR Purification Kit	Qiagen, Hilden
QuikChange II Site Directed Mutagenesis Kit	Agilent Technologies, Böblingen
GeneMorph II Random Mutagenesis Kit	Agilent Technologies, Böblingen

Protein biochemistry:	
Pierce Unstained Protein MW Marker	Thermo Fischer Scientific, Ulm

2.1.8 Devices

Automated liquid handling workstation Microlab STAR Plus	Hamilton, Bonaduz, GR, Switzerland
Automated liquid handling workstation Freedom EVO 200	Tecan Group, Männedorf, Switzerland
CD-Spektropolarimeter Jasco J-810	Jasco, Gross-Umstadt
Cell sorter FACSAria II	BD Biosciences, Heidelberg
Centrifuges	
Sigma 4K15C with rotors 11156 and 11118	Sigma, Osterode
Sorvall RC 3B Plus with rotor H6000A/HBB6	Kendro Laboratory Products, Munich
Sorvall RC 5C Plus and RC 6 Plus with rotors SS-34, SLA-1500, SLA-3000, F10-4x1000	Thermo Fisher Scientific, Waltham, MA, USA
Electroporator MicroPulser 411 BR	Bio-Rad Laboratories, München
Fermenter	
10-liter fermenter system	Schütt Labortechnik, Göttingen
flow-through sensor and control module	BCC Spezialgeräte, Göttingen
pH sensor and control module	BCC Spezialgeräte, Göttingen
pO_2 sensor and control module	BCC Spezialgeräte, Göttingen
Tube pump module	BCC Spezialgeräte, Göttingen
pH electrode (type 465)	Ingold Meßtechnik, Steinbach
O_2 sensor (12/320 A-type)	Mettler-Toledo, Steinbach
Circulation thermostat DC30/K20	Thermo Haake, Karlsruhe
Fluorescence spectrophotometers	
FluoroMax-3	Jobin Yvon, Grasbrunn
LS50B	Perkin-Elmer, Langen
FPLC	
Äkta Explorer	GE Healthcare Europe, Freiburg
Äkta Prime	GE Healthcare Europe, Freiburg
Äkta Purifier	GE Healthcare Europe, Freiburg
French Press High-Pressure homogenizer	SLM Aminco, Urbana, IL, USA
Incubator Minitron, with humidity control	Infors HT, Bottmingen, Switzerland

Laboratory chromatography devices	
Flow-through photometer Uvicord 2138 S and SII (with 276 nm bandpass)	LKB Instruments, Gräfelding
Flow-through photometer UVis-920 (with 280 nm bandpass)	GE Healthcare Europe, Freiburg
Fraction collector Redi Frac	GE Healthcare Europe, Freiburg
Peristaltic pump P1	GE Healthcare Europe, Freiburg
Line recorder REC 112	GE Healthcare Europe, Freiburg
Line recorder SE 120	ABB Goerz, Wien, Austria
Mass spectrometer	
maXis ESI-QTOF	Bruker Daltonics, Bremen
Plate washer ELx405	BioTek Instruments, Bad Friedrichshall
Roll mixer Stuart SRT1	Bibby Scientific, Staffordshire, UK
Surface Plasmon Resonance (SPR) spectrometers	
Biacore 2000	Biacore, Uppsala, Sweden
Biacore X	Biacore, Uppsala, Sweden
Thermocyclers	
Mastercycler gradient	Eppendorf, Hamburg
TPersonal	Biometra, Göttingen
UV-Vis-Photometers	
NanoDrop 2000	PEQLAB Biotechnologie, Erlangen
UltraSpec 2000 und 2100 pro	Amersham Pharmacia Biotech, Freiburg
96-well plate photometer SpectraMax 250	Molecular Devices, Sunnyvale, CA, USA
96-well plate photometer Synergy 2	BioTek Instruments, Bad Friedrichshall
Vacuum concentrator RVC 2-18 CDplus	Martin Christ Gefriertrocknungsanlagen, Osterode am Harz
Water purification systems	
ELGA PURELAB Classic	VWS Deutschland, Celle
Bidestillierapparat 2304	Gesellschaft für Labortechnik, Burgwedel

Other devices that comprise standard equipment in a biotechnological/biochemical laboratory are not listed.

2.1.9 Other materials

Affinity chromatography (material and kits):	
Strep-Tactin Superflow	IBA, Göttingen
Chelating Sepharose Fast Flow	GE Healthcare Europe, Freiburg
Ni Sepharose High Performance	GE Healthcare Europe, Freiburg
Proteus NoEndoS Column kit	Generon, Slough, UK
Beads for calibration of the FACS device	
BD FACS Accudrop Beads	BD Biosciences, Heidelberg
SPHERO Rainbow Calibration Particles	BD Biosciences, Heidelberg
Cell Scraper, 39 cm	Sarstedt, Nümbrecht
CrystalClear sealing film	Hampton Research, Aliso Viejo, CA, USA
Dialysis tubes and membranes:	
Spectra/Por, MWCO 6-8 kDa	Carl Roth, Karlsruhe
Type 27, MWCO 12-16 kDa	Biomol, Hamburg
Electroporation cuvettes, 0.2 cm	Bio-Rad Laboratories, Munich
HPLC columns:	
Gemini 3 µm C18 110 Å, 75×4.6 mm	Phenomenex, Torrance, CA, USA
Purospher STAR RP8e, 250×3 mm	Merck, Darmstadt
Endosafe-PTS endotoxin test system with a Limulus Amebocyte Lysate (LAL) chip	Charles River Laboratories, Wilmington, MA, USA
Membranes for filter sandwich colony assay:	
PVDF membrane Durapore GVWP, 0.22 µm	Millipore, Eschborn
PVDF membrane Immobilon-P, 0.45 µm	Millipore, Eschborn
Size exclusion chromatography columns:	
PD-10	GE Healthcare Europe, Freiburg
Superdex 75 HR 10/30	Amersham Pharmacia Biotech, Freiburg
Superdex 75 10/300 GL	GE Healthcare Europe, Freiburg
Superdex 75 HiLoad 16/60 prep grade	Amersham Pharmacia Biotech, Freiburg
Superdex 200 HR 10/30	Amersham Pharmacia Biotech, Freiburg

Superdex 200 10/300 GL	GE Healthcare Europe, Freiburg
Superdex 200 HiLoad 16/60 prep grade	Amersham Pharmacia Biotech, Freiburg
Ion exchange chromatography columns:	
Resource S, 1 and 6 mL	Amersham Pharmacia Biotech, Freiburg
Resource Q, 1 and 6 mL	Amersham Pharmacia Biotech, Freiburg
Concentrators (centrifugal filters):	
Vivaspin 500, MWCO 10 kDa	Sartorius, Göttingen
Amicon Ultra-4, MWCO 10 kDa	Millipore, Eschborn
Amicon Ultra-15, MWCO 10 kDa	Millipore, Eschborn
Multi-well plates:	
Immuno Plate F96-Maxisorp	Nunc, Roskilde, Denmark
MicroWell 96-well PP plates U96 PP-0.5 ML	Nunc, Roskilde, Denmark
96-well PS microtiter plate, flat bottom	Sarstedt, Nümbrecht
CrystalQuick 96-well crystallization plates	Greiner Bio-One, Kremsmünster, Austria
CrysChem 24-well crystallization plates (sitting drop)	Hampton Research, Aliso Viejo, CA, USA
VDX 24-well crystallization plates (hanging drop)	Hampton Research, Aliso Viejo, CA, USA
Petri plates:	
square, 120×120×7 mm	Greiner Bio-One, Frickenhausen
round, 94×16 mm	Greiner Bio-One, Frickenhausen
Pipettes:	
Eppendorf Reference, 0.1–2.5 µL	Eppendorf AG, Hamburg
Eppendorf Research, 0.5–10 µL	Eppendorf AG, Hamburg
SPR sensor chip CM5	GE Healthcare, Uppsala, Sweden
Sterile filters:	
Ultrafree centrifugal filters (PVDF), 0.22 and 0.45 µm	Merck, Darmstadt
Filtropur S syringe filters, 0.2 und 0.45 µm	Sarstedt, Nümbrecht

2.1.10 Media, antibiotics and common solutions

All media and solutions for the work with bacteria, bacteriophage and DNA were sterilized either by autoclaving for 20 min at 121 °C or by sterile filtration (0.45 or 0.22 µm). Culture media were prepared from deionized water, other solutions were prepared from high-purity water type I (18.2 MΩ-cm), if not stated otherwise. Antibiotics was added to the solid media directly before filling the plates, after the medium had cooled down to appr. 50 °C; for the liquid media, antibiotics were added directly prior to use.

Antibiotic stock solutions:

The solutions were stored at -20 °C; aqueous solutions were sterile-filtered.

Ampicillin (Amp)	100 mg/mL in H_2O (1:1000 to the medium)
Kanamycin (Kan)	35 mg/mL in H_2O (1:500)
Inducer stock solution:	
Anhydrotetracyclin (aTc)	2 or 5 mg/mL in DMF (1:10000 to the medium)

LB-Medium:

Bacto tryptone	10 g/L
Bacto yeast extract	5 g/L
NaCl	5 g/L
Bacto agar	15 g/L
(only for culture plates)	

pH was set to 7.5 with NaOH and medium was autoclaved.

TB medium components:

TB buffer (10x):

KH_2PO_4	0.17 M
K_2HPO_4	0.72 M

TB medium:

Bacto tryptone	12 g/L
Bacto yeast extract	24 g/L
Glycerol	4 mL/L

The TB buffer was autoclaved separately and added to the autoclaved medium in a dilution of 1:10 after both components cooled down.

SOC medium:

Bacto tryptone	20 g/L
Bacto yeast extract	5 g/L

NaCl	10 mM
KCl	2.5 mM

The pH value was adjusted to 7.5 with NaOH; then the following components were added per 1 liter medium:

20 % (w/v) Glucose	20 mL
1 M $MgCl_2$	10 mL
1 M $MgSO_4$	10 mL

GYT medium:

Bacto tryptone	0.25 % (w/v)
Bacto yeast extract	0.125 % (w/v)
Glycerol	10 % (v/v)

Solutions for the fermentation:

Mineral salt solution:

$Na_2HPO_4 \cdot 2\ H_2O$	5.51 g/L (31 mM)
KH_2PO_4	2.58 g/L (19 mM)
NH_4Cl	1.33 g/L (25 mM)
Na_3 citrate $\cdot 2\ H_2O$	0.47 g/L (5 mM)

The mineral salt solution has a pH of 6.9 after autoclaving.

Glucose solutions:

20 % (w/v) glucose (autoclaved separately)

50 % (w/v) glucose (autoclaved separately)

$MgSO_4$ stock solution:

1 M $MgSO_4$ (autoclaved separately)

Thiamine stock solution:

10 mg/mL thiamine hydrochloride (sterile-filtered)

$FeCl_3$ stock solution:

35 g/L $FeCl_3 \cdot 6\ H_2O$ (sterile filtered)

Zn acetate stock solution:

8.0 g/L Zn acetate $\cdot 2\ H_2O$ (sterile filtered)

Trace elements stock solution (sterile filtered) :

$MnCl_2 \cdot 4\ H_2O$	3.0 g/L
$CuCl_2 \cdot 6\ H_2O$	0.3 g/L
H_3BO_3	0.6 g/L
$CoCl_2 \cdot 6\ H_2O$	0.5 g/L

$(NH_4)_6Mo_7O_{24} \cdot 4\ H_2O$	1.2 g/L
Na_2 EDTA• 2 H_2O	4 mM

Other solutions for the fermentation:

12.5 % (w/v) NH_3 for pH regulation

Buffers and solutions for SDS-PAGE (Fling & Gregerson, 1986)

1x SDS running buffer:

Tris	50 mM
glycine	190 mM
SDS	1 g/L

pH of this solution is 8.8.

4x lower Tris buffer (for the resolving gel):

Tris/HCl pH 8.85	3 M
SDS	4 g/L

4x upper Tris buffer (for the stacking gel)

Tris/HCl pH 6.8	0.5 M
SDS	4 g/L
Ammonium persulfate (APS)	10 % (w/v)
TEMED	100 % (liquid)

5x loading buffer:

Tris/HCl pH 8.0	250 mM
SDS	7.5 % (w/v)
glycerol	25 % (v/v)
bromophenol blue	0.25 mg/mL
2-mercaptoethanol	2.5 % (v/v) (only in the reducing buffer)

Staining solution:

acetic acid	10 % (v/v)
isopropanol	25 % (v/v)
Coomassie brilliant blue R-250	0.1 % (w/v)

Destaining solution:

acetic acid	10 % (v/v)

Buffers for ELISA:

ABTS buffer (see Chapter 2.1.6)

AP buffer:

Tris/HCl pH 8.8	100 mM
NaCl	100 mM
$MgCl_2$	5 mM

Buffers for phage display:

BBS-E:	
$B(OH)_3$	20 mM
NaCl	160 mM
EDTA	1 mM

Anti-phage solution:

NaOH	0.1 M
SDS	1 % (w/v)

Other buffers:

PBS:

KH_2PO_4	4 mM
Na_2HPO_4	15 mM
NaCl	115 mM

pH of this buffer is 7.4; in some cases, PBS was supplemented with 0.1 und 0.005 % (v/v) Tween 20 (designated PBS/$T_{0.1}$ or PBS/$T_{0.005}$).

Periplasmic extraction buffer (PPE buffer):

sucrose	500 mM
Tris/HCl pH 8.0	100 mM
Na_2 EDTA	1 mM

Buffer for streptavidin affinity chromatography (SA buffer):

Tris/HCl pH 8.0	100 mM
NaCl	50 mM
Na_2 EDTA	1 mM

IMAC running buffer:

Na-phosphate buffer pH 7.5	40 mM
NaCl	500 mM

TE buffer:

Tris/HCl pH 8.0	10 mM
Na_2 EDTA	1 mM

2.2 Methods of molecular biology

2.2.1 Cultivation and conservation of *E. coli* strains

To obtain single colonies from *E. coli* suspensions, bacteria were spread on culture plates with LB agar and incubated overnight at 37 °C. Selection on plasmids was achieved via addition of corresponding antibiotics to the culture medium. The culture plates were stored at 4 °C and were used for inoculation of liquid media for up to 4 weeks.

Liquid cultures in LB or TB medium were inoculated with a single bacterial colony or a liquid culture, which had been prepared beforehand. Culture tubes of 13 mL were used for 2 mL cultures; other cultures were cultivated in Erlenmeyer flasks filled to ~40 % of their nominal volume. Cultivation was performed at 30 or 37 °C and 180 rpm if not stated otherwise.

For the long-term conservation of strains transformed with plasmids, 0.5 mL of a stationary-phase culture was mixed with 75 % or 87 % (v/v) sterile glycerol to a final concentration of 15 %, shock-frozen in liquid nitrogen and stored at -80 °C.

2.2.2 Isolation of plasmid DNA from *E. coli*

For the preparation of double-stranded plasmid DNA in analytical scale (“miniprep”, 10–20 µg) or preparative scale (midiprep, ~100 µg) from *E. coli*, corresponding kits from Qiagen were used according to the instructions of the manufacturer. The isolated plasmid DNA was eluted with ddH_2O or TE buffer and stored at -20 °C.

2.2.3 DNA sequencing

In cases when nucleotide substitutions in the DNA were introduced (e.g., for site-directed mutagenesis or determination of the mutation rate after error-prone PCR), purified plasmids were sequenced using the “Mix2Seq” service from Eurofins Genomics (Ebersberg). Therefore, 15 µL of 50–100 ng/µL plasmid DNA was mixed with 2 µL of 100 µM sequencing primer (see Chapter 2.1.4), sealed in a tube obtained from the service provider and shipped.

2.2.4 Transformation of *E. coli* using the $CaCl_2$ method

If not stated otherwise, competent *E. coli* cells were prepared using the classical $CaCl_2$-method (Cohen *et al.*, 1972). 50 mL LB medium without antibiotics was inoculated with a stationary overnight culture of the respective *E. coli* strain in a dilution of 1:100 and incubated at 37 °C. When the culture had reached an OD_{550} of 0.5, the whole culture was centrifuged in a 50 mL PP tube (Sigma 4K10, 4200 ×*g*, 4 °C for 10 min), and the pellet was resuspended in 40 mL sterile ice-cold 100 mM $MgCl_2$. After a similar second centrifugation step, the pellet was resuspended in 20 mL sterile ice-cold 50 mM $CaCl_2$ and incubated on ice for 30 min. After the

third centrifugation step, the pellet was resuspended in 2 mL sterile ice-cold 50 mM $CaCl_2$ with 15 % (v/v) glycerol, aliquoted in 50–200 µL, shock-frozen in liquid nitrogen and stored at -80 °C or used directly for transformation.

Transformation was usually performed with 10–100 ng plasmid DNA or 5 µL ligation mixture added to 50–200 µL cell suspension. After the addition of plasmid DNA and mixing, cells were incubated on ice for 5–30 min. Then the sample was heated to 42 °C for 45 s, put on ice for 5 min, transferred into 1 mL LB medium and incubated at 37 °C for 40–60 min. For transformation with plasmids based on ampicillin resistance, the last incubation step was omitted, as ampicillin does not kill the cells, but only prevents their growth. Finally, the cells were spread on LB agar plates with the corresponding antibiotic and incubated overnight at 37 °C.

2.2.5 Transformation of *E. coli* by electroporation

For the preparation of competent cells for electroporation, the method based on the protocols from Tung & Chow (1995) and Sambrook & Russell (2001) was used. Furthermore, the data from (Chuang *et al.*, 1995; Szostková *et al.*, 1999; Wang *et al.*, 2007) were taken into consideration. All steps after the cultivation were performed in a cold room with solutions pre-cooled to 4 °C.

A single colony from a fresh LB agar plate (less than two weeks old) with the corresponding *E. coli* strain (XL1-blue or JK321) was used to inoculate a preculture in 50 mL LB medium. The preculture was incubated at 30 °C, 200 rpm overnight. On the next day, 2 L TB medium was inoculated with the whole preculture to OD_{550} = 0.02–0.03 and incubated at 30 °C, 180 rpm. When the OD reached 0.3–0.4, the flask was put into a bucket with ice and stirred gently with a sterile magnet for 10–15 min. Afterwards, the cells were washed: (1) centrifuged in two 1 L CF tubes for 10 min at 2700 ×*g*, each pellet resuspended in 500 mL ddH_2O; (2) centrifuged for 13 min at 2700 ×*g*, each pellet resuspended 500 mL ddH_2O; (3) centrifuged for 15 min at 3500 ×*g*, each pellet resuspended in 400 mL 10 % (v/v) glycerol and transferred into two 0.5 L CF tubes; (4) centrifuged for 15 min at 3500 ×*g*. The remaining fluid was removed and each pellet was resuspended in 150-200 µL GYT medium, resulting in ~1 mL cell suspension. The cells were frozen in liquid nitrogen and stored at -80 °C or used directly for electroporation.

DNA for transformation was depleted from salts by precipitation in ethanol (see Chapter 2.2.6) and/or dialysis against ddH_2O in micro dialysis units. For the transformation, 10-20 µL plasmid DNA or ligation mixture (max. 1-2 µg) were mixed with 100–200 µL competent cells, transferred into an ice-cold electroporation cuvette (d = 2 mm) and incubated for 1 min. Then the electroporator (BioRad MicroPulser) was set into the mode “EC2” and an electric pulse of

12.5 kV/cm was applied. Optimal pulse time comprised ≥5.0 ms for a 110 µL sample or ≥5.5 ms for a 55 µL sample. Instantly after the pulse, 1 mL SOC medium prewarmed to ~37 °C was added and the cells were transferred to a fresh 13 mL culture tube. The remaining cells were recovered from the cuvette with an additional 1 mL SOC medium. The electroporated cells were then subjected to a heat shock for 6 min at 46 °C. In a one-to-one comparison, application of the heat pulse (Wang *et al.*, 2007) increased transformation efficiency around 2-fold. Afterwards, the cells were incubated for 1 h t 37 °C, 200 rpm, plated onto square LB/Amp agar plates (120 mm) and incubated at 37 °C overnight, if not stated otherwise.

2.2.6 Precipitation of DNA with ethanol

For the purification of plasmid DNA or ligation mixtures from impurities (agarose, salts, etc.), the DNA was precipitated by addition of an equal volume of 5 M Na acetate, 1/40 volume 10 mg/mL tRNA from *S. cerevisiae* and 4 volumes of 96 % ethanol. After incubation for 1 h at room temperature, the mixture was centrifuged for 1 h at 15,800 ×*g*, 4 °C, and the pellet was rinsed with 70 % (v/v) ethanol. The tube was centrifuged again for 1 min, the remaining liquid was carefully removed, and the pellet was dried under vacuum for 10 min at 40 °C using the rotational vacuum drier. The dry DNA pellet was dissolved in ddH_2O or TE buffer and used for transformation of *E. coli* or other purposes.

2.2.7 Gel-electrophoresis and purification of DNA

Size-dependent separation of DNA fragments via agarose gel electrophoresis was used for analytical and preparative purposes (Sambrook & Russell, 2001). Depending on the size range of the DNA fragments to separate, gels with 0.7–1.5 % (w/v) agarose were prepared in TAE buffer. For the visualization of the DNA bands under UV light, 1 % (w/v) ethidium bromide was added at a dilution of 1/10,000. For the preparative separation of DNA fragments for library ligation, high-purity “genetic engineering quality” GTQ agarose (Carl Roth) was used. Before application, 6x loading buffer was added to the DNA samples. The electrophoresis was performed at a constant voltage of 75 V.

For the preparation of DNA fragments, the DNA bands visualized in UV light (λ = 312 nm) were cut out of the gel with a scalpel. To prevent UV-induced damage of the DNA, UV light intensity was lowered, and the UV exposure time was decreased to the lowest possible. In addition, for the preparation of DNA fragments for library ligations, 1 mM guanosine was added to the electrophoresis buffer, as it was shown to prevent UV-induced DNA damage (Gründemann & Schömig, 1996). DNA was extracted from the gel fragments using the Wizard SV Gel and PCR purification kit according to the instructions of the manufacturer. DNA concentrations were determined via UV light absorption at 260 nm using Nanodrop 2000 (mode “DNA”).

2.2.8 *In vitro* modification of DNA

2.2.8.1 Polymerase chain reaction (PCR)

For analytical purposes, PCR was performed with *Taq* DNA-polymerase according to the manufacturer´s recommendations. For the amplification of DNA for further cloning, the high-fidelity Pfu Ultra II Fusion HS DNA polymerase was used. 10–100 ng purified DNA was used as template. If needed, the primers included additional non-complementary nucleotides at their 5'-ends, introducing restriction sites into the PCR product. For the purification of DNA, the Qiagen PCR Purification Kit or Wizard SV Gel and PCR purification system was employed.

2.2.8.2 Site-directed mutagenesis via QuikChange PCR

For the site-directed introduction of nucleotide mutations, QuikChange II Site-Directed Mutagenesis Kit was used according to the instruction of the manufacturer. The method is based on the synthesis of a complete plasmid via PCR from a plasmid template prepared from a dam^+ *E. coli* strain (e.g., XL1-blue or JM83) with two complementary primers containing the desired substitution, insertion or deletion. The template DNA was destroyed after the PCR via addition of the endonuclease DpnI, which specifically cleaves the dam-methylated plasmid. The resulting PCR-synthesized plasmid contains two single-strand breaks, which are repaired *in vivo* after the transformation of bacterial cells.

2.2.8.3 Random mutagenesis via error-prone PCR

For the introduction of multiple single-nucleotide mutations into the Anticalin genes, the GeneMorph II Mutagenesis kit was employed. The kit contains a mixture of two error-prone DNA polymerases, which enables the synthesis of partially mutated DNA strands with minimal transition/transversion mutation bias. The oligonucleotides BstXI_for and BstXI_rev were used as primers (annealing temperature 57 °C), while DNA fragments obtained via standard PCR (with *Taq* or *Pfu* DNA polymerase) with primers F83 and PR1 were used as template. The error rate of the polymerase mixture was determined to be approximately 0.71 nucleotides per kilobase per duplication. Thus, to obtain the desired mutation rate of 4–5 nucleotides per gene, 60 pg of the template DNA fragment (amount calculated for the 379 bp Anticalin gene region between the two BstXI restriction sites, the "BstXI-cassette") were used for a 50 µL PCR sample and amplified in 30 PCR cycles. Each cycle comprised 30 s at 95 °C, 30 s at 57 °C and 1 min at 72 °C, with a final elongation step of 10 min at 72 °C. After the PCR, BstXI endonuclease was added directly to the PCR mixture together with the BstXI buffer and incubated for 2 h at 37 °C. Although the presence of PCR buffer components might be suboptimal for the cleavage reaction, BstXI turned out to possess sufficiently high activity for a complete site-specific DNA cleavage under these conditions, as judged by agarose gel

electrophoresis and further sequence analysis. The digested PCR fragment was purified via agarose gel electrophoresis and used for the ligation with the appropriate plasmid: pNGAL108 for phage display, pNGAL146 for bacterial surface display.

2.2.8.4 Cleavage of double-stranded DNA with restriction endonucleases

For the site-specific cleavage of DNA molecules, these were digested using type II restriction endonucleases according to the recommendations of the manufacturer (Thermo Scientific). For the digestion of high-complexity Anticalin libraries with the endonuclease BstXI, a higher amount of 5 units per µg DNA was employed, using a DNA concentration of 100 ng/µL. The digestion was performed for 1 h at 37 °C.

2.2.8.5 Ligation of DNA fragments

Ligation of DNA fragments (sticky- or blunt-end) was performed using T4 DNA ligase according to the instructions of the manufacturer. The reaction proceeded for 15 min at 20 °C for standard ligations. For the ligation of gene libraries for phage display or bacterial surface display (with the plasmids pNGAL108 or pNGAL146, respectively), a DNA concentration of 10 ng/µL, and highly concentrated T4 DNA ligase (5 U/µL) was used at a final concentration of 0.1 U/µL. The reaction was performed for 48–72 h at 16 °C. Prior to the transformation of *E. coli* by electroporation, the ligation mixture was purified by ethanol precipitation (see Chapter 2.2.6).

2.3 Directed evolution methods

2.3.1 Preparation of lipocalin random libraries

Two types of gene libraries were applied in this work: phagemid library for phage display selection and *E. coli* cell surface library for bacterial cell surface display via FACS. The random combinatorial library of the Lcn2 gene cassette was prepared using Slonomics technology (van den Brulle *et al.*, 2008). The design of the Anticalin library (i.e., choice of the randomized positions and triplet mutagenesis) was described in detail by Gebauer *et al.* (2009). Compared with the wild-type Lcn2 sequence (UniProt ID: P80188), the library contains two additional mutations, Gln38His and Cys87Ser. The former introduces one of the pair of BstXI restriction sites, and the latter eliminates an unpaired Cys residue, which would complicate protein production and cause dimerization. All randomized positions are located between the two BstXI restriction sites, enabling simple cloning on different generic plasmids for Anticalin selection and expression (Gebauer & Skerra, 2012).

The second-generation randomized libraries were prepared using error-prone PCR (see Chapter 2.2.8.3). The resulting gene libraries were used to transform competent *E. coli* XL1-blue (for phage display) or JK321 (for bacterial surface display) by electroporation.

2.3.2 Phage display

Phage display enables the genotype-phenotype link via phages or phagemids (a phage particle containing a plasmid instead of the complete phage genome, and thus incapable of replicating on its own) displaying the protein on their surface. In this work, phagemid display based on the M13 filamentous phage was used (Skerra, 2001). The phasmid vector pNGAL108 (Gebauer & Skerra, 2012) carries a lipocalin 2 gene fused to the full-length M13 capsid protein pIII. Binding of the displayed Anticalin to an immobilized target followed by washing, elution and re-amplification of the bound phage leads to enrichment ('panning') of the binding phage population. The cycle is repeated several times, until the best binding species are enriched to such an extent that they can be detected by high-throughput screening (e.g., ELISA or filter sandwich colony assay). Since bacteriophages impose a contamination risk in a microbiological laboratory, strict safety rules were followed during the work with the phage: the gloves were regularly changed, the tubes were opened and the liquids were pipetted accurately to prevent formation of aerosols. At the end of the day, all work surfaces were wiped with a 1 % SDS, 0.1 M NaOH solution, and all used flasks and tubes were decontaminated by autoclaving.

One phage display cycle was performed in the course of three days. On "Day 0", a single colony of *E. coli* XL1-blue was used to inoculate 4 mL 2xYT medium without antibiotics, which was incubated at 30 °C, 180 rpm overnight. On Day 1, three 100 mL conical flasks with 50 mL 2xYT medium prewarmed to 37 °C were inoculated with the preculture at different dilutions (1:500, 1:200 and 1:100) and incubated at 37 °C, 200 rpm (the dilutions were chosen so that the cultures reached OD_{550} ≈0.5 by the time when they needed to be infected with the phage). In the first panning cycle, the phagemid library – precipitated in BBS-E with benzamidine and Pefabloc (serine protease inhibitors) – was centrifuged at 14,000 rpm, 4 °C for 20 min in a table-top centrifuge. The supernatant was removed, the pellet was resuspended in 308 µL sterile, ice-cold PBS with 50 mM benzamidine, incubated on ice for 30 min and centrifuged again at 14,000 rpm, 4 °C for 5 min to remove insoluble matter (each following panning cycle was started at this point). The supernatant containing the phagemid library was recovered (two 3 µL samples were taken for titer determination) and kept on ice. An aliquot of freshly resuspended paramagnetic beads (coated with streptavidin or NeutrAvidin; 50–100 µL of 10 mg/mL beads) was put into a 2 mL Eppendorf tube and washed by adding 400 µL $PBS/T_{0.1}$ rotating the tube on an overhead rotator for 1 min, collecting the beads at the tube wall for 2 min using a neodymium magnet, and removing the supernatant. Then the beads were incubated in 1 mL $PBS/T_{0.1}$ with 2 % (w/v) BSA for ≥1 h on ice in order to block the potential interaction sites on the bead surface. The phagemids in the library were blocked accordingly by adding 100 µL $PBS/T_{0.4}$ with 8 % BSA to the library and incubating on ice for 1 h.

The blocked beads were collected with the magnet and resuspended in 400 µL of the biotinylated target solution (colchicine or TSA) in PBS/$T_{0.1}$ with 2 % (w/v) BSA. In the first selection rounds, 100 nM target was used, but the concentration was reduced down to 5 nM at later stages, when higher selection stringency was needed. Thereafter, the weakly bound phagemids were removed by 10 subsequent washing steps using 500 µL PBS/$T_{0.1}$ with 0.1 mM D-desthiobiotin (the latter was added as a competitor to prevent binding of phagemids to streptavidin via the *Strep*-tag I located between the Anticalin and the pIII capsid protein sequence). The bound phagemids were then eluted using one of two techniques: (1) *elution under denaturing conditions* was performed by adding 408 µL of 4 M urea in PBS and incubating at RT for 30 min on the overhead rotator; (2) *competitive elution* was achieved by incubating the beads with 408 µL of 100 µM non-biotinylated target in PBS (with up to 10 % (v/v) DMF) for 1.5 h under the same conditions. Two 4 µL samples were taken from the elution fraction for determination of the phagemid titer. For the reamplification of the bound phagemid population, the eluted phagemid suspension was prewarmed to 37 °C and mixed with 4 mL of exponentially growing *E. coli* XL1-blue. The infection of bacteria with the phagemids was allowed to proceed for 30 min at 37 °C without shaking, after which the cells were pelleted by centrifuging at 1500 ×*g*, 4 °C for 5 min, resuspended in 0.9 mL 2xYT medium and plated onto four big square LB agar plates with ampicillin. The plates were incubated for 14–16 h at 32 °C. The phagemid samples of the initial phagemid library, wash fractions 1, 5 and 10, as well as the elution fraction, were used for infecting the exponentially growing *E. coli* in a similar way. The infected cells were diluted with LB medium (dilution ratios were chosen to provide a countable number of colonies on the plate), plated onto LB/Amp agar plates, and incubated overnight under the same conditions.

On Day 2, the colonies for the titer determination were counted, and the relative phagemid titer was calculated. Then the bacteria that were quantitatively infected with the enriched phagemids (on the big agar plates) were recovered from the 120 mm LB/Amp agar plates by overlaying each plate with 10 mL LB/Amp medium, scraping the cells with a cell scraper and collecting them in a 100 mL conical flask. To maximize the yield, the first plate was additionally rinsed with 10 mL LB/Amp, which was used to recover the bacteria from the next plate. The dense cell suspension was collected in a 100 mL conical flask and incubated at 37 °C, 180 rpm. This suspension was used for the preparation of a glycerol stock: 5 mL cell suspension was pelleted by centrifuging for 10 min at 3000 ×*g*, resuspended in 1.6 mL LB and 0.4 mL 87 % (v/v) glycerol, shock-frozen in liquid nitrogen and stored at -80 °C. This stock served as a backup for each selection round. After 30 min, OD_{550} was measured in a dilution of 1:100, and the cell suspension was used to inoculate 50 mL 2xYT/Amp to OD_{550} ≈0.1 (in the first selection round, a volume of ~100 mL was used due to the higher initial library complexity).

The culture was incubated at 37 °C, 180 rpm until it reached an OD_{550} of 0.5; then 1.5×10^{11} cfu of the VCS-M13 helper phage were added (10 cfu per *E. coli* cell). After mixing manually, the cells were incubated at 37 °C without shaking to ensure efficient phage infection via the F-pili. Then kanamycin was added to a final concentration of 70 µg/mL (kanamycin ensures survival of only the cells infected with the helper phage). The cells were shaken for 10 min at 26 °C, 140 rpm, and expression of the Anticalin-pIII fusion protein was started by adding aTc to a concentration of 25 µg/L. The production of phage and phagemid particles proceeded at 26 °C, 140 rpm. After 7 h, the cells were pelleted by centrifuging at 12,100 ×*g*, 4 °C for 15 min. The supernatant was sterile-filtered (0.45 µm) and mixed with ¼ volume of fresh, ice-cold 20 % (w/v) PEG8000, 15 % (w/v) NaCl. The phagemids were precipitated in two SS-34 centrifuge tubes overnight at 4 °C on a tube roller.

On Day 3, the precipitated phagemids were pelleted by centrifuging at 18,000 ×*g*, 4 °C for 20 min. The supernatant was discarded, and the tubes were shortly centrifuged to remove the residual liquid. Each pellet was resuspended in 1 mL sterile cool BBS/E with 50 mM benzamidine, collected in a 2 mL Eppendorf tube and incubated on ice for 30 min. After an additional centrifugation at 14,000 rpm, 4 °C for 5 min (to remove the insoluble matter), the supernatant was aliquoted into two 1.5 mL Eppendorf tubes, and the concentrated phagemids were precipitated again by mixing each 1 mL aliquot with 250 µL ice-cold 20 % (w/v) PEG8000, 15 % (w/v) NaCl and incubating on ice for at least 30 min. After centrifuging for 20 min at 14,000 rpm, 4 °C, one tube was frozen and stored at -80 °C as a backup, while the second was used for the next steps. The supernatant was carefully aspirated, and the phagemid pellet was dissolved in 308 µL sterile, ice-cold PBS with 50 mM benzamidine. After incubating the phagemid solution for 30 min and centrifuging for 5 min at 14,000 rpm, the supernatant was transferred to a fresh tube and used for the following panning round (see Day 1).

The described procedure corresponds to the so-called "*on-bead*" panning, in which the target is first immobilized on the surface of paramagnetic beads and then presented to the phagemid library. This technique makes use of the avidity effect on the surface of the ligand-coated beads, enabling better capturing of weakly binding protein species at the early stages of selection. For the affinity maturation of existing Anticalin variants via phage display selection, another technique called '*in-solution*' panning was used. In this case, the library was first incubated with the (monomeric) target in solution, which was followed by the immobilization of the phagemid-ligand complexes on the paramagnetic beads. This technique allows better discrimination between variants with different affinities, thus favoring the enrichment of high-affinity binders.

2.3.3 Bacterial surface display via FACS

The method used in this work is based on the protocol developed previously (Binder *et al.*, 2010). Usually, each selection round was finished in one day. On the previous day, 50 mL LB was inoculated with a single colony of *E. coli* JK321 and incubated at 37 °C overnight to be used as a negative control. For the affinity maturation, a culture of *E. coli* JK321 displaying the initial Anticalin variant was prepared accordingly in LB/Amp to be used as a reference.

The cells transformed with the gene library (see Chapter 2.3.1) were recovered from the 120 mm LB/Amp agar plates by overlaying each plate with 10 mL LB/Amp medium, scraping the bacteria with a cell scraper and collecting them in a 100 mL conical flask. After scraping, the first plate was additionally rinsed with 10 mL LB/Amp, which was used to recover the bacteria from the next plate. The scraped cells were incubated at 37 °C for 30 min, and the OD_{550} was measured in a dilution of 1:50 or 1:100. The cell suspension was used to inoculate 50 mL prewarmed LB/Amp to an OD_{550} of 0.15, and the culture was incubated at 30 °C, 200 rpm. After the OD_{550} reached 0.5, protein expression was induced by adding aTc at a concentration of 10 ng/mL. After 2.5 h (OD_{550} =1.8–2.0), a 200 µL aliquot (corresponding to 2×10^8 cells) was taken and the cells were pelleted by centrifuging at 10,000 ×*g* for 3 min. The supernatant was discarded, the pellet was resuspended in 500 µL PBS with 0.5 % (w/v) BSA, and the bacteria were centrifuged again. The pellet was resuspended in 50–1500 µL biotinylated ligand mixed with 3 µM anti-A3C5 Fab-DY634 conjugate in PBS and incubated on ice for 1 h. The volume of the ligand solution was calculated to ensure molar excess of the ligand over the amount of Anticalin displayed on the cell surface, assuming 3000 protein molecules per bacterial cell (Binder *et al.*, 2010). After 1 h, the cells were pelleted and washed with PBS as described above. Then the washed cells were resuspended in 25–50 µL of 100 nM streptavidin-PE in PBS, and incubated on ice for 10 min, followed by one more washing step.

The washed cells were resuspended in 0.5–1.5 mL PBS, transferred to a precooled tube for FACS analysis and the cells were subjected to FACS using a FACSAria II cell sorter (BD Biosciences). The cells were sorted into a cooled 15 mL tube containing ~2 mL LB. After the sorting was completed, the positively sorted cells were pelleted by centrifuging at 5000 ×*g* for 10 min. Because of the small size of the cell pellet and its invisibility, only ~¾ of the supernatant was removed, the pellet was resuspended in the remaining medium and plated onto one 120 mm LB/Amp agar plate. The plate was incubated overnight at 37 °C, next morning the cells were scraped from the plate, collected in a 50 mL conical flask and prepared for the next sorting round as described above. For the affinity maturation of the variant D6.1, the anti-

A3C5 Fab-DY634 conjugate was added only after the competitive dissociation step, as a mixture with streptavidin-PE in PBS (same concentrations as above).

Before each sorting round, the time delay between the registration of the fluorescence signal from the cell by the FACS device and electrical charging of drop was calibrated using Accudrop fluorescent particles. The flow speed was chosen so that the Event Rate lay between 10,000 and 15,000 s^{-1}. The drop device amplitude was adjusted to 35±5 V at the beginning of the sorting and was maintained automatically using the “Sweet Spot” controlling function. Delay and area scaling factors for the fluorescence signal detection were adjusted using bead standards SPHERO Rainbow Calibration Particles (BD Biosciences) according to the instructions of the manufacturer. An overview of all FACS settings is presented in Table 2.1.

Table 2.1. Settings of the FACS device.

Photomultiplier voltages		Laser settings		Stream settings	
FSC	300	Blue laser delay	0.00	Amplitude	30–40 V
SSC	500	Blue laser scaling factor	3.4	Frequency	89 kHz
PE	700	Red laser delay	39.2	Drop 1	180 px.
DY634	800	Red laser scaling factor	2.1	Gap	5 ± 2 px.
FITC	700	Window extension	2.00		
		FSC Area scaling	1.6		

2.3.4 Single-clone analysis via FACS

After several rounds of FACS enrichment from a library, single clones were individually analyzed via FACS. In principle, the procedure was similar to the previous chapter, but instead of a library, single clones were cultivated in 96-well plate format, and only FACS analysis was performed without subsequent cell sorting. Single clones of transformed *E. coli* JK321 after the last round of FACS enrichment, as well as negative controls, were used to inoculate 150 µL LB/Amp in a round-bottom 96-well plate (Nunc MicroWell U96 PP-0.5 ML), which was sealed with an air-pervious foil, and the cells were incubated overnight at 37 °C, 280 rpm in a humidity-controlled incubator Minitron (Infors HT; humidity setting 70 %). On the next morning, 35 µL of these precultures were used to inoculate a deep 96-well plate (PP Masterblock 2 mL) filled with 1 mL LB/Amp per well, leading to an initial OD_{550} = 0.1–0.2. The plate was incubated at 30 °C, 200 rpm. After 2 h, gene expression was induced by adding 50 µL of 420 ng/µL aTc (diluted in LB/Amp medium from a stock solution in DMF; final aTc concentration in the bacterial culture 20 ng/mL) for 2.5 h. Then 50 µL of each culture were transferred into a round-bottom 96-well plate (Nunc MicroWell U96 PP-0.5 ML), and the cells were pelleted by

centrifuging at 4100 ×*g* for 10 min. Each pellet was resuspended in 100 µL of 4 nM biotinylated colchicine in PBS, incubated for 20 min on ice, centrifuged again as above, resuspended in 100 µL PBS, centrifuged again and finally resuspended in 50 µL of 20 nM streptavidin-PE and 740 nM anti-A3C5 Fab-DY634 conjugate in PBS. After 30 min, 150 µL PBS were added, the cells were centrifuged again, and each pellet was transferred into a precooled tube for FACS analysis and analyzed by FACS using the setting described in Chapter 2.3.3.

2.3.5 Library pre-enrichment via magnet-assisted cell sorting (MACS)

In order to reduce the initial complexity of the error-prone randomized library during affinity maturation of the Anticalin D6.1, it was pre-enriched using magnet-assisted cell sorting. The method is based on the selective immobilization of bacterial cells on the surface of paramagnetic beads coated with the ligand. First, the cells freshly transformed with the randomized library were scraped from the agar plates as described in Chapter 2.3.3 and used to inoculate 200 mL prewarmed LB/Amp medium to OD_{550} = 0.2, corresponding to 2.4×10^{10} cells, or 20 times the number of transformants. The cells were incubated at 30 °C, 200 rpm to an OD_{550} = 0.5, and gene expression was induced by addition of aTc to a concentration of 10 ng/mL. After 1.5 h (OD_{550} ≈ 1.2), 50 mL of the culture was centrifuged at 5000 ×*g* for 10 min and the pelleted bacteria were washed twice by resuspending in 10 mL PBS with 0.5 % (w/v) BSA and pelleted again. The washed cells were resuspended in 50 mL of 10 nM biotinylated colchicine in PBS with 0.5 % (w/v) BSA and incubated for 1 h on ice. Then the cells were pelleted and washed as described above. In parallel, 100 µL (1 mg) streptavidin-coated paramagnetic beads were washed three times in 500 µL PBS with 0.5 % (w/v) BSA and transferred into a 15 mL PP tube. The washed cells were resuspended in 10 mL PBS with 0.5 % (w/v) BSA and transferred into the tube with paramagnetic beads. The cells were incubated with the beads for 1 h at 4 °C on a tube roller, after which the beads with the bound cells were collected at the tube well for 10 min using a neodymium magnet, the supernatant was discarded, and the cells were washed twice with 5 mL PBS containing 0.5 % (w/v) BSA. The washed beads with the cells were resuspended in 1 mL LB medium and plated onto five 120 mm LB/Amp agar plates. The plates were incubated overnight at 37 °C and used for the FACS selection as above (see Chapter 2.3.3).

2.4 Production of recombinant proteins in *E. coli*

2.4.1 Shake flask cultivation

2.4.1.1 Periplasmic protein production

50 mL LB medium supplemented with the appropriate antibiotic were inoculated with a single colony of *E. coli* JM83 (for the production of Anticalins) or BL21 (for the production of wild-type

Lcn2) and incubated overnight at 30 °C, 180 rpm. On the next day, the complete stationary preculture was used for inoculation of 2 L of the same medium in a 5 L conical shake flask, which was incubated under the same conditions until OD_{550} reached 0.3. Then the incubation temperature was lowered to 22 °C, and at OD_{550} = 0.5–0.6 gene expression was induced by addition of aTc to a final concentration of 200 µg/L. After 2.5 h, the flasks were put on ice for 10 min, and the cells were pelleted by centrifugation in two 1 L CF beakers (15 min at 4,500 ×*g*, 4 °C). All further procedures were performed on ice or at 4 °C in a cold room. The supernatant was carefully removed, the pellets were resuspended in ice-cold PPE buffer (20 mL per flask) and gently mixed on a tube roller in 50 mL PP tubes for 30 min. The resulting spheroplasts were pelleted by centrifugation for 20 min at 4500 ×*g*, and the supernatant was further depleted from cell debris by a second centrifugation for 15 min at 27,000 ×*g*. The periplasmic extract was dialyzed overnight against ≥100 volumes of the corresponding chromatographic buffer (e.g., SA or IMAC buffer), filtered using a 0.45 µm syringe filter and subjected to purification.

2.4.1.2 Cytoplasmic protein production

Since Anticalins possess a structural disulfide bond in their three-dimensional structure, they cannot be expressed in the cytoplasm of the most bacterial strains due to its reducing redox potential. However, the specially designed *E. coli* strain Origami B carries mutations in the thioredoxin reductase (*trxB*) and glutathione reductase (*gor*) genes, leading to a shift of the redox balance in its cytoplasm to a more oxidizing side and thus making the formation of disulfide bonds possible (Rabhi-Essafi *et al.*, 2007).

For the cytoplasmic expression, 2 mL LB medium with antibiotic was inoculated with a single colony of *E. coli* Origami B carrying the desired expression vector and incubated at 37 °C for 6–10 h. In the evening, the preculture was used to inoculate 2 L LB or TB medium (with the corresponding antibiotic) in a dilution of 1:1000. The main culture was incubated overnight at 26 °C, 180 rpm, and in the morning, as soon as the OD_{550} reached at least 0.5, protein expression was started by addition of aTc to a final concentration of 200 µg/L. In the case of preparative-scale expression of PASylated proteins, TB medium was used for the main culture, and protein expression was started at OD_{550} >1. Protein expression was continued for 3 h (4 h in case of preparative-scale expression). Then the cells were pelleted by centrifugation at 4500 ×*g*, 15 min, 4 °C, frozen and stored at -20 °C till further use. The pellet was then thawed at 4 °C, resuspended in 20 mL chromatography buffer (or more, depending on the viscosity of the resulting cell suspension) and supplied with lysozyme to a final concentration of 200 µg/mL. After 30 min incubation at 4 °C, the cells were disrupted in a French press homogenizer (1100 psi, 3–5 cycles in total). The cell homogenate was centrifuged for 1 h at 18,000 ×*g*, and the

supernatant was filtered through a 0.45 µm syringe filter. The resulting total cell extract was used directly for the purification via column chromatography (usually IMAC).

2.4.2 High-density fermentation

The method for the periplasmic production of Anticalins in a bioreactor was based on a protocol developed by Schiweck & Skerra (1995). The *E. coli* strain W3110 or KS272 was cultivated in a 10 L bioreactor with mineral medium, glucose as a carbon source and ammonium as a nitrogen source. By controlling the temperature, pH value and oxygen partial pressure, homeostatic conditions were maintained during the whole fermentation cycle.

Fermentation was preceded by two precultures. The first preculture in 2 mL LB medium with antibiotic was inoculated with a single colony of the freshly transformed strain and incubated for 6–8 h at 37 °C, 200 rpm. It was used for the inoculation of the second preculture prepared from 360 mL mineral salt solution, 40 mL 20 % (w/v) glucose, 4 mL 1 M $MgSO_4$, 400 µL antibiotic stock solution and 400 µL thiamine stock solution. This medium was inoculated at a dilution of 1:1000 and incubated for 24–26 h at 30 °C, 200 rpm. The second preculture usually reached OD_{550} = 1.5–2.0. The bioreactor was filled with ~ 7 L mineral salt solution, sterilized by autoclaving, fixed on a magnetic stirring module, and the rotation speed was set to 470 rpm. Prior to inoculation, the bioreactor was equilibrated at 25 °C and supplemented with 800 mL 20 % (w/v) glucose, 80 mL 1 M $MgSO_4$, 8 mL antibiotic stock solution, 8 mL thiamin stock, each 4 mL $FeCl_3$ and Zn-acetate, 10 mL trace element solution and 1–2 mL Antifoam Y-30 emulsion. The bioreactor was also supplied with pressurized air, and the condition prior to inoculation was used to set the relative oxygen partial pressure to “100 %”. The pH value was kept at 7.0 via feedback-controlled titration with a 12.5 % (w/v) ammonium solution. Eventually, the bioreactor was inoculated with the entire second preculture (400 mL, dilution 1:20) and the fermentation proceeded for 12 h without supervision.

Table 2.2. Glucose feeding scheme during the fermentation runs.

OD_{550} [AU]	Glucose feed [mL/h]
7.5	28
12.5	40
18.5	60
22.5	80

On the next morning, the pure oxygen supply was opened, the oxygen level control turned on (at this fermentation stage, supply with pressurized air was insufficient to keep the relative oxygen partial pressure at >80 %), and an oxygen partial pressure of ≥30 % was maintained

using a combination of pressurized air and pure oxygen supply. Starting from this point, samples of the culture broth were taken every 30–60 min via an integrated metal tube probe connected to a 20 mL syringe, and the OD_{550} was measured in dilutions 1:20 to 1:50. Glucose was supplied depending on the culture OD_{550} according to the scheme in Table 2.2.

At OD_{550} = 13, additional 4 mL $FeCl_3$, 4 mL Zn-acetate and 10 mL trace salt solution were added. At OD_{550} = 20, gene expression was started via the addition of 800 µL aTc stock solution (5 mg/mL) to a final concentration of 0.5 mg/L and continued for 2.5 h. After 2.5 h (usually the culture reached OD_{550} = 30–40), the whole bioreactor was cooled down to 1–4 °C using a water bath partly filled with ice, then disassembled, and the cells were pelleted by centrifugation at 4500 ×*g*, 4 °C for 20 min. The pellets were resuspended in a volume of PPE buffer calculated according to the formula

$V\ [mL] = OD_{550} \times \text{culture volume [L]} \times 2$

First, the pellets were manually squeezed with a small volume of buffer, followed by stirring on a magnetic stirrer at ~180 rpm, 4 °C for 20 min. Prior to stirring, 20 mL of 500 mM EDTA pH 8.0 stock solution and 200 mg lysozyme dissolved in 5 mL water were added (final concentrations 15 mM and 0.25 mg/mL, respectively). The spheroplasts were pelleted by a centrifugation at 21,500 ×*g*, 4 °C for 20 min, and the supernatant was centrifuged again at the same conditions for 40 min to remove the cell debris. The resulting periplasmic extract was dialyzed three times against 5 L chromatography buffer (SAC or IMAC) at 4 °C for at least 12 h each. The dialyzed extract was filtered through 0.45 µm sterile syringe filters (sometimes preceded by filtration through paper filters, “black-” or “red ribbon”) and supplied with 1 nmol wild-type streptavidin per liter culture medium and OD_{550} unit (1 nmol/L×OD_{550}) to “mask” BCCP and remaining free biotin in case a subsequent SA chromatography was planned. Then the extract was either used directly for purification, or shock-frozen in liquid N_2 and stored at -20 °C till further use.

2.5 Protein biochemistry and chromatographic methods

2.5.1 Protein chromatography

2.5.1.1 Strep-Tactin affinity (SA-) chromatography

For the purification of recombinant proteins carrying a *Strep*-tag II affinity tag, the SA chromatography was used, which enabled one-step purification from periplasmic extracts to ≥95 % purity (Schmidt & Skerra, 2007). All chromatography steps were performed at 4 °C; the column was connected to a peristaltic pump upstream, and to a flowthrough UV-photometer (λ = 280 nm) downstream. The UV signal was recorded using a line recorder. The SAC column was equilibrated with 10 volumes of SA buffer and the periplasmic extract, previously dialyzed

against SA buffer and sterile-filtered (0.45 µm), was applied. The column volume was chosen assuming that 1 mL Strep-Tactin resin binds 0.5 mg recombinant protein with a *Strep*-tag II. The column was then washed with SA buffer until the UV signal reached a baseline, and competitive protein elution was started by the application of 2.5 mM D-desthiobiotin in SA buffer. After the eluted protein was collected, the column was regenerated with 5 mM HABA in SA buffer. HABA competitively elutes D-desthiobiotin from Strep-Tactin, which is evidenced by the dark-red coloring of the resin. HABA was eluted with 10 mM Tris (pH 10.5). Finally, the regenerated column was equilibrated with SA buffer and used for the next purification cycle.

2.5.1.2 Immobilized metal ion affinity chromatography (IMAC)

IMAC allows efficient affinity purification of recombinant proteins carrying an oligohistidine (usually His_6 or His_{10}) tag and is based on the complexation of immobilized transition metal ions (e.g., Zn or Ni) by the imidazole side chains of histidine (Skerra *et al.*, 1991b). Compared with SAC, it delivers lower purity but enables purification of a much higher (>10-fold) amount of protein per resin volume. For the most applications, 5 mL Ni Sepharose High Performance (HisTrap HP, based on NTA) columns were used, which are operated using an Äkta Prime or Äkta Purifier chromatography system.

First, the column was rinsed with deionized water and loaded with one volume of 100 mM $NiSO_4$. After rinsing with water until the baseline of A_{280} was reached, the column was equilibrated with 5–10 volumes IMAC buffer, and the bacterial extract (periplasmic or cytoplasmic) dialyzed against IMAC buffer, or a pre-purified protein solution, was loaded at a flow rate of ~2 mL/min. The column was then washed with IMAC buffer until the baseline was reached, end elution with a linear concentration gradient of 0 to 250 mM imidazole in IMAC buffer was applied in 15–20 column volumes. The eluate was collected in fractions, to which 0.5 M EDTA (pH 8.0) was added at a concentration of 1 mM. This step served to prevent metal-induced precipitation of the protein during dialysis, when imidazole is removed and the remaining metal ions that leak from the column may cause aggregation of histidine-rich (or His-tagged) proteins. The fractions were analyzed via SDS-PAGE, the desired fractions were pooled and used for further purification.

For the purification of PASylated Anticalins in the course of animal experiments, a Ni-NTA Sepharose column with a bed volume of 60 mL was used. The flow rates and buffer volumes were adapted accordingly.

2.5.1.3 Ion exchange chromatography (IEX)

For the fine purification of proteins previously purified from cell extracts via affinity chromatography, ion exchange chromatography was used. It enables separation of proteins

based on their specific surface charge. Therefore, Resource S (strong sulfonate-based cation exchanger) or Resource Q (strong quaternary ammonium-based anion exchanger) columns with bed volumes of 6 mL were used, operated using Äkta Purifier or Äkta Explorer FPLC systems. The running buffers were chosen individually for every protein, but in most cases 20 mM MES/NaOH, pH 5.5–6.5 or 20 mM HEPES/NaOH, pH 7.0 was used for CEX, and 20 mM CHES/NaOH, pH 9.0–9.5 was used for AEX. In some cases, the running buffer was supplied with 10–20 mM NaCl to prevent protein aggregation. The protein solution was dialyzed against the running buffer and loaded onto the column at a flow rate of 1–2 mL/min, and the column was washed with the same buffer until the baseline was reached. Elution was performed with a linear concentration gradient of 0 to 500 mM NaCl (in the running buffer) applied in 10–20 column volumes. The columns were regenerated with 2 M NaCl and 0.5 M NaOH according to the recommendations of the manufacturer.

2.5.1.4 Size exclusion chromatography (SEC)

Preparative size exclusion chromatography was used for the fine purification of the proteins from aggregates, oligomers and/or small-molecule impurities or for changing the buffer. Analytical SEC was used for the characterization of the aggregate/oligomer/monomer ratio of the purified protein in a given buffer. Depending on the application, column resins of two types were used: Superdex S75 for the efficient separation of proteins below 50 kDa and Superdex S200 for proteins with higher molecular mass. Columns with a bed volume of ~24 mL (dimensions 10×300 mm, operated at 0.5 mL/min) were used for preparative as well as for the analytical purposes, while 121 mL columns (16×600 mm, operated at 1 mL/min) were used for preparative purposes. Prior to the purification by SEC, the proteins were concentrated using Amicon centrifugal filters with an MWCO of 10 kDa. For the purification, 250 µL (10×300 mm columns) or up to 1 mL (16×600 mm columns) of the concentrated protein solution was loaded onto the column. Then, the eluate was fractionated, the fractions corresponding to the monomeric peak were pooled and used for further analysis or application.

For the determination of the apparent molecular mass, a mixture of the following proteins was used: BSA (66 kDa), carbonic anhydrase (29 kDa), cytochrome C (12.4 kDa) and aprotinin (6.5 kDa). A calibration curve was created by linear regression (logarithms of the obtained molecular masses *vs* elution volume) and used for the interpolation of the apparent molecular mass of the protein of interest.

2.5.2 SDS polyacrylamide gel electrophoresis (SDS-PAGE)

The apparent molecular masses and purity of the recombinant proteins was routinely determined via discontinuous SDS polyacrylamide gel electrophoresis (Laemmli, 1970) using

the buffer system of Fling & Gregerson (1986). The gel consisted of a stacking gel with 7 % (w/v) polyacrylamide and a resolving gel with 15 % (w/v) polyacrylamide and dimensions of 55×85×0.75 mm (see Table 2.3; for the buffer composition, see Chapter 2.1.10). For efficient separation of PASylated proteins, resolving gels with 10 % (w/v) or 12 % (w/v) polyacrylamide were prepared.

Table 2.3. Composition of the SDS-PAGE gels.

Component	Stacking gel	Resolving gel (15/12/10 %)
30 % acrylamide with 0.8 % bis-acrylamide	0.4 mL	3/2.4/2 mL
Upper Tris buffer	0.6 mL	–
Lower Tris buffer	–	1.5 mL
APS	25 µL	45 µL
TEMED	2.5 µL	3 µL
H_2O	1.4 mL	1.5/2.1/2.5 mL
Total	2.428 mL	6.048 mL

For the gel preparation, the acrylamide stock solution, Tris buffer and water were mixed, and the polymerization was started by the addition of APS (donor of free radicals) and TEMED (catalyst). First the resolving gel was prepared, transferred into the assembled glass gel chamber, overlaid with 1 mL water (prevention of contact with air oxygen) and allowed to polymerize for 10–15 min. The water was carefully removed, then the stacking gel was prepared and sealed with the well comb. The gels could be stored at 4 °C in a humid environment for up to 3 days.

For the SDS-PAGE analysis, 10–15 µL of the protein sample (usually 5–10 µg protein) was mixed with 5x SDS loading buffer, heated to 95 °C for 5 min (not for the non-reducing SDS-PAGE) and loaded into the gel wells. The protein marker (5 µL) was also loaded. The electrophoresis was performed at 120 V for 2 h. Afterwards, the gel plates were disassembled, the gel was placed in the staining solution in a large petri dish and incubated for 15 min with gentle shaking. The excessive dye was removed in the unstaining solution for 1–16 h. For faster and more complete unstaining, a piece of absorbing paper was put into the petri dish. Finally, the gel was photographed on on a white light source and used for documentation.

2.5.3 Protein methylation

To prevent chemical reaction of surface-exposed Lys residues with amine-reactive chemicals, or to improve the formation of crystal contacts between protein molecules, some proteins were

methylated using dimethylaminoborane (DMAB) and formaldehyde (Walter *et al.*, 2006). Therefore, 1 mL protein in ≥50 mM amine-free buffer (e.g., HEPES/NaOH) pH 6–8 was mixed with 1/50 volume of 58 mg/mL DMAB and 1/25 volume of 3 % (w/v) formaldehyde. Both solutions were freshly prepared (<4 h), and the mixing was be performed as fast as possible. The mixture was incubated on ice for 45–75 min, after which this step was repeated. After additional 45–75 min, the protein was separated from the reactants using a PD-10 column or SEC. This protocol resulted in double methylation of every Lys residue. Mass spectrometric analysis was performed to confirm the degree of methylation (a mass difference of 28 per Lys residue was expected, excluding the methylation of the N-terminus, which also occurs).

2.5.4 Quantification of colchicine via HPLC

Colchicine was extracted from the rat plasma samples with dichloromethane. Therefore, a 10 µL plasma sample was mixed with 10 µ of 100 mM Tris-HCl pH 8.5 and overlaid with 400 µL CH_2Cl_2. The mixture was vortexed for 15 min, centrifuged at 5000 rpm for 10 min, and the floating protein-containing pellet was removed with a pipette tip. Then, the and CH_2Cl_2 phase was evaporated in a vacuum evaporator for 10 min at 40 °C. The extract was dissolved in 50 µL PBS (the tube was vortexed, and the tube walls were thoroughly rinsed with PBS), centrifuged at 14,000 rpm for 1 min to remove insoluble matter, and 30 µL of the supernatant was analyzed via HPLC with a Gemini C18 column (Phenomenex, part no. 00C-4439-E0, dimensions 150x4.6 mm, particle size 3 µm). The HPLC analysis was performed under the following conditions: flow rate 0.7 mL/min, buffer A = 0.1 % (w/v) TFA in H_2O, buffer B = 100 % acetonitrile, gradient: 30–60 % buffer B in 7.5 min. For the calibration, a standard solution of colchicine in PBS was prepared, the peak area per mole applied colchicine (elution time 6.2 min) was determined and used for the quantification purposes.

2.5.5 Measurement of the Diels-Alder reaction via HPLC

For the quantification of the Diels-Alder reaction, the reaction mixture was separated and analyzed using HPLC on a reversed-phase column. In the initial experiments, a Purospher STAR RP8e column (Merck, part no. 1.50273, dimensions 250x3 mm, particle size 5 µm) was used. After testing other columns, the best separation efficiency was reached with the Gemini C18 column (Phenomenex, part no. 00C-4439-E0, see above). The runs were performed using ddH_2O with 0.1 % (w/v) TFA as buffer A and 100 % acetonitrile as buffer B with the settings listed in Table 2.4. During the analysis, the vials were kept in the autosampler thermostatted to 25 °C. Formation of the oxidized product (cf. Figure 1.5, **8**) was monitored at 238 nm (absorption peak of P_{ox}) with a bandwidth of 16 nm with a reference channel at 400 nm, bandwidth 50 nm. To increase the throughput, overlapping injection of the next sample was started after 4 min for each run; the total run time comprised 4.79 min.

Table 2.4. HPLC settings for the kinetic analysis of the Diels-Alder reaction.

Setting	Value
Injection volume	10 µL
Injection speed	100 µL/min
Equilibration time	2 s
Flow rate	1.00 mL/min
Column temperature	25 °C
Gradient	0 min – 80 %B 2.5 min – 85 %B 3 min – 80 %B
Run time	4.79 min
Time between injections	5.00 min

2.6 Immunological methods

2.6.1 Sandwich ELISA for the high-throughput screening of an Anticalin sublibrary

For screening of Anticalin libraries enriched via phage display, a sandwich ELISA optimized for high-throughput was employed. Several steps were performed using the automated liquid handling workstation Microlab Star Plus (Hamilton). First, the central gene cassette between the two BstXI restriction sites was subcloned onto the plasmid pNGAL98 (Gebauer & Skerra, 2012) allowing periplasmic expression of the Anticalins. The subcloned library was used to transform *E. coli* TG1-F^- cells, which were plated onto plane rectangular plates (Nunc no. 140156) filled with 25 mL LB/Amp agar medium to a density of 100–200 colonies per plate to allow the robotized isolation of single colonies. The plates were always prepared freshly to prevent formation of satellite colonies; in some cases, a 50 % higher concentration of Amp was used for this purpose. On Day 1, the colonies were picked by the robot and used to inoculate a round-bottom 96-well plate (Nunc MicroWell U96 PP-0.5 ML) filled with 150 µL LB/Amp liquid medium per well. The plate was incubated overnight at 25 °C, 300 rpm in a Multitron shaker (rotation amplitude 5 cm). On Day 2, a 96-deep-well plate (PP Masterblock 2 mL) was filled with 1 mL TB/Amp medium per well and inoculated with 5 µL of the preculture. The deep-well plate was incubated for 1.5–2 h at 37 °C, 300 rpm, humidity 70 %, and then at 20 °C (humidity control disabled) to OD_{550} = 0.3–0.5. Protein expression was induced by adding 50 µL of 4.2 µg/mL aTc dissolved in TB/Amp, and the plate was incubated for 13–17 h. In the evening, an ELISA microtiter plate (Nunc MaxiSorp) was filled with 50 µL 10 µg/mL *Strep*MAB-Immo in PBS per well, sealed and incubated at 4 °C overnight. On Day 3, 340 µL BBS with 1 mg/mL lysozyme was added in each well and the plate was incubated for 1 h at 750 rpm, 4 °C. Then 340 µL PBS/$T_{0.1}$ with 10 % (w/v) BSA was added, followed by 1 h

incubation under the same conditions. The resulting spheroplasts were pelleted by centrifuging for 10 min at 3100 ×*g*, 4 °C, and the supernatant (crude periplasmic extract) was used further. At the same time, the ELISA microtiter plate coated with *Strep*MAB-Immo was washed 5 times with 300 µL PBS/$T_{0.1}$ using an ELISA plate washer (ELx405, BioTek Instruments), and 200 µL of 3 % (w/v) BSA in PBS/$T_{0.1}$ per well was added. After 1 h incubation at RT, the plate was washed again as described above, and 200 µL of the crude periplasmic extract from the deep-well plate were added to each well. The plate was incubated for 1.5 h at 500 rpm, RT. In parallel, 0.5 µM biotinylated ligand (colchicine or TSA) was pre-incubated with 0.125 µM ExtrAvidin-AP conjugate in PBS for 1 h at RT. The ELISA plate was washed again, and 50 µL of the ligand/ExtrAvidin-AP complex was added, followed by incubation for 1 h at 500 rpm, RT. Finally, the ELISA plate was washed again, with an additional washing step performed using 150 µL AP buffer. Then 100 µL of 0.5 mg/mL 4-NPP in AP buffer was added, and the change in absorbance at 405 nm was monitored for 30 min using a 96-well-format photometer (Synergy 2, BioTek Instruments). Clones corresponding to the highest signals were recovered from the pre-culture plate and analyzed further.

2.6.2 Filter sandwich colony screening assay

The filter sandwich colony screening assay (Skerra *et al.*, 1991a; Schlehuber *et al.*, 2000) served the same purpose as the ELISA high-throughput screening (see Chapter 2.6.1), while providing higher throughput and diminishing the clone-to-clone variation due to differences in the bacterial growth rate. For the assay, the Anticalin library enriched via phage display was subcloned onto pNGAL124 (Gebauer & Skerra, 2012), enabling expression of the Anticalins as fusion proteins with the albumin binding domain of *streptococcal* protein G. First, two sets of petri dishes were prepared: one half with LB/Amp and one with LB/Amp and 0.2 µg/mL aTc (inducer plates). The plates were freshly prepared (<2 days) and stored at 4 °C. In addition, two sets of PVDF membranes were cut in circles to the size of the Petri plates: the hydrophilic GVWP (pore size 0.22 µm, Millipore) and the hydrophobic Immobilon-P (pore size 0.45 µm, Millipore). On Day 1, *E. coli* TG1-F^- was transformed with the sublibrary subcloned on pNGAL124 and plated onto the LB/Amp agar plate covered with the hydrophilic membrane. The number of cells was calculated in order to achieve 500–1000 colonies per plate. The plate was incubated for 7–9 h at 37 °C until the colonies reached a diameter of ~0.5 mm. In the meantime, the hydrophobic membrane was activated by sinking subsequently into methanol, ddH_2O and PBS, each for 5 min. The activated membrane was placed in 10 mL 10 mg/mL HSA in PBS and incubated for 4 h, followed by blocking in 10 mL 3 % (w/v) BSA in PBS/$T_{0.5}$. The blocked membrane was washed twice in 20 mL PBS and sunk into 10 mL of LB/Amp with 0.2 µg/mL aTc. The plate was placed onto the inducer LB/Amp plate avoiding formation of air bubbles under the membrane.

As soon as the colonies had reached the desired size, the hydrophilic membrane was transferred onto the hydrophobic membrane on the inducer plate, both membranes were marked at several spots with a needle, and the plate with the membrane sandwich was incubated overnight at 22 °C. On Day 2, the upper, hydrophilic membrane with the colonies was transferred onto a fresh LB/Amp agar plate and stored at 4 °C. The hydrophobic membrane was also removed from the plate and washed three times in 20 mL PBS/$T_{0.5}$ for 10 min under gentle agitation. The washed membrane was incubated in 10 mL of a solution containing 200 nM biotinylated colchicine and 50 nM ExtrAvidin-AP conjugate in PBS for 1 h. The membrane was washed twice in 20 mL PBS/$T_{0.5}$, twice in 20 mL PBS and once in 20 mL AP buffer. The bound ligand/ExtrAvidin-AP complex was detected by incubating the membrane in 10 mL of 75 µg/mL BCIP, 19 µg/mL NBT in AP-buffer. The formation of the blue tetrazolium dye was allowed to proceed to an optimal signal-to-background ratio (usually 10–30 min); if the signal was too low, the staining solution was changed, and staining was repeated. The stained hydrophobic membrane was dried, the colonies with the strongest signal were identified, and the corresponding colonies were picked from the hydrophilic membrane stored on the LB/Amp plate at 4 °C. Thereby, the needle marks on both membranes were used to identify the correct coordinates of the desired colonies. These colonies were subjected to secondary tests using corresponding positive and negative controls.

2.6.3 Capture ELISA for the quantification of the Colchicalin in rat plasma

For the quantification of the Colchicalin in rat plasma, a capture ELISA was used, which utilized the high binding affinity of the Colchicalin D6.2 towards both colchicine and its biotinylated analog (see Figure 3.1). Prior to the test day, wells of an ELISA microtiter plate (Nunc MaxiSorp) were filled with 50 µL of 5 µg/mL NeutrAvidin in PBS, sealed and incubated at 4 °C overnight. On the test day, the ELISA plate was washed 5 times with 300 µL PBS/$T_{0.1}$ using an ELISA plate washer ELx405 (BioTek Instruments) and filled with 200 µL 3 % (w/v) BSA in PBS/$T_{0.1}$ per well. After 1 h incubation at RT and washing, 50 µL of 1 µM biotinylated colchicine was added and the plate was incubated in a Minitron incubator for 30 min at 600 rpm, RT. In the meantime, a series of 1:2 dilutions (100 µL + 100 µL) of the plasma samples and of the calibration standard was prepared in PBS/$T_{0.1}$ in a separate round-bottom 96-well plate (Nunc U96 PP-0.5 ML). The microtiter plate was washed as described above, filled with 100 µL of the diluted plasma and calibration samples from the round-bottom plate, and incubated for 2 h at 500 rpm, RT. After another washing step, 50 µL of anti-polyhistidine antibody/HRP conjugate (Sigma-Aldrich, prod. code A7058; diluted 1:2000 in PBS/$T_{0.1}$) was added, and the plate was incubated for 1 h at 500 rpm, RT. Finally, the plate was washed again 5 times with PBS/$T_{0.1}$ and once with PBS, the wells were emptied, and filled with 100 µL of 1 mg/mL ABTS

in ABTS buffer. The change in absorbance at 405 nm was monitored for 30 min using a 96-well-format photometer (Synergy 2, BioTek Instruments).

2.6.4 Competitive ELISA for quantification of colchicine

The competitive ELISA for the quantification of colchicine in biological fluids was developed in the course of this work and employed the high affinity of the selected Anticalins towards colchicine. Some of the steps were optimized while the assay was established; the optimization is described in Chapter 3.4.1. The described method corresponds to the optimized protocol.

Prior to the test day, wells of an ELISA microtiter plate (Nunc MaxiSorp) were filled with 50 µL of 5 µg/mL Colchicalin D6.2 in PBS, sealed and incubated overnight at 4 °C. On the test day, the ELISA plate was washed 5 times with 300 µL PBS/$T_{0.1}$ using an ELISA plate washer (ELx405, BioTek Instruments) and filled with 200 µL 3 % (w/v) BSA in PBS/$T_{0.1}$. In parallel, a series of 1:2 dilutions (100 µL + 100 µL) of the sample in PBS, as well as the calibration standard, was prepared in a separate round-bottom 96-well plate (Nunc U96 PP-0.5 ML) and mixed with an equal volume of 20 nM tracer (biotinylated colchicine) in PBS (or in 2 % human serum in PBS for the experiment shown in Figure 3.33D; final tracer concentration was 10 nM). The microtiter plate coated with the Colchicalin was washed again, and the samples with the tracer (200 µL) were transferred from the round-bottom plate to the ELISA plate. The plate was incubated for 1 h at 500 rpm, RT in a Minitron incubator, washed as described above, and filed with 100 µL ExtrAvidin-AP conjugate in PBS (diluted 1:5000 from a 3.7 mg/mL stock solution). After 1 h, the plate was washed again and filled with 100 µL of 0.5 mg/mL 4-NPP in AP buffer. The change in absorbance at 405 nm was monitored for 30 min using a 96-well-format photometer (Synergy 2, BioTek Instruments). The calibration curve was fitted to the equation $A_{405} = A_{max} + (A_{min} - A_{max})/(1 + ([colchicine] / EC_{50})^{slope})$, which was used for the quantification of the colchicine samples.

2.6.5 Detection and removal of endotoxin

The bacterial lipopolysaccharide (endotoxin) content of the protein samples prepared for the animal experiments was tested using the Endosafe-PTS test system with a Limulus Amebocyte Lysate (LAL) chip (Charles River Laboratories). This system is based on the hydrolysis of a chromogenic peptide substrate by a proteolytic enzyme the becomes activated in a cascade triggered by the endotoxin or by (1,3)-*β*-D-glucan (Iwanaga, 2007). For the test, 3 µL SEC-purified protein was diluted 1:50 with ddH_2O, heated for 5 min at 95 °C, incubated for 1 min at RT and then loaded onto the chip (4 channels, 25 µL per channel). The protein was considered sufficiently endotoxin-free if the measured endotoxin concentration was <10 EU/mL. For the specific removal of endotoxin from the protein preparations prior to the

animal experiments, subtractive affinity chromatography using Proteus NoEndoS Column Kit (Generon) was used according to the manufacturer's instructions.

2.7 Biophysical methods

2.7.1 Measurement of protein concentration

Concentrations of purified protein solutions were determined by measuring the absorbance at 280 nm using the micro-scale photometer Nanodrop 2000 (Thermo Scientific). The concentration was calculated according to the Lambert-Beer law. Extinction coefficients of the individual proteins were estimated according to the content of the amino acids that contribute to the absorption at 280 nm (tryptophan, tyrosine, cysteine) using Geneious software (Biomatters, Auckland, New Zealand). Protein-free buffer was used as a reference; if needed, the protein was diluted with the appropriate buffer.

2.7.2 Fluorescence titration

For the determination of equilibrium dissociation constants in solution, the method of fluorescent titration was used. The method is based on the change of the intrinsic fluorescence of tryptophan and/or tyrosine side chains (emission wavelength 345 nm) located in the proximity of the ligand binding site upon binding of the ligand. Several components may contribute to the change of fluorescence: first, fluorescence depends on the polarity of the environment, which may change upon binding of a hydrophobic or a hydrophilic ligand in comparison with the aqueous solvent; second, the ligand may directly absorb the light emitted by Trp/Tyr, thus lowering the apparent fluorescence; third, the ligand itself might possess fluorescent properties and interfere with the protein fluorescence.

For the assay, 2 mL of a purified Anticalin solution in PBS (usually 1 µM) was filled into a 4 mL quartz cuvette (S = 1 cm^2) and placed into the cuvette holder of the fluorescence photometer (Perkin Elmer LS50B) thermostatted to 25 °C. Stirring of the solution was achieved via a small magnet placed onto the cuvette bottom. The measurement was performed with the following settings: excitation wavelength 280 nm (slit 5.0 nm), emission wavelength 345 nm (slit 6.0 nm for the 1 µM protein solutions or 16.0 nm for the ≤100 nM protein solutions), integration time 15 s. After equilibrating the cuvette temperature for at least 10 min, the ligand stock solution (colchicine or TSA; usually 400 µM in DMF for the 1 µM protein solutions, 40 µM in PBS/10 % (v/v) DMF for the 100 nM protein solutions, and 8 µM in PBS/0.8 % (v/v) DMF for the 20 nM protein solutions) was added to the cuvette in 0.25–2 µL aliquots using a high-precision pipette (Eppendorf Reference). The binding equilibrium was allowed for 45 s (1.5 min for the 20 nM protein solutions) and the fluorescence signal was recorded. The pipetting scheme was chosen such that the highest density of data point was achieved near the region

of equimolarity; the titration was finished at a 3-fold ligand concentration compared with the protein. Fluorescence of the pure buffer was subtracted from each value after the measurement.

The obtained fluorescence values were corrected for the inner filter effect (see below), and the resulting corrected values were plotted against the ligand concentration. The data were fitted to an equation derived from the Law of Mass Action (Vopel, 2016):

$$K_D = \frac{([P]_t - [P \cdot L])([L]_t - [P \cdot L])}{[P \cdot L]} \tag{1}$$

by applying the relation of the measured fluorescence to the concentrations of the individual components (protein, ligand and protein-ligand complex) under the assumption that they contribute to the total fluorescence additively. Combining the mathematical solutions of the Law of Mass Action for the individual components

$$[P \cdot L] = \frac{([P]_t + [L]_t + K_D)}{2} - \sqrt{\frac{([P]_t + [L]_t + K_D)^2}{4} - [P]_t[L]_t} \tag{2}$$

$$[P] = \frac{([P]_t - [L]_t - K_D)}{2} - \sqrt{\frac{([P]_t + [L]_t + K_D)^2}{4} - [P]_t[L]_t} \tag{3}$$

while the definition for the total fluorescence

$$F = f_P[P] + f_L[L] + f_{PL}[P \cdot L] \tag{4}$$

and assuming no intrinsic ligand fluorescence under the test conditions leads to the equation

$$F = ([P]_t - [L]_t - K_D)\frac{f_P}{2} + ([L]_t + [P]_t + K_D)\frac{f_{PL}}{2} + (f_P - f_{PL})\sqrt{\frac{([P]_t + [L]_t + K_D)^2}{4} - [P]_t[L]_t} \tag{5}$$

where F is the measured fluorescence intensity, $[P]_t$ is the total protein concentration, $[L]_t$ is the total ligand concentration, f_P is the molar intrinsic fluorescence coefficient of the protein, f_{PL} is the fluorescence coefficient of the protein-ligand complex, and K_D is the equilibrium dissociation constant. Fitting was performed via non-linear regression using OriginPro 2015G. $[L]_t$ was set as independent variable, F as dependent variable, and the parameters f_P, f_{PL}, $[P]_t$ and K_D were obtained from the non-linear regression.

The described model assumes that the ligand lacks intrinsic fluorescence (which was the case for both ligands used in this work) and influences the fluorescence signal only when bound to

the protein. However, these assumptions are not met if the free ligand absorbs either the excitation light from the photometer or the light emitted by the protein or the protein/ligand complex. This was especially important for the ligand colchicine as it possesses a strong absorption peak at 346 nm, which is close to the measured Trp/Tyr emission wavelength. Hence, prior to the plotting, the original fluorescence data were corrected with respect to the so-called inner filter effect.

Correction of the inner filter effect aimed at separating the fluorescence changes caused by the ligand binding to the protein from all other interactions. The most appropriate control experiment for doing this would be creating a system consisting of the same counterparts but lacking the ligand binding. As an approximate solution, the protein was substituted by *N*-acetyl-L-tryptophanamide (NATA). NATA possesses spectral properties similar to the protein, thus mimicking the spectral interaction of the protein with the free ligand without complex formation. For the control experiment, a 5 µM solution of NATA in PBS was titrated with the same ligand solution, and the change of absorbance was recorded. If the ligand absorbs the excitation light from the photometer, the measured Trp/Tyr fluorescence becomes lower than without the ligand. The same happens if the ligand absorbs the fluorescence light emitted by the protein. The apparent fluorescence F_{app} depends on the intrinsic protein fluorescence f_P, the protein concentration $[P]$ and the intensity of the excitation light I_{ex}:

$$F_{app} = f_P \cdot [P] \cdot I_{ex} \tag{6}$$

According to the Lambert-Beer law, the following relation applies to the absorption of the excitation light by the (non-interacting) ligand:

$$log\frac{I_{ex}^0}{I_{ex}} = \varepsilon_L \cdot [L] \cdot d \tag{7}$$

where ε_L is the molar extinction coefficient of the ligand, $[L]$ is the ligand concentration and d is the path length. If NATA is titrated instead of the protein, the extinction coefficient corresponds only to the light absorbed by the free ligand. The following half-logarithmic plot of the fluorescence intensity versus the ligand concentration in the presence of a fixed NATA concentration yields a line with a slope equal to the apparent extinction coefficient ε_{app} (Vopel, 2016):

$$logF_{app} = logF - \varepsilon_{app} \cdot [L] \tag{8}$$

This coefficient ε_{app} can then be used to correct the I_{ex} and, hence, F_{app} in (6):

$$F = F_{app} \cdot 10^{\varepsilon_{app} \cdot [L]} \tag{9}$$

The corrected fluorescence values were then used for the curve fitting according to eq. (5).

2.7.3 Surface plasmon resonance (SPR) spectroscopy

Real-time binding kinetics of the Anticalins selected against colchicine was studied via surface plasmon resonance spectroscopy on a Biacore 2000 or Biacore X SPR spectrometer with a CM5 sensor chip. For this assay, a special derivative of colchicine was synthesized that carries a free amino group at the end of a hexaethylene glycol linker (Figure 2.1). The derivative was synthesized by Dr. Martin Dauner (Chair of Biological Chemistry, TU Munich).

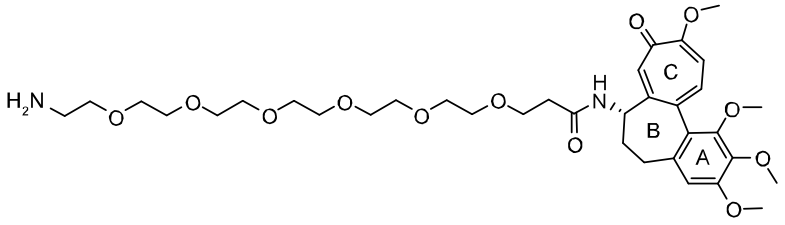

Figure 2.1. Colchicine derivative with a free amino group on a PEG_5 linker.

All buffers for the SPR measurement were degassed under ultrasound for at least 1 h. The colchicine derivative was immobilized on the surface of the sensor chip according to the manufacturer's instructions by activating the carboxyl groups by injecting 35 µL of a fresh solution containing 25 mM NHS and 50 mM EDC at a flow rate of 5 µL/min. Afterwards, 5 µL of 10 µM colchicine derivative were applied, followed by blocking of the unreacted activated carboxyl groups by injecting 35 µL of 100 % ethanolamine. A reference measurement channel was prepared using the same steps, but omitting the injection of the colchicine derivative. This protocol resulted in a signal intensity of 70–150 ΔRU upon saturation with the Anticalin.

The binding analysis was performed at 25 °C at a flow rate of 25 µL/min. First, the device was equilibrated with PBS-$T_{0.005}$ until a stable baseline was reached. Then 100 µL of the Anticalin in PBS-$T_{0.005}$ was injected (association phase of 4 min), the flow was changed to the running buffer, and the sensorgram was recorded for at least 100 min (dissociation phase). After regenerating the chip by injecting 5 µL of 0.5 % (w/v) SDS twice and reaching a stable baseline again, the next run with a different Anticalin concentration was started. Usually, a 1:2 dilution series of the Anticalin from 128 nM to 1 nM was analyzed in multi-cycle kinetics mode. The obtained signals represent the difference between the measurement channel and the reference channel. Furthermore, each curve was corrected using the curve from a blank measurement in which running buffer was injected instead of the analyte. The resulting curves were fitted according to a 1:1 Langmuir binding model $dAB/dt = k_{on} \times A \times B - k_{off} \times AB$ (where A and B are the binding partners, AB is the complex, k_{on} and k_{off} are the association and the dissociation rate constants, respectively) using BIAevaluation software (Karlsson *et al.*, 1991).

2.7.4 Circular dichroism (CD) spectroscopy

Purified protein was diluted to 10 µM with CD buffer (20 mM KH_2PO_4, 50 mM K_2SO_4, pH 7.5) and dialyzed against 1000 volumes of CD buffer. Prior to the measurement the protein was diluted with CD-buffer to 2 µM. The measurement was performed in a 500 µL cuvette with a path length of 1 mm on a Jasco J-810 spectropolarimeter. The protein was heated from 20 °C to 95 °C with a temperature gradient of 1 K/min and the CD signal at 222 nm was recorded (bandwidth 1 nm, data pitch 0.1 °C, response time 4 s). The measured ellipticity values were plotted against the temperature and the resulting curve was fitted to the equation assuming a two-state model of protein unfolding

$$\Psi = \frac{(m_N \mathrm{T} + b_N) + (m_U \mathrm{T} + b_U)\left\{\exp\left[\frac{\Delta H_m}{R}\left(\frac{1}{T_m} - \frac{1}{T}\right)\right]\right\}}{1 + \exp\left[\frac{\Delta H_m}{R}\left(\frac{1}{T_m} - \frac{1}{T}\right)\right]} \qquad (10)$$

where Ψ is the ellipticity at 222 nm, T_m is the melting temperature (temperature corresponding to the state when the half of the protein molecules is unfolded), R is the universal gas constant and ΔH_m (in J/mol) is the enthalpy of unfolding at T_m (Schlehuber, 2001). The terms $m_N \mathrm{T} + b_N$ and $m_U \mathrm{T} + b_U$ correspond to the signal slopes of curve before and after the transition. The fitting was performed using the Spectra Manager Suite software (Jasco, Tokyo, Japan).

The resulting fitted curves were normalized with regard to the fraction of unfolded protein at each temperature point using the equation

$$f(u) = \frac{\exp\left[\frac{\Delta H_m}{R}\left(\frac{1}{T_m} - \frac{1}{T}\right)\right]}{1 + \exp\left[\frac{\Delta H_m}{R}\left(\frac{1}{T_m} - \frac{1}{T}\right)\right]} \qquad (11)$$

with the help of Microsoft Excel (Microsoft, Redmond, WA, USA).

2.7.5 Mass spectrometry (MS)

To determine the exact molecular masses of the Anticalins, ESI-TOF mass spectrometry was used. Therefore, purified protein solution (usually 100 µL of 10 µM protein) was dialyzed against a 1000-fold volume of 10 mM ammonium acetate (pH 6.6). Prior to the measurement, the protein was mixed with an equal volume of 100 % methanol, followed by addition of 0.5–1 % (v/v) formic acid. The measurement was performed on a maXis ESI-TOF mass spectrometer with the friendly support of Andreas Reichert (Chair of Biological Chemistry, TU Munich). The raw data were processed and deconvoluted with Compass v1.3 (Bruker Daltonics) using the MaxEnt (Ferrige *et al.*, 1991) and MaxEntX algorithms.

2.8 Protein crystallization

2.8.1 Precipitant screens

To identify protein crystallization conditions, an in-house set of 480 screening conditions, the so-called *Vector Screen* (Chair of Biological Chemistry, TU Munich; see Appendix, Table 8.3) was applied. This screen was designed to minimize the redundancy and optimized according to the BDP – a databank of crystallization conditions for X-ray structures deposited in the Protein Data Bank (PDB; www.wwpdb.org) (Peat *et al.*, 2005). The screen consisted of five 96-well plates, whereby the first plate contained conditions with the highest success rate in the BDP. The crystallization screens were performed using the vapor diffusion technique with sitting drops in CrystalQuick 96-well plates. The screens were pipetted using a Tecan Freedom EVO automated liquid handler, each drop consisting of 250 nL precipitant buffer and 250 nL protein-ligand complex solution. The drop was equilibrated against 100 µL of the precipitant buffer. The plates were sealed using a CrystalClear sealing film and incubated at 20 °C or 4 °C. The formation of crystals was controlled under a microscope each week for the first four weeks and then once in 1–2 months. The protein concentration for the screens was chosen so that, if possible, approximately one third of the drops contained protein precipitate.

2.8.2 Refinement screens

The crystallization conditions identified in the Vector Screens (see Chapter 2.8.1) were taken as a starting point for systematic refinement. Usually, the concentration of the main precipitant and the pH value were varied first; if necessary, other parameters were also varied, such as protein concentration, drop volume, incubation temperature and influence of additives. The refinement screens were performed using the handing drop technique in VDX 24-well plates, whereby the drop usually consisted of 1 µL ddH_2O, 0.7 µL precipitant buffer and 0.7 µL protein-ligand complex and was equilibrated against 1 mL precipitant buffer. For the ‘hanging drop’ technique, the drops were mixed on a glass cover slip; this was placed upside down onto the reservoir of the 24-well VDX plate, whose fringe had been greased with a viscous mixture of vaseline and light mineral oil. For the ‘sitting drop’ technique, the drops were mixed in the ‘isle’ well of a specially designed 24-well plate CrysChem and sealed with a sticky foil. The formation of crystals was controlled under a microscope every 1–2 days. The best-looking protein crystals were harvested, soaked into a cryoprotecting solution (precipitant buffer supplied with 30 % (v/v) glycerol) and frozen in liquid nitrogen.

2.8.3 Collection of the X-ray diffraction pattern, data processing and building of the 3D model

The X-ray diffraction data set was collected by Dr. Andreas Eichinger (Chair of Biological Chemistry, TU Munich) at 100 K at the BESSY (Berliner Elektronenspeicherring-Gesellschaft

für Synchrotronstrahlung, Berlin, Germany) beamline 14.3 at the wavelength 0.89429 Å (for the Colchicalin D6.2/M69Q) or 14.2 at the wavelength 0.91840 Å (for the Catacalin C3A5).

The X-ray data were processed with the friendly support of Dr. Andreas Eichinger (Chair of Biological Chemistry, TU Munich) using MOSFLM and SCALA (CCP4, 1994). Molecular replacement was performed using the structure of an Anticalin selected against Y-DTPA (PDB code 3DTQ; Kim *et al.*, 2009) using Phaser (CCP4, 1994). The 3D model was built and adjusted with Coot (Emsley & Cowtan, 2004). ARP/wARP (Lamzin *et al.*, 2012) was used to add the water molecules, NQ-Flipper (Weichenberger & Sippl, 2007) was used to adjust rotamers of Asn and Gln side chains and Refmac5 (CCP4, 1994) was used to refine the protein model. The model was additionally corrected using the PDB_REDO server (Joosten *et al.*, 2014). The final model was validated using PROVE (Pontius *et al.*, 1996), ERRAT (Colovos & Yeates, 1993), Verify3D (Luthy *et al.*, 1992), PROCHECK (Laskowski *et al.*, 1993), WHAT_CHECK (Hooft *et al.*, 1996) and MolProbity (Chen *et al.*, 2010). DSSP (Kabsch & Sander, 1983) was used to assign the elements of secondary structure; PISA (Krissinel & Henrick, 2007) was used to analyze the crystal contact sites.

The graphics were prepared using the UCSF Chimera software (Resource for Biocomputing, Visualization, and Informatics at the University of California, San Francisco, CA, USA; Pettersen *et al.*, 2004) and the molecular surfaces were calculated using the MSMS package (Sanner *et al.*, 1996). Structure alignments were performed at the 58 conserved Cα atoms of the residues 28-37, 52-58, 63-69, 77-84, 91-94, 106-113, 118-124, 133-139 (Skerra, 2000). RMSD for the superimposed structures was calculated using the MatchMaker module of UCSF Chimera.

2.9 Animal experiments

Experiments with rats were performed by Dr. Nicole Jung and Dr. Jochen Stenzel (Abteilung für Klinische Toxikologie, TUM, Univ.-Prof. Dr. Eyer) in a specially equipped laboratory. The application for animal experiments was submitted to the authorities of Upper Bavaria by Prof. Dr. Florian Eyer on 17th March 2015 and approved in January 2016 (AZ 55.2-1-54-2532-43-2015). Healthy adult male Sprague-Dawley rats aged at least three months and weighing 300–600 g were purchased from Charles River (Sulzfeld, Germany). They were housed in temperature-controlled cages with a 12 h light/dark cycle and fed with standard laboratory diet. Acclimatization was allowed for two weeks before an experiment started.

For the determination of colchicine pharmacokinetics, the rats were anesthetized under monitoring of ECG, body temperature (37 +/- 0.5 °C) and pulsoxymetry. The anesthesia was initiated with intramuscular injection of Midazolam 2 mg/kg, Medetomidin 150 µg/kg and

Fentanyl 5 µg/kg. After that, one-third of the starting dose was injected approximately every 30 min, depending on the deepness of the narcosis. Then a tracheotomy was performed, and the rat was intubated tracheally using a 17 G plastic tube, which was connected to an artificial ventilation device. Ventilation parameters were adjusted according to arterial blood gas analysis. Stable body temperature was maintained using a heating mattress placed on the operation table, and loss of liquid was compensated by subcutaneous injection of Ringer solution after two hours. After the cannulation of the right *Vena jugularis* and *Arteria carotis interna*, a blood pressure monitor was connected, and the first 200 µL blood sample was collected from the *A. carotis interna*. Afterwards, the urinary bladder was cannulized and collection of urine was started.

To ensure exact dosing, each animal was weighed directly before the experiment. Colchicine dissolved in PBS (~1 mL) was injected into the *V. jugularis* via the cannula, and blood samples were collected from the *A. carotis interna* at pre-defined time points. The blood sample volume varied, since other biochemical and clinical parameters (creatinine, troponin, blood gas analytics, etc.) were also determined at various time points. The blood samples were collected in tubes coated with EDTA to prevent blood coagulation. The samples were centrifuged 10 min at 1,300 ×*g* directly after collection and the supernatant was stored at 4 °C if analyzed on the same day or frozen and stored at -20 °C till further analysis. During the experiment, changes in heart rhythm, blood circulation parameters and body temperature were documented every 10–30 min. Unless the death occurred during the experiment, the animal was euthanized after 3.5 h by an intravenous injection of pentobarbital.

For the determination of the Anticalin pharmacokinetics, the rats were put under mild narcosis via nasal inhalation with isoflurane (initiated with 2–5 %, maintained with 1.5–2.5 % (v/v) in oxygen), the Anticalin in PBS (~0.5–1 mL) was injected into the tail vain using a 25–27 G needle and 100 µL blood samples were collected after pre-defined time intervals. The rats were kept under narcosis during the first 0.5–1 h, then kept normally in cages and put under isoflurane narcosis again only for taking the next blood samples. The plasma was separated from the blood cells by centrifugation as described above, frozen and stored at -20 °C till further analysis. The animal was euthanized after completion of the experiment by an intravenous injection of pentobarbital.

The 95 % confidence interval (CI95) for the plasma half-file values was calculated using the Microsoft Excel function CONFIDENCE.NORM, which uses the formula

$$CI95 = \bar{x} \pm 1.96\left(\frac{\sigma}{\sqrt{n}}\right)$$

where $\bar{x}$ is the mean, σ is the standard deviation and n is the number of measurements.

3. Results

3.1 Selection of Anticalins against the plant toxin colchicine

The selection campaign was conducted with a published combinatorial Anticalin library (Gebauer *et al.*, 2013) having a complexity of 1.0×10^{10}. The library was based on the scaffold of human lipocalin 2 (Lcn2, also called neutrophil gelatinase-associated lipocalin, NGAL) containing 20 randomized amino acid positions and was prepared in form of phagemids, with the Anticalin moiety presented on the N-termini at the pIII capsid protein of the phage M13 (Skerra, 2001).

3.1.1 Selection from a combinatorial Anticalin library via phage display

For phage display selection, the ligand was immobilized on a solid phase. Therefore, the colchicine moiety was chemically coupled to biotin via a PEG-homoalanine linker (Figure 3.1), enabling its subsequent immobilization on the surface of streptavidin- or NeutrAvidin-coated paramagnetic particles.

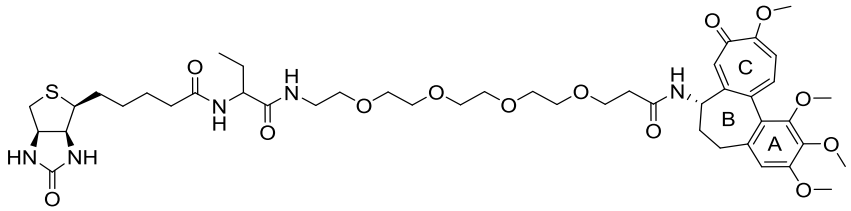

Figure 3.1. Colchicine (right) conjugated with biotin (left) via a PEG-homoalanine linker. The compound was synthesized by Dr. Martin Dauner (Chair of Biological Chemistry, TU Munich).

The library stored at -80 °C was reconstituted from the precipitated phagemids as described in Chapter 2.3.2, yielding a total titer of 4.8×10^{12} cfu. To prevent potential enrichment of streptavidin or NeutrAvidin binding lipocalin variants, every second panning round was performed with a different bead type. The ligand concentration was kept constant (100 nM) for the first three rounds and then reduced to 20 nM and 5 nM for the fourth and fifth round, respectively, to increase the stringency of selection. As shown in Figure 3.2, the relative phagemid titer increased in the later panning rounds, indicating enrichment of a subpopulation from the library. After the fifth panning round, plasmid DNA was isolated from the phagemids, and ten arbitrary clones were sequenced (Figure 3.3).

As expected, the majority of mutations was located at the randomized positions; only three further mutations were found elsewhere (possibly due to DNA synthesis errors during preparation of the library or during replication of the single-stranded phagemid DNA in *E. coli*). No frame shifts, stop codons or additional cysteine residues were detected in the analyzed

sequences, suggesting that selection was driven by the properties of functional full-length Anticalins. Notably, some amino acid positions at the tips of the structurally variable loops were enriched with positively charged residues (Lys or Arg).

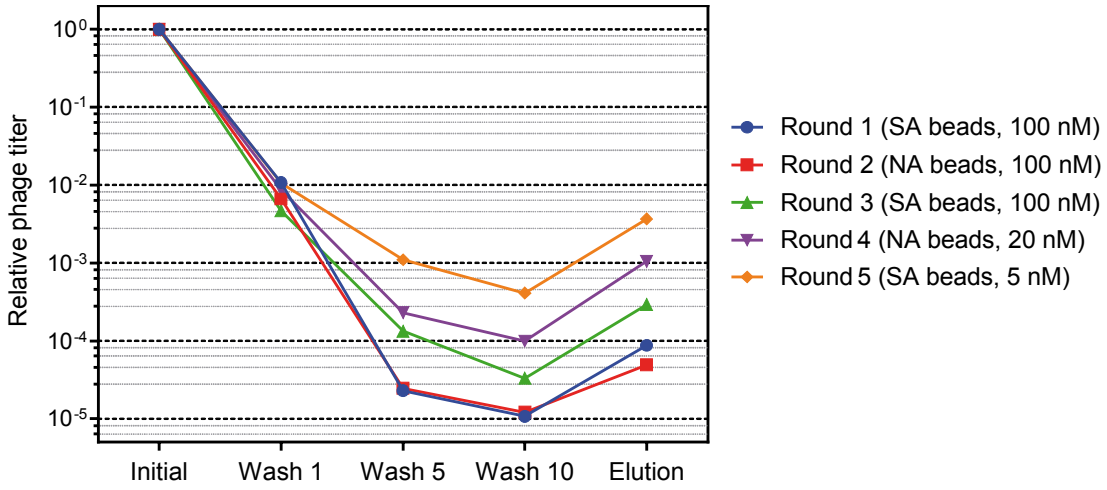

Figure 3.2. Phagemid titer during the panning against colchicine. The titer was calculated in relation to the titer at the beginning of each selection cycle. The bead type and ligand concentration used for each round is indicated in the legend.

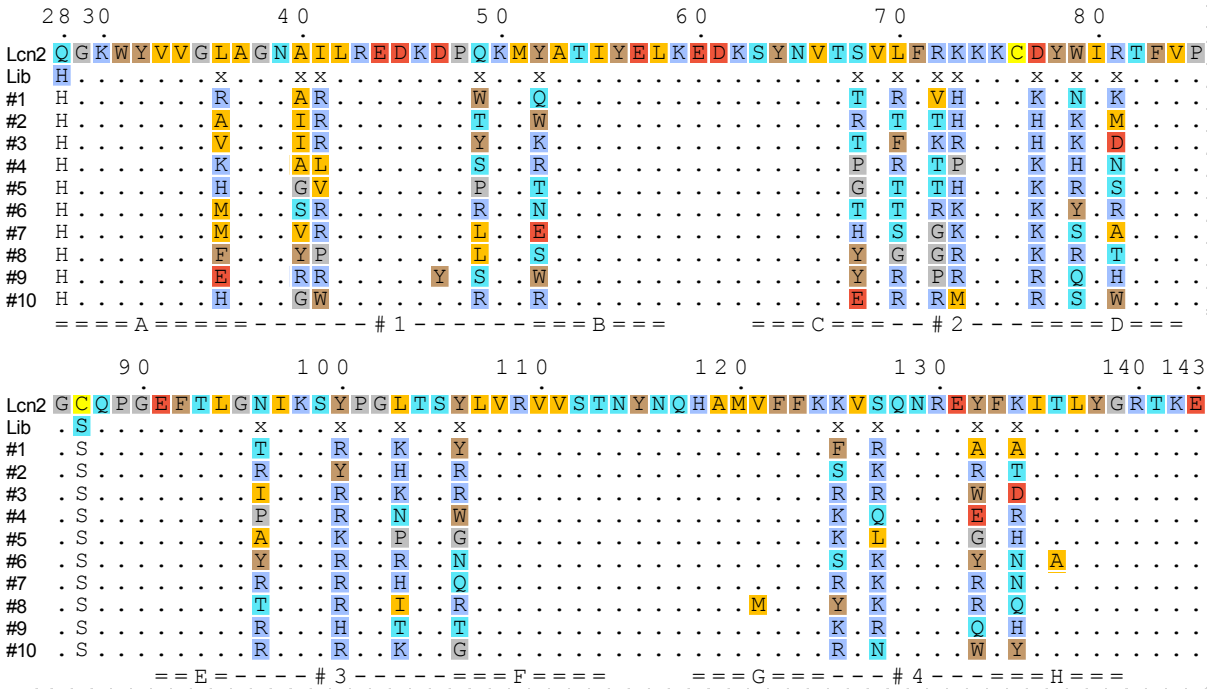

Figure 3.3. Amino acid sequence alignment of the Anticalin genes from ten randomly picked clones after 5 rounds of phage display. Only the central lipocalin gene region flanked by the BstXI restriction sites is shown. The 20 randomized positions are marked with 'x'. Amino acid residues corresponding to the β-strands are marked with double lines, structurally variable loops with dashes. Coloring scheme: orange for aliphatic, brown for aromatic, cyan for hydrophilic, blue for positively charged, red for negatively charged, yellow for cysteine, grey for glycine or proline. The mutations His28 and Ser87 were fixed in the library design and are not colored.

For the screening of the enriched Anticalin sublibrary by means of ELISA (Figure 3.4), the Anticalin gene cassette flanked by the BstXI restriction sites ('BstXI cassette') was subcloned on the plasmid vector pNGAL98 (Gebauer & Skerra, 2012). Apart from the Lcn2 gene, this plasmid also includes an N-terminal secretion signal of the outer membrane protein OmpA (which enables translocation of the protein into the periplasmic compartment) and a C-terminally fused *Strep*-tag II. Single clones obtained after the transformation of *E. coli* TG1-F$^-$ were grown in 96-well-plate format using 1 mL cultures and, after 2.5 h of heterologous protein production, periplasmic extracts were prepared as described in Chapter 2.6.1.

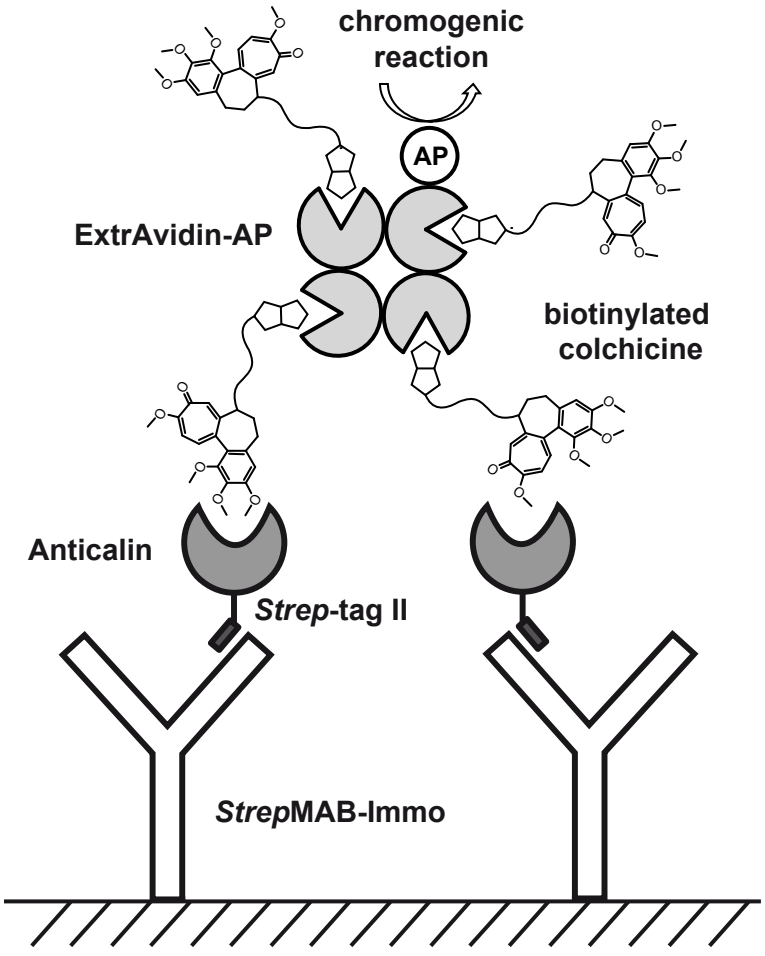

Figure 3.4. Schematic representation of the ELISA setup for Anticalin screening. *Strep*MAB-Immo was immobilized on the ELISA plate and used for capturing of the Anticalins from the crude periplasmic extract via the C-terminal *Strep*-tag II. Anticalins with binding activity towards colchicine were then detected via an ExtrAvidin-AP conjugate catalyzing a chromogenic reaction.

To increase the detection sensitivity of the ELISA with the help of the avidity effect, biotinylated colchicine was pre-incubated with the tetrameric ExtrAvidin-AP conjugate before applying the complex to the Anticalins captured at the surface of the microtiter plate. Five plates with a total of 460 clones from the final sublibrary (Round 5) were analyzed in this screening (Figure 3.5).

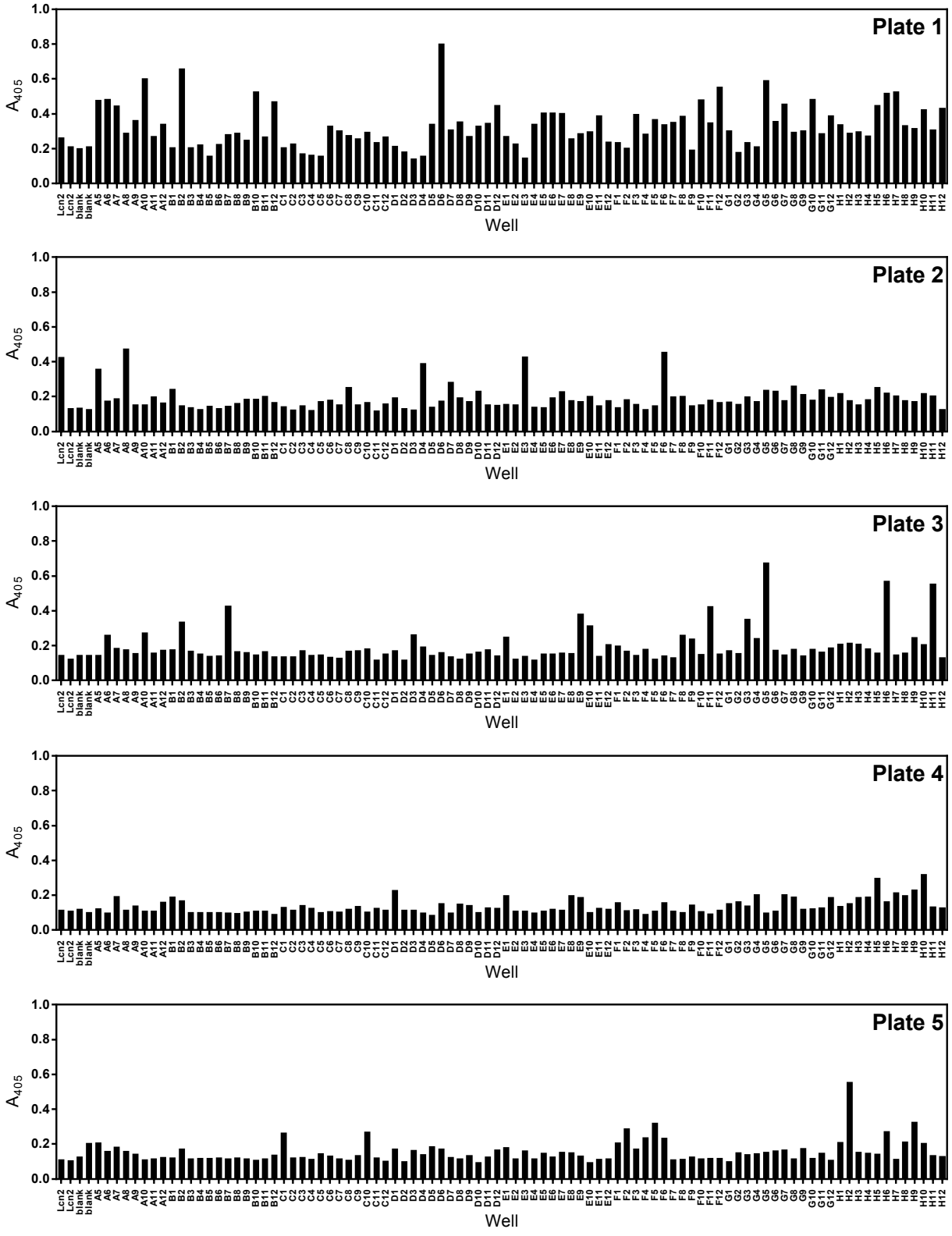

Figure 3.5. Read-out of the primary ELISA screening for colchicine binding. Variation in the background signal between the plates resulted from slightly varying incubation times. Lcn2 – clone expressing wild-type Lcn2 (negative control 1); blank – wells with LB medium not inoculated with bacteria (negative control 2).

After the primary screening, 28 clones with the highest signals were chosen for a secondary ELISA screening. In this assay, each clone was additionally tested with two negative controls:

in the first control, biotinylated colchicine was substituted by biotinylated fluorescein and, in the second, a 100-fold excess of free colchicine was added to the biotinylated colchicine. In case of specific colchicine binding, both controls should show lower signal. Of all clones tested in the secondary ELISA, only clone #23 showed an at least 1.5-fold higher signal than the respective negative controls (Figure 3.6A). However, repetition of the secondary ELISA screening with clones #23 and #5 in triplicates did not reproduce the initial observations (Figure 3.6B). This could have resulted either from enrichment of the library with unspecific binders or from a methodological problem with the ELISA test. To test the former and exclude the latter possibility, a different screening approach was applied: the filter sandwich colony assay.

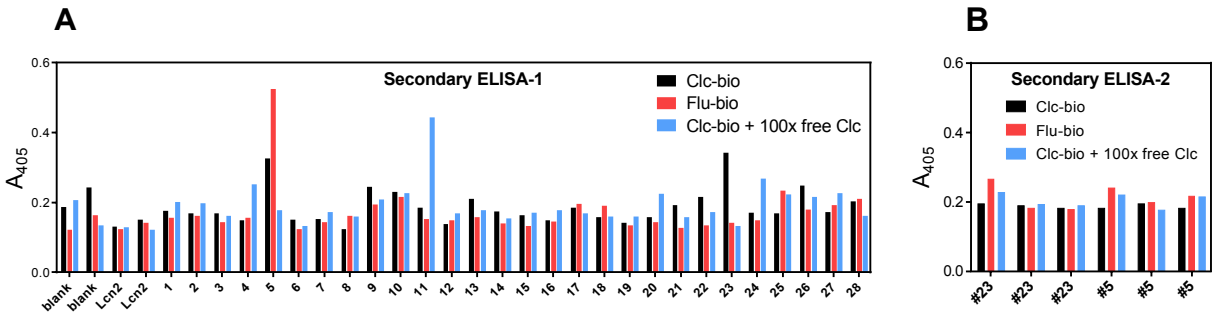

Figure 3.6. Read-out of the secondary ELISA screenings with two negative controls. Clc-bio – biotinylated colchicine; Flu-bio – biotinylated fluorescein; Clc-bio + 100x free Clc – biotinylated colchicine combined with a 100-fold excess of native (non-derivatized) colchicine. Prior to application, 500 nM biotinylated colchicine or fluorescein was pre-incubated with 125 nM ExtrAvidin-AP conjugate; for the second negative control (shown in blue), native colchicine was added at a concentration of 500 µM. **A:** The initial experiment with one replicate per clone. **B:** Repeat of the initial experiment on (A) with the clones #23 and #5, each analyzed in triplicate. The signal pattern from the primary test was not reproduced.

3.1.2 Screening for colchicine binding using the filter sandwich colony assay

Filter sandwich colony assay was developed to screen antibody fragments (Skerra *et al.*, 1991a) and was later adapted for the selection of Anticalins (Kim *et al.*, 2009; Schlehuber, 2001). The ‘sandwich’ consists of two membranes lying one on top of another on the surface of an agar plate with culture medium. Bacterial cells are plated onto the upper, hydrophilic membrane. Protein expression is initiated by placing the sandwich onto a new agar plate containing the appropriate concentration of inducer. For the assay, the plasmid vector pNGAL124 (Gebauer & Skerra, 2012) was used, encoding the albumin-binding domain (ABD) of the protein G from *Streptococcus spp.*, C-terminally fused to the Anticalin gene (Figure 3.7A). The fusion protein is secreted into the periplasm and diffuses through the pores in the outer cell membrane towards the lower, hydrophobic membrane, which had been coated with human serum albumin (HSA). After several hours of incubation, the upper membrane with

the colonies is removed and stored on a fresh agar plate, while the lower membrane is washed and probed for binding activity in a similar manner as a bottom of an ELISA plate.

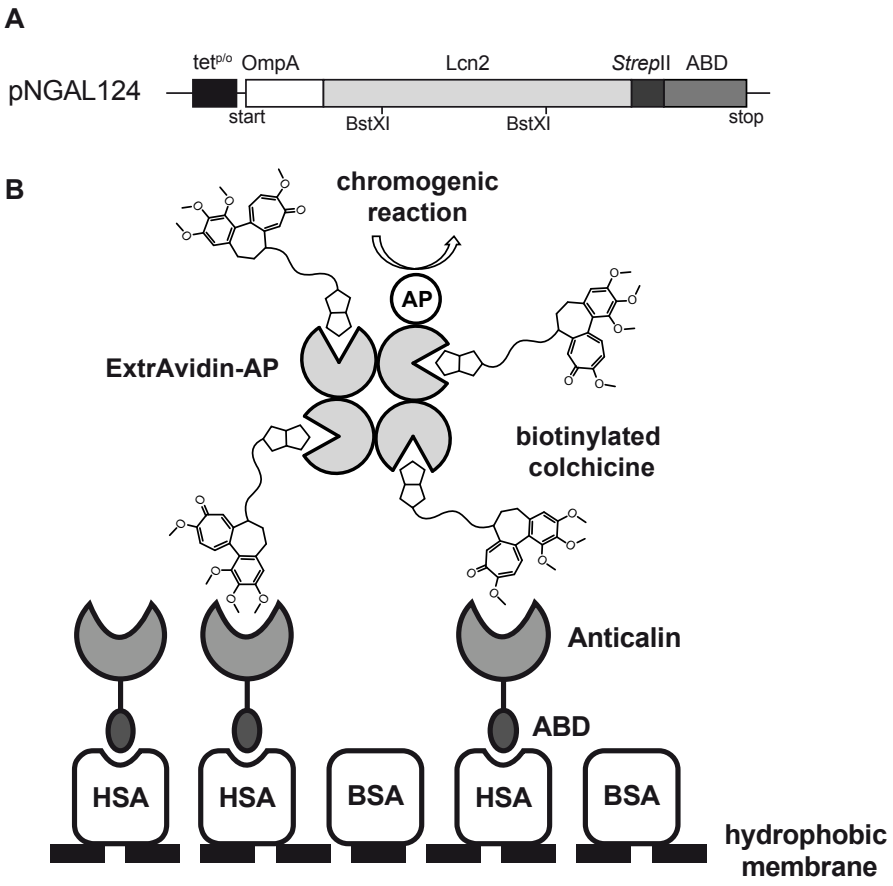

Figure 3.7. Filter sandwich colony assay. **A:** Scheme of the expression cassette on the plasmid vector pNGAL124. $tet^{p/o}$ – tetracycline promoter/operator; OmpA – OmpA signal sequence; *Strep*II – *Strep*-tag II, ABD – albumin-binding domain. **B:** Schematic representation of the assay setup. Only the hydrophobic membrane (after removal of the hydrophilic membrane supporting the bacterial colonies) is depicted. Anticalins are selectively immobilized via the ABD on the HSA-coated hydrophobic membrane, and the Anticalins that bind colchicine are detected via ExtrAvidin-AP conjugate, which had been pre-incubated with a stoichiometric amount of colchicine.

Compared with ELISA, this method has two important advantages. First, the filter sandwich assay offers much higher throughput: 1–2 thousand colonies can be easily sampled on a single agar plate, compared with the 96 wells on the ELISA plate. Second, the clone-to-clone growth variability is inherently low because colony growth is limited by the diffusion of nutrients from the agar medium. The assay variability is further reduced by the absence of the periplasmic extraction step, leaving basically only two variables that influence signal intensity of each colony: the binding activity of the tested Anticalin clone and the level of its expression.

The central Lcn2-encoding cassettes (flanked by the two BstXI restriction sites) of the sublibrary after the fifth round of phage display were subcloned on pNGAL124, and three plates with more than 5000 colonies in total were screened. An example of one hydrophobic

membrane after staining is depicted in Figure 3.8. Colonies with the brightest signals were picked from the upper membranes (stored at 4 °C), plasmid DNA was prepared and used for sequence determination (Figure 3.9). Similar to the randomly sequenced clones after the 5th round of phage display (Figure 3.3), the obtained sequences displayed the expected pattern of mutations, with the exception of Clone #1, which carried an insertion of tyrosine after residue 77. Enrichment of positively charged amino acids at loop positions was also noticeable, yet less pronounced.

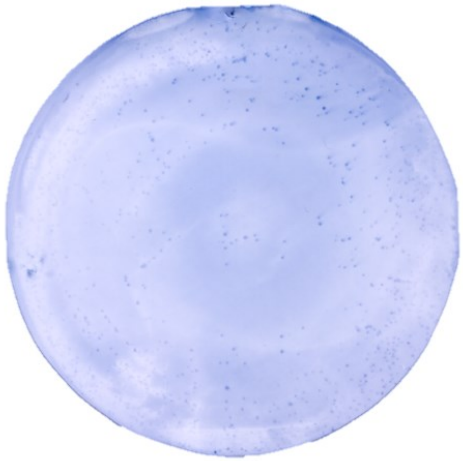

Figure 3.8. Hydrophobic membrane from the primary screening via filter sandwich assay, after staining with biotinylated colchicine, ExtraVidin-AP and BCIP/NBT. Dark blue dots correspond to Anticalin-producing colonies.

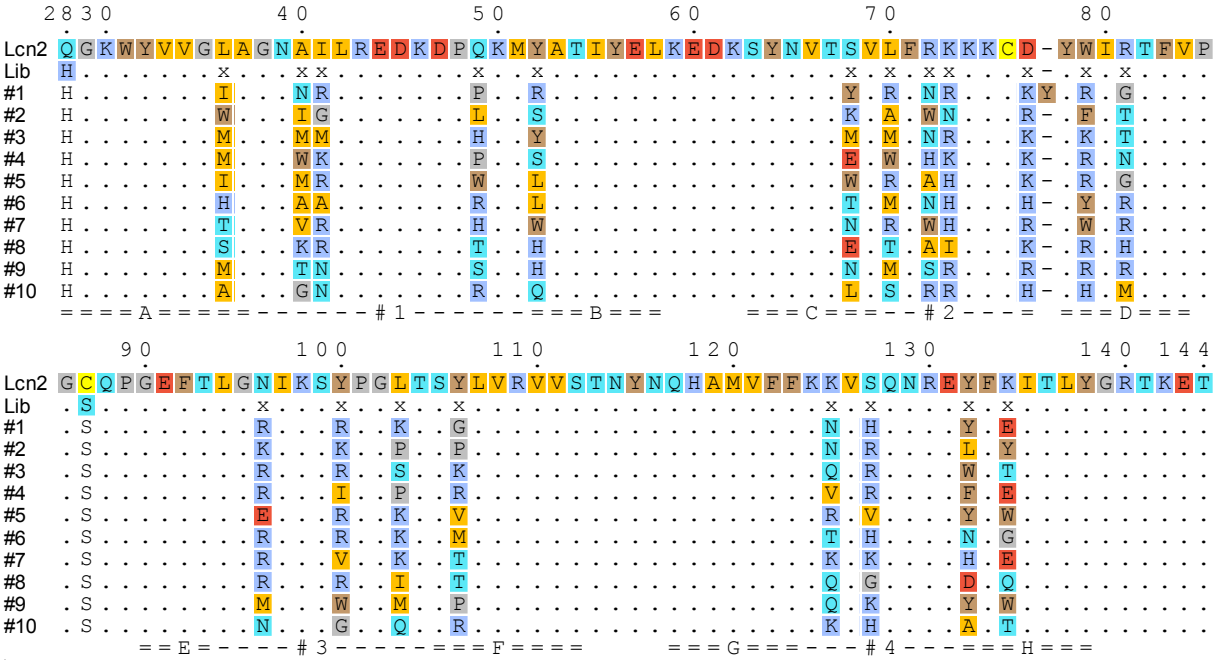

Figure 3.9. Amino acid sequence alignment of the central mutated Lcn2 regions from the best ten clones after the first filter-sandwich colony assay. For the coloring scheme, cf. Figure 3.3.

The best 6 clones were compared with wild-type Lcn2 in a secondary test, also carried out with a negative control, for which the clones were streaked as sectors on two membranes in parallel. After protein expression from the colonies, one hydrophobic membrane was developed using ExtrAvidin-AP pre-incubated with biotinylated colchicine, the other with ExtrAvidin-AP alone (Figure 3.10). Surprisingly, the negative control gave rise to a stronger signal than the first plate. Such a signal for all clones, including wild-type Lcn2, had to be explained by a non-specific interaction between ExtrAvidin-AP and some bacterial proteins that were unspecifically adsorbed to the membrane. For instance, ExtrAvidin-AP could bind to the biotin carboxyl carrier protein (BCCP) from *E. coli*, and the high affinity of ExtrAvidin to biotin could compensate for a comparatively low amount of the adsorbed BCCP. To exclude this possibility, in an additional experiment ExtrAvidin-AP was pre-incubated with a saturating amount of free biotin. This second negative control (Figure 3.10, right) showed much lower signal intensity, thus supporting the assumption.

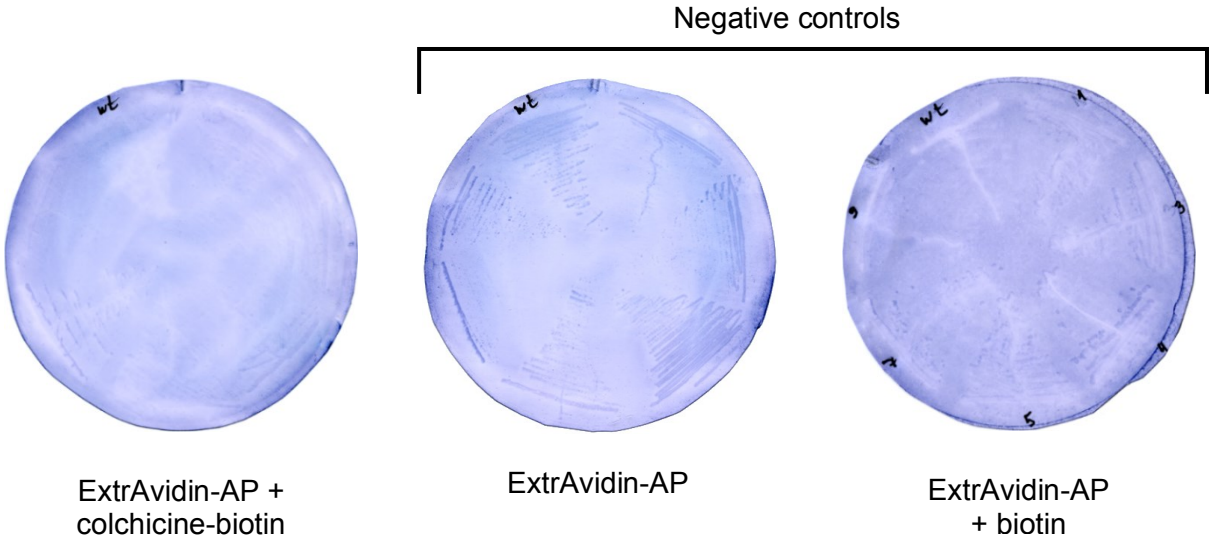

Figure 3.10. Results of the secondary filter-sandwich test (left) with the negative controls (middle and right). The signal on the negative control missing the binding ligand (middle) was stronger than on the experiment membrane (left), unless ExtrAvidin-AP was pre-saturated with free biotin (right).

Even though over 5000 clones had been screened, no specific colchicine binders appeared, suggesting insufficient enrichment after the five rounds of phage display. Consequently, three additional rounds of phage display (Figure 3.11) were performed. These additional rounds were conducted under higher selection stringency, with ligand concentration decreased to 1 nM. In addition, BSA was substituted by ovalbumin as blocking agent, since literature evidence was found suggesting that BSA can complex with colchicine (Hu *et al.*, 2005) and, thus, interfere with the assay. For ovalbumin, no colchicine binding could be detected in a fluorescence titration experiment (data not shown).

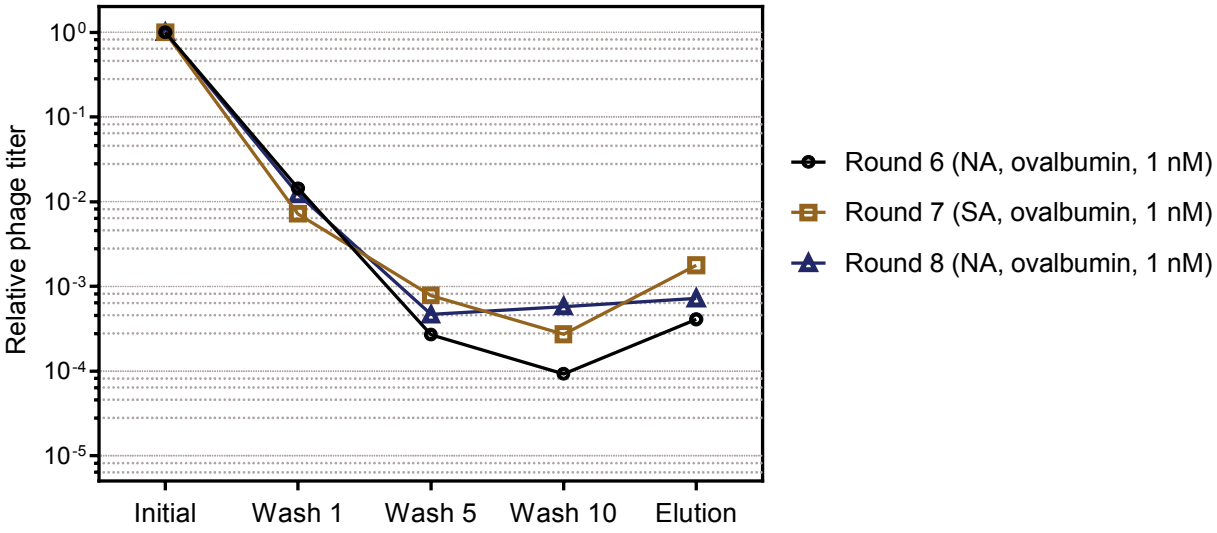

Figure 3.11. Phage titer after three further rounds of phage display. Bead type (NeutrAvidin-coated, NA, or streptavidin-coated, SA), blocking agent and ligand concentration used for each round are indicated in the legend.

After the three additional rounds of phage display, another filter-sandwich colony assay was carried out. In order to obtain an overview on the course of phage display selection from Round 1 to Round 8, sublibraries from the panning Rounds 1, 5 and 8 were screened in parallel (Figure 3.12A). Although the bacteria transformed with the sublibraries from different rounds were plated to the same final density, the signal density on the membranes after staining notably increased from Round 1 to 8. While for the sublibrary after Round 1 only a portion of the colonies produced a signal, nearly every colony from Round 8 gave rise to a signal of similar intensity. This demonstrated that the library actually was enriched for binding, although specificity of this enrichment remained in question. As all colonies after Round 8 had similar intensities, it was difficult to determine a distinct ‘hit’. At the same time, after Round 1 the contrast between the colonies was much higher: at least four colonies with stronger signals were clearly distinguishable from the others. These four clones, together with two new clones from Round 5 (freshly picked, not the ones shown in Figure 3.10) and two clones from Round 8, were tested for binding specificity in a secondary test (Figure 3.12B). This time, biotinylated fluorescein was used as a negative control as before. Interestingly, all four clones isolated from the sublibrary after Round 1 showed specific binding to biotinylated colchicine. The same was true for the two new clones isolated from Round 5, while both signals for the clones from Round 8 were unspecific.

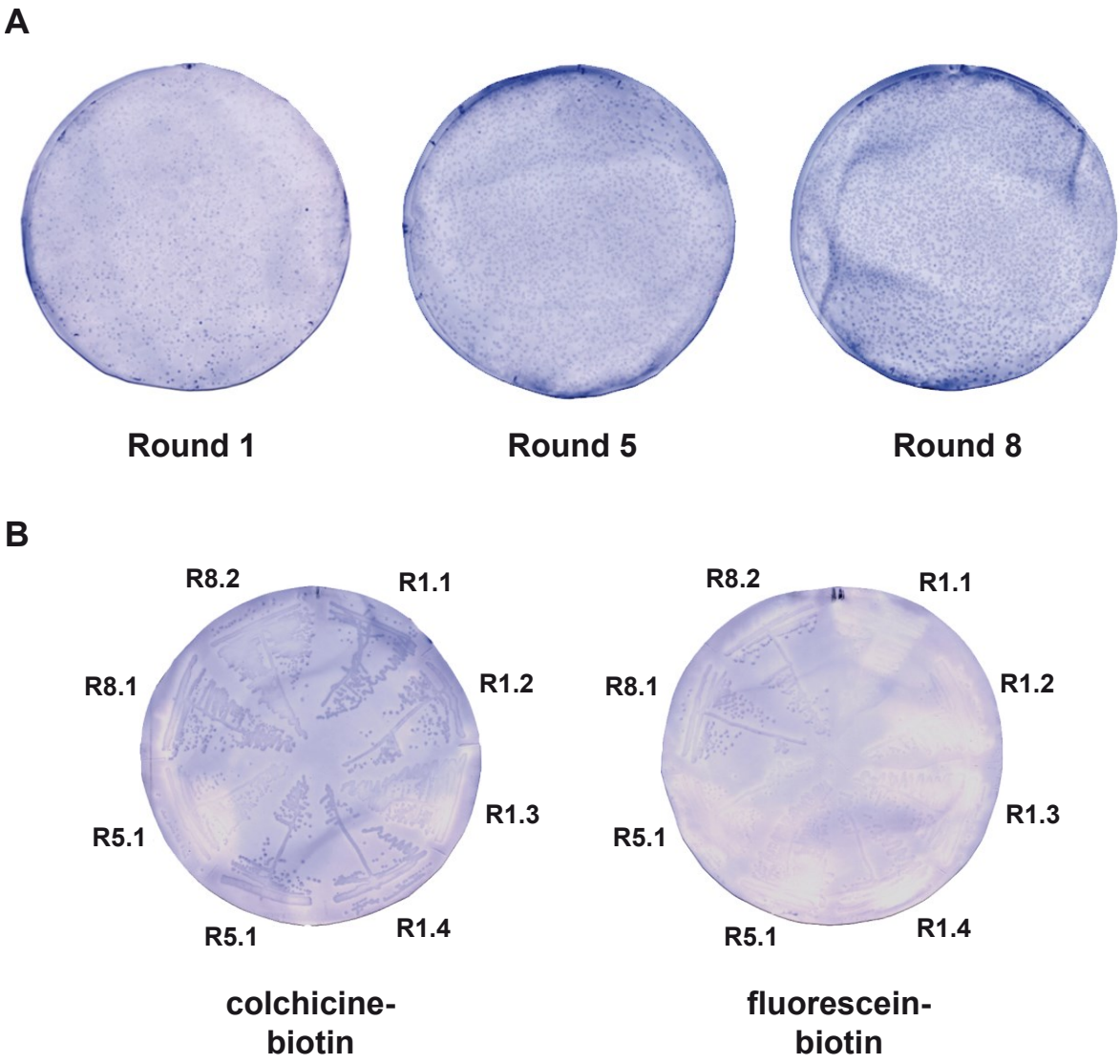

Figure 3.12. Results of the filter-sandwich colony screening of sublibraries after individual rounds of phage display. **A:** Primary test. Increasing signal density from Round 1 to Round 8 implied library enrichment, which was, however, found to be unspecific for colchicine binding. **B:** Secondary test performed with biotinylated fluorescein as negative control. All clones showed specific binding to colchicine, except for the clones isolated from Round 8.

Sequence analysis of the tested clones (Figure 3.13) revealed that all Anticalins contained mutations only at the randomized positions; neither stop codons nor frameshifts were detected. Enrichment of positively charged residues at the tips of the loops was noticeable, but less pronounced than in the previous experiments. Four clones with the strongest specific signal – R1.1, R1.2, R1.4 and R5.1 (see Figure 3.12B) – were subcloned on the expression plasmid pNGAL98 and produced in shake flasks in 2 L scale. After purification via *Strep*-tag affinity chromatography, the oligomeric state of each protein was analyzed by SEC (Figure 3.14). The clones R1.1, R1.2 and R1.4 were present as monomers; the minor deviations in retention volumes may be attributed to differences in hydrophobicity and interaction with the column matrix. For the clone R5.1, which was mostly present as a dimer, only the second half of the

monomer peak (shoulder) was used for the further analysis of ligand-binding activity by fluorescence titration.

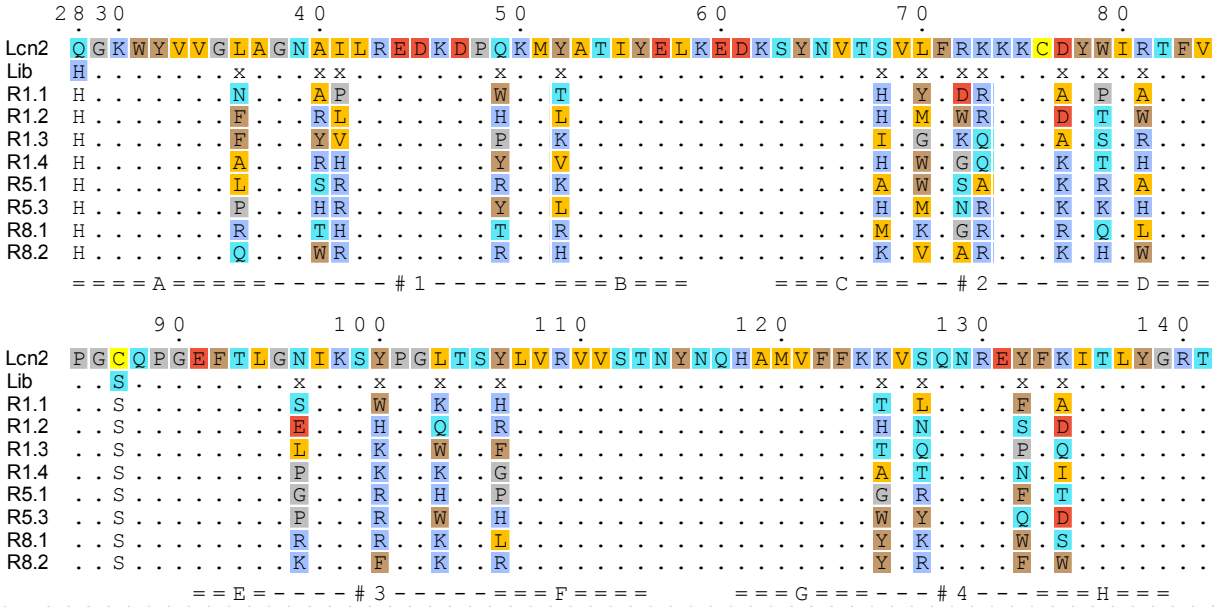

Figure 3.13. Amino acid sequence alignment of the central Lcn2 regions from the clones analyzed in the secondary filter-sandwich assay (see Figure 3.12B). All clones except R8.1 and R8.2 showed specific binding to colchicine. For the coloring scheme, cf. Figure 3.3.

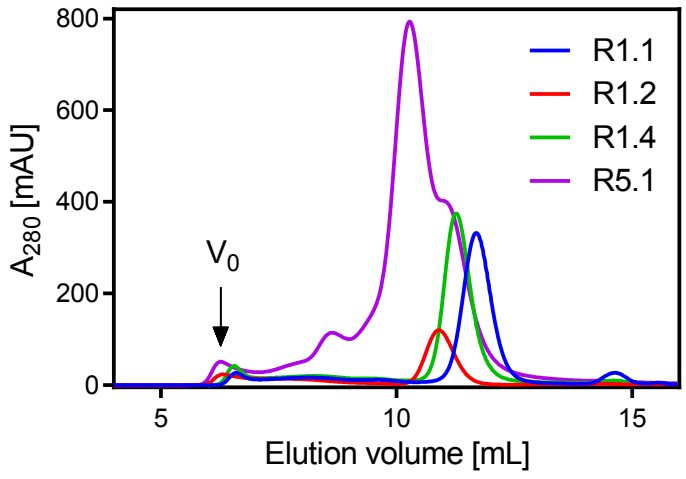

Figure 3.14. Size exclusion chromatographic analysis of four clones with the strongest specific binding signal in the filter-sandwich colony assay (see Figure 3.12 and 3.13). All Anticalins showed monomeric behavior, except for R5.1, which was predominantly present as a dimer.

3.1.3 Determination of affinity towards colchicine by fluorescence titration

Fluorescence titration is a method based on changes of intrinsic protein Trp and Tyr fluorescence upon binding of a ligand. The changes of intrinsic fluorescence are caused by two factors: change of hydrophobicity of the fluorescent side chain microenvironment and, potentially, energy transfer between the protein and the ligand. The latter can occur if the absorption spectrum of the ligand overlaps with the emission spectrum of Trp/Tyr in the protein, or *vice versa* (for fluorescing ligands). In fact, the absorption spectrum of colchicine strongly overlaps with the protein emission spectrum (Figure 3.15), which makes the method especially sensitive for studying colchicine-protein interactions. However, colchicine will also absorb some Trp/Tyr emission in the unbound state. To correct for this so-called inner filter effect, a control titration of *N*-acetyltryptophanamide with colchicine was performed, and the data points of the Anticalin titrations were corrected according to the Lambert-Beer Law (Vogt & Skerra, 2001; see Chapter 2.7.2).

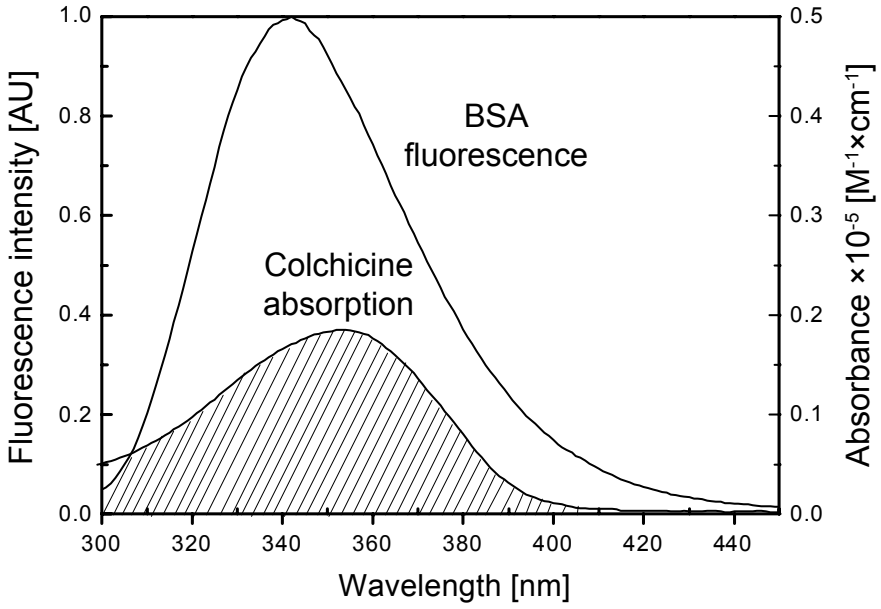

Figure 3.15. Spectral overlap of colchicine absorption with BSA fluorescence, adapted from Hu *et al.* (2005).

Results of the titration experiments are presented in Figure 3.16. Although it was possible to perform curve fitting according to Equation 5 and calculate the dissociation constants for all four clones, only the clone R1.4 provided an amplitude of fluorescence change that significantly exceeded the data scattering after correction of the inner filter effect. As a result of this analysis, clone R1.4 bound colchicine specifically with a dissociation constant of 1.5 µM and, thus, was the most promising Anticalin candidate at this stage of the project. Since its affinity was insufficient for complexation of colchicine *in vivo,* clone R1.4 was subjected to affinity maturation.

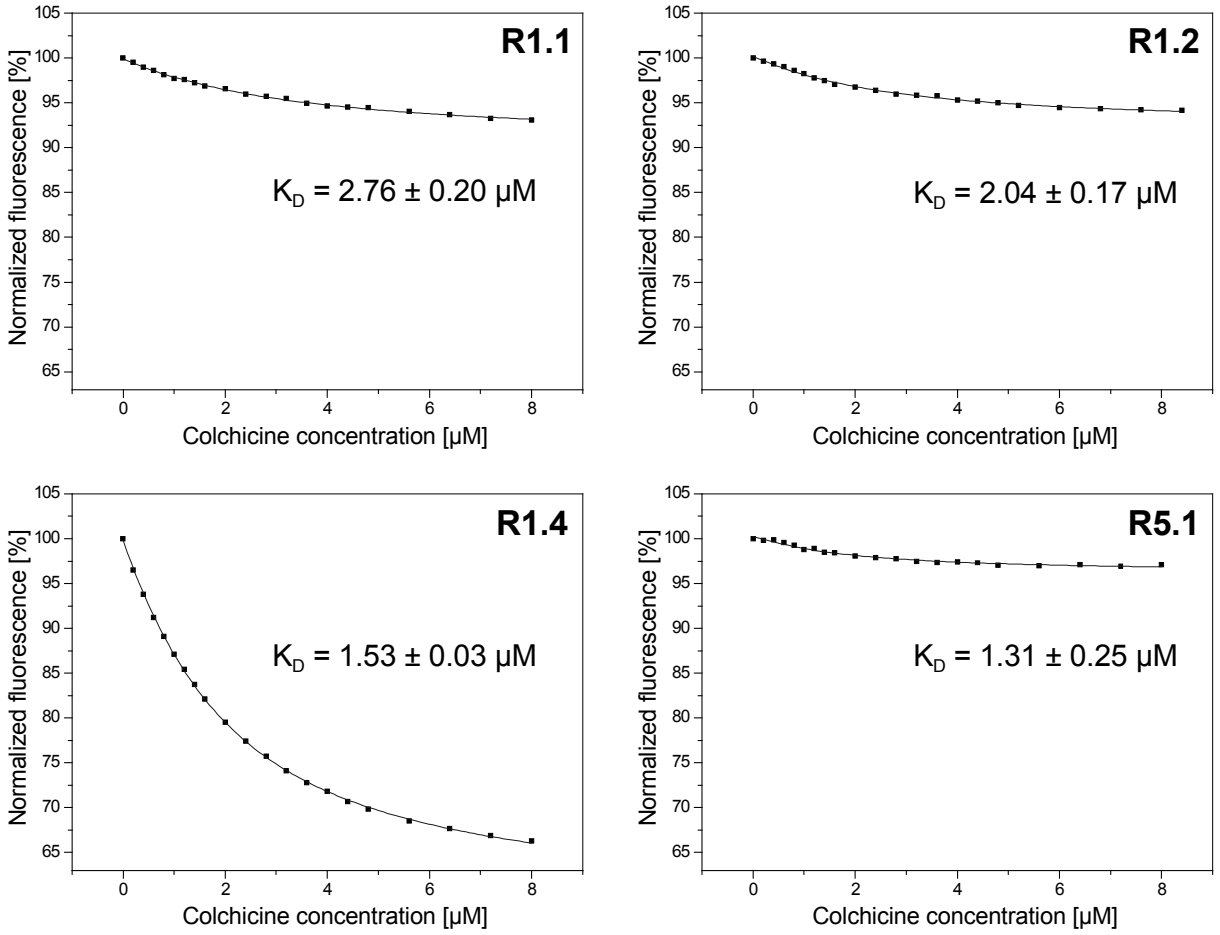

Figure 3.16. Fluorescence titration of the purified lipocalin variants from clones that showed strong specific binding signals in the filter-sandwich colony assay. Clone R1.4 demonstrated the highest amplitude of fluorescence quenching. Curve fitting according to Equation 5 was performed using Origin Pro software as described in 2.7.2.

3.1.4 Affinity maturation of the Anticalin candidate R1.4

For the affinity maturation, the coding region for R1.4 was randomized via error-prone PCR, followed by selection of improved binders via phage display. Only the part of the gene flanked by the two BstXI restriction sites (the 'BstXI-cassette') was subjected to randomization, since the rest of the gene corresponds to the conservative N- or C-terminal protein regions outside of the binding pocket. In preparation for the mutagenesis, the BstXI-cassette was first amplified using standard PCR (with *Taq* DNA polymerase and primers BstXI_for and BstXI_rev) and purified from agarose gel. For the error-prone PCR, 60 pg of the purified DNA fragment were used, which should lead to a predicted mutation rate of 3–4 amino acid substitutions per gene. A commercially available mixture of error-prone polymerases ('Mutazyme II') was applied, which incorporates transitions and transversions with a nearly equal frequency. Directly after the error-prone PCR (without additional amplification), the DNA fragment was digested with BstXI directly in the PCR mixture to minimize the losses associated with DNA extraction and purification. In parallel, the plasmid vector pNGAL108 was digested with the same enzyme

under recommended conditions. For the gel-purification of the digested DNA fragments, high purity agarose was used, and 1 mM guanosine was added to the electrophoresis running buffer in order to protect the DNA from UV light (λ = 312 nm) damage during excision of the gel pieces (Gründemann & Schömig, 1996). Before the preparative ligation, a test ligation and transformation (with 200 ng DNA) was performed for determination of the mutation rate. In the 6 sequenced clones, the average rate lay at 3.8 amino acid mutations per gene.

For the generation of the error-prone library, 11.2 µg of the digested pNGAL108 were ligated with 1.3 µg of the BstXI-cassette, and electrocompetent *E. coli* JK321 were transformed with the purified ligation product by electroporation. A post-electroporation heat pulse (46 °C for 6 min) was also performed (Wang *et al.*, 2007) to further increase transformation efficiency. The complexity of the resulting library was 3.6×10^9 (under assumption of independently transformed cells), with a transformation efficiency of 3×10^8 cfu/µg DNA. This library was used for the phage display selection.

The phage display selection was executed in the same way as with the combinatorial library, starting with 100 nM ligand and using ovalbumin as blocking agent. Since at this point it became evident that, at least in the late selection rounds, phage display might lead to enrichment of clones not specific for colchicine binding, the panning was stopped after the second round, and the selection strategy was changed by applying bacterial surface display (Binder *et al.*, 2010). The main advantage of bacterial surface display *versus* phage display is the tighter control over each selection cycle by using FACS instrumentation, thus increasing the chances for ligand-directed enrichment of the library.

It should be noted that the Anticalin candidate R1.4 had been isolated from a sublibrary obtained after one cycle of phage display. Considering the high complexity of the naïve phage display library, it was probable that other (possibly better) colchicine binders were present in the library but were not detected due to technical limitations of the selection and screening procedures. For this reason, it was decided to make another attempt of isolating a potent colchicine-specific Anticalin from the combinatorial phage display library. Therefore, the sublibrary after Round 2 of the phage display selection from the naïve library (Chapter 3.1.1) was additionally screened using bacterial surface display and FACS.

3.1.5 Screening for colchicine binding via bacterial cell sorting

The BstXI-cassettes from both sublibraries (affinity maturation of R1.4 and additional screening of the naïve library) were cloned on the plasmid vector pNGAL146, which enables EspP-mediated functional presentation of the Anticalin on the surface of the outer bacterial membrane. The selection procedure was performed mostly as described by Binder *et al.*

(2010). After cultivation and recombinant gene expression, approximately 2x10^8 bacterial cells were washed in PBS and incubated in a 10 µM solution of biotinylated colchicine in PBS. Bound biotinylated colchicine was detected in the FACS instrument after staining of the bacteria with streptavidin-phycoerythrin (Strep-PE) conjugate.

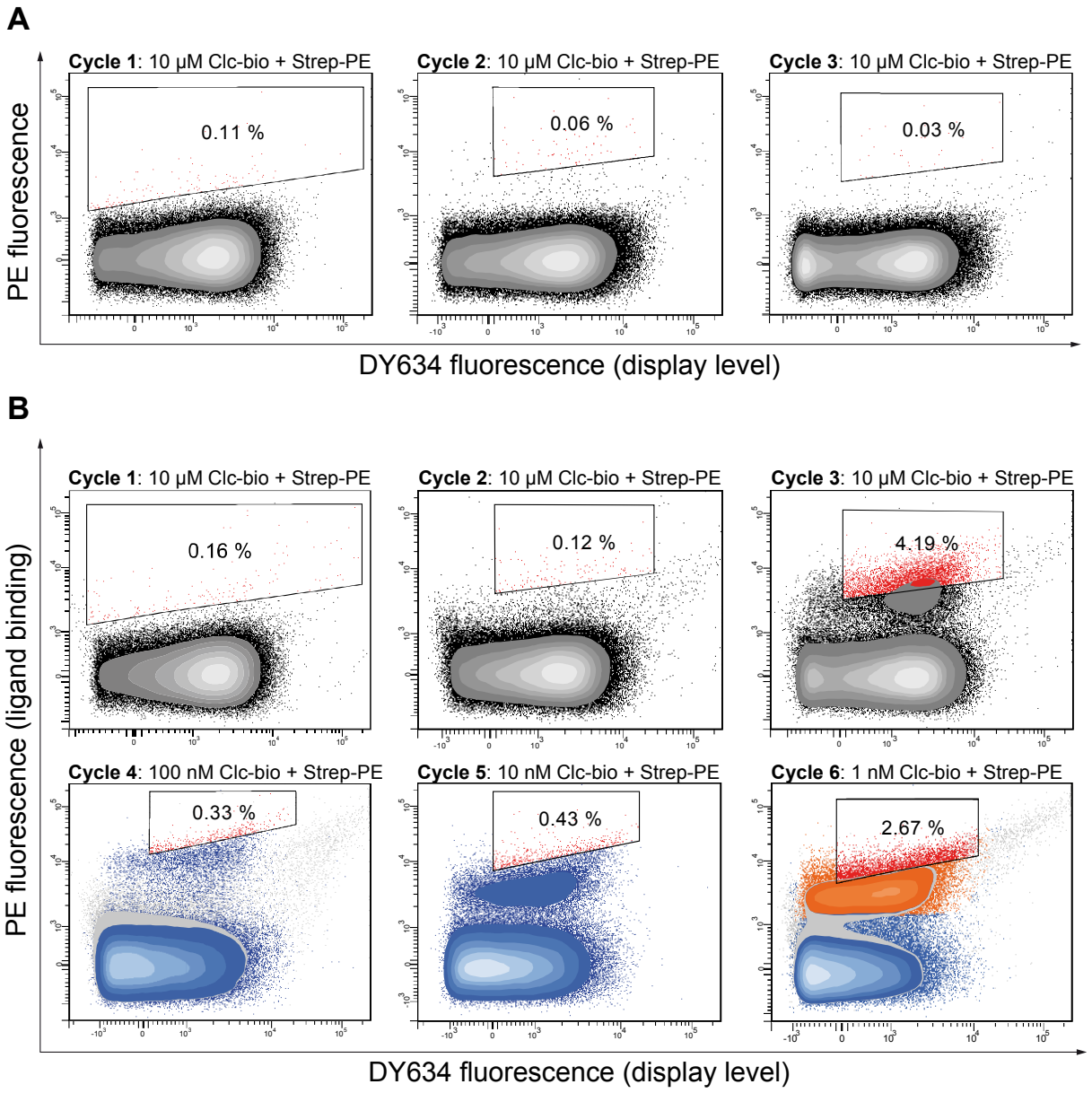

Figure 3.17. FACS read-out from the bacterial surface display selection campaigns. **A:** Affinity maturation of Anticalin candidate R1.4 – screening of the sublibrary after two rounds of phage display. **B:** Selection from the combinatorial Anticalin library – screening of the sublibrary after two initial rounds of phage display. Each cell is shown as a dot. The cells within the forward/side scattering sorting gate (see below) are colored blue, the emerged upper population (population with binding signal higher than for the negative control – bacteria displaying wild-type Lcn2) for Cycle 6 is marked orange. The PE/DY sorting gate is shown with a tetragon; the percentage of cells inside the gate is indicated.

Both selection campaigns (from the error-prone and from the naïve library) were performed in parallel for the first three cycles. As seen in Figure 3.17A, no enrichment was observed after three FACS cycles for the error-prone library derived from the Anticalin candidate R1.4. In contrast, for the preselected combinatorial library a distinct second population with elevated PE signal emerged (Figure 3.17B). This population was shown to bind colchicine specifically, since omitting of the ligand resulted in complete loss of the binding signal (data not shown). Because of these promising findings, selection from the error-prone library of the clone R1.4 was stopped, whereas the combinatorial sublibrary was screened further.

Starting from the fourth FACS cycle (Figure 3.17B, 'Cycle 4'), the selection pressure was increased by gradually reducing the ligand concentration (Cycle 4 – 100 nM, Cycle 5 – 10 nM, Cycle 6 – 1 nM). Furthermore, an additional superordinate sorting gate on the forward/side scattering plot was introduced (in order to filter out dead cells and cell debris) and the main sorting gate was shifted upwards (towards stronger binding). As a result of the increased stringency, the fluorescence signal of the upper population slightly shifted downwards, but continued growing from cycle to cycle, reaching almost 30 % of the total cell population after the sorting Cycle 5 and eventually 63 % after Cycle 6.

After Cycle 6, seven clones were picked randomly and sequenced. Five sequences were found to be identical (Figure 3.18), corresponding to a full-length lipocalin variant carrying mutations only at the 20 randomized positions of the combinatorial library. This variant was designated as lead candidate 'D6.1' and subjected to further analysis.

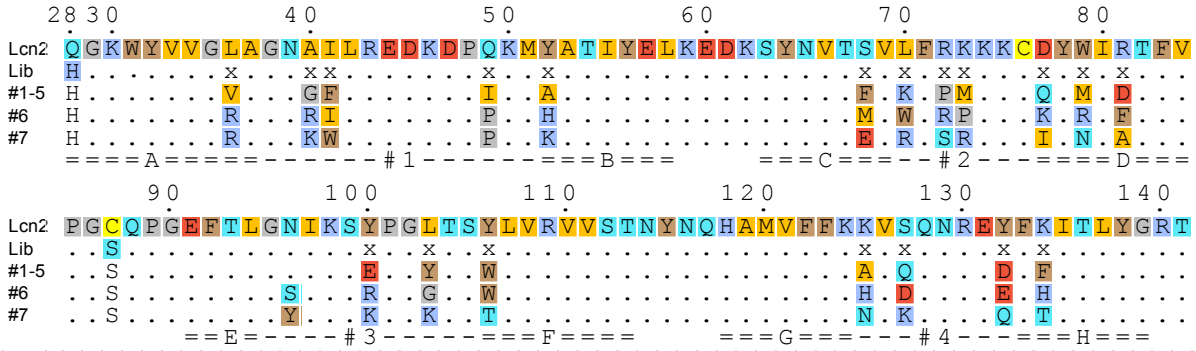

Figure 3.18. Amino acid sequence alignment of the central gene regions from the seven randomly picked Anticalin clones after the 6th FACS cycle (shown in Figure 3.17B). The repeating sequence (No. 1–5) belongs to the Anticalin D6.1, which was enriched during bacterial surface display selection. Variants #6 and #7 showed no binding, as tested by FACS single-clone analysis. For the coloring scheme, cf. Figure 3.3. The nucleotide sequences of Lcn2 and D6.1 can be found in the Appendix, Figure 8.1.

3.1.6 Biochemical characterization of the Anticalin D6.1

To determine the specificity and affinity of the lipocalin variant D6.1, 'on-cell' analysis by FACS was performed (Figure 3.19). The procedure was carried out similarly to the bacterial surface display of a library, but this time a single clone was analyzed. Several aliquots of *E. coli* JK321 presenting the Anticalin D6.1 were incubated with a dilution series of biotinylated colchicine, stained with streptavidin-PE and analyzed via FACS. D6.1 showed strong binding signals in FACS, indicating that the selected sequence belonged to an Anticalin that specifically recognizes colchicine. Its apparent dissociation constant was calculated to be ~7 nM.

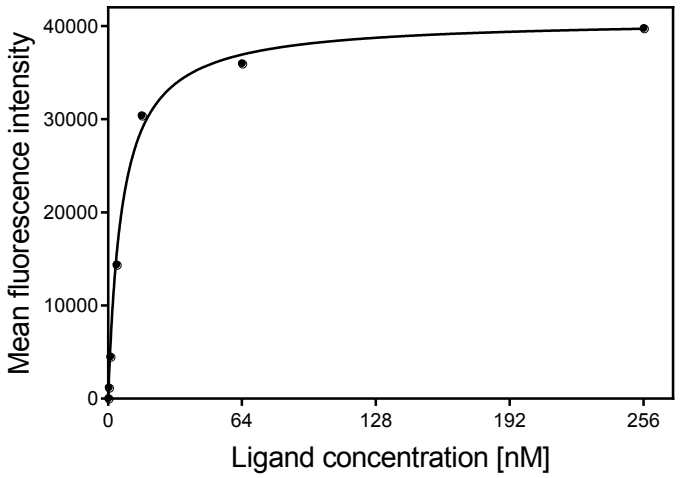

Figure 3.19. 'On-cell' determination of affinity of the Anticalin D6.1 via FACS titration. Bacteria were incubated with a dilution series of biotinylated colchicine (0.25–256 nM) in PBS. If two populations were detectable in FACS (the upper-right, protein-presenting, and the lower-left, lacking the Anticalin on the surface, see Figure 3.17), the mean fluorescence intensity was calculated only for the upper (protein-presenting) population.

This value can only be regarded as a rough estimate of the true dissociation constant, because both the ligand and the protein are present in modified forms, i.e. the Anticalin – as a fusion protein on the bacterial cell surface, and colchicine – as a biotinylated derivative. For proper biochemical characterization of the Anticalin D6.1, its BstXI gene cassette was cloned on pNGAL98, the protein was produced in 2 L shake flask and purified in a soluble state via SAC and SEC. The protein was obtained almost exclusively as a monomer with a yield of 1.1 mg/L×OD_{550} (as measured after SAC; Figure 3.20A&B). Finally, the pure monomer fraction after SEC was used for the determination of the true dissociation constant by fluorescence titration, resulting in a value of 7.5 ± 0.5 nM (Figure 3.20C). Thus, the apparent constant determined in the 'on-cell' analysis and the true dissociation constant measured in solution coincided in this case.

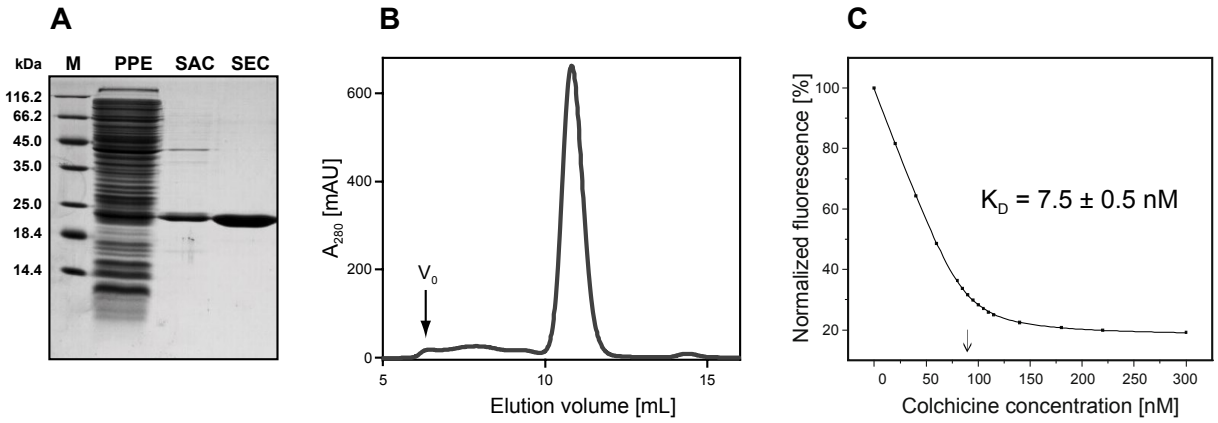

Figure 3.20. Expression and characterization of the Anticalin D6.1. **A:** SDS-PAGE analysis of the protein purification (reducing conditions). M – protein marker, PPE – periplasmic extract, SAC – elution fraction of the *Strep*-Tactin affinity chromatography, SEC – elution fraction of the size exclusion chromatography. **B:** Size exclusion chromatographic analysis using a Superdex S75 13/300 GL column. V_0 indicates the void volume of the column. **C:** Determination of the dissociation constant for colchicine by fluorescence titration. The error value represents standard deviation of the curve fitting; the point of equimolarity is indicated with an arrow.

Ultimately, using a combination of phage display and bacterial surface display, a lead candidate Anticalin D6.1, was successfully isolated and expressed as a monomeric protein with acceptable yield. However, in order to serve as an antidote *in vivo*, the desired Anticalin needed to be capable of complexing the poisonous colchicine quantitatively in blood. Colchicine concentration in blood can fall to the single-digit nanomolar range already several hours after intoxication; hence, an Anticalin with a dissociation constant of 1–2 orders of magnitude below was desired. To this end, the Anticalin D6.1 was subjected to affinity maturation.

3.2 Affinity maturation of the Anticalin D6.1

3.2.1 Sequence randomization and screening

The error-prone randomized library was prepared in the same way as described for the Anticalin candidate R1.4 (see Chapter 3.1.4), yielding a final library complexity of 2.2×10^9. In contrast to phage display, the throughput of bacterial surface display is limited by the speed of the FACS device. In practice, it is difficult to process more than 10^8 cells per cycle with a sorting rate of 10,000 cells per second. To ensure 95 % probability of each clone being analyzed by FACS at least once, the amount of screened clones has to exceed the complexity of the library 3-fold (Bosley & Ostermeier, 2005). Thus, FACS is useful for screening libraries with a complexity of up to 3×10^7 – two orders of magnitude less than the complexity of the obtained error-prone library. In order to overcome this bottleneck, an approach called Magnet-Assisted Cell Sorting (MACS) was implemented (Friedrich *et al.*, 2017).

MACS involves a simple pre-enrichment step in which the bacteria are incubated with ligand-coated magnetic beads. Since the throughput of this method is only limited by the amount of used beads, the library complexity can be oversampled and shrunk to a size that can be screened by FACS. First of all, MACS eliminates defective proteins that arise during error-prone library randomization and usually constitute a considerable part of the library. In addition, it helps to enrich the library for stronger binders, although discrimination of binders by affinity is hampered due to strong avidity effects between the bacterial surface, which presents thousands of Anticalin molecules, and the surface of the ligand-coated magnetic beads.

Sufficient oversampling of the initial library was ensured by applying a 10-fold higher number of bacteria than the starting library complexity. Accordingly, 2.2×10^{10} transformed *E. coli* JK321 cells were incubated with 10 nM biotinylated colchicine (500 pmol in total) immobilized on streptavidin-coated magnetic beads.

In order to estimate the effect of this pre-enrichment step, the error-prone Anticalin library was also used for the selection by FACS directly, without MACS. The first cycle of this FACS experiment was performed on the same day as the MACS pre-enrichment, which was also regarded as the first selection cycle. The two libraries were then processed in parallel and sorted under equal conditions, whereby the higher complexity MACS pre-enriched library was sorted in the second step in order to prevent a possible cross-contamination in the FACS instrument.

As the starting affinity of the Anticalin D6.1 was relatively high, the stringency of selection had to be increased considerably. For the previous selections, this had been achieved solely through reduction of the ligand concentration, i.e. selection was driven by the equilibrium constant of complex formation. Equilibrium-driven selection can proceed optimally when the ligand is present in excess.

As an alternative, selection can be performed under ‘kinetic’ conditions. Considering that the dissociation constant is the quotient of the dissociation and association rate constants, k_{off}/k_{on}, the selection strategy was adapted to favor binders with lower dissociation and higher association rates. For this, selection for fast association was achieved through shortening of the incubation period with biotinylated colchicine, whereas selection for slow dissociation – through introduction of a competition step with an excess of free colchicine, in order to prevent rebinding of the biotinylated colchicine (Figure 3.21).

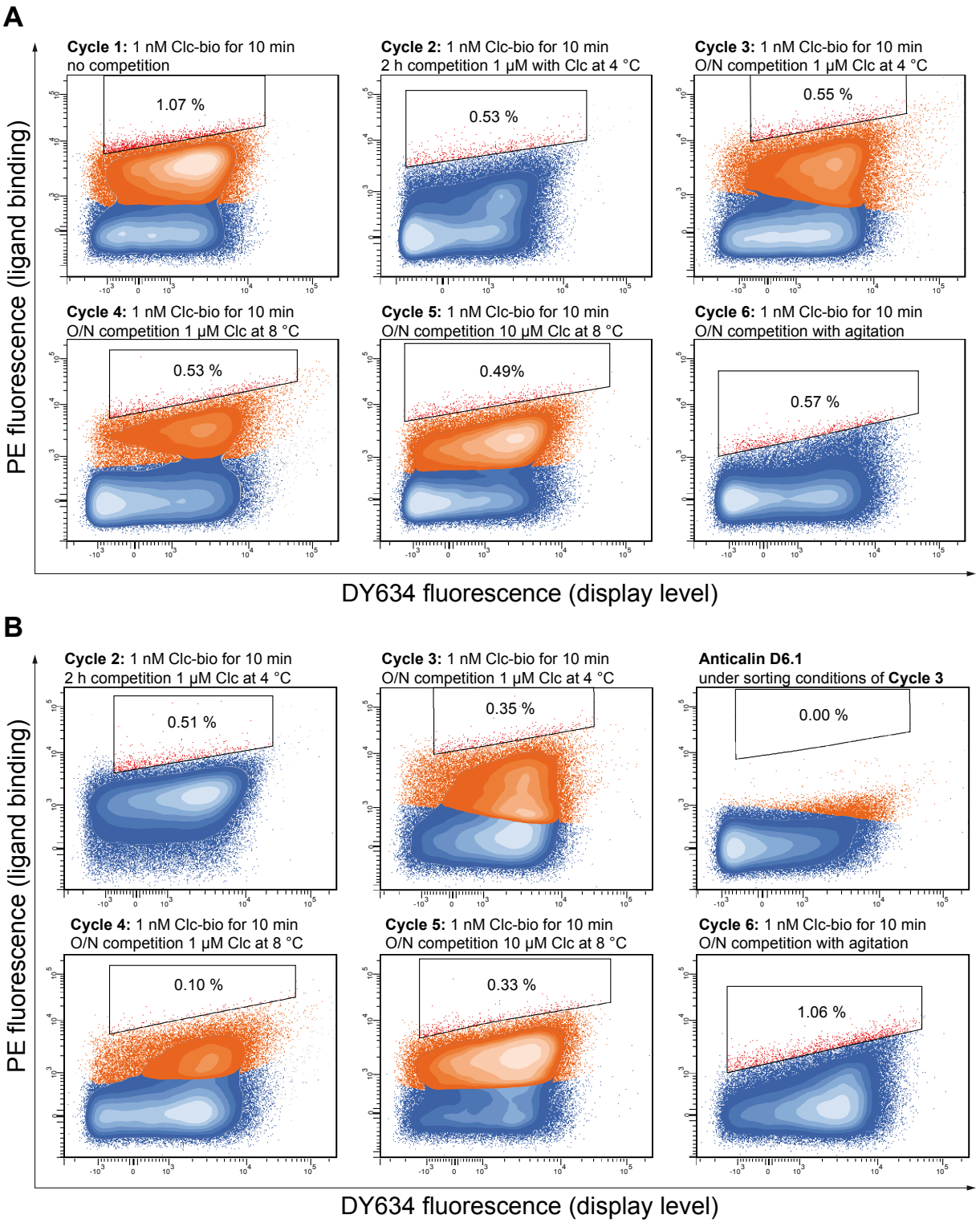

Figure 3.21. FACS read-outs during the affinity maturation of the Anticalin D6.1. **A:** Selection without MACS pre-enrichment. **B:** Selection after a MACS pre-enrichment step. The cells within the forward/side scattering sorting gate are colored blue, the upper population (population with binding signal higher than for the negative control – bacteria displaying wild-type Lcn2) is marked orange. The PE/DY sorting gate is shown with a tetragon; the percentage of cells inside the gate (colored red) is indicated. In Cycle 6, the bacterial suspension was gently agitated during the competition step to accelerate the dissociation.

Notably, after MACS pre-enrichment (Figure 3.21B, Cycle 1) the library appeared as a homogeneous population with high PE signal, demonstrating successful depletion of Anticalin variants with hampered folding and/or binding activity. Otherwise, both libraries behaved similarly throughout the six selection cycles with increasing stringency and revealed signs of enrichment: the main population shifted downwards, while a second (upper) population with stronger binding signal emerged (Figure 3.21). After the last round (Cycle 6), single-clone analysis by FACS was executed. To this end, 94 clones from both setups after Cycle 6 were picked randomly and, together with the wild-type Lcn2 and Anticalin D6.1, were grown in 1 mL scale and analyzed one-by-one. For each clone, the ratio of the PE over the DY634 signal was calculated, representing the ligand binding normalized to the cell surface expression level. By normalization to the corresponding ratio for the Anticalin D6.1, a coefficient '$k_{D6.1}$' was obtained and used to rank the clones (Table 3.1).

Table 3.1. Results of the single-clone analysis after the affinity maturation of Anticalin D6.1.

FACS only (without MACS)								With MACS							
Clone	PE	DY	$k_{D6.1}$	Clone	PE	DY	$k_{D6.1}$	Clone	PE	DY	$k_{D6.1}$	Clone	PE	DY	$k_{D6.1}$
Before O/N incubation				4	70,761	3,057	2.9	**Before O/N incubation**				35	25,169	1,944	1.6
Lcn2	43	1,111	0.0	12	25,648	1,151	2.8	Lcn2	43	1,111	0.0	5	31,261	2,442	1.6
D6.1	21,371	2,721	1.0	11	61,150	2,777	2.8	D6.1	21,371	2,721	1.0	3	36,338	2,917	1.6
7	51,745	1,885	3.5	8	58,363	2,695	2.8	20	42,413	989	5.5	30	39,082	3,203	1.6
16	54,454	1,994	3.5	38	38,424	2,038	2.4	9	64,520	1,703	4.8	21	35,860	3,023	1.5
8	49,877	1,853	3.4	28	42,449	2,336	2.3	1	50,510	1,813	3.5	24	31,449	2,654	1.5
9	50,180	1,962	3.3	36	45,597	2,567	2.3	16	50,815	1,945	3.3	29	37,522	3,283	1.5
10	51,950	2,069	3.2	31	44,173	2,487	2.3	7	43,208	1,662	3.3	33	31,006	2,872	1.4
33	48,978	2,019	3.1	29	41,797	4,121	1.3	10	50,933	2,181	3.0	27	21,946	2,271	1.2
25	42,601	1,802	3.0	5	28,072	3,187	1.1	4	70,761	3,057	2.9	18	34,395	3,706	1.2
11	50,241	2,231	2.9	3	26,198	3,481	1.0	12	25,648	1,151	2.8	**After O/N incubation**			
20	44,165	1,975	2.8	2	28,355	3,788	1.0	11	61,150	2,777	2.8	Lcn2	34	1,140	0.0
26	41,981	1,884	2.8	**After O/N incubation**				8	58,363	2,695	2.8	D6.1	10,935	2,810	1.0
6	40,532	1,868	2.8	Lcn2	34	1,140	0.0	38	38,424	2,038	2.4	20	47,223	973	12.5
23	39,648	1,850	2.7	D6.1	10,935	2,810	1.0	28	42,449	2,336	2.3	9	77,006	1,832	10.8
27	40,654	1,906	2.7	16	54,544	2,134	6.6	36	45,597	2,567	2.3	16	57,578	1,979	7.5
4	46,534	2,278	2.6	9	54,578	2,237	6.3	31	44,173	2,487	2.3	1	55,468	1,914	7.4
28	41,812	2,049	2.6	33	49,425	2,111	6.0	37	39,923	2,376	2.1	7	45,041	1,773	6.5
12	28,998	2,004	1.8	7	45,996	1,968	6.0	23	32,605	1,954	2.1	10	51,494	2,076	6.4
30	33,585	2,460	1.7	8	43,691	1,895	5.9	2	40,876	2,763	1.9	4	86,240	3,531	6.3
17	33,920	2,489	1.7	10	51,251	2,279	5.8	13	42,948	2,968	1.8	11	68,679	2,871	6.1
36	33,111	2,458	1.7	6	42,510	2,035	5.4	14	48,340	3,372	1.8	8	62,929	2,717	6.0
16	50,815	1,945	3.3	20	41,484	2,003	5.3	22	35,041	2,462	1.8	38	43,504	2,035	5.5
7	43,208	1,662	3.3	26	38,446	1,853	5.3	34	39,919	2,846	1.8	12	24,634	1,152	5.5
10	50,933	2,181	3.0	11	47,582	2,399	5.1	39	32,573	2,378	1.7	28	42,907	2,254	4.9

Underlined are the sequenced clones.
Clones that showed no binding activity (12 in total) were omitted from the table.

To better discriminate between the lipocalin variants with slow dissociation kinetics, the analyzed suspensions of bacterial clones with $k_{D6.1} \geq 2.5$ were incubated in PBS (without ligand) at 4 °C overnight and analyzed again on the next morning. The ranking according to $k_{D6.1}$ (see above) was performed again, and the clones that reached a $k_{D6.1} \geq 5.5$ after overnight incubation were sequenced. The six analyzed clones from the library without pre-enrichment contained only two unique sequences, whereas all 11 clones from the MACS library were unique, demonstrating higher end diversity (Figure 3.22). Four candidates with the highest $k_{D6.1}$ values were chosen, their BstXI-cassettes were cloned on pNGAL98, the proteins were expressed and purified, and their affinities were measured by fluorescence titration (Figure 3.23). All four Anticalins turned out to have sub-nanomolar affinities, muteins MACS1 and MACS20 reaching the lowest K_D values.

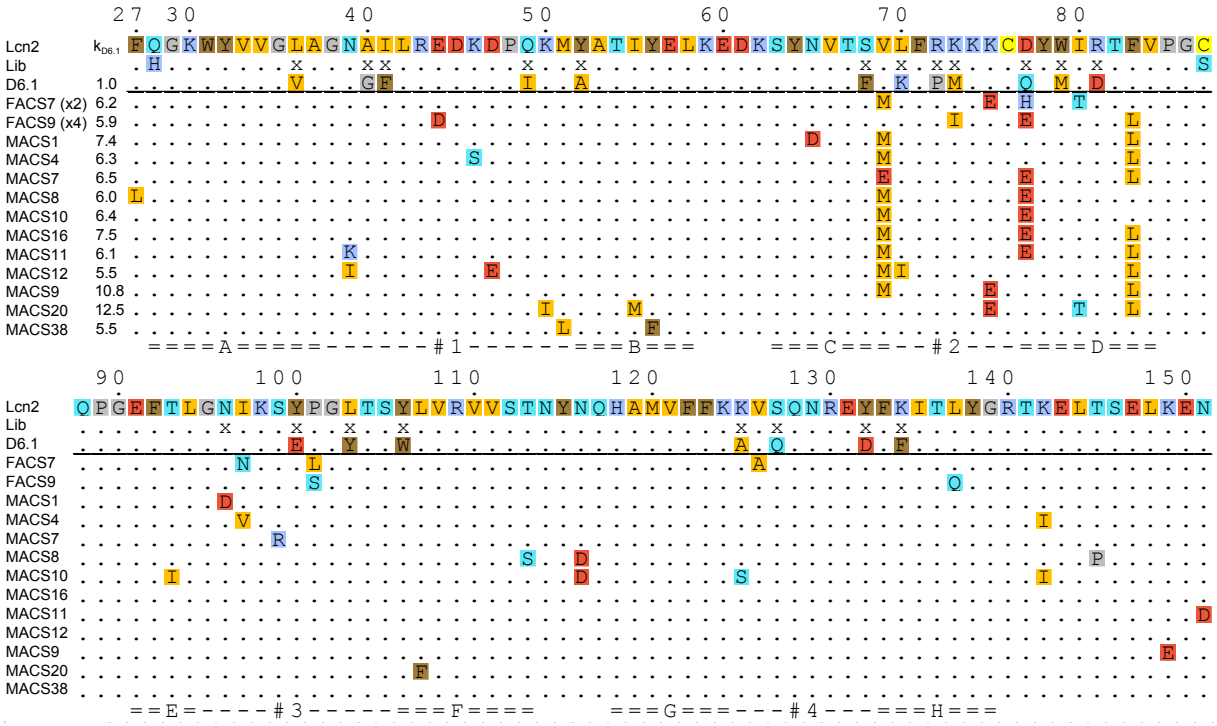

Figure 3.22. Amino acid sequence alignment of the BstXI-flanked gene regions from the best clones identified in the single-clone analysis via FACS. The Anticalin D6.1, the starting point of the affinity maturation, serves as a reference for all sequences under the black line. For the coloring scheme, cf. Figure 3.3. The corresponding nucleotide sequences can be found in the Appendix, Figure 8.2.

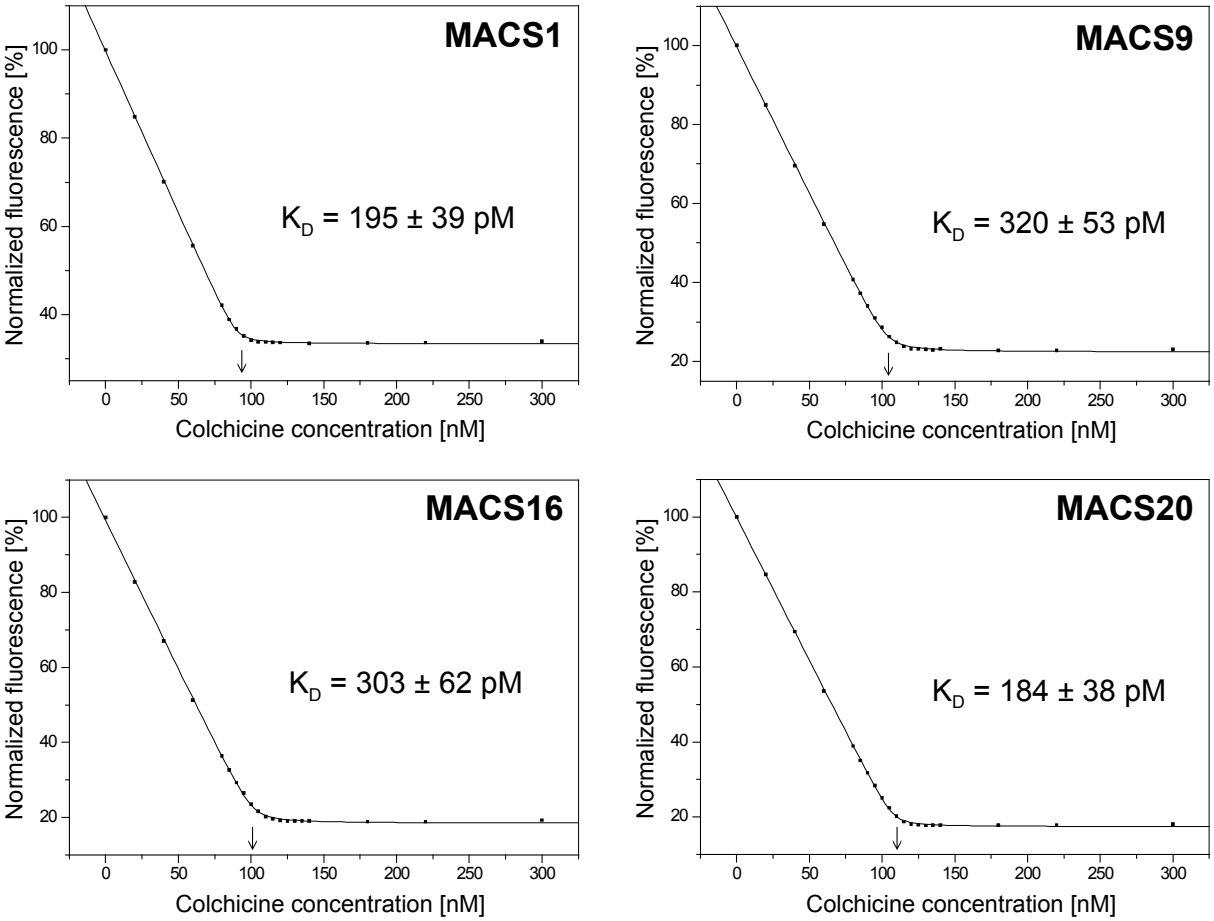

Figure 3.23. Fluorescence titration of the Anticalin variants isolated after the affinity maturation of Anticalin D6.1. Starting from this fluorescence titration, the protein concentration was set to 100 nM (decreased 10-fold compared with the previous titrations) in order to decrease the sharpness of transition at the point of equimolarity (indicated with an arrow) and thus improve the reliability of curve fitting for the high-affinity Anticalins.

3.2.2 Rational mutagenesis and generation of the Colchicalin D6.2

As seen from the sequence alignment (Figure 3.22), most sequenced clones shared a pattern of mutations V69M, K75E/Q77E and F83L. In order to understand the influence of each amino acid substitution on colchicine binding, two of the substitutions were introduced one-by-one into the original Anticalin D6.1 using site-directed mutagenesis, and affinities of each mutein were measured by fluorescence titration (Table 3.2). The mutations K75E and Q77E were not tested at this stage, because based on their localization, it was assumed that they could interact only with the PEG linker of the biotinylated colchicine, rather than with colchicine itself. Instead, the mutation I80T was included, which appeared twice (cf. Figure 3.22) including the best mutein MACS20.

Table 3.2. Dissociation constants of Anticalin D6.1 and its muteins obtained via site-directed mutagenesis, as determined by fluorescence titration with 100 nM protein.

Anticalin version	K_D ± SD [nM]
D6.1	3.6 ± 0.1
D6.1-V69M	0.26 ± 0.03
D6.1-I80T	2.6 ± 0.1
D6.1-F83L	1.3 ± 0.1
D6.1-V69M/I80T	0.23 ± 0.01
D6.1-V69M/F83L	0.094 ± 0.025
D6.1-I80T/F83L	0.60 ± 0.07
D6.1-V69M/I80T/F83L (= D6.2)	0.047 ± 0.004

Surprisingly, the mutation V69M turned out to have the strongest influence on the dissociation constant, leading to a 10-fold increase in affinity. The crucial role of this amino acid position – with the amino acid side chain directed away from the binding pocket – was understood only after the crystal structure of the Anticalin was solved (see Chapter 3.3.8). The other two mutations, I80T and F83L, increased the affinity 1.3- to 2.7-fold, respectively, while also improving the protein yield. The triple mutant V69M/I80T/F83L, which reached a K_D of 47 pM (tested at 100 nM protein), was chosen as the new lead candidate and was designated ‘Colchicalin D6.2’.

In order to understand which structural features resulted in the development of the high affinity against colchicine, and which amino acid residues were responsible for it, Colchicalin D6.2 was subjected to crystallographic analysis.

3.3 Crystal structure determination of the Colchicalin D6.2

3.3.1 Crystallization of the Colchicalin D6.2 with C-terminal affinity tags

First, the Colchicalin D6.2 was expressed in the form of two constructs: with a C-terminal *Strep*-tag II or a hexahistidine (His_6) tag; the expression vectors were based on the plasmids pNGAL98 and pNGAL118, respectively. After the production in *E. coli* JM83 at elevated cell density (OD_{550} 2–4), both proteins were purified via affinity, cation exchange and size exclusion chromatography (Figure 3.24). The pure proteins were concentrated to ~20 mg/mL in 10 mM MES/NaOH pH 5.5 with 50 mM or without NaCl. Free colchicine was added at 5-fold molar concentration from a 100 mM stock solution in DMF. The drops in the in-house precipitant screen comprising 480 different conditions consisted of 250 nL protein solution and 250 nL reservoir solution.

Table 3.3. Behaviour of Colchicalin D6.2 with C-terminal affinity tags in the crystallization screens.

NaCl	50 mM		0 mM	
Temperature	20 °C	4 °C	20 °C	4 °C
% Precipitate	20 %	12 %	12 %	16 %
Phase separation	< 5 %	< 5 %	21 %	23 %

As indicated in Table 3.3, for all conditions used (different NaCl concentrations and incubation temperatures), the proportion of drops with precipitate was far below the range of 30-35 %, which is normally considered optimal. The only crystalline structures formed in some drops with sodium malonate had spherolit morphology and did not improve upon refinement of crystallization conditions (Figure 3.24D).

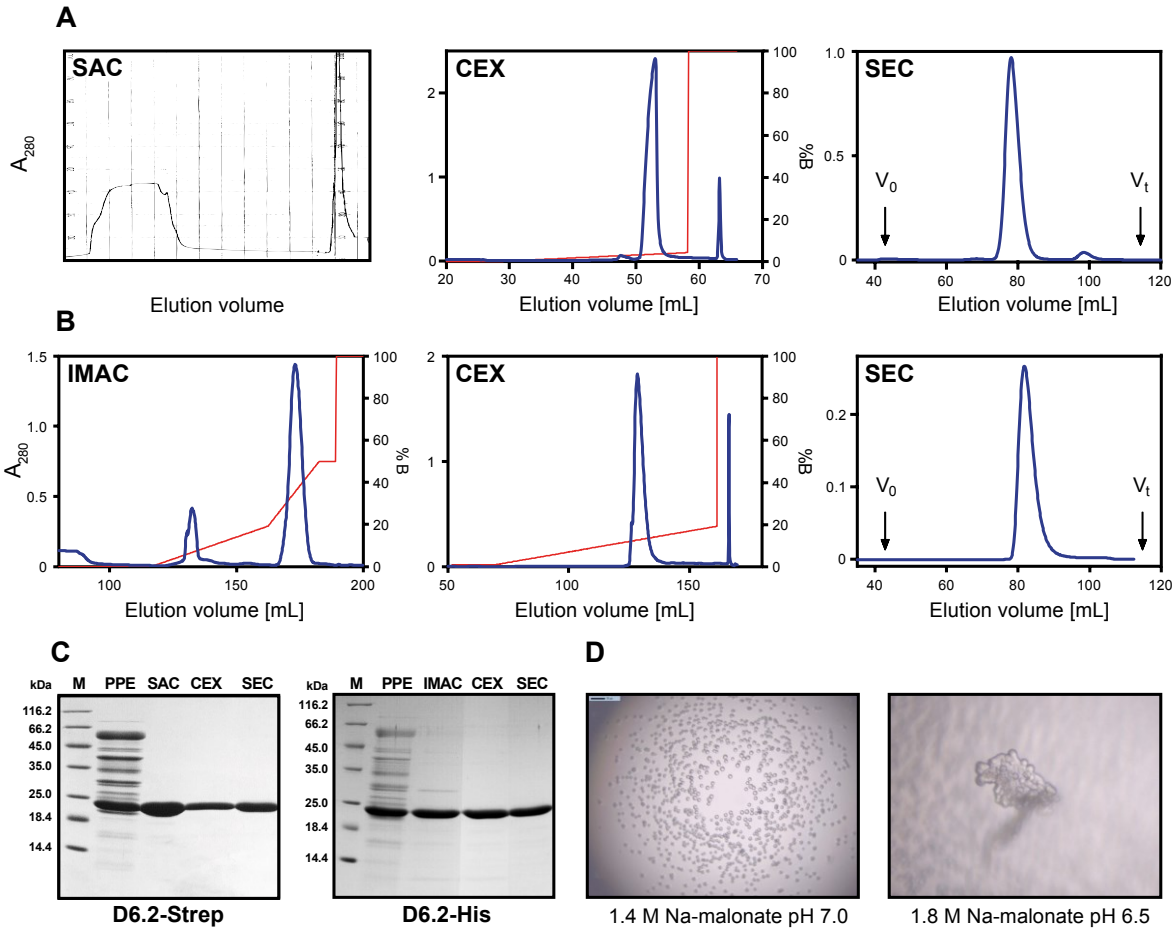

Figure 3.24. Purification and crystallization of the Colchicalin D6.2 with different C-terminal affinity tags. Protein yield from *E. coli* culture was ~1.5 mg/L*OD_{550} for both variants. **A:** Purification of the Colchicalin D6.2 with a C-terminal *Strep*-tag II. V_0 and V_t indicate the void and the total column volume, respectively. **B:** Purification of D6.2 with a C-terminal His_6-tag. **C:** SDS-PAGE analysis of the purification steps (reducing conditions). M – protein marker, PPE – periplasmic extract, SAC – elution fraction from SAC, IMAC – elution fraction from IMAC, CEX – elution fraction from CEX, SEC – elution fraction from SEC. **D:** Pseudo-crystals with spherolit morphology formed under conditions with sodium malonate.

3.3.2 Crystallization of the Colchicalin D6.2(M69Q) with an N-terminal affinity tag

The plasmid pASK-IBA4 (IBA, Göttingen) was used as a vector for the expression constructs. It contains the OmpA signal sequence followed by a *Strep*-tag II and a KasI restriction site that allows in-frame insertion of a coding region starting with two codons for a Gly-Ala linker (Figure 3.25A).

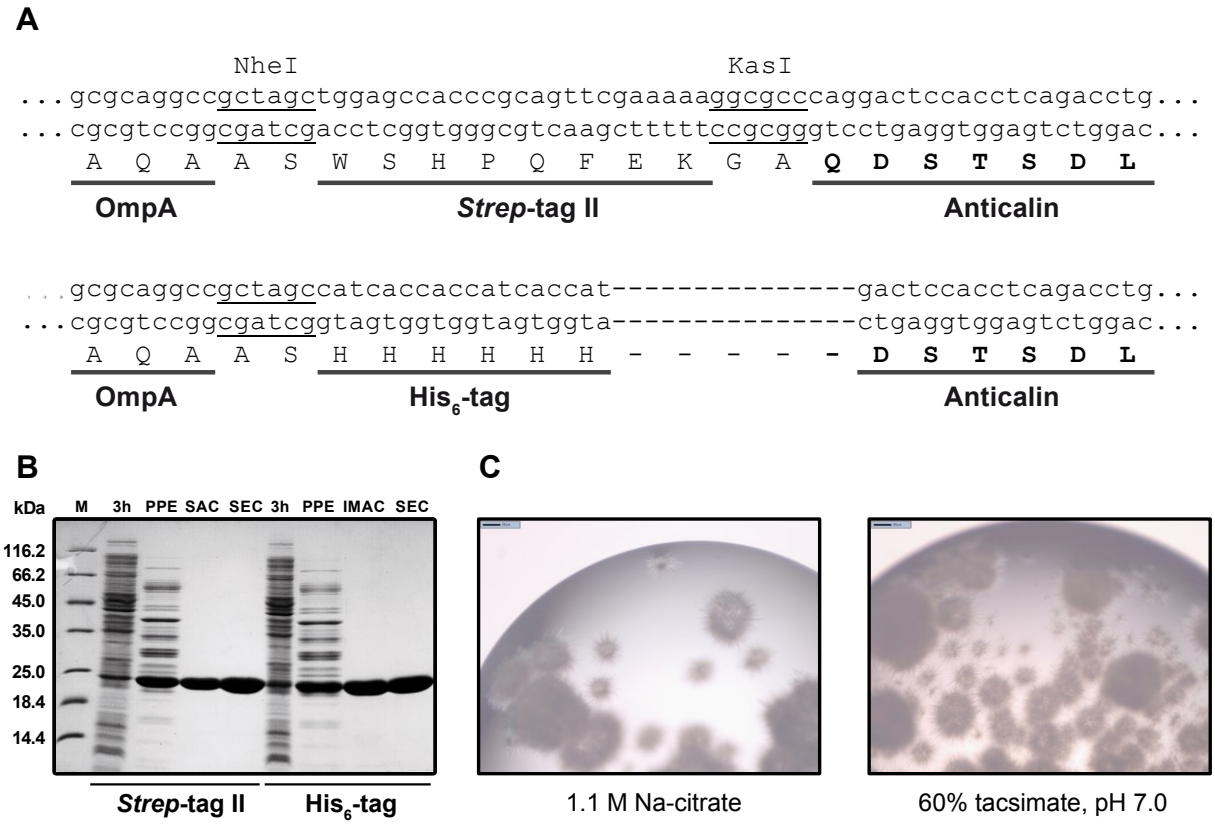

Figure 3.25. Purification and crystallization of the Colchicalin D6.2(M69Q) with an N-terminal affinity tag. **A:** Sequence alignment of the two expression constructs used for crystallization. The BstXI-cassette was inserted into the plasmid pASK-IBA4, which carried a gene of a different Lcn2-based Anticalin. The second construct (with a His_6-tag) was obtained from the first via PCR using the primers N-His-(DST)-Lcn2_for and PR1. **B:** SDS-PAGE analysis of the protein expression and purification (reducing conditions). The yield of the *Strep*-tag II version was 2.8 mg/L*OD_{550} and for the His_6-tag version 2.5 mg/L*OD_{550}. **C:** Aggregates covered with crystalline needles appeared for both *Strep*- and His-tagged versions in the refinement screens.

For the construction of N-terminal affinity tag fusions, several changes in the expression cassettes were made. First, a point mutation M69Q was introduced. The aim of this substitution was to eliminate the surface-exposed methionine residue: these are particularly prone to oxidation by air and can bring heterogeneity into the protein sample, thus deteriorating the crystal quality. The variant D6.2(M69Q) was originally obtained and tested by Elena Ilyukhina as part of her internship; the mutation led to a slight (~1.5-fold) decrease in affinity but also to an almost 2-fold increase in expression yield. The mutant is also referred to as ‘D6.3’ and was

used for all further crystallization trials. The second change concerned only the construct with a His_6-tag: during construction of the gene cassette by PCR, the Gly-Ala-linker between the tag and the N-terminus of the Anticalin was deleted together with the first Gln residue of the mature lipocalin. This allowed shortening of the flexible N-terminus and simultaneously reduced the required length of the PCR primers.

Both proteins were expressed according to the same protocol as in Chapter 3.3.1. Ion exchange chromatography was omitted because both proteins were pure already after the affinity chromatography step, as judged by SDS-PAGE analysis (Figure 3.25B). Since the use of NaCl-free buffers or incubation at lower temperature did not improve crystallization of the previous protein constructs, 10 mM MES/NaOH, 50 mM NaCl, pH 6.0 and incubation at 20 °C were applied for all following crystallization experiments. Both proteins were concentrated to 34 mg/mL and colchicine was added at a 2-fold molar concentration. After filtration with 0.45 µm spin-off filter units, in-house crystallization screens were set.

Despite the 50 % higher protein concentration, only 5 % of drops contained precipitate after one week, demonstrating even higher solubility of the new protein constructs. Many drops contained spherical pseudo-crystals, and some – mostly with sodium malonate, sodium citrate or tacsimate – contained protein aggregates covered with a ‘fur coat’ of thin needles (Figure 3.25C). Variation of precipitant concentrations, pH values or inclusion of additives did not improve the crystal morphology.

3.3.3 Crystallization of the methylated Colchicalin D6.2(M69Q) with an N-terminal affinity tag

Exhaustive methylation of protein Lys side chains is a common approach for reducing protein solubility and improving the crystallizability, because it can promote formation of crystal contacts by increasing the hydrophobicity. For the chemical protein modification, formaldehyde was used as a methyl group donor in combination with dimethylaminoborane for reducing the intermediate imines to amines in the Eschweiler–Clarke methylation.

Methylation was performed with purified proteins, which were separated from the reaction side products by an additional SEC step. Interestingly, the methylated proteins showed a slightly increased retention volume, most probably due to the increased hydrophobicity causing stronger interaction with the SEC column matrix (see Figure 3.26A). Complete methylation of all lysines was confirmed by ESI-MS analysis for both the *Strep*- and the His-tagged version (results for the *Strep*-tag II version are presented in Figure 3.26B). Ligand affinities of the native and the methylated versions were tested by fluorescence titration, which confirmed that methylation did not decrease affinity of the Anticalin towards colchicine (Figure 3.26C).

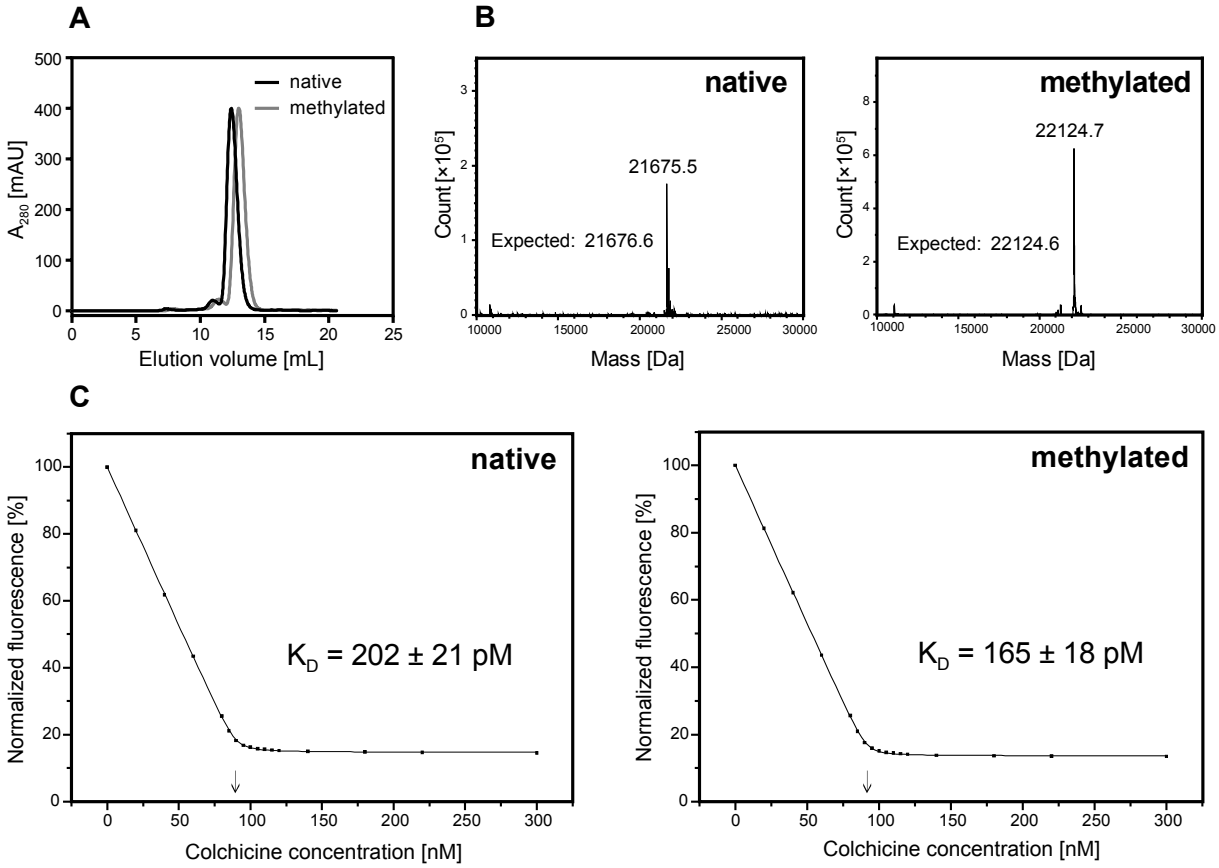

Figure 3.26. Purification and analysis of the methylated Colchicalin D6.2(M69Q) with an N-terminal *Strep*-tag II. **A:** Size exclusion chromatography using a Superdex S75 13/300 GL column. The methylated protein migrated through the column slower than the native version, presumably due to stronger interaction with the column matrix. **B:** ESI-MS analysis of the native and the methylated Anticalin. The expected molecular mass was calculated assuming formation of the structural disulfide bond, and for the methylated version, double methylation of all Lys residues, including the one in the *Strep*-tag II and the N-terminus. **C:** Determination of dissociation constants of the Anticalin by fluorescence titration before and after methylation at 100 nM protein concentration. The point of equimolarity is indicated with an arrow.

After concentration of the *Strep*- and His-tagged versions to 25 and 30 mg/mL, respectively, the crystallization screens were set as described before. These screens revealed 7.5 % of drops with precipitate and produced spherical pseudo crystals of similar morphology. Thus, in this case methylation failed to improve the protein crystallizability.

3.3.4 Purification of the tag-free Colchicalin D6.2(M69Q)

The presence of unstructured, flexible peptide termini increases the protein entropy and usually contributes negatively to its ability to form well-ordered crystals. In the previous trials, the Anticalins carried an affinity tag at the N- or C-terminus. At the expense of purification simplicity and yield, it was decided to try crystallizing the Colchicalin D6.2(M69Q) without any affinity tags.

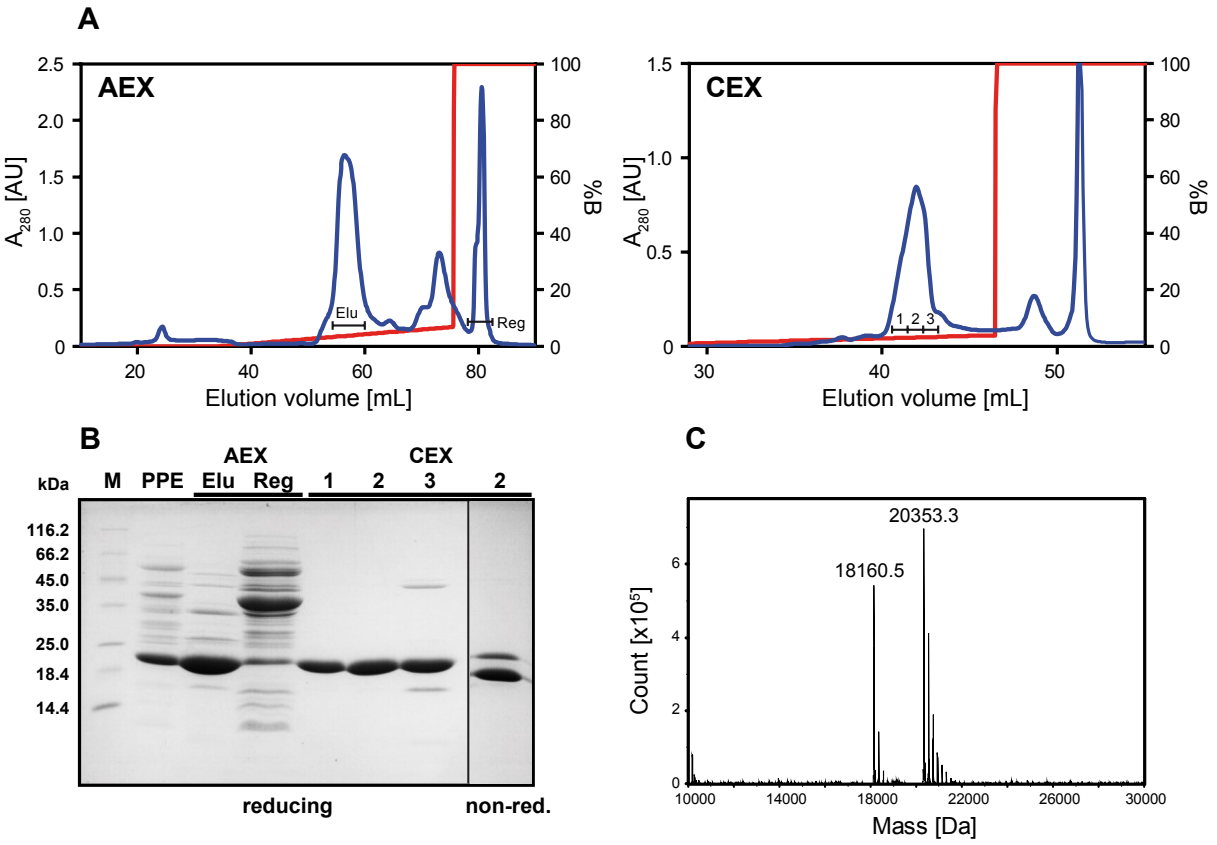

Figure 3.27. Purification and analysis of the tag-free Colchicalin D6.2(M69Q). **A:** Purification using ion exchange chromatography. AEX was performed on a 6 mL Resource Q column (GE Healthcare) with 20 mM CHES/NaOH, pH 9.5 as running buffer; CEX was performed on a 6 mL Resource S column (GE Healthcare) with 20 mM MES/NaOH, 10 mM NaCl, pH 5.5 as running buffer. In both cases, elution was triggered by a concentration gradient of 0–500 mM NaCl in 120 mL (20 column volumes; solvent B = 2 M NaCl). **B:** SDS-PAGE analysis of the purification (reducing conditions). M – protein marker, PPE – periplasmic extract, Elu – elution fraction from AEX, Reg – fraction during regeneration with 2 M NaCl. **C:** ESI-MS analysis of the CEX fraction 2. The higher mass corresponds to the tag-free Colchicalin D6.2, the lower one to the contaminant, the periplasmic *E. coli* protein OsmY.

The C-terminal *Strep*-tag II was deleted from the expression plasmid pNGAL98 using PCR (with the primers D20 and pNGAL98_del_Strep) by introducing a stop codon directly after the last amino acid (Gly). The protein was produced periplasmically in *E. coli* JM83, the periplasmic extract was dialyzed against 20 mM CHES/NaOH, pH 9.5 and purified by anion and cation exchange chromatography (Figure 3.27A). As judged by reducing SDS-PAGE, the first two fractions of the CEX eluate were virtually pure; however, when the fraction 2 was analyzed on a non-reducing SDS-PAGE gel, a second band became visible (Figure 3.27B). To determine the origin of this band, fraction 2 was analyzed by ESI-MS (Figure 3.27C). Indeed, a second molecular species with a mass of 18160.5 Da was found, which did not correspond to any possible proteolytic fragment of Colchicalin D6.2(M69Q). A search for similar proteins in the *E. coli* Protein Database EcoProDB (https://eecoli.kaist.ac.kr) revealed an exact match with osmotically inducible protein Y (OsmY) having a mass of 18161.2 Da and a theoretical

p*I* of 5.42. In the original article, the protein was shown to migrate on SDS-PAGE 'with an apparent molecular mass of 22 kDa' (Yim & Villarejo, 1992), thus making it undistinguishable from the Colchicalin D6.2 on a reducing SDS-PAGE. Surprisingly, even though possessing a theoretical p*I* of 6.79, D6.2 was not separated from OsmY even after two ion exchange chromatography steps.

Although it would have been possible to purify the tag-free Colchicalin D6.2 by further optimization of the purification strategy (e.g. change of the ion exchange matrix or use of hydrophobic interaction chromatography), a more elegant strategy was developed instead to crystallize the tag-free Colchicalin D6.2(M69Q).

3.3.5 Construction of expression vectors for the cytoplasmic expression of lipocalin variants as fusion proteins with SUMO

SUMO (Small Ubiquitin-like Modifier) is a 11 kDa eukaryotic protein, which is covalently attached to other proteins *in vivo*, thus modifying their functions in a manner similar to ubiquitin. Due to its small size, robustness and high expression yield in *E. coli*, SUMO is often used as a fusion partner to increase solubility, stability and expression yields of other proteins. Availability of a highly specific protease Ulp1, which recognizes the tertiary structure of SUMO protein and efficiently cleaves it from the fusion partner downstream of the C-terminal Gly-Gly motif, makes this pair a valuable tool for production of tag-free proteins for various purposes (Malakhov *et al.*, 2004).

For production of the fusion protein in *E. coli*, the expression system was changed from periplasmic to cytoplasmic. Generally, Anticalins based on human lipocalin 2 cannot be expressed in the *E. coli* cytoplasm because formation of the structural disulphide bond requires oxidizing environment. However, the *E. coli* strain Origami B facilitates formation of the disulfide bond because of its less reducing cytoplasmic milieu, which is achieved by mutations in the thioredoxin reductase (trxB) and glutathione reductase (gor) genes (Prinz *et al.*, 1997). The plasmid pASK75-T7RBS2 (Figure 3.28A) was chosen as expression vector, carrying a T7-derived ribosome binding site that enhances efficient translation of heterologous proteins in *E. coli* (Olins *et al.*, 1988).

In order to express the cleavable fusion protein, an expression cassette consisting of an N-terminal His_6-tag, the SUMO protein and the mature Colchicalin D6.2(M69Q) was constructed (Figure 3.28B). Due to the location of the Ulp1 cleavage site, the resulting tag-free Anticalin carried an additional Ala residue on its N-terminus (Figure 3.28C, above). The Anticalin sequence from the plasmid pASK-IBA4 (Chapter 3.3.2, Figure 3.25A) was inserted into the cassette using digestion with KasI and XhoI restriction sites.

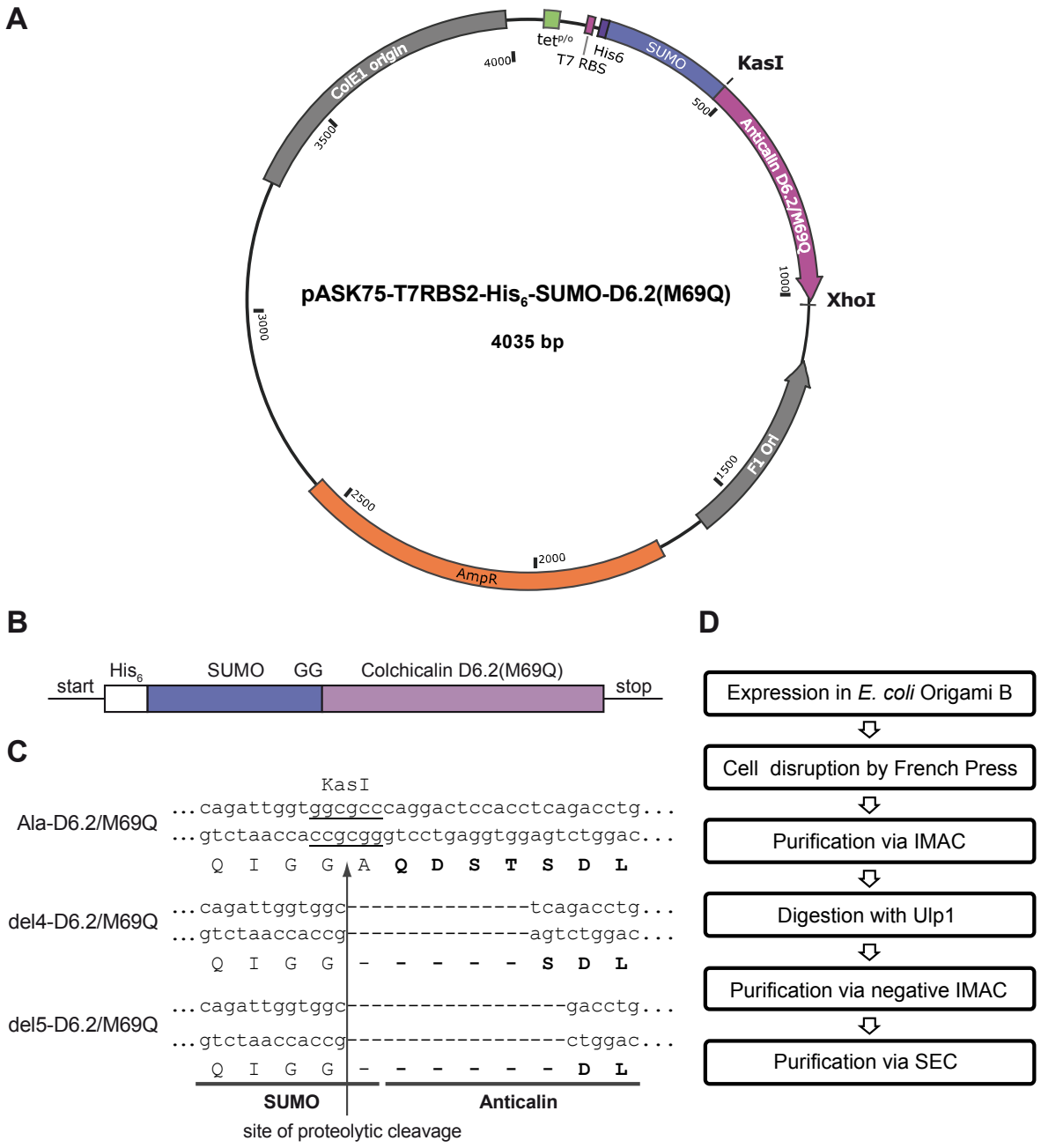

Figure 3.28. Production of the Colchicalin D6.2(M69Q) as a fusion with SUMO. **A:** Map of the plasmid vector pASK75-T7RBS2-His$_6$-SUMO-D6.2(M69Q). **B:** Scheme of the expression cassette. **C:** Nucleotide and amino acid sequences of the linker region between SUMO and the Anticalin. The Ulp1 protease cleaves the fusion protein after the second Gly residue. **D:** Workflow of protein expression and purification.

3.3.6 Production of the SUMO fusion protein and crystallization of the tag-free Colchicalin D6.2(M69Q)

For cytoplasmic production, *E. coli* Origami B cells were grown at 30 °C to an OD_{550} of 0.5, then the temperature was decreased to 22 °C, and 30 min later protein expression was induced by addition of 200 µg/L aTc. After 4 hours, cells were harvested, disrupted by a French press in IMAC buffer, centrifuged for 30 min at 18,000 ×*g* and purified by IMAC (Figure 3.29B).

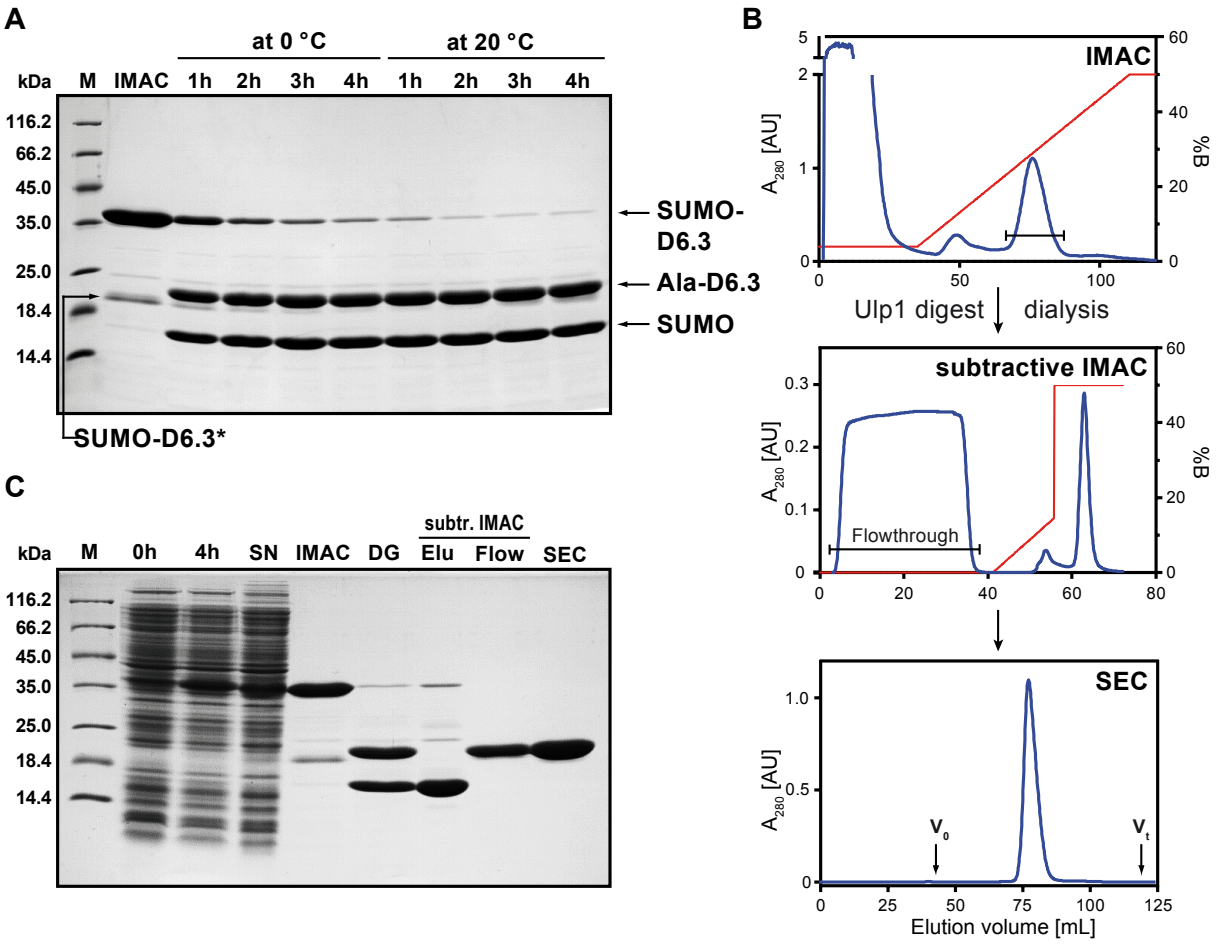

Figure 3.29. Production, proteolytic digest and purification of the tag-free Colchicalin D6.2(M69Q) (=D6.3). **A:** SDS-PAGE analysis (reducing) of a test digest of the fusion protein SUMO-Colchicalin with Ulp1 protease at two different temperatures. SUMO-D6.3* most probably corresponds to a prematurely terminated protein. **B:** Purification of the tag-free Colchicalin D6.2(M69Q). A standard IMAC was followed by a subtractive IMAC, whose flowthrough was concentrated and purified by SEC. **C:** SDS-PAGE analysis (reducing) of the proteolytic digest and purification. 0h – whole-cell extract before induction of protein expression, 4h – whole-cell extract after 4 hours of protein expression, SN – supernatant after centrifugation of the whole-cell extract, IMAC – elution fraction of the first IMAC, DG – sample after the Ulp1 digest, Elu – elution fraction of the subtractive IMAC, Flow – flowthrough of the second, subtractive IMAC.

In the next step, the fusion protein was cleaved by the Ulp1 protease. In order to determine the optimal temperature and incubation time for the proteolytic reaction, the IMAC elution fraction was dialyzed against Ulp1 buffer (40 mM KP_i, 150 mM NaCl, pH 7.5) and two aliquots of 1 mg protein were mixed each with 1 µg of Ulp1 protease. The first aliquot was kept at 20 °C and the second was put on ice. During the incubation, 20 µL samples were taken each hour, mixed with SDS-PAGE loading buffer and heated to 95 °C for 5 min to stop the proteolysis reaction. As seen in the SDS-PAGE analysis (Figure 3.29A), most protein was completely digested after 4 h even at 0 °C. An additional band at ~20 kDa visible in the IMAC-purified fraction (Figure 3.29A) most probably corresponded to a prematurely terminated fusion protein

consisting of full-length SUMO and part of the Anticalin. This assumption is supported by the fact that this protein species also underwent proteolysis by Ulp1. The resulting contaminating fragment must have passed the purification by subtractive IMAC together with the Anticalin but must have been fully separated from the full-length Anticalin via SEC.

The rest of the IMAC elution fraction from above was then digested with Ulp1 for 4 h at 20 °C and purified by subtractive IMAC (Figure 3.29B&C). The flowthrough from the IMAC was already pure on SDS-PAGE, but preparative SEC was performed to change the buffer and to ensure complete separation of possible fragments, aggregates or oligomers. Finally, 13 mg of pure full-length Colchicalin D6.2(M69Q) in 10 mM MES/NaOH, 50 mM NaCl, pH 6.0 were mixed with a double molar amount of colchicine (0.1 mM final), concentrated to 42 mg/mL via a centrifugal ultrafiltration unit and used for random factorial screens (see Table 8.3).

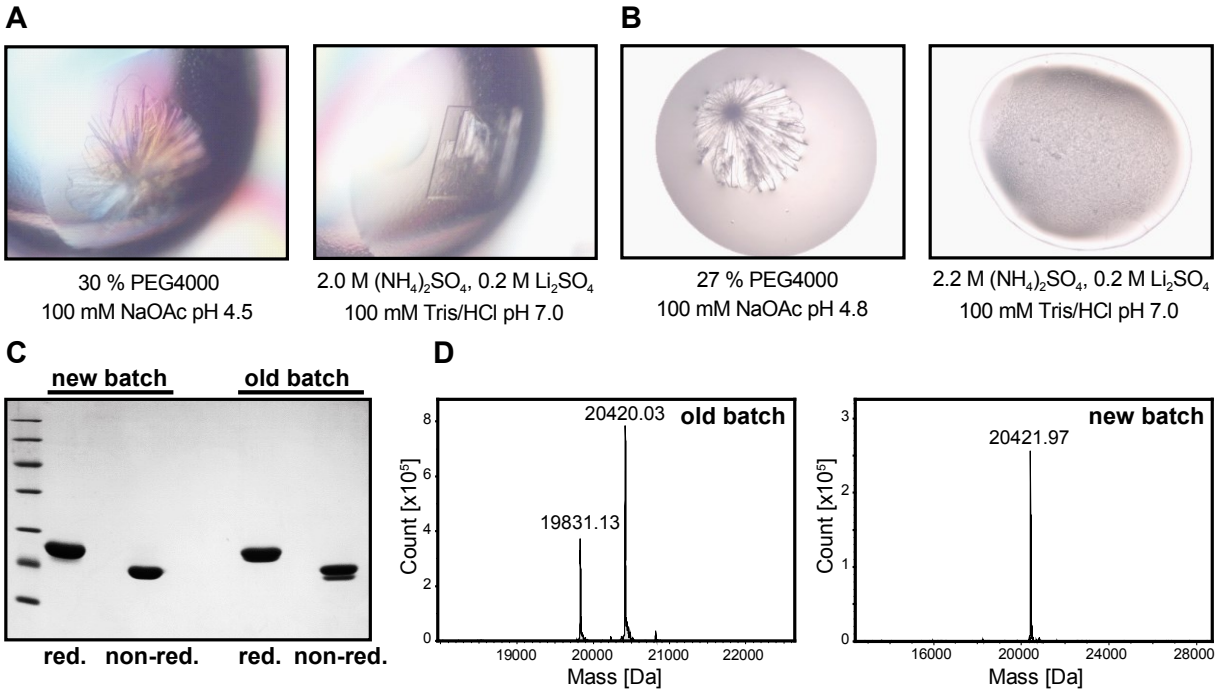

Figure 3.30. Crystallization and analysis of the tag-free Colchicalin D6.2(M69Q) expressed as fusion with SUMO. **A:** Crystals in the random factorial screens. **B:** Platelet-shaped (left) and spheroid (right) crystals in the refinement screens. **C:** SDS-PAGE analysis (reducing and non-reducing) of the protein batches used for crystallization. Both samples were analyzed under reducing and non-reducing conditions. **D:** ESI-MS analysis of the two protein batches. The higher masses correspond to the tag-free Colchicalin D6.2(M69Q) with an additional N-terminal alanine; the smaller mass in the old batch corresponds to the same Anticalin, from which the first 6 N-terminal amino acids AQDSTS were cleaved off proteolytically.

Already on the next day, clear platelet-like crystals appeared in three wells containing 30 to 36 % PEG4000. Two days later, thin crystals in drops with 25 % PEG monomethyl ether could be distinguished, and a week later a thick, clear crystal with sharp edges was found in a well containing 2 M ammonium sulfate and 200 mM lithium sulfate (Figure 3.30A). For the

refinement screens, a fresh batch of protein was produced, purified accordingly and concentrated to 52 mg/mL. Refinement screens were set using the hanging drop technique, with drops consisting of 2 µL water, 0.7 µL protein and 0.7 µL reservoir solution.

Crystals formed in the presence of PEG4000 were easily reproduced in the refinement screens but retained their thin platelet morphology. However, an attempt to reproduce the crystals grown in the presence of ammonium sulfate, which exhibited the best morphology, resulted in thousands of spherical pseudocrystals in the whole concentration range 1.6– 2.2 M ammonium sulfate (Figure 3.30B). Since a fresh batch of protein was used for the refinement screens, batch-to-batch variation needed to be excluded as a possible reason for the observed inconsistency. Hence, samples from the two batches were analyzed on reducing SDS-PAGE with lower protein amount, leading to detection of a vague second band in the sample from the first, older batch. This band migrated so close to the main Anticalin band that it was hardly detectable; however, it appeared distinct on non-reducing SDS-PAGE (Figure 3.30C). ESI-MS analysis of the samples revealed the presence of an abundant second species, whose mass corresponded to the Colchicalin D6.2(M69Q) with the N-terminus shortened by 5 amino acids (as well as the N-terminal Ala residue that remained after the cleavage; see Figure 3.30D).

The presence of a shortened species in the old protein batch and the failed attempt to reproduce the well-looking crystals with the fresh protein implied that the shortened species itself could have produced the crystals. Making use of this coincidence, an Anticalin with a similarly shortened N-terminus was designed (see below). This idea found additional support in the fact that the N-terminal polypeptide segments were not resolved in any of the X-ray structures of Anticalins available to date. In most of them, electron density starts with the 5th or the 6th amino acid. Accordingly, two expression constructs with a deletion of the first 4 or 5 amino acids of the Colchicalin D6.2(M69Q) were created and tested for crystallizability.

3.3.7 Production of the SUMO fusion Anticalin and crystallization of the tag-free Colchicalin D6.2(M69Q) with a shortened N-terminus

The constructs with N-terminal deletions (Figure 3.28C) were prepared using QuikChange mutagenesis with the primer pairs SUMO-del4-Lcn2 and SUMO-del5-Lcn2 (Figure 3.28C). The Ala residue following the SUMO protein sequence was also deleted. Both protein versions were produced in *E. coli* Origami B, and the cell extract was purified by IMAC as described in the previous chapter. Since the N-terminal shortening of the Anticalin could have reduced sterical accessibility of the Ulp1 cleavage site, the proteolytic reaction was performed for 4 h at room temperature and further kept on ice for 2 days. After 2 days, nearly all protein with the deleted 4 amino acids QDST (‘del4’) was found digested, while for the shorter version (‘del5’) roughly a half remained undigested (Figure 3.31A).

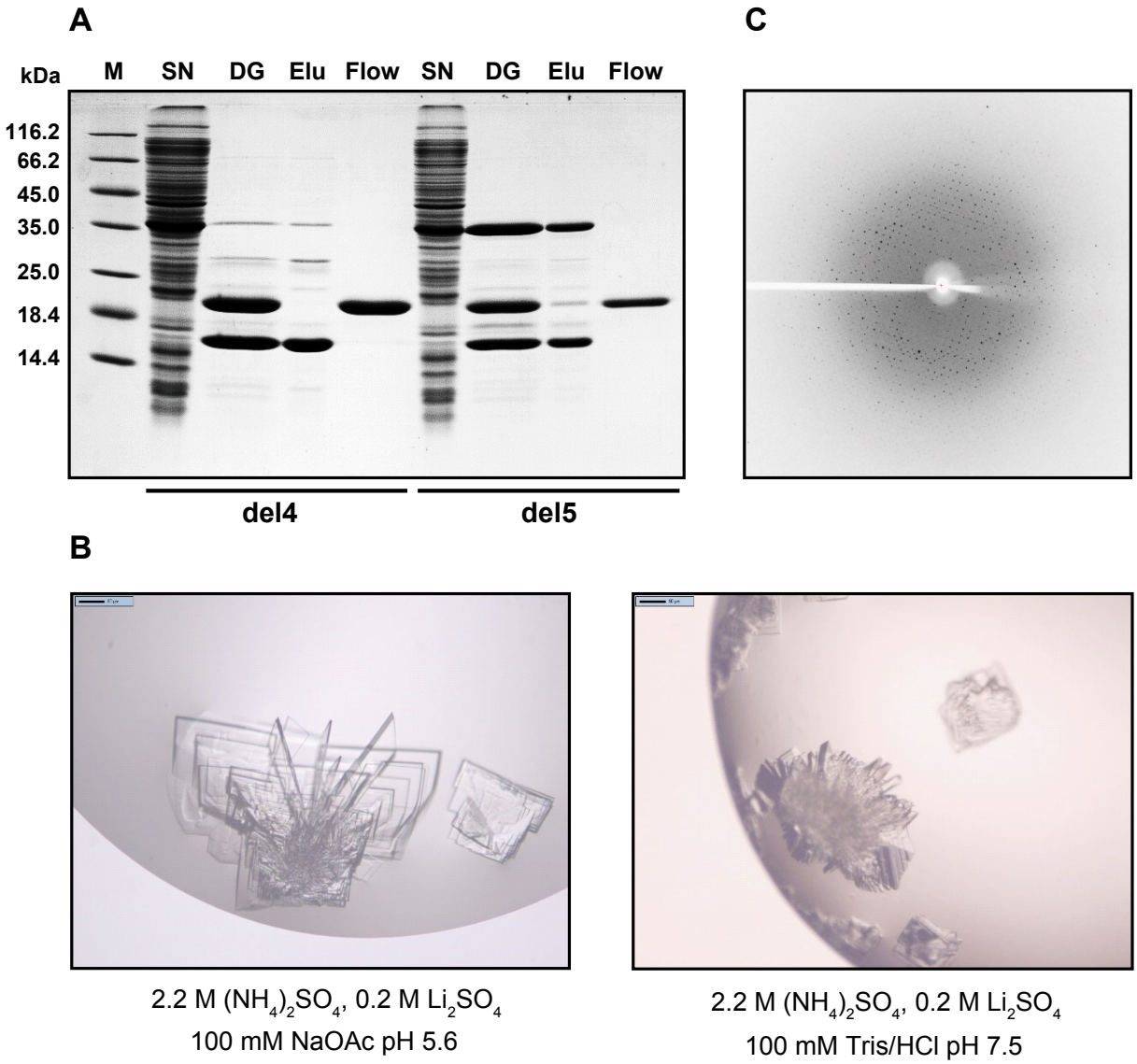

Figure 3.31. Purification and crystallization of tag-free Colchicalin D6.2(M69Q) with shortened N-terminus from a fusion with SUMO. **A:** SDS-PAGE analysis. M – protein marker, SN – supernatant after centrifugation of the whole-cell extract, DG – sample after Ulp1 digest, Elu – elution fraction of the subtractive IMAC, Flow – flowthrough. **B:** Protein crystals of the Anticalin del4-D6.2(M69Q). **C:** The X-ray diffraction pattern obtained using the BESSY beamline 14.2 (Berlin, Germany) from a fragment of the crystal in the left picture in (B).

After both proteins were purified by subtractive IMAC and SEC, random factorial screens consisting of 3 drops were set: drop 1 contained the full-length Colchicalin D6.2(M69Q) (52 mg/mL), drop 2 contained the Anticalin lacking the first 4 amino acids (42 mg/mL), and drop 3 containing the shortest construct with the deletion of the first 5 amino acids (41 mg/mL). Ligand-to-protein ratio of 2:1 was kept constant for all drops. The construct ‘del4’ reproduced crystals under all conditions also seen for the full-length construct (including the ‘best’ crystals previously obtained with ammonium sulfate) while ‘del5’ formed crystals only in one well. Hence, only the ‘del4’ construct was used for the further refinement.

Refinement of the crystallization conditions containing ammonium sulfate and lithium sulfate yielded clear crystals with a pronounced three-dimensional morphology (Figure 3.31B). Although organized in clusters, it was possible to prepare and freeze a sufficient number of monocrystals. Preparation of the crystals and collection of the X-ray diffraction datasets at the Berliner Elektronenspeicherring-Gesellschaft für Synchrotronstrahlung mbH (BESSY; Berlin, Germany) was performed by Dr. Andreas Eichinger.

3.3.8 X-ray structure of the Colchicalin D6.2/M69Q in complex with colchicine

A suitable dataset with a resolution of 2.2 Å was obtained from a fragment of the crystal grown in 2.2 M ammonium sulfate, 200 mM lithium sulfate and 100 mM MES/NaOH pH 7.5 (Figure 3.31B, right). The crystal acquired a space group $P4_122$ with one protein chain in the asymmetric unit, whose structure was solved using molecular replacement with the coordinate set of an engineered Lcn2 with specificity for Y-DTPA (PDB:3DTQ, Kim *et al.*, 2009). The initial operations during the process of structure solution up to early structure refinement were performed by Dr. Andreas Eichinger (see Appendix, Table 8.1 for the refinement statistics).

Sequence of the crystallized Anticalin construct started with residue Ser5, which was also the first amino acid visible in the electron density. The density continued to Ile176 and included complete colchicine ligand, leaving only the two last C-terminal amino acids, as well as residues Ile97 to Pro101, poorly resolved (Figure 3.32).

The core fold of the engineered lipocalin appeared intact, as illustrated by the low RMSD of 0.834 Å for the 58 Cα-atoms of the β-barrel (see Chapter 2.8.3) if superimposed with the crystal structure of lipocalin 2 (mutant K125A, PDB:3CMP). However, the flexible loops at the opening of the ligand pocket underwent deep structural changes, adapting the protein for the high shape complementarity towards colchicine. The total RMSD of 2.512 Å for the flexible loops resulted from loop #2 being bent inwards by up to 11.1 Å, loop #3 bent inwards by up to 6.4 Å and loop #4 bent outwards by up to 7.3 Å, while the conformation of loop #1 remained similar to lipocalin 2. Loops #2 and #3 form a narrow entrance to a binding pocket 12 Å deep with a mostly hydrophobic inner surface. The complexed colchicine ligand protrudes deeply down to the bottom of this pocket while its acetamide group is positioned at the opening of the cleft and is exposed to the solvent.

Analysis of the complex crystal structure using PISA (Krissinel & Henrick, 2007) revealed that 88.7 % (547.7 of 617.7 $Å^2$) of the accessible surface of colchicine is buried upon binding to the Anticalin. This large buried surface results from 25 amino acid residues of the engineered lipocalin that form van-der-Waals contacts with the ligand (Table 3.4). 15 of their side chains are of hydrophobic nature (7 aliphatic and 8 aromatic) and are responsible for the high

hydrophobicity of the binding pocket. Thr136 represents an exception, being located in a hydrophobic environment at the bottom of the β-barrel, in just 3.5 Å distance to the ligand. Although 4 of the 9 hydrophilic amino acids are charged, they interact with the ligand via their backbone, their side chains being directed away from the ligand.

Table 3.4. Residues of the Colchicalin•colchicine complex that form van der Waals contacts with the ligand.

Residue	Buried surface [Å^2]	Residue	Buried surface [Å^2]	Residue	Buried surface [Å^2]
Val33	6.4	Gln69	6.0	Trp106	37.2
Val36	3.7	Lys70	13.0	Phe123	10.2
Gly40	8.3	Phe71	64.7	Arg130	12.8
Phe41	17.7	Met73	2.6	Asp132	12.5
Met51	12.6	Met79	13.8	Phe134	34.9
Thr54	2.6	Asp81	3.0	Thr136	6.2
Tyr56	1.4	Leu94	15.6	Tyr138	8.6
Val66	5.5	Gly102	1.8		
Phe68	45.0	Thr104	0.3	**Total:**	**547.7**

As noted above, the aromatic amino acids are responsible for a considerable part of the ligand-protein interactions. Trp106 with a 37.2 Å contact surface (6.8 % of the total buried surface on the protein side) covers a large part of the colchicine molecule on one side, while Phe68 stacks to the planar colchicine ring A (45.0 Å^2 or 8.2 %) on the other side, and Phe71 interacts with the tropone ring C (64.7 Å^2 or 11.8 %). In addition, residues Phe41, Phe123 and Phe134 mutually form a triple π-stack, the latter involved in a 34.9 Å^2 contact surface (6.4 % of total).

Figure 3.32. Crystal structure of the Colchicalin D6.2(M69Q). **A:** Van der Waals surfaces of Colchicalin D6.2(M69Q) and wild-type Lcn2 (PDB:3CMP), view from the top of each binding pocket. The ligands (colchicine and ferric enterobactin, respectively) are shown as stick models. **B:** Superposition of Colchicalin D6.2(M69Q) (purple) and wild-type Lcn2 (green) crystal structures, shown as ribbon models in two projections. The two structures were aligned via the conserved residues of the β-barrel (see Chapter 2.8.3). **C:** Electrostatic surface of Colchicalin D6.2(M69Q). Negative charge is shown in red, positive in blue. Several amino acid residues interacting with the ligand are shown as stick models under the translucent surface. **D:** Close-up view of colchicine in the binding pocket. Several amino acid residues interacting with the ligand are shown as stick models. Thin blue lines represent hydrogen bonds. The three water molecules fixed at the bottom of the binding site are indicated as red spheres.

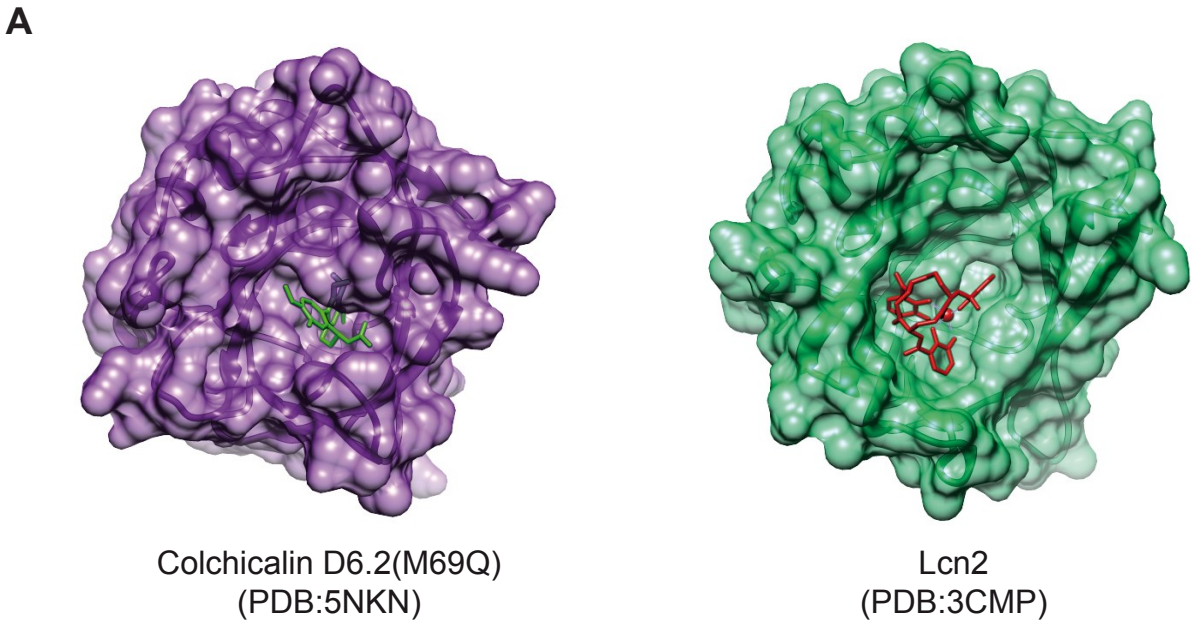
A
Colchicalin D6.2(M69Q)
(PDB:5NKN)
Lcn2
(PDB:3CMP)

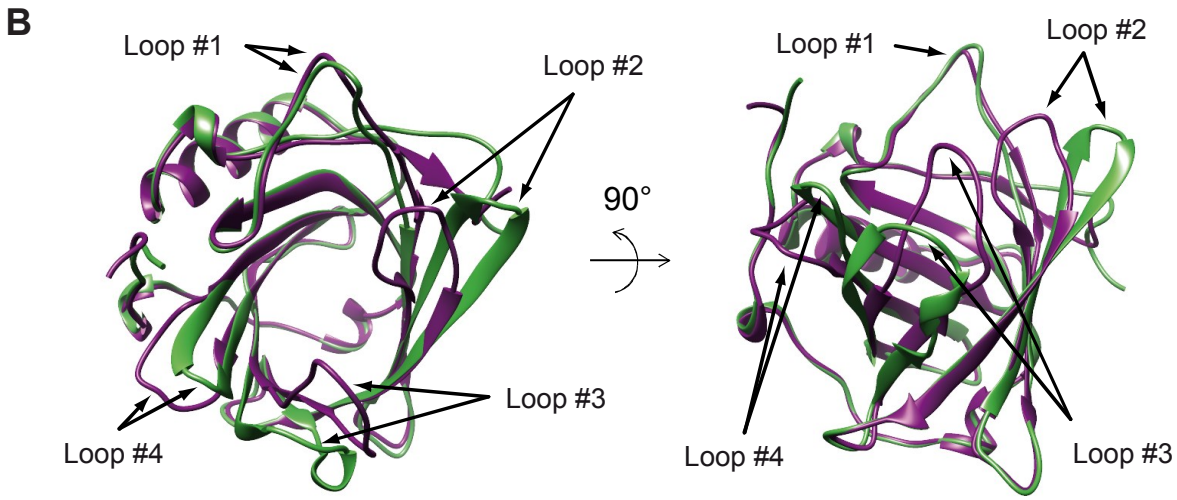
B
Loop #1
Loop #2
Loop #3
Loop #4
90°
Loop #1
Loop #2
Loop #4
Loop #3

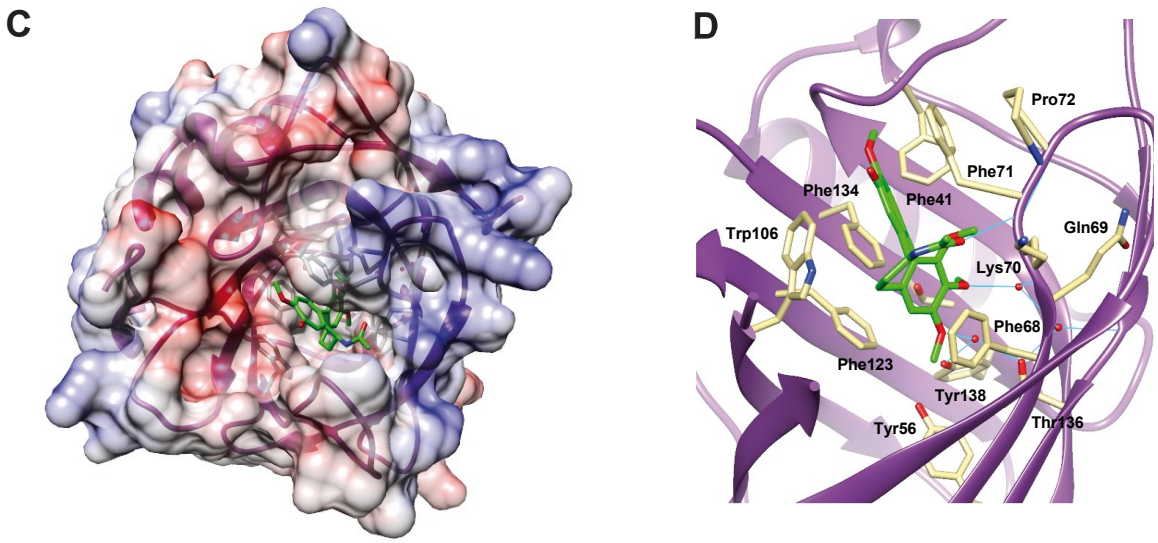
C
D
Pro72
Phe71
Phe134
Phe41
Trp106
Gln69
Lys70
Phe68
Phe123
Tyr138
Tyr56
Thr136

A special feature of this Anticalin structure is the conformation of its loop #2 (residues 70–76). The 11 Å inward shift does not only narrow the entrance to the ligand cleft but also allows Phe71 to stack to the tropone ring, thus shielding this highly hydrophobic moiety from solvent and improving the shape complementarity. In addition to the π-stacking explained above, Phe71 forms a hydrogen bond with the oxygen atom of the *N*-acetamide group of colchicine. The orientation of Phe71 in the complex is defined by another unusual feature – the *cis*-conformation of the peptide bond between Phe71 and Pro72. Interestingly, bending of loop #2 starts at residue 69, which was mutated from Val to Met in the original Anticalin D6.1 (and later to Gln; see Figure 3.32B) accompanied by a 10-fold increase in affinity.

Even though colchicine possesses only few atoms capable of forming hydrogen bonds, the structure of the complex is stabilized by a complex hydrogen bond network. Apart from the mentioned H-bond between the *N*-acetamide group and Phe71, several H-bonds are mediated by the three crystallographically defined water molecules at the bottom of the binding pocket. From the total of 10 H-bonds in this network, 3 connect to the two methoxy groups of colchicine and 7 anchor them in the protein scaffold (via OH-groups of Tyr54 and Tyr138, the peptide carbonyl of Ala52, as well as the peptide amide and carbonyl of Gln69). An additional hydrogen bond is formed between residues Tyr56 and Tyr138, which both directly contact the ligand.

3.4 Design of Anticalins against colchicine as biochemical tools

3.4.1 Development of a competitive ELISA for colchicine quantification

The high affinity of the Colchicalin D6.2 should allow its use as a capturing reagent for the detection and quantification of colchicine in biological fluids. To this end, a simple competitive ELISA was developed and tested for applicability as a tool for colchicine analytics.

Setup of the ELISA is depicted in Figure 3.33A. First, the bottom of a plastic 96-well plate is coated with the Colchicalin in PBS overnight and washed. The analyte is then supplied with a predefined concentration of the tracer (biotinylated colchicine, see Figure 3.1) and incubated in the Colchicalin-coated plate, followed by washing. Then ExtrAvidin-AP conjugate is added, and, after the final washing step, the bound tracer is detected by adding p-nitrophenol (pNP). For the proper functioning of the assay, several parameters had to be determined: (1) optimal Anticalin concentration for coating of the ELISA plate, (2) optimal tracer concentration, (3) sensitivity range and (4) influence of plasma components on the sensitivity of the assay.

As seen in Figure 3.33B, increase of the Anticalin concentration used for coating to more than 6.4 µg/mL did not lead to an increase in the signal strength, indicating saturation of the well binding capacity or exhaustion of ExtrAvidin used as secondary reagent. Thus, an Anticalin concentration of 5 µg/mL was chosen for subsequent experiments. To determine the optimal

tracer concentration and sensitivity range, a dilution series of free colchicine in PBS was tested with four different tracer concentrations (Figure 3.33C). As expected, the highest tracer concentration led to the highest signal; however, resolution in the low analyte concentration range decreased. As a compromise, a tracer concentration of 10 nM was set as standard. As seen in Figure 3.33C, for the samples with low tracer concentrations the curve shape was close to linear down to sub-nanomolar concentrations.

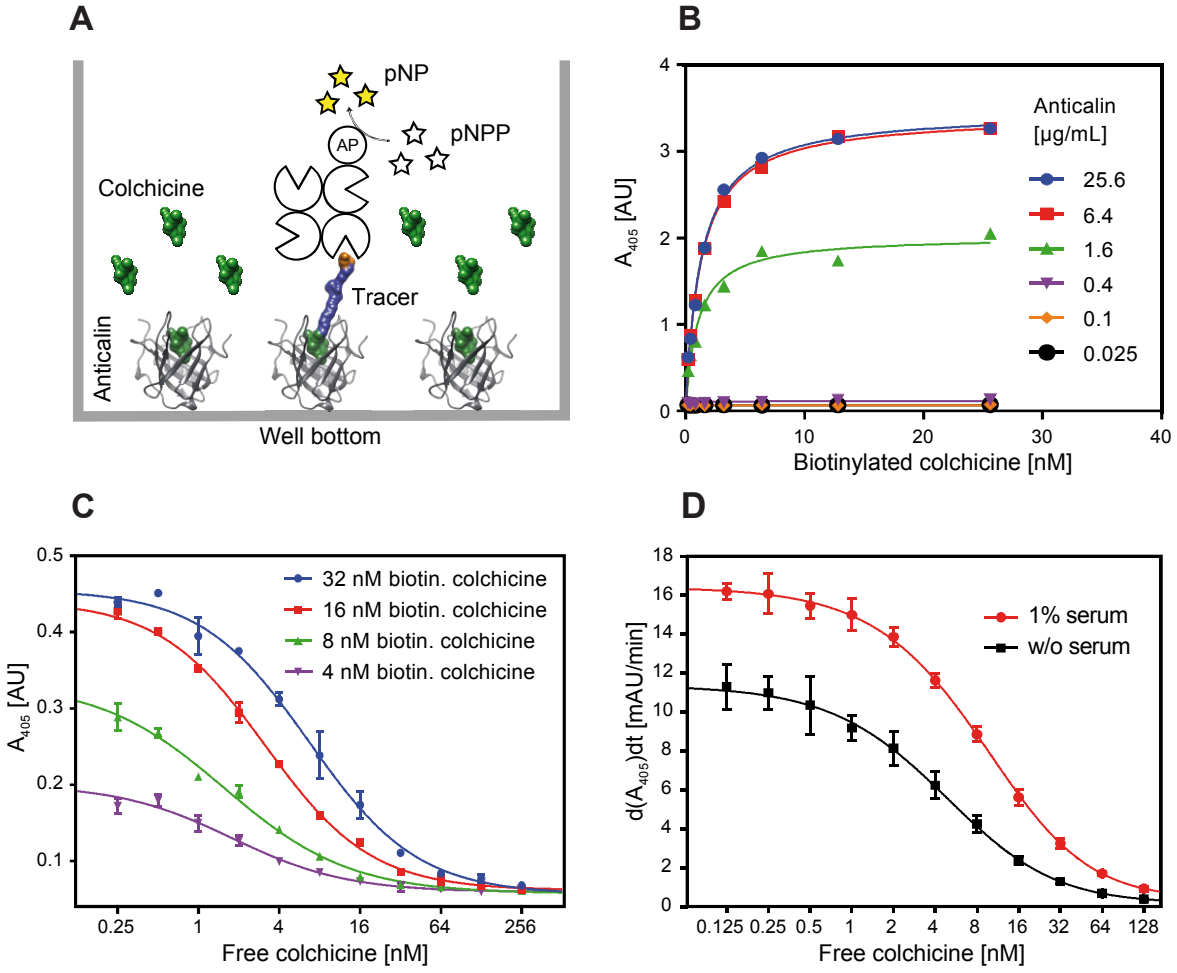

Figure 3.33. Competitive ELISA for quantification of colchicine. **A:** Schematic representation of the ELISA setup. The ELISA plate was coated with the Anticalin, and a mixture of free colchicine (analyte) and biotinylated colchicine (tracer) was applied, followed by detection of the bound tracer via ExtrAvidin-AP conjugate and p-nitrophenol phosphate. **B:** Determination of optimal concentrations for the Anticalin and the tracer. In this experiment, no free colchicine was added. **C:** Determination of the sensitivity range with 5 µg/mL Colchicalin and different tracer concentrations. **D:** Assessment of the effect of human serum in the sample. Black curve – colchicine dilution in PBS, red curve – colchicine dilution in 1 % human serum in PBS.

Finally, in order to estimate the influence of human serum in the sample, a dilution series of colchicine was prepared in parallel in pure PBS and in PBS with 1 % (v/v) human serum (corresponding to a 100-fold dilution of the theoretical samples). As seen in Figure 3.33D, the average signal intensity was shifted upwards for all data points, but the shape of the curve

remained virtually unchanged, indicating that the developed ELISA can be applied for colchicine quantification in blood directly, with no need for sample extraction or purification.

3.4.2 Engineering of Colchicalins with very slow dissociation kinetics

The high affinity of D6.2 towards colchicine and its biotinylated form prompted the idea of using the Colchicalin/colchicine affinity pair as a general-purpose immobilization anchor, similar to (strept)avidin/biotin or to antibodies binding fluorescein, digoxigenin or other small molecules. For such applications, not only high affinity, but also a long complex half-life of several hours is necessary. To measure the half-life of the Colchicalin D6.2 in complex with colchicine, surface plasmon spectroscopic (SPR) analysis was implemented.

The Colchicalin D6.2 revealed a dissociation rate constant of 1.3×10^{-4} $M^{-1}sec^{-1}$, corresponding to a complex half-life of 1.5 h (Figure 3.34A). Even though this represents a fairly stable complex between a protein and a small-molecule ligand, a half-life of around 10 h would be more desirable for practical applications. To achieve this, the Colchicalin D6.2 was subjected to further affinity maturation.

The affinity maturation of D6.2 was performed by Elena Ilyukhina in the course of her internship. Generation of the error-prone library, pre-enrichment by MACS and further selection by FACS was performed in the same manner as the previous affinity maturation campaign (see Chapter 3.2). As a result, three new mutants were identified. Two of them, EI.1 and EI.3, demonstrated a more than two-fold increase in the half-life (Table 3.5, Figure 3.34B), with EI.3 exhibiting the longest complex half-life. In the next step, mutations from the Colchicalin EI.1 (K46M, K75E, K142I) were introduced one-by-one into EI.3. As a results, the mutation K142I increased the half-life of EI.3 to over 5 h, yielding the Colchicalin ‘D6.4’.

The crystal structure of D6.2(M69Q) provided guidance for the further improvement of the Colchicalin. Assuming that the mutant EI.3 retained substantial shape identity to D6.2, several mutations were suggested to improve the shape, hydrophilicity or charge complementarity between EI.3 and colchicine. In total, five point mutants of EI.3 (F41Y, T54K, T54Q, V66I, T136V) were created and tested by SPR. One of the mutations, T136V, led to a slight increase in the complex half-life. The same amino acid exchange was introduced into D6.4 to yield the Colchicalin ‘D6.5’ with a half-life of 6.8 h. Finally, an additional mutation Q77E was introduced, which had appeared several times during the affinity maturation of D6.1 (see Figure 3.22) but was not tested separately. The resulting Colchicalin ‘D6.6’ reached an impressive dissociation half-life of 9.4 h (Table 3.5, Figure 3.34B).

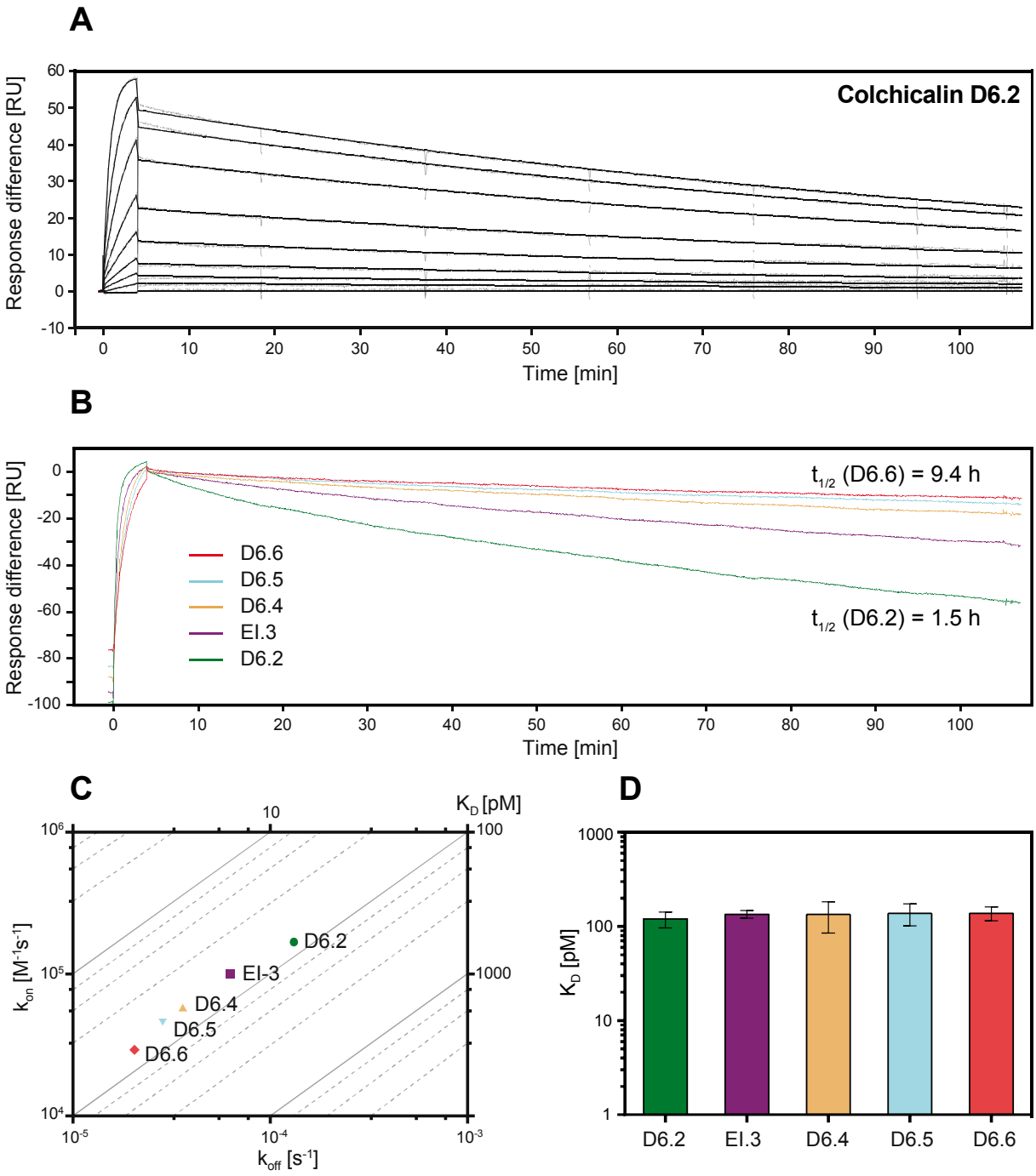

Figure 3.34. Generation of Anticalins against colchicine with superior dissociation kinetics. **A:** SPR analysis of the Colchicalin D6.2. A 1:2 dilution series of the Colchicalin in PBS-$T_{0.005}$ (128–1 nM) was injected for 4 min and allowed to dissociate for 100 min. The binding curves were fitted according to a 1:1 Langmuir biding model $dAB/dt = k_{on} \cdot A \cdot B - k_{off} \cdot AB$. **B:** Comparison of the dissociation kinetics of the generated Anticalins against colchicine. All runs were performed with the same SPR chip under identical conditions, at 256 nM protein concentration. Technical fluctuations of the signal were removed, and the curves were aligned to zero at the beginning of the dissociation phase. **C:** k_{off}/k_{on} plot with the same Anticalins. Note that the reduction of the dissociation rates was compensated by trade-offs in the association rates. **D:** Determination of equilibrium dissociation constants against free colchicine in solution via fluorescence titration. Titration was performed in duplicates or triplicates with a protein concentration of 20 nM in order to improve the resolution in the picomolar affinity range. Error bars represent standard deviations from the duplicate or triplicate titrations (see Table 3.5).

Interestingly, equilibrium binding constants of the k_{off}-optimized Anticalins remained virtually unchanged, since both the on- and the off-rate decreased gradually from variant to variant (Figure 3.34C). This observation was confirmed by measuring the equilibrium dissociation constants of the optimized Anticalins against free colchicine in solution via fluorescence titration (Figure 3.34D). The discrepancy between the K_D values determined via SPR and via fluorescence titration can be explained by surface effects on the SPR chip as well as by the fact that colchicine used for SPR was modified by biotinylation.

Table 3.5. Binding kinetics of the Anticalins against colchicine.

Mutant	k_{on} [$M^{-1}s^{-1}$]	k_{off} [s^{-1}]	K_D^{kin} [pM] [1]	K_D^{eq} [pM] [2]	$t_{1/2}$ [h]
D6.2	1.67×10^{5}	1.32×10^{-4}	790	120 ± 23	1.5
EI.1	7.44×10^{4}	6.17×10^{-5}	829	not tested	3.1
EI.3	1.03×10^{5}	5.64×10^{-5}	548	135 ± 12	3.4
EI.3/K142I = D6.4	5.80×10^{4}	3.61×10^{-5}	622	134 ± 49	5.3
D6.4/Q77E	6.41×10^{4}	2.89×10^{-5}	451	127 ± 45	6.7
D6.4/T136V = D6.5	4.60×10^{4}	2.85×10^{-5}	620	137 ± 36	6.8
D6.5/Q77E = D6.6	2.92×10^{4}	2.05×10^{-5}	702	139 ± 23	9.4

[1] Calculated as k_{off}/k_{on} from the kinetic binding constants obtained via real-time SPR analysis (cf. Figure 3.34C).
[2] Equilibrium K_D values obtained via the fluorescence titration with 20 pM protein (see also Figure 3.34D). Error bars represent standard deviations for duplicate or triplicate titrations.

The physicochemical stability of a protein is one of the key factors of its applicability as a biochemical tool. One of the most important parameters of protein stability is the resistance to thermal denaturation. Hence, the thermal denaturation profile of the Anticalin D6.6 was investigated using circular dichroism (CD) spectroscopy. Two lead candidates from the earlier engineering stages, namely D6.2 and EI.3, were tested in comparison (Figure 3.35). Melting points of all three tested Anticalin candidates turned out to be around 70 °C and higher. The variant D6.2 was the most stable protein with 76 °C, while EI.3 showed a slight trade-off in thermal stability, which was partly restored in the successor D6.6 with a melting point of 71 °C.

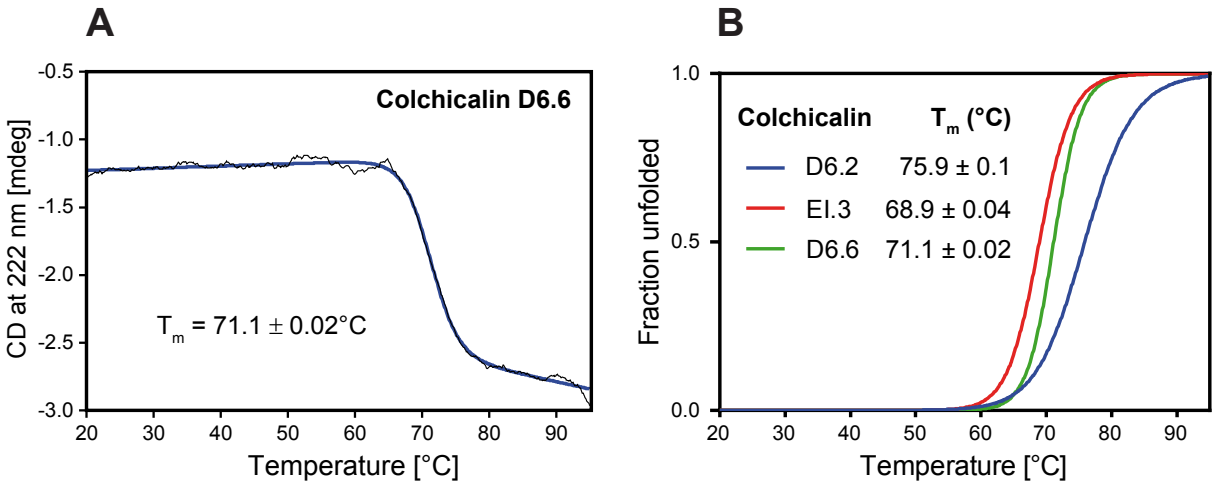

Figure 3.35. Thermal denaturation profiles of the Colchicalins D6.2, EI.3 and D6.6 measured via CD spectroscopy. **A:** Thermal denaturation curve for D6.6. The black line corresponds to the raw CD signal, the smooth blue line is the curve fit to Equation 10 (see Chapter 2.7.4). **B:** Thermal denaturation curves for the three tested proteins normalized via Equation 11. The curves represent the fraction of unfolded protein at each temperature point.

3.5 Proof of principle experiments for an Anticalin as colchicine antidote in a rat model

In cooperation with the Chair of Clinical Toxicology at the Klinikum rechts der Isar (Munich, Germany), a series of experiments was planned, in which the effectiveness of our Colchicalin D6.2 as antidote against acute colchicine intoxication was tested in a *Rattus norvegicus* model. The planned pre-clinical trials were divided into three phases: (1) pharmacokinetics of colchicine, (2) pharmacokinetics of the Colchicalin and its PASylated versions (see below), and (3) simulation of colchicine poisoning and its treatment with the Colchicalin. Only the first two phases were accomplished in the scope of the current PhD thesis.

3.5.1 Pharmacokinetic study of colchicine in the rat model

Two main goals were set for this experiment. On the one hand, the pharmacokinetic profile of colchicine after high-dose intravenous injections was to be determined. By the time when the experiment was prepared, corresponding data was absent in the literature. On the other hand, clinical effects of such intoxication within the time scope of the experiment needed to be described. This was essential for diagnosing toxicity in the third experimental phase.

To minimize suffering of the animals, colchicine injections were made under narcosis. Since narcosis impairs normal breathing, lung ventilation was maintained through a punctured trachea. To simplify the injection as well as blood and urine sampling, the *arteria carotis*, the *vena jugularis* and the urinary bladder were cannulated. Because of the surgical intervention and the deep narcotization, the whole experiment had to be accomplished within 3–3.5 hours.

In order to maximize the toxic effects of colchicine within the experiment time span, high colchicine concentrations were chosen, exceeding the reported LD50 of 1.6 mg/[kg body mass] six- to twelve-fold (Ferguson, 1952; Rosenbloom & Ferguson, 1968).

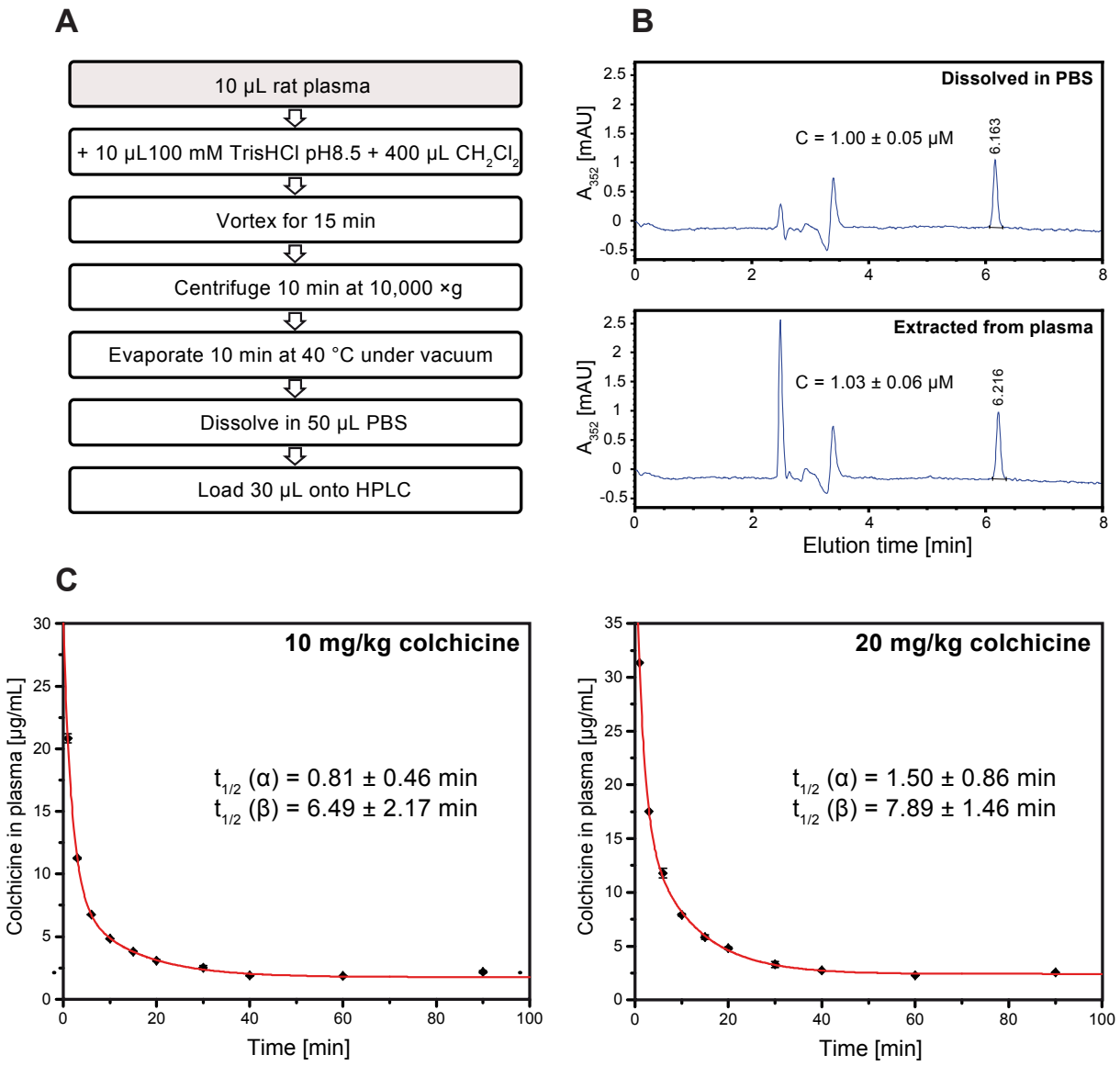

Figure 3.36. Pharmacokinetics of colchicine in the rat model. **A:** Scheme of the colchicine extraction protocol from rat plasma. **B:** Quantification of colchicine dissolved in PBS or extracted from rat plasma using HPLC. Triplicate 10 µL samples of 1 µM were prepared and the measured concentrations were compared. Extraction did not influence the colchicine recovery. The errors of the concentration values represent 95 % confidence intervals. **C:** Exemplary pharmacokinetic profiles of colchicine in rat. The data were fitted using a bi-exponential equation $A = A_1 \times e^{(-t/\tau_1)} + A_2 \times e^{(-t/\tau_2)} + A_0$ using Origin Pro. The indicated half-life values were calculated from triplicates (three animals for each colchicine concentration); the errors represent 95 % confidence intervals.

After successful surgical preparation (installation of artificial breathing device, cannulation of the blood vessels) and stabilization of the heart and breathing rhythm, a 2 mg/mL sterile colchicine solution was injected into the *vena jugularis*. The injected volume was adjusted

within the range of 0.8–1.2 mL depending on the weight of the animal to achieve equal injected dose per body mass. For the measurement of colchicine concentrations, 100–500 µL blood samples were taken after 1, 3, 6, 10, 15, 20, 30, 40, 60 and 90 min. Colchicine was extracted from plasma using dichloromethane (Abe *et al.*, 2006) according to the protocol outlined in Figure 3.36A (see also Chapter 2.5.4). The quantification was performed via HPLC, which was calibrated using rat plasma samples spiked with colchicine (Figure 3.36B). Plasma from each sample was analyzed in duplicates or triplicates. The first three animals were treated with 10 mg/[kg body mass] colchicine (Figure 3.36C). For the next three animals, the colchicine concentration was increased to 20 mg/[kg body mass]. The determined half-life values showed no statistically significant difference, with the α-phase half-life of around 1 min and the β-phase half-life of around 7 min. Notably, the fitted curves did not reach the zero asymptote, suggesting a third, much slower elimination phase.

3.5.2 Production of the Colchicalin D6.2 and its PASylated variants for preclinical trials

First of all, a suitable candidate had to be chosen for this experiment from the existing portfolio of the Colchicalins. Starting from the variant D6.2, all engineered lipocalins had similar dissociation constants for colchicine, making them suitable for *in vivo* tests. However, in contrast to the use as a biochemical tool, fast binding kinetics is preferable for an antidote application: faster dissociation can facilitate more efficient colchicine excretion through the kidneys. For this reason, the Colchicalin D6.2 possessing the fastest binding kinetics was chosen for the preclinical tests in *Rattus norvegicus*.

Colchicine poisoning is characterized by fast toxin distribution into the tissues and a slow secondary elimination phase. Since lipocalins usually possess plasma half-lives no longer than 1 h in rodents (Schlehuber & Skerra, 2005), injection of an Anticalin would cause fast depletion of colchicine from the plasma but should have little effect on the larger intra-tissue pool. Hence, it appeared useful to increase the plasma half-life of the Anticalin using PASylation technology (Schlapschy *et al.*, 2013). For the preliminary tests, three protein variants were compared: (1) the original Colchicalin D6.2, (2) Colchicalin D6.2 fused with a PA200 moiety, and (3) Colchicalin D6.2 with a PA600 moiety. The PA sequences were excised from the plasmids pXL2-PA#1.2(200) and pXL2-PA#1.2/1.3/1.2(600) using EarI restriction sites (Binder & Skerra, 2017). Both plasmids were kindly provided by XL-protein GmbH.

The ‘native’ Colchicalin was produced in the periplasm of *E. coli* JM83 using the expression plasmid pNGAL118, a derivative of pNGAL98 carrying a C-terminal His_6-tag instead of the *Strep*-tag II. After shake-flask production in LB medium, the periplasmic extract was subjected to IMAC and SEC (data not shown), the purified protein was passed through a Proteus NoEndo column for endotoxin removal and finally concentrated to 2 mg/mL.

Since larger amounts of the PASylated Colchicalins were required, these two protein variants were produced in the cytoplasm of *E. coli*. To this end, the D6.2 gene was subcloned onto the plasmid pNGAL117 carrying a SapI restriction site upstream of the C-terminal His_6-tag. Then the PA sequences were inserted using the SapI/EarI restriction site and, subsequently, the genes of the two PASylated Anticalin versions were recloned on the vector pASK75-T7RBS2 using the XbaI and HindIII restriction sites. In the final expression constructs, the PA sequences were attached to the C-terminus of the Anticalin and carried His_6 tags at their C-termini (Figure 3.38A). After gene expression in *E. coli* Origami B (three 2 L flasks with TB-medium for each protein variant), the proteins were purified by IMAC from the whole-cell extracts using a 60 mL Ni-NTA column (Figure 3.37A,C). The pooled elution fractions were dialyzed against 10 mM MES/NaOH, 10 mM NaCl, pH 6.5 and subjected to cation exchange chromatography (Figure 3.37B,C). After the final SEC polishing step in PBS, the proteins were concentrated using centrifugal ultrafiltration units to a molar concentration equal to that of 2 mg/mL non-PASylated Colchicalin D6.2.

All three proteins were sterile-filtered (0.22 µm pore diameter) and shock-frozen in liquid nitrogen in 0.6 mL aliquots. Three quality controls were performed: (1) analysis of purity on reducing and non-reducing SDS-PAGE, (2) confirmation of the absence of aggregates via SEC after freezing, and (3) comparison of the protein concentration before and after freezing. After all controls had been passed (Figure 3.38B,C), the frozen protein samples were handed over to our cooperation partners at the Klinikum rechts der Isar.

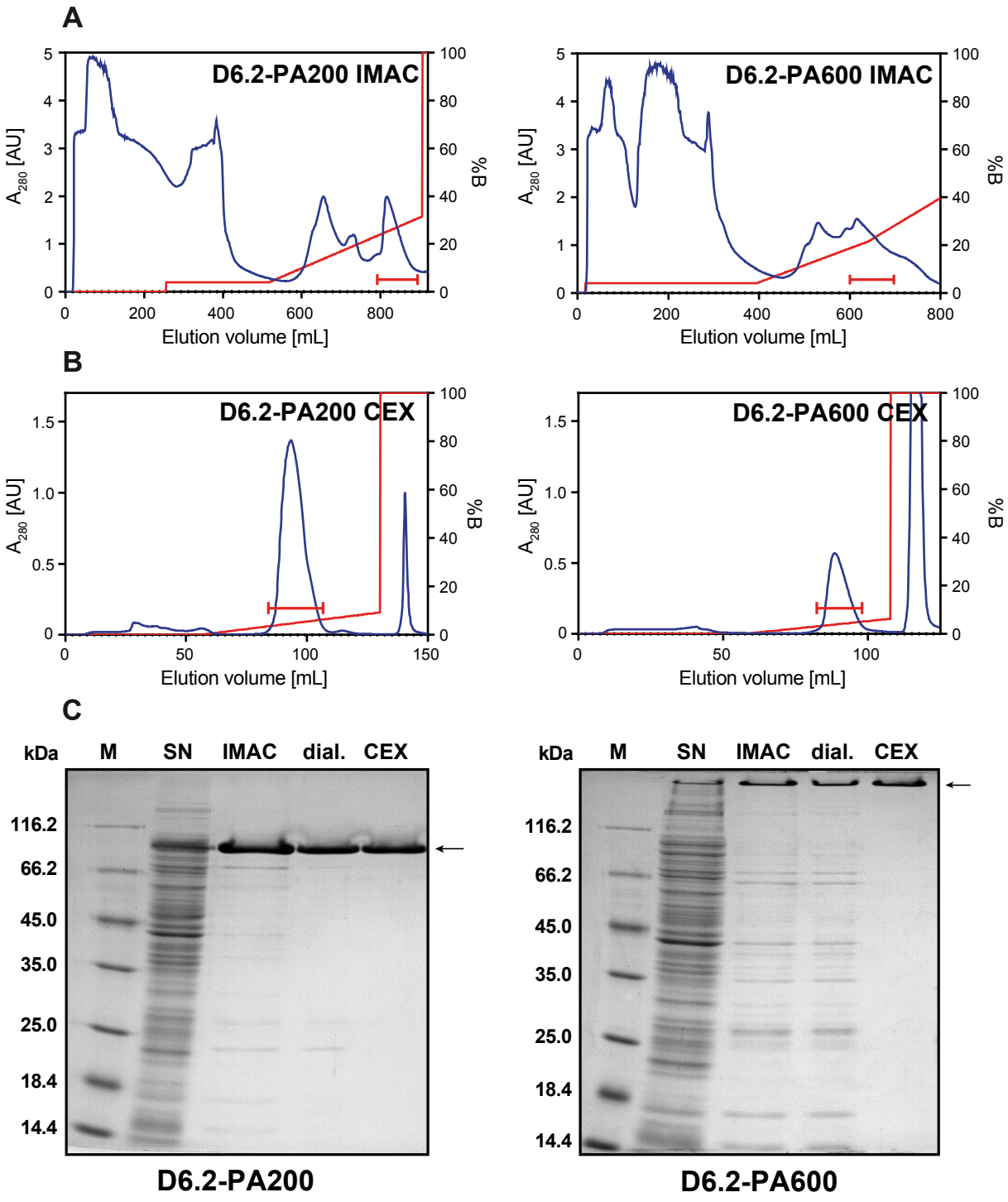

Figure 3.37. Purification of the PASylated versions of Colchicalin D6.2. **A:** Purification via IMAC. The whole cell extracts were applied on a 60 mL Ni-NTA column, the column was washed with 20 mM imidazole in IMAC buffer and a gradient of 20–250 mM in 10 column volumes was applied. **B:** Purification via CEX. The dialyzed IMAC elution fraction was applied on a 10 mL MacroCap SP column and eluted using a gradient of 10–500 mM NaCl in 20 column volumes. **C:** SDS-PAGE analysis. M – protein marker, SN – supernatant after centrifugation of the whole-cell extract, IMAC – elution fraction, dial. – IMAC elution fraction after dialysis, CEX – elution fraction.

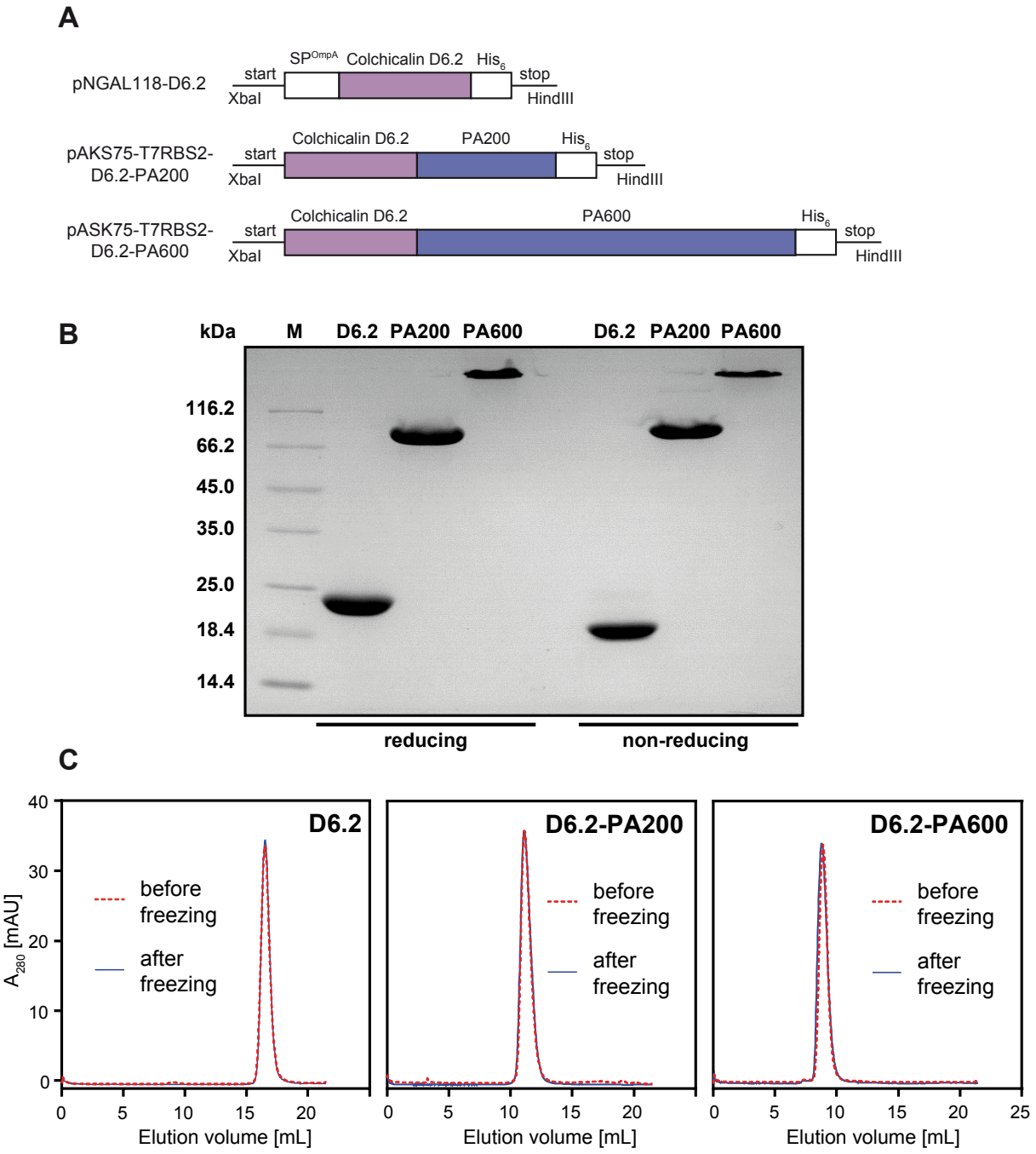

Figure 3.38. Quality control of the Colchicalin D6.2 and its PASylated versions. **A:** Expression constructs used for the bacterial production of Anticalins for the preclinical trials in a rat model. The first construct contained the OmpA signal peptide for the periplasmic expression, while the constructs for the PASylated Anticalins enabled cytoplasmic expression via the ribosome binding site of the bacteriophage T7. **B:** SDS-PAGE analysis. M – protein marker, 'D6.2' –Colchicalin D6.2, 'PA200' – Colchicalin D6.2 with a PA200 moiety, 'PA600' – Colchicalin D6.2 with a PA600 moiety. **C:** SEC analysis before and after freezing/thawing. 100 µL of the protein samples concentrated to 2 mg/mL were loaded onto a Superdex 200 13/300 column with PBS as running buffer. The peak heights were normalized for each pair of curves; protein concentration after freezing remained constant as confirmed via UV spectrometry.

3.5.3 Pharmacokinetic study of the Colchicalins in the rat model

For the pharmacokinetic study, the 2 mg/mL solution of the Colchicalin in PBS (calculated for the Anticalin portion, neglecting the mass of the PAS polypeptide; ~94 µM) was injected into the tail vain of rats at a dose of 2.5 mg (117 nmol) Colchicalin per kg body mass. The time scheme for blood sampling was elaborated individually for each protein variant to ensure optimal distribution of the data points for the curve fitting (Table 3.6). The blood samples were centrifuged as described (Chapter 3.5.1) and the 50–70 µL plasma samples were either stored at 4 °C and analyzed on the same day or stored at -20 °C till the analysis.

Table 3.6. Time points of the blood sampling during the Anticalin pharmacokinetic study.

Time [h]	1'	5'	10'	20'	30'	45'	1	1.5	2	3	4	6	12	24	36	48	N
D6.2	x	x	x	x	x	x		x									7
D6.2-PA200			x		x		x	x		x	x	x					7
D6.2-PA600					x		x		x			x	x	x	x	x	8

The Colchicalin was quantified using a sandwich ELISA, which employed the binding of the protein to colchicine (Figure 3.39A; see also Chapter 2.6.3). Each protein version was tested in three animals; exemplary curves are presented in Figure 3.39 and the calculated half-life values are listed Table 3.7. PASylation drastically increased the plasma half-life of the Colchicalin over 25-fold for the PA200 version and almost 400-fold for PA600, thus exceeding expectations. Notably, the used ELISA setup employed binding events via both termini of the fusion proteins (Colchicalin as the N-terminal part and the His_6-tag at the C-terminus; see Figure 3.39A), thus guaranteeing that only the full-length polypeptides were quantified. Thus, functional stability of all three Anticalin variants in rat plasma could be demonstrated.

Table 3.7. Determined plasma half-life values of the Colchicalin D6.2 and its PASylated versions.

Protein	Plasma half-life					
Animal No.:	1	2	3	Mean	CI95	
D6.2	2.68	2.81	2.64	**2.71**	**± 0.10**	min
D6.2-PA200	80.5	59.2	85.9	**75.2**	**± 16.0**	min
D6.2-PA600	16.9	18.6	17.2	**17.6**	**± 1.0**	h

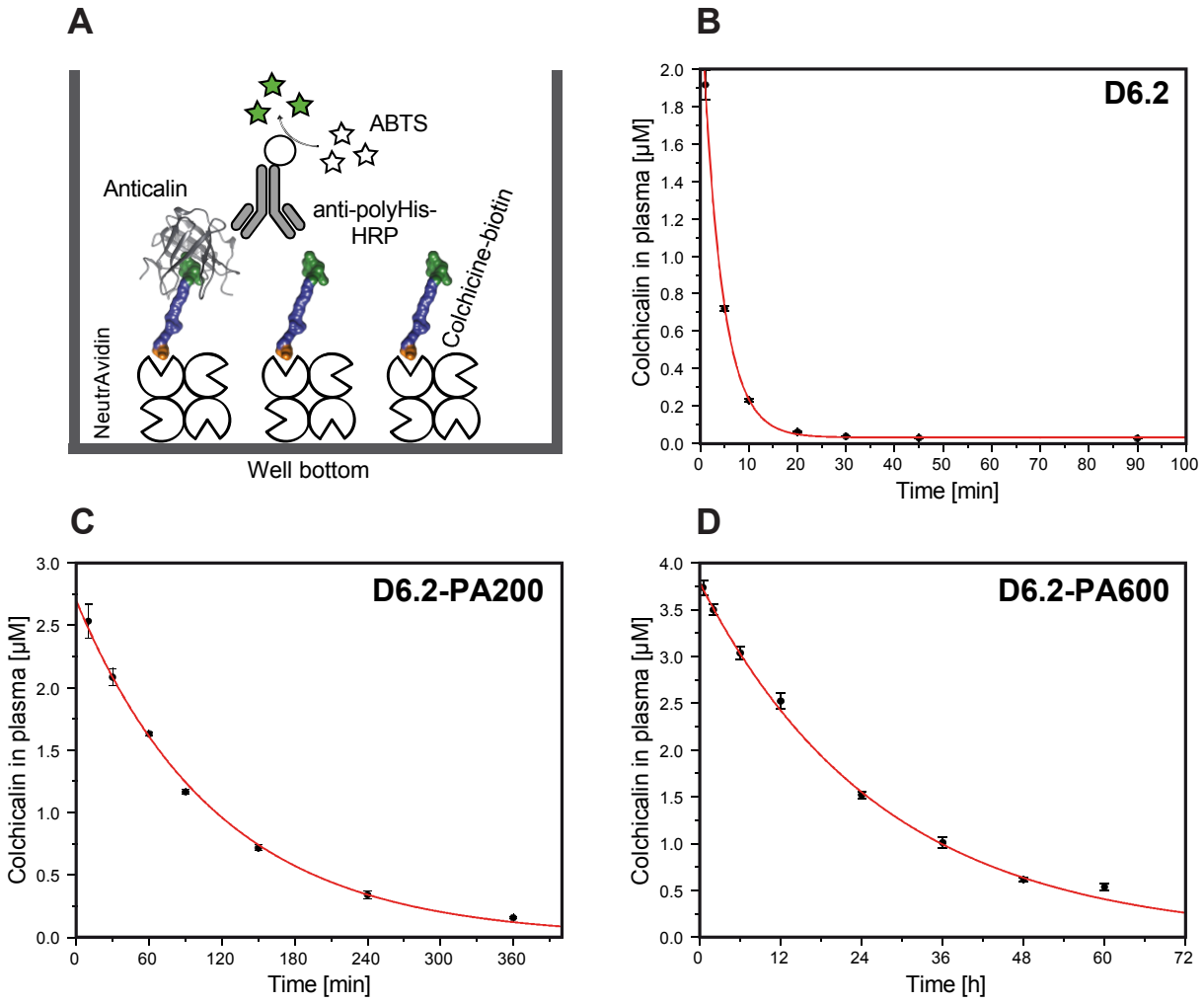

Figure 3.39. Measurement of the pharmacokinetics of the Colchicalin D6.2 and its PASylated versions in rats. **A:** Capture ELISA setup for the quantification of the Anticalin in rat plasma. **B-D:** Exemplary pharmacokinetic profiles of the Colchicalin and its PASylated versions. The error bars represent standard deviations for N = 3. Data points were fitted to a monoexponential decay equation $A = A_1 \times e^{(-t/\tau)} + A_0$ using Origin Pro.

3.6 Enzymatic characterization of TSA-specific Anticalins

3.6.1 Development of an HPLC-based analytics for the Diels-Alder reaction

Another subproject of this thesis was the engineering and functional characterization of lipocalins with catalytic activity. As explained in Chapter 1.2.5, prior to the current work Stephan Dickgießer in his Master's thesis (2011) selected two Anticalins that bind a transition state analog (TSA) for the Diels-Alder cycloaddition between NEM and TCTD. Initially, two TSA-binding Anticalins were selected via phage display from the combinatorial library, which were dubbed C3A5 and C1G2. Later on, C1G2 was modified via affinity maturation, resulting in the version E1G2 (Figure 3.40). The affinities towards the TSA are in the lower nanomolar range for C3A5 and in the lower micromolar range for E1G2. Despite initial investigation, the ability of these Anticalins to catalyze the Diels-Alder cycloaddition between NEM and TCTD remained in question. Therefore, the reliable experimental detection of catalytic activity for C3A5 and E1G2 was the first goal of the present project.

```
      1        10        20        30        40        50        60        70        80
      .        .         .         .         .         .         .         .         .
Lcn2  QDSTSDLIPAPPLSKVPLQQNFQDNQFQGKWYVVGLAGNAILREDKDPQKMYATIYELKEDKSYNVTSVLFRKKKCDYWIRTFVPGCQP
lib   ........................H.......x...xx.......x..x..............x.x.xx...x.x.x.....S..
C3A5  ........................H.......M...GD.......Y..R..............W.W.LP...K.F.N.....S..
E1G2  ........................H.......L...GW.......A..F..............R.W.GN...N.T.W.....S..
NFY   ........................H.......L...GW.......A..F..............R.W.GN...N.N.F.....S..
                              ====A=====------#1------===B===    ===C===--#2---====D===
                             ----
                            BstXI

      90        100       110       120       130       140       150       160       170     178
      .         .         .         .         .         .         .         .         .       .
Lcn2  GEFTLGNIKSYPGLTSYLVRVVSTNYNQHAMVFFKKVSQNREYFKITLYGRTKELTSELKENFIRFSKSLGLPENHIVFPVPIDQCIDG
lib   ......x...x..x..x.................x.x....x.x.........................................
C3A5  ......L...Y..Q..L.................T.I....R.Y.........................................
E1G2  ....F.H...A..L..I.................R.N....L.W.........................................
NFY   ....F.H...A..L..I.................R.N....L.Y.........................................
       ==E=----#3-----===F====    ===G===---#4---===H===
                                                      ----
                                                     BstXI
```

Figure 3.40. Amino acid sequence alignment of the catalytic Anticalins C3A5, E1G2 and NFY (Lib – initial combinatorial library). The variant NFY was obtained later from E1G2 by rational mutagenesis, as discussed in Chapter 3.6.3.

The reaction analytics was accomplished via separation of the reaction products using RP-HPLC, followed by quantification of the relevant product peak via absorbance measurement in the near UV range. In the first attempt, the reactants NEM and TCTD were mixed in equimolar ratio at 0.1 mM concentration each in order to observe the uncatalyzed background reaction. As seen in Figure 3.41A, it was possible to completely separate the reaction product (P_{ox}, see Figure 1.5, **8**) from the educts NEM and TCTD on a C18 reverse phase column using a linear gradient of 30–60 % acetonitrile.

As soon as the analytical method was established (see Chapter 2.5.5), it was used to study the Diels-Alder reaction kinetics in more detail. To define optimal educt concentrations, a pair

of experiments was performed: concentration of one reactant was varied, while concentration of the other was kept constant (Figure 3.41B). Since the mathematical products of the respective educt concentrations were equal for both experiments, the resulting kinetic profiles resembled each other. However, the initial rate for the reaction between 0.1 mM NEM and 0.8 mM TCTD was lower than expected, which is explained by the limited solubility of TCTD in the aqueous reaction solution. The actual concentration of TCTD in the '0.8 mM' sample was later found to be only around 0.6 mM, which is in line with the reported values (Hilvert & Hill, 1989). The poor water solubility of TCTD imposes a fundamental limitation on the determination of true Michaelis constants for artificial enzymes catalyzing this Diels-Alder transformation. Therefore, TCTD was applied substantially below the solubility limit in subsequent experiments.

Another observation that became evident from the experiment shown in Figure 3.41B was the fast decline in the product concentration after 10–20 hours. In theory, this decline can be explained by the loss of product by precipitation as well as by the chemical degradation of the educts and/or the product. Precipitation of P_{ox} can be excluded since it would imply a constant solubility limit regardless of the educt concentration, which was not the case. However, it is possible that P_{ox} was degraded by further oxidation or hydrolysis. In addition, the educts could be unstable in the reaction buffer and degrade independently from the Diels-Alder reaction.

To test whether the substrates remained stable under the reaction conditions, NEM or TCTD were individually dissolved in the reaction buffer (20 mM MES/NaOH, 100 mM NaCl, pH 6.0) at a concentration of 0.1 mM, and samples were taken for HPLC analysis every 2 h. In addition, the pH of the buffer was varied to investigate a possible influence on the degradation (Figure 3.41C). As a result, both NEM and TCTD turned out to degrade considerably. While NEM degraded by 20 % after 24 h, the concentration of TCTD decreased by 85 %. Interestingly, the decay rate was pH-dependent only for NEM, for which it slightly increased towards pH 7, but not for TCTD, which degraded with a constant rate of ~3.7 % per hour in the tested pH range (5.5 to 7.0), corresponding to a zero-order decay constant of $1.03 \times 10^{-3}\ s^{-1}$. Change of the buffer substance, application of argon atmosphere or addition of mild reducing agents did not prevent TCTD degradation. In fact, TCTD remained stable only if kept in pure acetonitrile (data not shown). Thus, the only efficient measure against the fast degradation of TCTD was the reduction of the period used for the analysis and calculation of the initial reaction rate for the first 2–3 h so that the educt decay could be reasonably neglected.

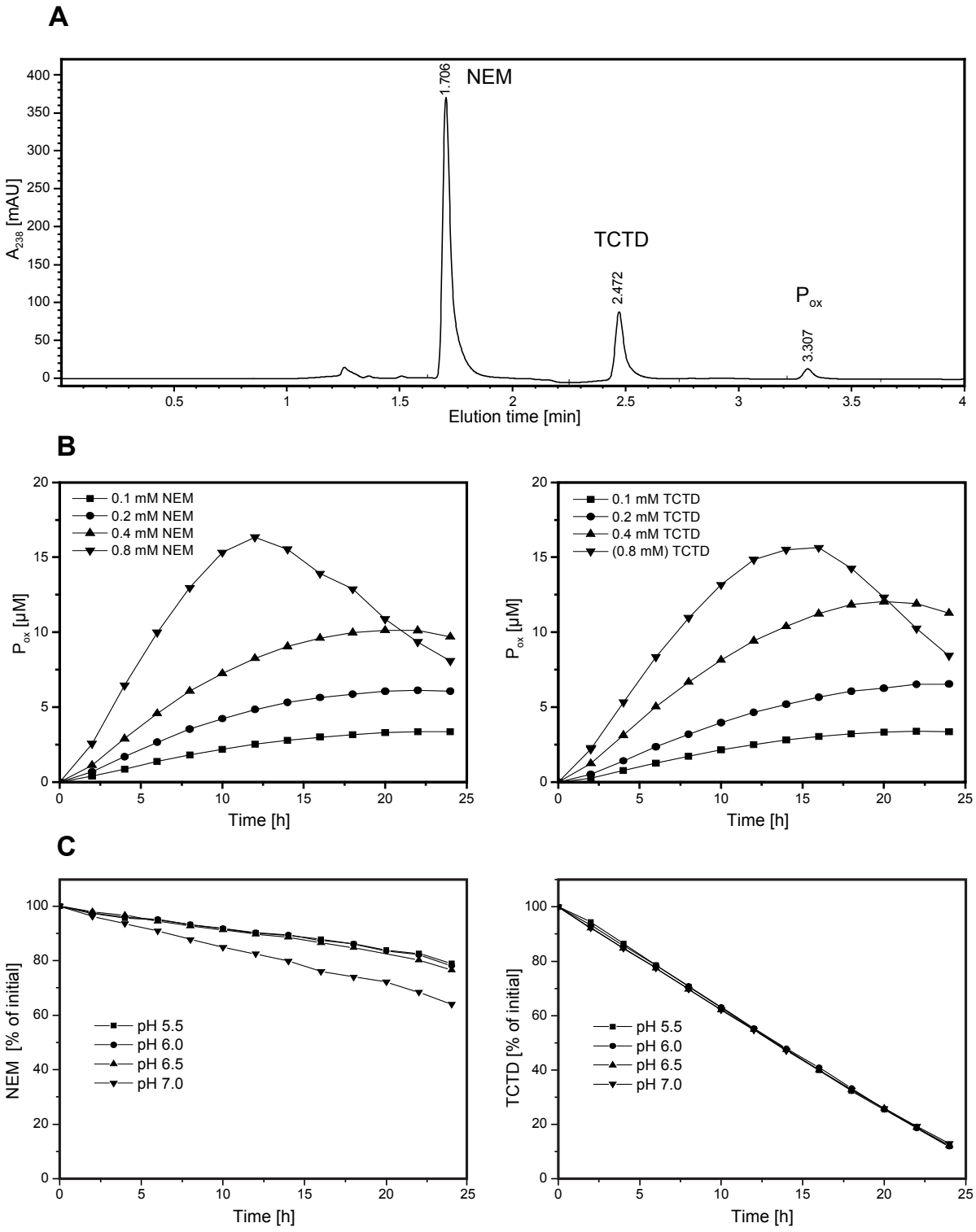

Figure 3.41. Analytics and characterization of the Diels-Alder reaction between NEM and TCTD. **A:** Chromatographic separation of the reaction mixture using a C18 RP-HPLC column in a gradient of acetonitrile. NEM eluted at 1.71 min, TCTD at 2.47 min, the oxidized cycloaddition product P_{ox} at 3.31 min. **B:** Reciprocal variation of educt concentrations. Different concentrations of one educt (as indicated in the diagram) were mixed with 0.5 mM of the other educt. The educts were added from stock solutions in acetonitrile, leading to 10 % (v/v) acetonitrile in the reaction mixture. The actual maximal TCTD concentration was around 0.6 mM because of its limited solubility, as was discovered later. **C:** Degradation of the individual educts in the reaction buffer at various pH values. Both educts decayed linearly, NEM at a rate of ~0.8 % per hour, TCTD up to ~3.7 % per hour.

3.6.2 First detection of catalytic activity for an Anticalin

After the behavior of the uncatalyzed Diels-Alder reaction was characterized, the Anticalins selected against the transition state analog were probed for catalytic activity. For a pilot experiment, the Anticalins E1G2 and C3A5 were produced in the periplasm *of E. coli* using the vector pNGAL98, purified via SAC and SEC and concentrated to 20 µM in the reaction buffer (20 mM MES, 100 mM NaCl, pH 6.0). Both reactants were added from 2 mM stock solutions in acetonitrile to a final concentration of 0.1 mM, resulting in a final acetonitrile content of 10 %. As seen in Figure 3.42A, the presence of an Anticalin in the reaction mixture led a noticeable increase in the initial reaction rate. Since the recombinant wild-type Lcn2, which was used as negative control, caused no rate acceleration, the observed effect was specific for the Anticalins E1G2 and C3A5, which were selected against the TSA. Consequently, it appeared that these proteins acted as true catalysts, lowering the activation energy by binding the transition state of the Diels-Alder cycloaddition.

Although the catalytic effect was measurable, the difference between the catalyzed and the background reaction did not exceed a factor of two. In order to improve the ratio of the catalytic reaction over the background, two optimization steps were performed. First, activity of the more efficient Anticalin E1G2 was tested at different pH values to determine its pH optimum, which lay around pH 5.6 (Figure 3.42B). Second, the effect of organic solvent content (reagent stocks were prepared in acetonitrile) was tested (Figure 3.42C). As expected, specific activity of the proteins increased when the concentration of organic solvent was reduced. For practical reasons (pipettable volumes), the acetonitrile content was kept at 5 % for all further experiments.

Optimization of the reaction mixture simplified the discrimination between the catalyzed and the background reaction, but the catalytic activity was still insufficient for measurement of proper Michaelis-Menten kinetics, which assumes large excess of educts over the enzyme. Making use of the fact that the two proteins with their different amino acid sequences catalyzed the same reaction, rational mutagenesis was engaged to improve the efficiency of the catalytic Anticalins, now dubbed ‘Catacalins’.

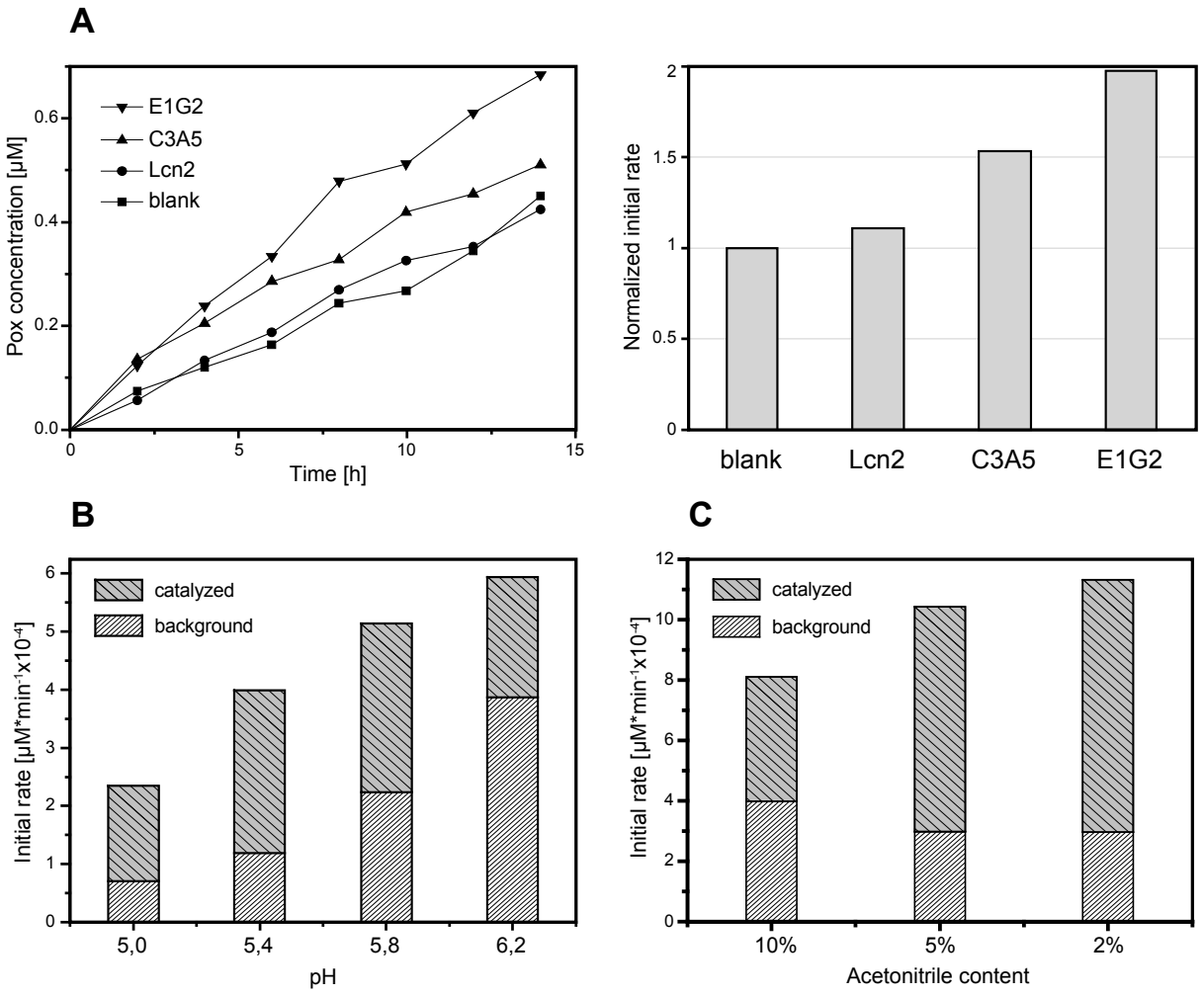

Figure 3.42. Detection of catalytic activity for the Anticalins C3A5 and E1G2 and enzymatic characterization of the Anticalin E1G2. **A:** First detection of catalytic activity for the Anticalins C3A5 and E1G2 using wild-type Lcn2 as control. NEM and TCTD (0.1 mM each) were mixed with 20 µM Anticalin in reaction buffer (20 mM MES, 100 mM NaCl, pH 6.0) in a total volume of 150 µL. The concentration of acetonitrile was kept at 10 % for all samples and the reaction was performed at room temperature (22 °C as measured by a liquid thermometer). The buffer was prepared in a 1.11-fold concentration to compensate for the dilution with 10 % acetonitrile. The initial rate was calculated for the first four measurement points (0–8 h). **B:** Determination of the pH optimum for the Anticalin E1G2. NEM and TCTD (0.15 mM each) were mixed with 0 or 20 µM Anticalin in 50 mM sodium citrate, 20 mM NaCl in a total volume of 75 µL. Otherwise, the conditions were as in (A). The catalyzed reaction rate was maximal between pH 5.4 and 5.8. **C:** Influence of the acetonitrile content on the background and the catalyzed reaction rates. The reaction was performed at pH 5.6 at the same conditions as in (B).

3.6.3 Rational mutagenesis of the Catacalin E1G2

The Catacalin E1G2 proved to be a better catalyst than C3A5 despite having an almost 1000-fold lower affinity against the TSA (K_D = 2 µM *vs* 3 nM, respectively). Thus, it was assumed that the catalytic activity of E1G2 can be further increased by improving its shape complementarity towards the TSA. Comparison of the amino acid sequences of the two proteins (see Figure 3.40) revealed some analogies such as amino acids with aliphatic side

chains at positions 36 and 106, aromatic amino acids at position 134 as well as the reciprocal pairs of a hydrophobic and a hydrophilic amino acid at positions 52/68 and 79/81. Based on these observations, a set of amino acid substitutions was introduced into the Catacalin E1G2, after which the new protein variants were expressed, purified and tested for catalytic activity (Figure 3.43A). Although most mutations did not lead to improvement, one single mutation W134Y and a double exchange T79N/W81F led to a substantial increase in the initial rate. Eventually, the triple mutant T79N/W81F/W134Y (Figure 3.40) achieved a more than two-fold higher catalytic activity than the initial Anticalin E1G2 and was designated 'NFY'. Interestingly, the affinity of the new Catacalin NFY towards the TSA was not better, as determined by fluorescence titration (Figure 3.43B).

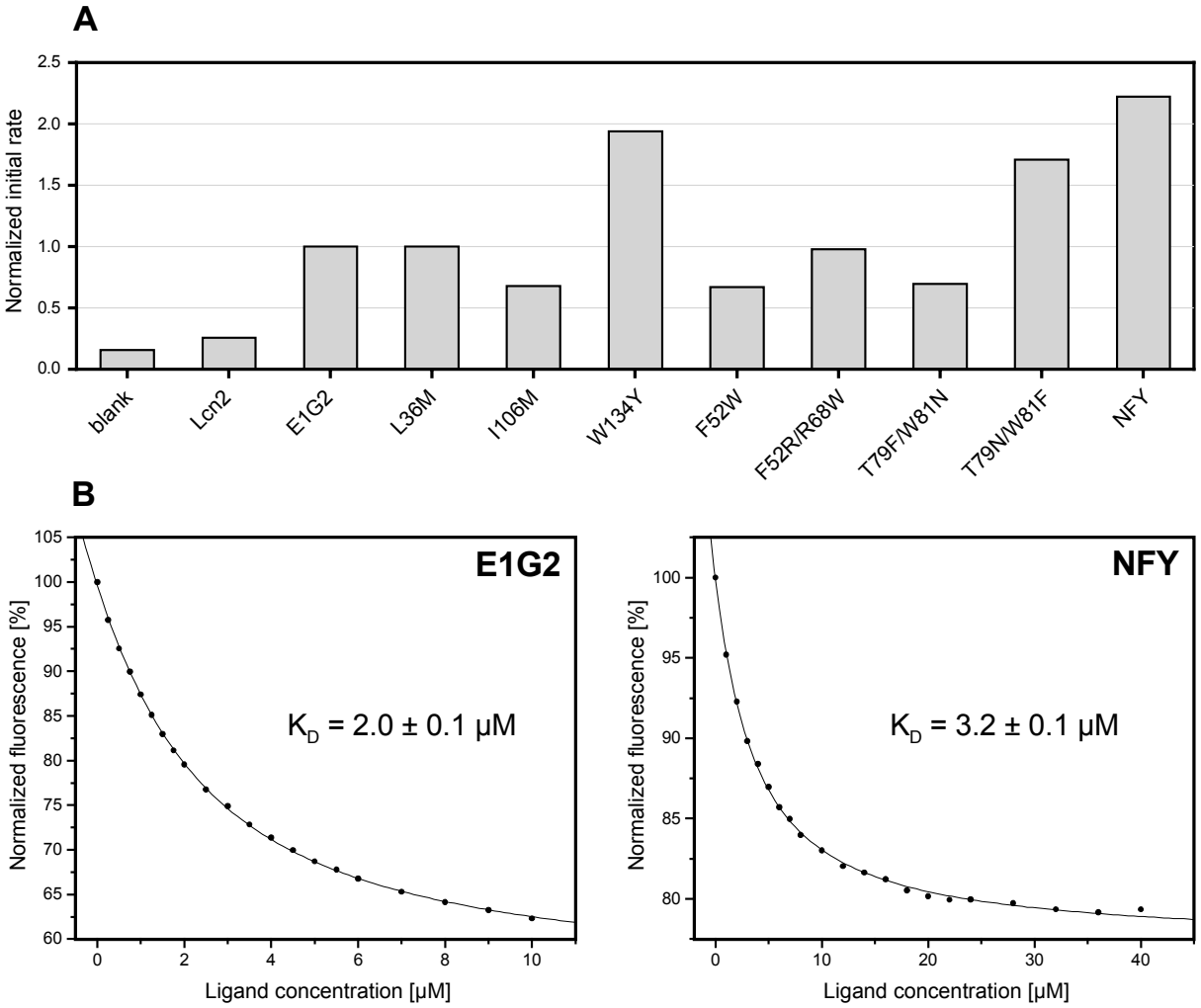

Figure 3.43. Rational mutagenesis of the catalytic Anticalin E1G2. **A:** Reaction rates measured for mutants of E1G2. The mutants were tested in separate runs, E1G2 was included as reference in each run, and the activities were then normalized to that of E1G2. **B:** Determination of the dissociation constants for the TSA by fluorescence titration. The TSA was added from a 500 µM (for E1G2) or 2 mM (for NFY) stock solution in DMF to a 1 µM Catacalin solution in 10 mM HEPES/NaOH, 150 mM NaCl, pH 7.0. Curve fitting was performed using Origin Pro software.

3.7 Affinity maturation of the Catacalin NFY via phage display

The low catalytic efficiency and the absence of reaction products detectable via photometry made it impossible to perform directed evolution coupled to direct screening for catalytic activity in order to improve the Catacalin. However, due to the fundamental link between the catalytic function of an enzyme and its affinity towards the transition state of the reaction, an increase in such affinity can also lead to improvement of the catalytic activity. Therefore, the Catacalin NFY was subjected to an affinity maturation towards the TSA.

To this end, the central gene cassette of NFY flanked by the pair of BstXI restriction sites (see Figure 3.40) was randomized as described in Chapter 3.1.4 with an average mutation frequency of 3.8 nucleotides per gene and subcloned on the vector pNGAL108 for phage display selection. Biotinylated TSA used for the selection was kindly provided by Prof. Donald Hilvert (Eidgenössische Technische Hochschule Zürich, Switzerland). The biotinylated TSA was immobilized on the surface of streptavidin or NeutrAvidin-coated magnetic beads, as it was done during the previous selection campaigns (see Chapter 3.1.1). Panning was performed with 10 nM biotinylated TSA according to the 'in-solution' protocol, i.e. the phages were incubated with the biotinylated TSA prior to the incubation with the magnetic beads, whereas the elution was carried out under denaturing conditions in the presence of 4 M urea (Figure 3.44A). Since it is known that harsh elution conditions can lead to enrichment of unspecific binders, competitive elution with an excess of free TSA was used as an alternative approach. To this end, phagemids from the first panning round with urea elution were taken (the backup aliquot stored at -80 °C, cf. the phage display protocol in Chapter 2.3.2), and further three panning rounds were performed using competitive elution with 100 µM TSA. After in total four rounds of panning, the gene cassettes from each phage display experiment were subcloned on pNGAL98 for the ELISA screening.

For the ELISA, the biotinylated TSA was pre-incubated with ExtrAvidin-AP conjugate in a ratio of 4:1 to enhance the assay sensitivity by means of the avidity effect. The Catacalin C3A5 was used as a positive control because of its high affinity towards the TSA. In total, three ELISA plates were analyzed for each elution approach; exemplary read-outs from two plates are shown in Figure 3.44B. Plasmid DNA from the clones that gave higher signals than NFY was prepared and used for sequence determination (Figure 3.45). From the 15 sequenced clones, 5 were chosen for further analysis based on their sequence properties (e.g., mutation proximity to the binding pocket and absence of excessive positive charge). The muteins were expressed in the periplasm of *E. coli* JM83, purified via SAC and SEC, and their activity was tested using the HPLC assay with 150 µM NEM and 150 µM TCTD in 20 mM MES/NaOH, 100 mM NaCl, pH 5.6. All proteins were concentrated to 4 µM except for U1D10 and U2A8, for which the yield

was only sufficient for a concentration of 0.66 µM. For U2A8, no catalytic activity was detected; the initial rates for the other four NFY mutants are shown in Figure 3.46A.

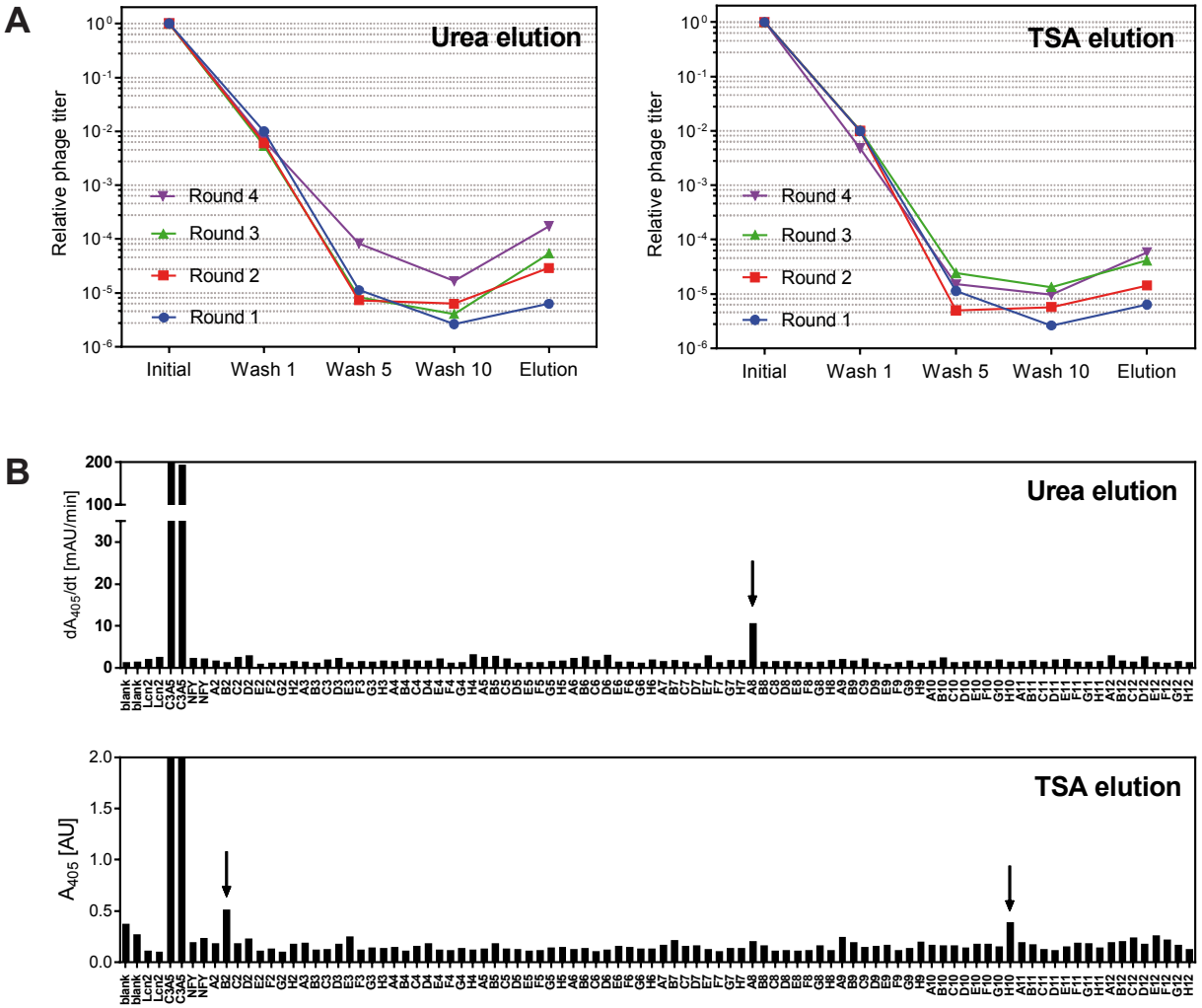

Figure 3.44. Affinity maturation of the Catacalin NFY. **A:** Phage titer during the panning against the TSA (left – denaturing elution with urea, right – competitive elution with free TSA, except for the first cycle, which is identical to the left). **B:** ELISA screening. Blank – empty wells with LB medium. Wild-type Lcn2 was used as negative control, C3A5 as positive control for TSA binding. NFY was also used as positive control, but its affinity was insufficient to produce a binding signal. Clones with the highest signal (marked by arrows) were chosen for further characterization.

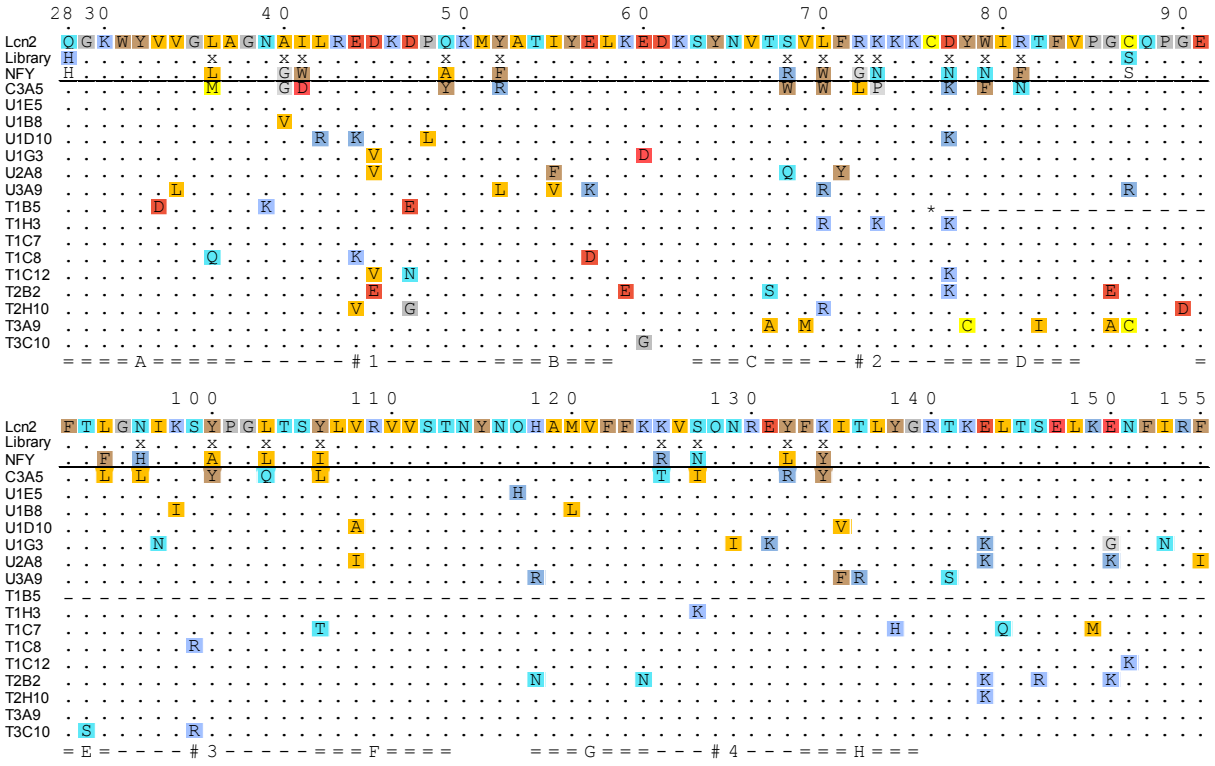

Figure 3.45. Amino acid sequence alignment of the NFY mutants with the highest signal in the ELISA. NFY serves as a reference for all sequences below the black line. One of the mutations introduced a stop codon indicated by an asterisk. For the amino acid coloring, cf. Figure 3.3.

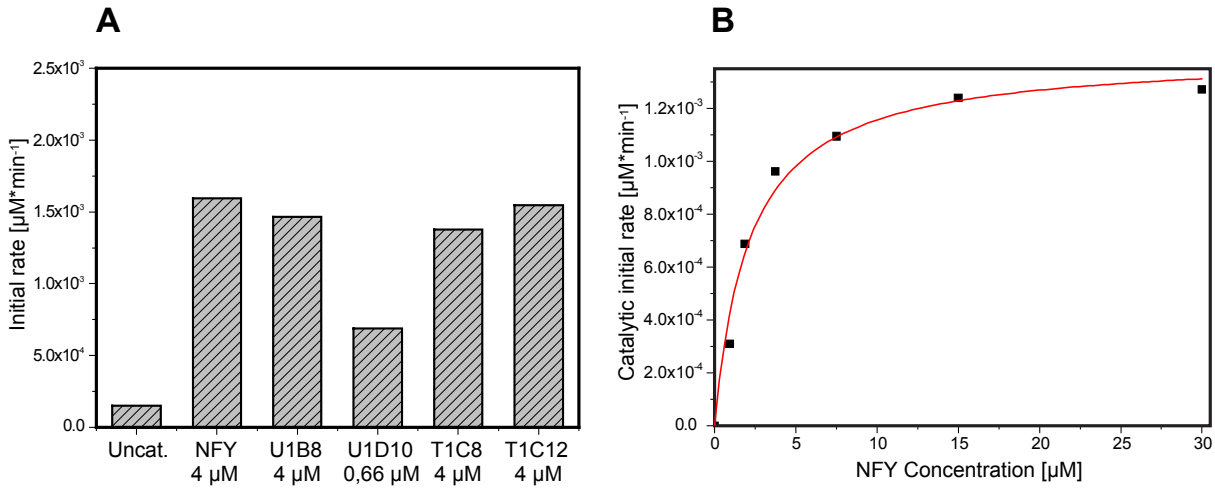

Figure 3.46. Characterization and affinity maturation of the Catacalin NFY **A:** Activity test of the muteins after the affinity maturation of NFY. NEM and TCTD (250 µM each) were mixed with the Catacalin solution at the given concentration in 20 mM MES/NaOH, 100 mM NaCl, pH 5.6, with a final acetonitrile content of 5 %. All mutants were tested in parallel at 25 °C. **B:** Dependence of the catalytic rate on the NFY concentration. Reaction conditions were same as in (A).

As a result, none of the muteins showed higher activity than NFY, with the exception of U1D10, which could possess higher activity if a linear dependence of the activity on the protein concentration is assumed. To test this assumption, an activity assay with varying NFY concentration was performed (Figure 3.46B). Contrary to the expectation, the reaction was saturated at high protein concentrations, reaching a plateau at around 30 µM Catacalin. This contradicted the linear concentration dependence, which is usually observed for enzymes, and could be at least in part explained by the relatively high enzyme-to-substrate ratio used in this assay (up to 1:5).

If a similar saturation behavior is assumed for U1D10, the expected activity improvement would be marginal. Together with its low expression yield (<100 µg/(L×OD_{550})) and a tendency towards aggregation, further characterization of U1D10 was considered impractical.

3.8 Crystallization of the catalytic Anticalins

Further effort in this project aimed at the crystallization of the two catalytic Anticalins in order to obtain a basis for structure-guided rational design.

3.8.1 Crystallization trials with the Catacalin NFY

Initially, the Catacalin NFY was subjected to crystallization with a C-terminal *Strep*-tag II. As these trials were unsuccessful, the SUMO fusion approach (see Figure 3.28) was employed. Subcloning, expression and purification was performed as described in Chapter 3.3.7, with the exception that a CEX purification step was used instead of SEC (Figure 3.47). The buffer was changed to 10 mM MES/NaOH, 100 mM NaCl, pH 6.0 via dialysis. Eventually, the Catacalin was concentrated to 7 mg/mL, mixed with TSA at a molar ratio of 5:1 and used for random factorial screens with 250 nL protein solution and 250 nL reservoir solution per drop. TSA was added after protein concentration to ensure complete ligand loading of NFY, which has 1000-fold lower affinity towards the TSA than C3A5. After two days, 29 % of the wells contained precipitate, corresponding to a nearly optimal proportion.

After two weeks, small (<40 µm) but well-shaped crystals were found in several wells containing mainly PEG3350 and PEG6000. These crystals were reproduced on refinement screens, and the best of them (grown in the presence of 22–26 % PEG 3350, 0.1–0.3 M Li_2SO_4 and 100 mM Bis-Tris/HCl pH 5.5) were harvested by Dr. Andreas Eichinger and used for dataset collection at the BESSY synchrotron. Unfortunately, the recorded diffraction pattern revealed that the harvested crystals comprised inorganic salt. Whether some of the crystals in other conditions corresponded to protein crystals, remains in question.

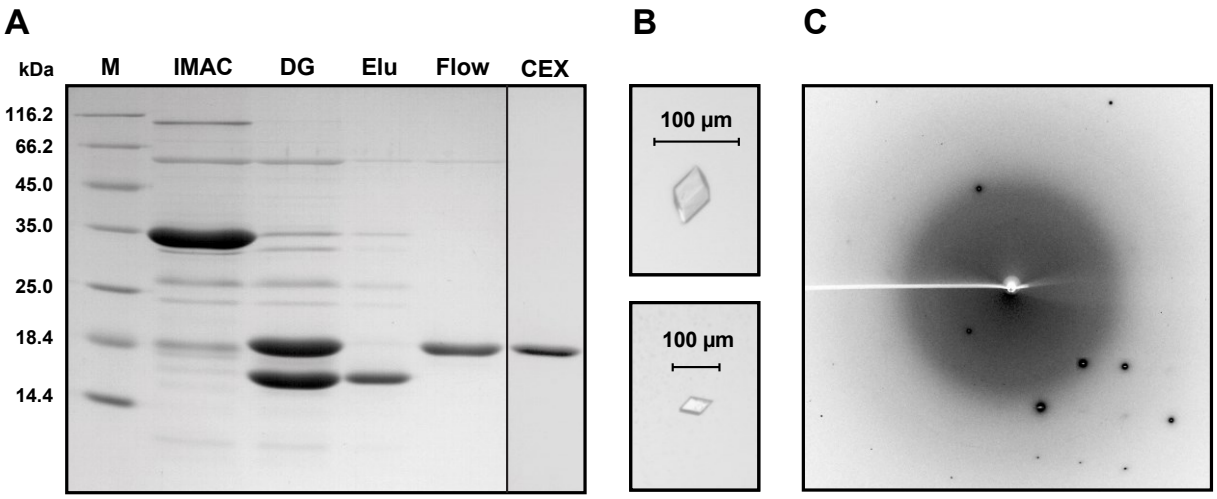

Figure 3.47. Purification and crystallization of the tag-free Catacalin NFY with a shortened N-terminus. **A:** SDS-PAGE analysis of the protein purification (reducing conditions). M – protein marker, IMAC – elution fraction of the first IMAC, DG – sample after the Ulp1 digest, Elu – elution fraction of the subtractive IMAC, Flow – flowthrough of the subtractive IMAC, CEX – elution fraction of the CEX. **B:** Crystals grown in the presence of 26 % PEG 3350, 0.1–0.3 M Li_2SO_4 and 100 mM Bis-Tris/HCl pH 5.5, which turned out to be salt crystals. **C:** X-ray diffraction pattern of a crystal from (B). The small number of reflections indicates an inorganic salt.

3.8.2 Successful crystallization of the Catacalin C3A5

Attempts to crystallize C3A5 were initiated by Dominik Hinz as part of his PhD work. He was able to obtain crystals of sufficient size for C3A5 with a C-terminal *Strep*-tag II; however, these showed considerable inner disorder, which prevented evaluation of the X-ray diffraction dataset. Thus, as a first step in this work, it was attempted to reproduce those crystals and improve their quality.

Therefore, the Catacalin C3A5 was expressed in the periplasm of *E. coli* JM83 using the vector pNGAL98 and purified via SAC and SEC, following the procedure of Dominik Hinz (Figure 3.48A,B). The purified protein in 10 mM HEPES, 50 mM NaCl, pH 7.0 at a concentration of 0.2 mg/mL was mixed with the TSA (Figure 1.5, **9**) at a molar ratio of 1:10 (2.3 µL TSA was added from a 100 mM stock solution in DMF to 2.8 mL protein solution) and concentrated to 6.5 mg/mL via ultrafiltration. The TSA was added before concentrating the protein because precipitation was observed in preliminary experiments when the TSA in DMF was added to the concentrated protein. It this way, ~15 % higher final protein concentration was reached than was achieved previously.

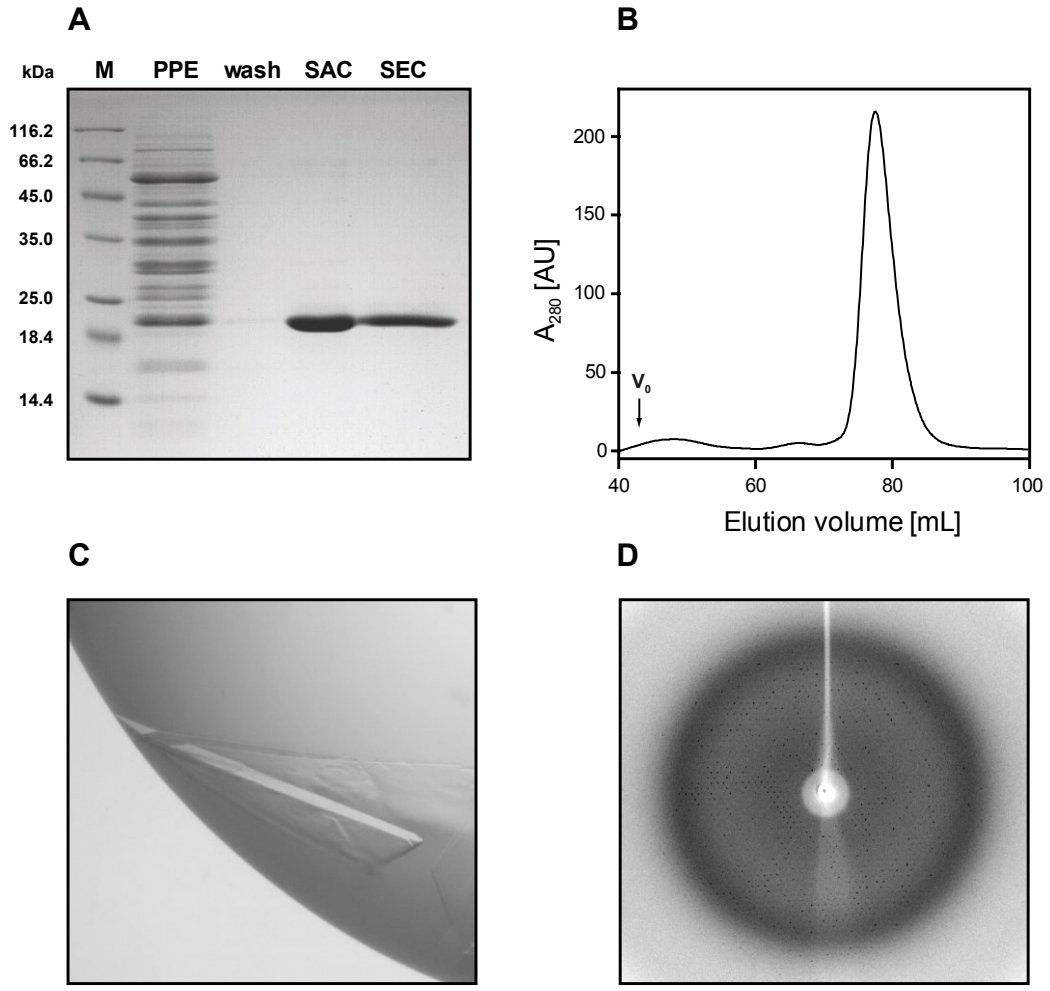

Figure 3.48. Purification and crystallization of the Catacalin C3A5 with a C-terminal *Strep*-tag II. **A:** SDS-PAGE analysis of the protein purification (reducing conditions). M – protein marker, PPE – periplasmic extract, wash – wash fraction of the SAC, SAC – elution fraction of the SAC, SEC – elution fraction of the SEC. **B:** Size-exclusion chromatography (SEC) using a Superdex S75 16/60 column with 10 mM HEPES, 50 mM NaCl, pH 7.0 as running buffer. **C:** The protein crystal used for the dataset collection. **D:** X-ray diffraction pattern of the crystal in (C) obtained at the BESSY synchrotron (Berlin, Germany).

The crystals previously obtained by Dominik Hinz (grown in the presence of PEG4000 and Li_2SO_4) had platelet-like morphology and were poorly developed in the third dimension. This time, crystals with a pronounced three-dimensional morphology were obtained in the presence of 21 % PEG4000, 260 mM Li_2SO_4 and 100 mM Na-acetate at pH 4.6 (Figure 3.48C). An X-ray diffraction pattern of this crystal was recorded at BESSY by Dr. Andreas Eichinger (Figure 3.48D). Although seemingly displaying straight and sharp edges, the crystal revealed multiple intergrown layers, which complicated diffraction data analysis and prevented solution of the crystal structure.

Fortunately, after additional optimization of the protein preparation performed by Irmgard Neumaier (Chair of Biological Chemistry, TU Munich), it was possible to obtain one crystal that provided a suitable diffraction pattern. The Catacalin C3A5 with a C-terminal *Strep*-tag II was

produced as described above, purified via SAC and SEC, and the buffer was changed to 10 mM MES/NaOH pH 6.5, 0.02 % (w/v) NaN_3 via dialysis. The protein crystal was obtained in a sitting drop containing 300 nL of the protein solution concentrated to 21.7 mg/mL with a 10-fold molar excess of the TSA and 300 nL of 20 % (w/v) PEG3350, 0.2 M diammonium tartrate (Figure 3.49). The crystal was frozen after addition of 25 % (v/v) glycerol and an X-ray diffraction pattern was measured at the BESSY synchrotron beamline 14.2. The crystal structure was solved by Dr. Andreas Eichinger via molecular replacement using the Anticalin N7E (PDB:5N47; Schiefner *et al.*, 2018) as search model (Figure 3.50; for the refinement statistics, see Appendix, Table 8.2). The crystal belonged to the space group P2 with 3 molecules per asymmetric unit; the best-resolved chain A was used for further analysis.

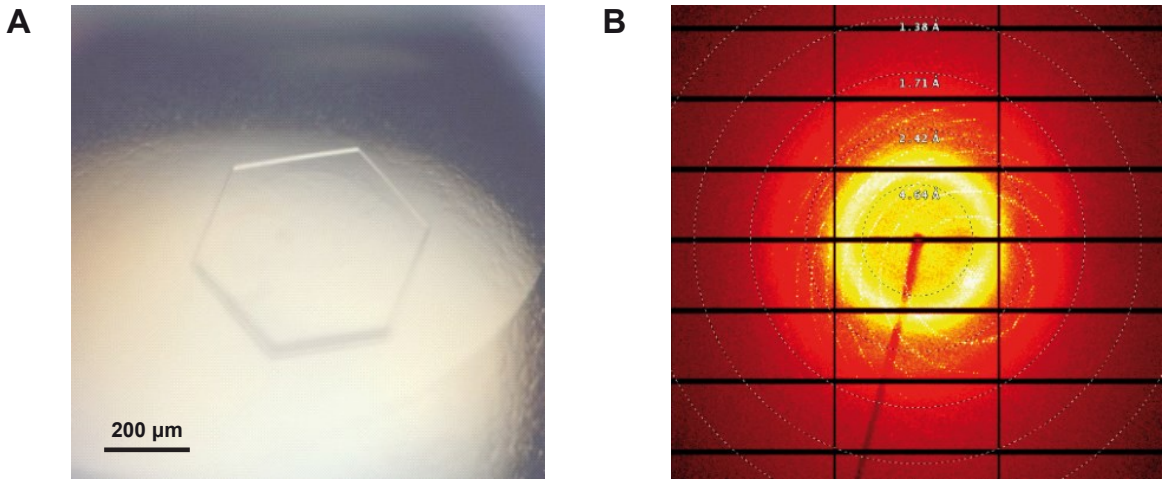

Figure 3.49. Successful crystallization of the Catacalin C3A5 with a C-terminal *Strep*-tag II. **A:** Crystal of C3A5 in complex with the TSA in the presence of 20 % (w/v) PEG3350 and 0.2 M diammonium tartrate. **B:** X-ray diffraction pattern of the crystal in (A) collected at the BESSY synchrotron beamline 14.2 (Berlin, Germany). The data were kindly provided by Dr. Andreas Eichinger.

The crystal structure was refined at a high resolution of 1.7 Å. The electron density was defined for residues Ser3–Gly180 as well as the TSA ligand including the hexanoyl linker, which was directed towards the solvent. Only the two N-terminal amino acids and the C-terminal *Strep*-tag II with the Ser-Ala-linker remained unresolved. As seen in Figure 3.50A, the Catacalin C3A5 forms a ~12 Å deep ligand pocket, narrower than in the wild-type lipocalin 2, as could be expected from the smaller dimensions of the TSA. Similar to the orientation of enterobactin in Lcn2 (and deviating from the orientation of colchicine in the Colchicalin D6.2 described earlier, cf. Chapter 3.3.8), the TSA 'lies' on the surface of the binding pocket, with a considerable portion of the ligand exposed to solvent. The dichloromethylene bridge that corresponds to the sulfoxide bridge in the actual transition state (cf. Figure 1.5) points sideward and is only partly accessible from solvent.

The superposition of the C3A5 structure with the crystal structure of lipocalin 2 (mutant K125A; PDB:3CMP) via the 58 conserved Cα atoms of the β-barrel (see Chapter 2.8.3) yielded a low RMSD of 0.592 Å, indicating that the overall lipocalin fold remained virtually unchanged. At the same time, the corresponding superposition of all 174 common resolved Cα atoms led to a higher RMSD of 2.841 Å, which results from the deviating conformations of several structurally variable loops at the open end of the β-barrel (Figure 3.50B). The most striking deviation concerns loop #1: compared with Lcn2, it is folded inward by up to 13.6 Å (if measured at the α-carbons of residue 45), thus narrowing the entrance to the pocket. Its conformation is stabilized by the formation of a 4-residue α-helix with 3 intrahelical hydrogen bonds as well as by up to 8 backbone- and side chain-mediated hydrogen bonds. Loop #3 also underwent substantial changes, although its shift by up to 9.8 Å is directed tangentially along the ridge of the β-barrel. In contrast, the positions of loop #2 and loop #4 are practically identical to those in the wild-type lipocalin.

Analysis of the protein-ligand interactions using PISA (Krissinel & Henrick, 2007) showed that the TSA binding is mediated via 14 amino acids, which is a low number compared with other engineered lipocalins (cf. Table 4.1). However, these relatively few amino acids are arranged with sufficient precision to cover 79.6 % of the accessible ligand surface (441 of 554 Å), including the flexible solvent-oriented hexanoyl linker, and build to 58 van der Waals contacts. The ligand pocket is paved predominantly by hydrophobic amino acids: the 3 hydrophilic residues (Asp47, Asn81, Thr125) account for only 11 % of the contact surface on the protein side, while the remaining 89 % contact surface is contributed by 5 aliphatic and 6 aromatic residues (Table 3.8, see also Figure 3.50C). Notably, only 5 of the 14 ligand-contacting amino acids belong to the set of 20 randomized positions, which can be explained by the fact that the employed library was designed as a compromise to enable selection against both protein-type and hapten-type ligands (Gebauer *et al.*, 2013) and was not optimized for selecting binding proteins against small haptens such as the TSA. However, some other randomized residues are also located in the ligand proximity and might interact with the ligand indirectly, while the more distant residues might contribute to the overall shape fit of the protein-ligand pair, contributing to the high affinity of C3A5 for the TSA.

Figure 3.50. Crystal structure of the Catacalin C3A5. **A:** Van der Waals surfaces of the Catacalin C3A5 in comparison with and the wild-type Lcn2, view from the top. The ligands (TSA and ferric enterobactin, respectively) are shown as stick models. **B:** Superposition of the Catacalin C3A5 (red) and wild-type Lcn2 (green) crystal structures in two projections, shown as ribbon models. The two structures were aligned at the 58 conserved residues of the β-barrel (see Chapter 2.8.3). **C:** Surface electrostatics of the Catacalin C3A5. Negative charge is shown in red, positive in blue. **D:** Close-up view of the bound TSA in the ligand pocket. The amino acid residues interacting with the ligand are shown as stick models. Dashed cyan lines represent hydrogen bonds.

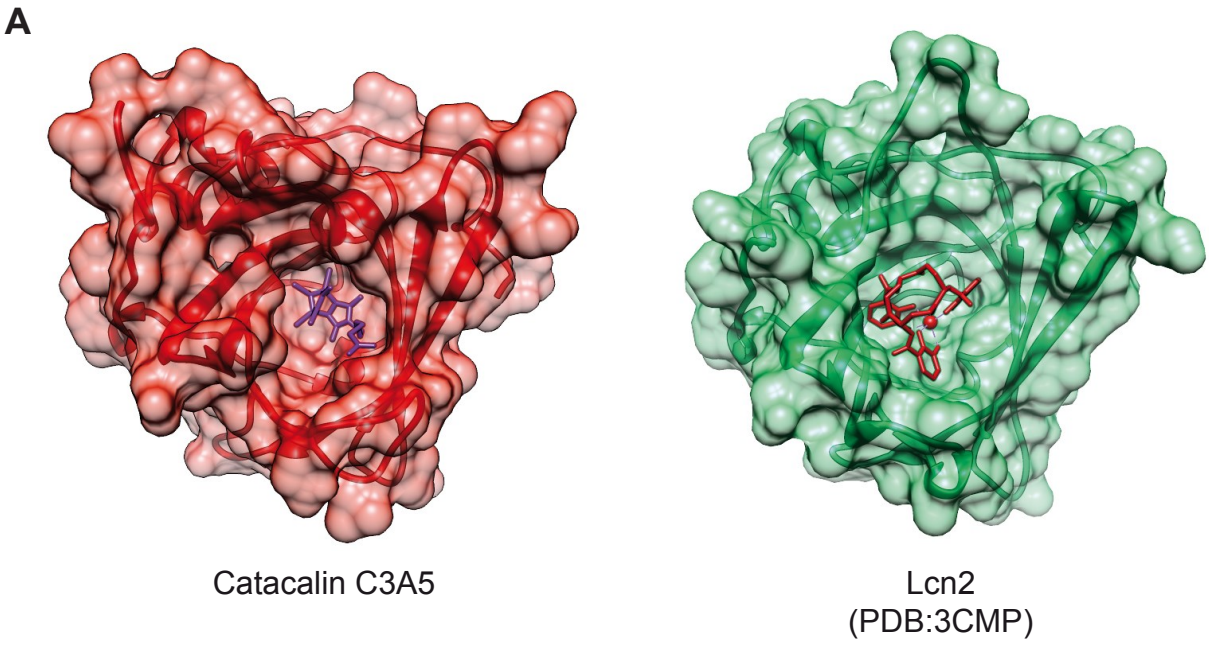
A
Catacalin C3A5
Lcn2
(PDB:3CMP)

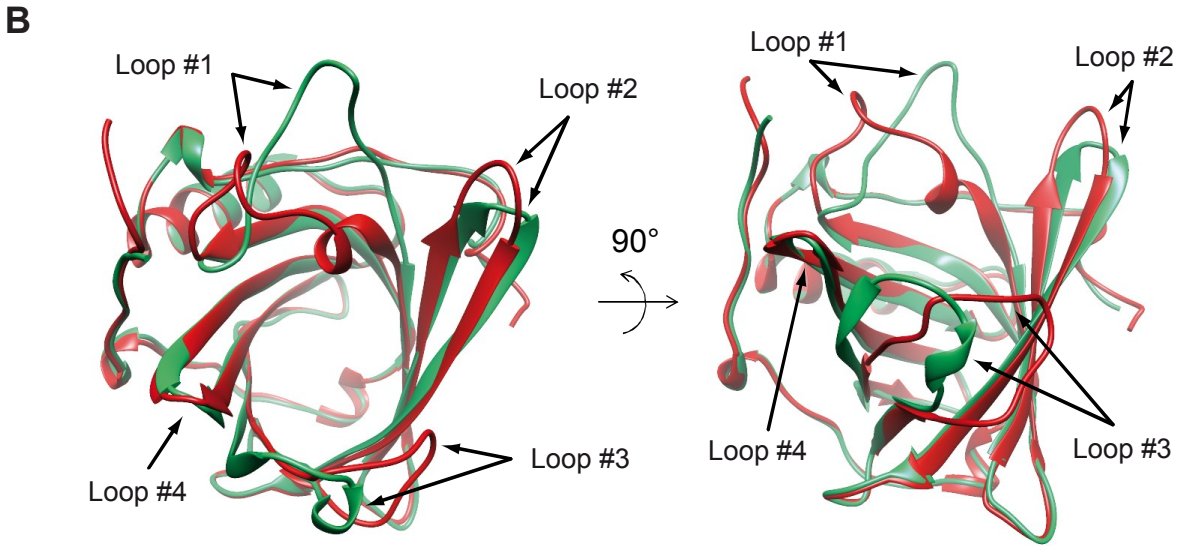
B
Loop #1
Loop #2
Loop #3
Loop #4
90°
Loop #1
Loop #2
Loop #4
Loop #3

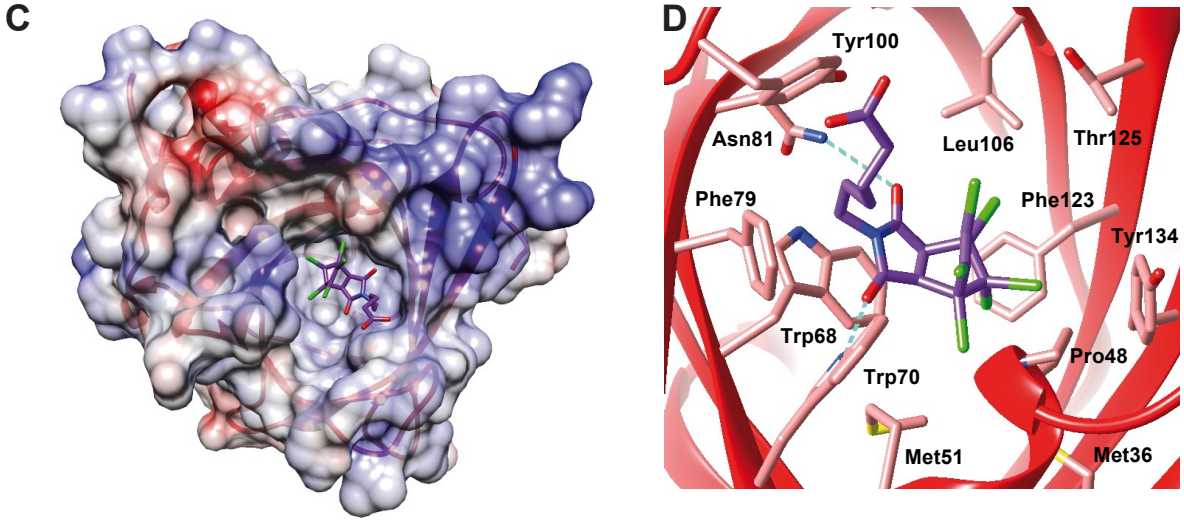
C
D
Tyr100
Asn81
Leu106
Thr125
Phe79
Phe123
Tyr134
Trp68
Pro48
Trp70
Met51
Met36

The chlorine atoms of the TSA are mainly surrounded by hydrophobic and aromatic amino acids (Met36, Met51, Pro48, Leu106, Phe123, Tyr134), whereas the succinimidyl ring rests on the benzene ring of Trp68 and forms a π-stacking interaction (Figure 3.50C,D). Notably, Tyr100 contributes 17.3 % of the contact area from the protein side and interacts mainly with the hexanoyl side chain of the TSA, implying that the flexible linker, originating from a short ethyl chain of NEM in the actual transition state, is important for the TSA recognition by the Catacalin C3A5. Apart from the hydrophobic interactions, the TSA is bound via two hydrogen bonds involving both carbonyl groups of its succinimidyl ring as well as the indole nitrogen of Trp70 and the amide nitrogen of Asn81 (Figure 3.50D).

Table 3.8. Residues of the Catacalin•TSA complex forming van der Waals contacts with the ligand.

Residue	Buried surface [Å^2]	Percentage	Residue	Buried surface [Å^2]	Percentage
Met36	10.1	4.1 %	Asn81*	11.1	4.5 %
Asp47	1.5	0.6 %	Tyr100	42.5	17.3 %
Pro48	20.8	8.5 %	Pro101	7.9	3.2 %
Met51*	8.9	3.6 %	Leu106	17.2	7.0 %
Trp68	28.9	11.8 %	Phe123	17.3	7.1 %
Trp70*	28.0	11.4 %	Thr125	15.2	6.2 %
Phe79*	22.9	9.3 %	Tyr134*	13.0	5.3 %
			Total:	**245.4**	**100.0 %**

Amino acids with a contact surface of ≥1 Å^2 as analyzed with PDBe PISA (Krissinel & Henrick, 2007). Individual contributions of the amino acids are indicated as absolute values and as portions of the total buried surface area from the protein side. Amino acid positions randomized in the lipocalin library are marked with an asterisk.

Overall, the high-resolution crystal structure unravels that the Catacalin C3A5 addresses several structural features of the TSA: the complex is stabilized predominantly via hydrophobic interactions as could be expected from the highly hydrophobic nature of the polychlorinated TSA, and are supplemented by a π-stacking, whereas both polar carbonyl groups are engaged in hydrogen bonding. The availability of this structure should enable the structure-guided design of new Catacalin variants with improved Diels-Alderase activity.

4. Discussion

4.1 Selection of Anticalins against colchicine

Since the invention of phage display in the mid 1980's, the methodology of directed protein evolution has been expanded by a variety of approaches (Sergeeva *et al.*, 2006; Packer & Liu, 2015). Some of them use living cells to link phenotype and genotype (cell surface display techniques), while others engage extracted or synthetic molecular machines for *in vitro* protein translation (ribosome and mRNA display as well as compartmentalized self-replication). Phage display is situated somewhere in the middle of the classifications because molecular recognition ('antigen presentation') takes place *in vitro*, while the genetic material is amplified *in vivo* (Jäckel *et al.*, 2008). This research project involved a multitude of protein engineering approaches, which are summarized in a scheme reflecting the path from the initial 'naïve' library to the final high-affinity Colchicalins (Figure 4.1, also Figure 4.2 and Table 4.4)

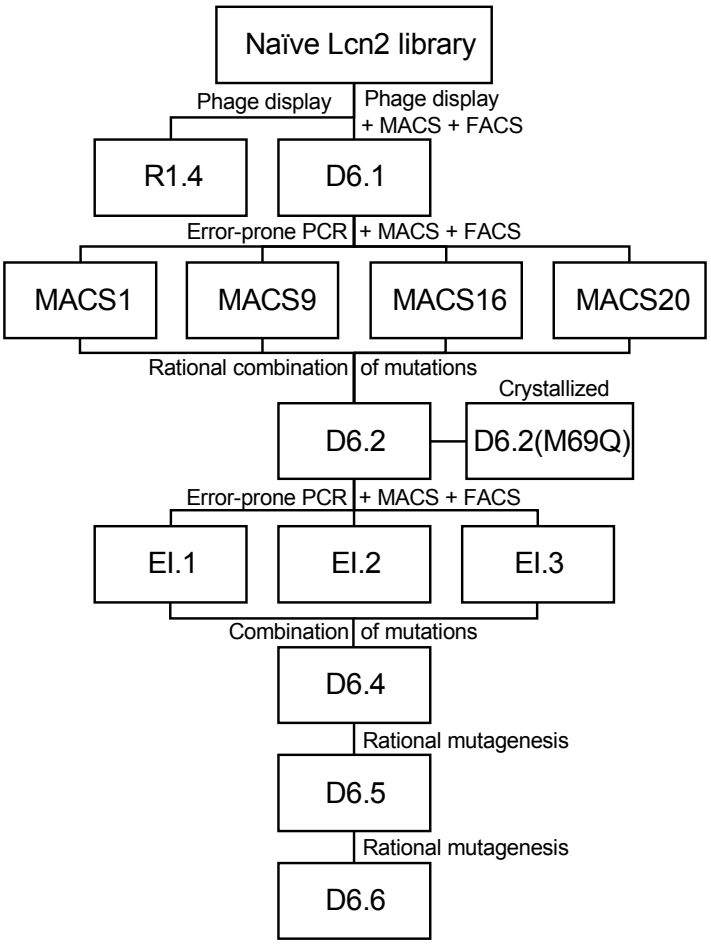

Figure 4.1. Schematic overview of anti-colchicine Anticalins developed in this work. The most important variants and their origins are indicated. While more than 20 unique clones were identified after the affinity maturation of D6.1, only the four variants that were analyzed as isolated proteins are shown. The variants EI.1–EI.3 were obtained by Elena Ilyukhina in the scope of her internship research project.

Originally, it was planned to pursue the selection of an Anticalin against colchicine via phage display. Phage display, historically the first method of directed evolution, is a well-established procedure verified in thousands of successful applications (Smith, 1985; Paschke, 2006) and in particular for Anticalin technology (Skerra, 2001). However, phage display offers limited possibilities to monitor the progress of selection. For example, determination of phage titers at each panning stage can help following the enrichment of the library, but its predictive power is limited to the elucidation of major deviations and does not provide sufficient information on the specificity of the enrichment. Exhaustive sequencing of the sublibraries from intermediate selection rounds is costly, labor- and time-consuming and also delivers only limited information. The so-called phage ELISA, in which phage or phagemid particles displaying protein variants are detected in a sandwich immunoassay, can be used as an 'in-process' control after each panning cycle to estimate enrichment of a target-specific subpopulation, but this only yields useful results if it constitutes a considerable portion of the library by the end of a successful selection campaign.

The initial selection of a colchicine-binding Anticalin performed via phage display in this work (see Chapter 3.1.1) did not lead to the expected ligand-dependent library enrichment, thus raising the question of the possible cause of this failure. During the phage display selection, the relative phage titer rose gradually from round to round, indicating that some sort of enrichment did take place. However, an unusual observation was made during the sequence analysis of the mutated lipocalin genes after the last panning round: these were unexpectedly rich in positively charged amino acids (mainly Lys and Arg), as can be seen in Figures 3.3 and 3.9 (Chapter 3.1.1). Such a phenomenon was observed in previous phage display selection campaigns of Anticalins, although in one case the prevalence of positive charges could be linked to the electrostatic interaction of the selected Anticalins with a patch of negative charges on the target protein (Richter, 2018). Since colchicine was uncharged under the selection conditions (pH 7.4), enrichment of Lys and Arg residues must be linked to other factors, such as unspecific interaction of the Anticalin with a component of the selection setup.

The most obvious candidates that might act as "unspecific" binding partners are streptavidin and NeutrAvidin on the surface of the paramagnetic beads. Indeed, according to the manufacturer's data, streptavidin possesses an isoelectric point of 5.5, implying prevalent negatively charged residues. Nonetheless, enrichment of streptavidin binders was prevented by alternating between streptavidin- and NeutrAvidin-coated paramagnetic beads after each round. In contrast to the bacterial streptavidin, NeutrAvidin is derived from the eukaryotic protein avidin and engineered to a more neutral isoelectric point of 6.3, thus reducing the chance of unspecific electrostatic binding (Vermette *et al.*, 2003). Interestingly, the prevalence of positively charged Anticalins was also noticeable among the clones that showed strong

signals in ELISA and filter-sandwich assays, which further supports the assumption of unspecific enrichment against a setup component.

Another possibility of target-independent enrichment might arise from factors related to phage biology, e.g. more favorable translocation of the Anticalin-pIII fusion proteins carrying multiple positive charges prior to virion assembly, or increased infectivity of corresponding phagemid particles. The former is unlikely because positive charges are known to decrease the efficiency of Sec-dependent translocation of the pIII phage protein, which is used as a lipocalin fusion partner in the employed phagemid library (Peters *et al.*, 1994; Schuenemann *et al.*, 1999; Rodi *et al.*, 2002; Wilson & Finlay, 1998). With regard to the latter, infectivity of the phagemid particles indeed might be influenced by the charge distribution on the phage surface, e.g. through interaction with the negatively charged phospholipid heads on the bacterial membrane (Rakonjac *et al.*, 2011). However, the electrostatic properties of the M13 virion are predominantly defined by the thousands of copies of the major coat protein pVIII, so that contribution of the 4–5 copies of pIII should be negligible. Furthermore, in the 'monovalent' phagemid-based display setup used in this work ("type 3+3" phage display according to Smith, 1993), each virion contains a mixture of Anticalin-pIII fusion proteins and wild-type pIII (originating from the helper phage), with only 1 copy per virion on average (Skerra, 2001). Nevertheless, the hypothesis cannot be completely rejected because the precise sequence of interactions leading to the phage intrusion into the inner membrane is not yet fully understood (Rakonjac *et al.*, 2011).

The absence of reproducible binding signal observed in the ELISA screening (cf. Figure 3.6) supported the assumption that the library enrichment was not driven by colchicine binding. This was elegantly confirmed by means of the filter sandwich assay screening that was performed with the sublibraries from the beginning, the middle and the end of the panning campaign (rounds 1, 5 and 8). While originally aiming at identifying specific binders, application of the filter sandwich assay allowed to investigate 'snapshots' of the whole selection process, finally elucidating that the phage display selection went in a wrong direction. Thanks to the high throughput of this method, it was possible to isolate an Anticalin with micromolar-range affinity towards colchicine (R1.4) from the sublibrary after the first panning round, i.e. from an early population with extremely high complexity. But, more importantly, this observation also showed that the original phagemid library actually contained specific colchicine-binding Anticalins, which were not sufficiently enriched during the panning.

The lack of success at isolating a potent colchicine binder via phage display alone stimulated the search for an alternative selection approach. A FACS-based bacterial surface display selection system was established before at the Chair of Biological Chemistry (Binder *et al.*,

2010) and was chosen here for the affinity maturation of R1.4 because of the possibility of tighter control over the selection process: in contrast to phage display, the enrichment progress can be quantitatively evaluated according to the distribution of cellular fluorescence signals after each selection round. Furthermore, the mean binding signal can be normalized to the amount of displayed protein on the bacteria, which allows to outweigh factors related to protein translation and/or translocation efficiency, thus directing selection to the target binding. Furthermore, since it was assumed that the initial lipocalin library could contain other colchicine-specific Anticalins, bacterial surface display was also used for screening the sublibrary obtained after round 2 of the phage display selection.

While providing better control over the selection, bacterial surface display is limited by the throughput of the FACS instrument, which makes screening of more than 10^8 clones per selection round impractical (Binder *et al.*, 2010; Doerner *et al.*, 2014). However, the library complexity can be reduced prior to FACS with the help of magnet-assisted cell sorting (MACS). Thereby, bacterial cells displaying the protein of interest are first incubated with target-charged paramagnetic beads and, after the elimination of non-binding variants by washing, the cells are released, amplified and sorted via FACS. Successful selection of Anticalins from a naïve library via bacterial surface display with MACS pre-enrichment was previously demonstrated by Friedrich *et al.* (2017). While MACS allows to overcome the throughput limitation of the FACS device, it must be mentioned that it possesses a potential disadvantage. Due to the presence of multiple Anticalin moieties on the bacterial cell surface and multiple streptavidin units on each paramagnetic bead, a large avidity effect might arise and lead to low discriminative power with regard to the binding affinity. The strength of the avidity effect depends on the protein densities both on the bacterial cell surface (Anticalins) and on the paramagnetic beads (streptavidin with bound target compound). Assuming 3000 displayed protein molecules per cell (Binder *et al.*, 2010), the density of the displayed protein on a *E. coli* cell should comprise ~380 molecules/μm^2 (as a rough approximation, assuming the bacterial cell to be a 2 µm long and 0.5 µm wide cylinder with even surface). This should correspond to an average distance between the centers of the Anticalin molecules of around 60 nm. The streptavidin-coated paramagnetic beads used for MACS in this work (Roche Diagnostics, Cat. No. 11641778001) have an average diameter of 1 µm and can bind ≥1800 pmol biotin per mg beads, corresponding to a nearly side-to-side surface packing of the streptavidin tetramers (assuming a spherical bead with even surface and considering streptavidin as a flat cylinder with a diameter of 4.2 nm). Thus, polyvalent binding should be sterically possible, meaning that one bacterial cell can be bound to multiple beads via hundreds of protein molecules per bead. Such an avidity effect will be highly unselective with respect to the affinity strength and might disfavor proteins with tight binding but slow association kinetics.

However, the results obtained in this work demonstrated that application of MACS pre-enrichment was able to boost the functional diversity of the mutein pool prior to FACS, resulting in the selection of a much richer sequence pool of high-affinity binders compared with FACS carried out without pre-enrichment (Chapter 3.2.2). This allowed to identify the mutations responsible for the affinity gain, especially the Val69Met substitution that alone led to an order-of-magnitude leap in affinity. Finally, it resulted in the creation of Colchicalin D6.2, which contained only three mutations compared with D6.1 but had an up to 60-fold higher affinity (depending on the assay). The "MACS+FACS" approach was used again for the affinity maturation of D6.2, yielding the variants EI.1 and EI.3 (performed by Elena Ilyukhina) whose most relevant mutations were rationally combined to create D6.4. In this case, the affinity gain was not so drastic, as it is to be expected for proteins that already possess high affinity. Furthermore, it must be noted that the selection process for EI.1–EI.3 was designed to favor variants with slow dissociation kinetics, which was indeed achieved. Eventually, the most slow-dissociating variants D6.5 and D6.6 were created on the basis of D6.4 using the structural information from the high-resolution crystal structure of D6.2(M69Q) in complex with the ligand. To sum up, the combination of various protein engineering and selection methods employed in the current study yielded colchicine-binding proteins with varying affinity and kinetics that open potential applications in clinical toxicology and bioanalytics. As an overview, the amino acid sequences of all Colchicalins created in this study are listed in Figure 4.2.

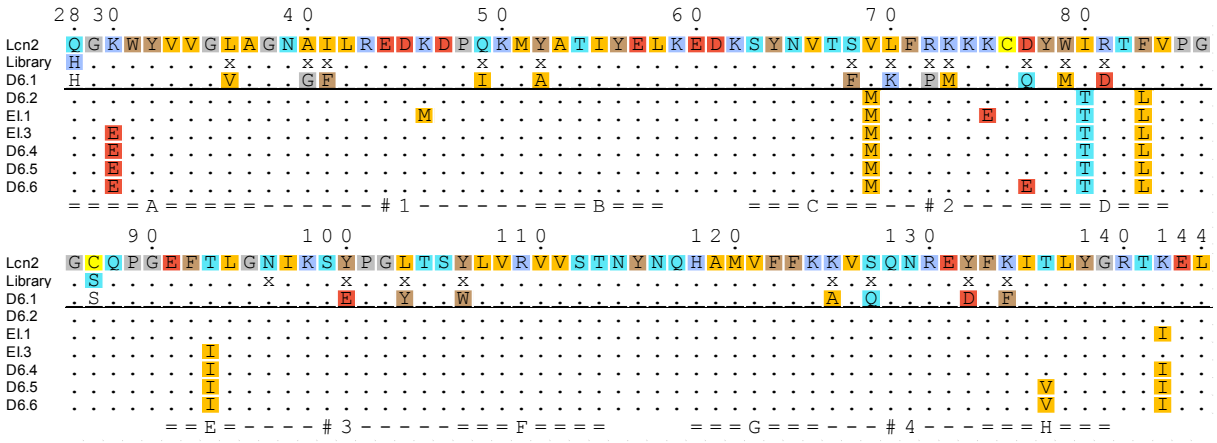

Figure 4.2. Amino acid sequence alignment of the high affinity Anticalins developed against colchicine. Only the mutation-containing central sequence (amino acids 28–144) is shown. The Anticalin D6.1 serves as a reference for the sequences underneath the black line. Sequences of the intermediate "MACS" variants mentioned in Figure 4.1 can be found in Figure 3.22. For the coloring scheme, cf. Figure 3.3.

4.2 Insights into the structural mechanism of the Anticalin complex formation with colchicine and other small-molecule ligands

Human lipocalin 2 (also known as NGAL or siderocalin) naturally evolved as a binding protein for the catecholate-type bacterial siderophores enterobactin, bacillibactin, carboxymycobactins

as well as their degradation products such as 2,5-dihydroxybenzoic acid, which serves as an iron scavenger in mammals (Goetz *et al.*, 2002; Abergel *et al.*, 2006; Holmes *et al.*, 2005). Both Lcn2-based engineered lipocalins selected against haptens prior to this work target metal chelators Y^{III}•DTPA (Kim *et al.*, 2009; Eggenstein *et al.*, 2014) and Fe^{III}•petrobactin (Dauner *et al.*, 2018) – haptens, which are somewhat distantly related to the natural Lcn2 ligands. On the other hand, colchicine consists of three condensed hexa- and heptacarbon cycles and has little similarity to any of these metal chelators.

By now, binding proteins based on human Lcn2 have been selected against four small-molecule ligands: the artificial metal chelator DTPA, the bacterial siderophore petrobactin, the plant toxin colchicine as well as the transition state analog **9** (Figure 1.5) described in Chapter 3.6. For all these Anticalins, the selection strategies involved phage display and/or bacterial surface display followed by high-throughput screening and rational mutagenesis, resulting in 'genera' of variants with gradually varying affinity, stability and binding kinetics. For most of them, at least one crystal structure of the protein•ligand complex has been solved and published in the Protein Data Bank in Europe (http://pdbe.org). In case of the DTPA-specific lipocalins, crystal structures of the complexes were obtained for three members of the 'genus' representing various stages of selection, affinity maturation and rational design: Tb7.N9 (PDB:3DSZ; Kim *et al.*, 2009), C26 (PDB:4IAW) and CL31 (PDB:4IAX; Eggenstein *et al.*, 2014). CL31 was chosen for the comparison with D6.2 shown below due to the pronounced changes in the conformation of the flexible loops. The structure of the Anticalin•petrobactin complex charged with gallium (Ga^{III}) was obtained only for the best variant M2, dubbed Petrocalin (PDB:6GR0). M2 was selected in the second round of affinity maturation with the help of bacterial surface display, which was preceded by selection and affinity maturation via phage display and filter sandwich colony screening (Dauner *et al.*, 2018). Eventually, for the colchicine-specific lipocalins described here, a crystal structure of the complex was obtained for the first variant that bound colchicine with subnanomolar affinity, namely D6.2 (PDB:5NKN; Barkovskiy *et al.*, 2018). D6.2 was additionally modified by a mutation M69Q to prevent possible oxidation of the solvent-oriented methionine residue (Chapter 3.3.8).

The affinities of all further colchicine-binding variants selected on the basis of D6.2 (Figure 4.1) remained virtually unchanged, while the binding kinetics gradually slowed down (see Table 3.5). Thus, it is conceivable that the overall shape complementarity in the protein•ligand complex was preserved, whereas the energy barrier of the transition between the unbound and bound state was increased. Nevertheless, it cannot be excluded that the binding mode for the 'slow' variants, e.g. D6.6, underwent certain changes. For instance, such changes were traced in the crystal structures of the three different stages of affinity maturation for the DTPA-binding Anticalins (Tb7.N9, C26 and CL31).

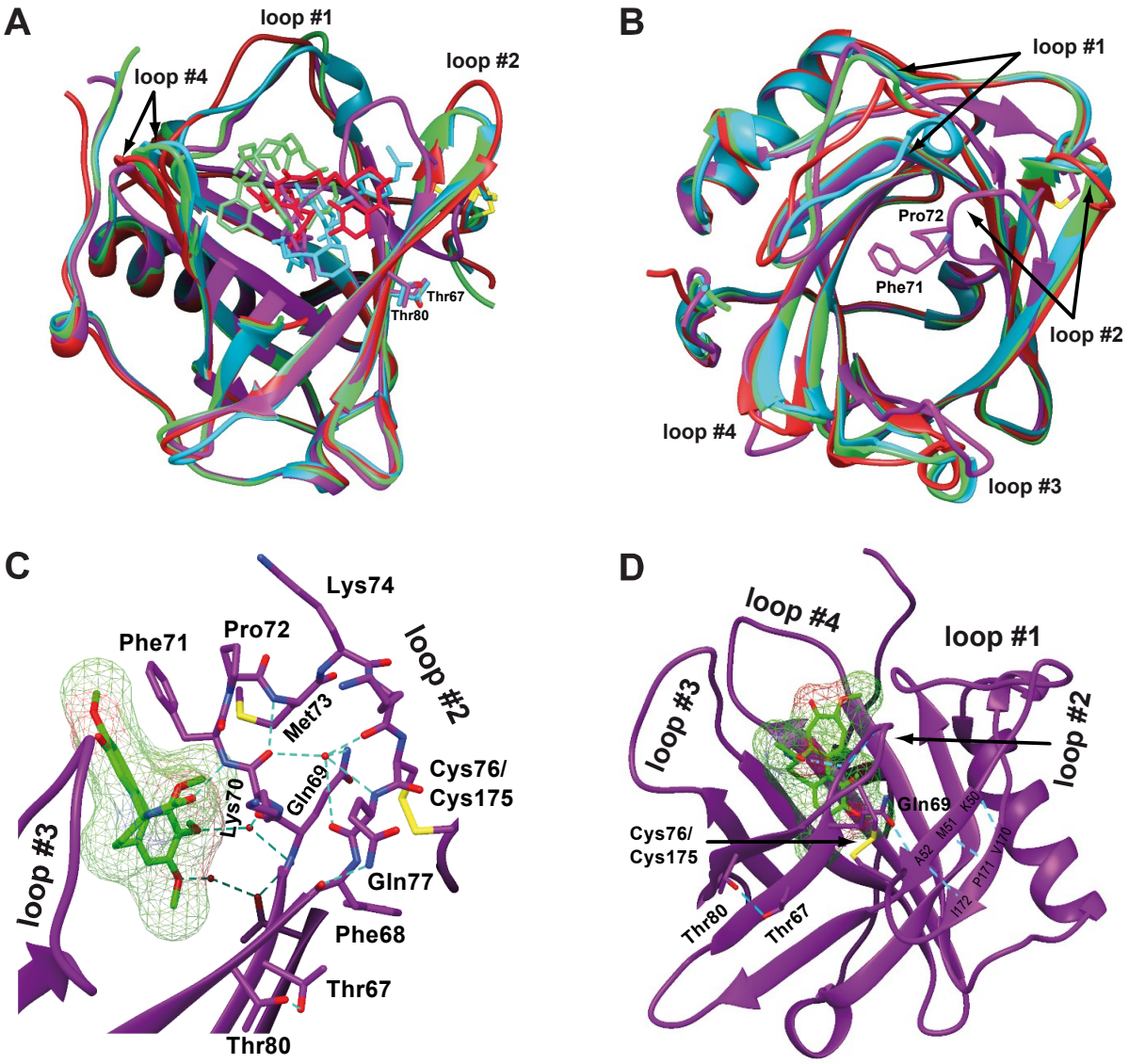

Figure 4.3. Structural features of D6.2(M69Q) in comparison with wtLcn2 and two other hapten-binding Anticalins. **A:** Structural alignment of Lcn2 (PDB:3CMP, green) with three Anticalins selected against hapten-type ligands: Colchicalin D6.2(M69Q) (PDB:5NKN, purple), Petrocalin M2 (PDB:6GR0, red) and Y-DTPA binder CL31 (PDB:4IAX, cyan). Alignment was performed via the 58 conserved Cα-positions (see Chapter 2.8.3). Other haptens intrude into the binding pocket more deeply than the natural ligand enterobactin (light green). Note residues Thr67 and Thr80, which form an H-bond with each other both in D6.2 and CL31. The structure was clipped at the front (hiding loop #3) to enable complete view on the ligands. **B:** Same superposition as (A), view from the top of the binding pocket. The residues Phe71 and Pro72 on Colchicalin D6.2(M69Q), which form the 'closing lid', are shown as sticks. Note the different conformations of loop #1 and loop #2 between Colchicalin D6.2(M69Q) and CL31. **C**: D6.2(M69Q) from the right side relative to the view in (A). Colchicine is shown in green, its accessible ligand surface is shown as mesh. Note the H-bond between Gln69 and Ala52 as well as the pair of short parallel β-strands between the stretches Lys50-Ala52 and Val170-Ile172. **D**: Close-up view at loop #2 (shown as sticks) of D6.2(M69Q) and its peculiar network of hydrogen bonds. Note residue Gln69, which is located directly on the bending edge of the loop #2, suggesting a role for the lid-like conformation of this loop. Also note the hydrogen bonds formed between the oxygen of the acetamide group of colchicine and the backbone nitrogen of Phe71 as well as between the oxygen of Lys70 and the nitrogen of Met73.

Both similarities and differences can be observed in the available structures of the various hapten-binding Anticalins, as illustrated in Figure 4.3. At first glance it appears that DTPA, petrobactin and colchicine intrude into the β-barrel more deeply compared with the wtLcn2•enterobactin complex (Figure 4.3). Similar to Lcn2, Petrocalin forms a shallow funnel-like cavity to which the petrobactin•Ga^{III} complex is bound mostly with one side, large molecule branches protruding to the solvent, as reflected in the comparably large solvent-accessible surface for the bound petrobactin (Table 4.1; see also Figure 3.32A,B). In contrast, both DTPA in complex with CL31 and colchicine bound D6.2(M69Q) are oriented more 'vertically' along the axis of the β-barrel; thereby, the acetylated amino group of colchicine points to the solvent, as expected from the design of the biotinylated colchicine derivative used for the selection. In both complexes, more than ¾ of the ligand become buried upon binding. In the case of D6.2(M69Q), merely 11 % of the colchicine surface remains solvent-accessible.

Table 4.1. Structural characteristics of hapten binding in some engineered lipocalins and tubulin.

Protein	Ligand surface [Å^2]	Buried ligand surface [Å^2]	Buried ligand surface [%]	Number of contacting amino acids	Source PDB structure[2]
Lcn2 (K125A)	729	532	73	20	3CMP (C)
Anticalin C26	747	533	71	21	4IAW (B)
Anticalin CL31	747	572	77	22	4IAX
Petrocalin M2	860	557	65	21	6GR0 (A)
Catacalin C3A5	554	441	80	14	n.a.
D6.2(M69Q)	618[1]	548	89	25	5NKN
Tubulin	608[1]	484 (β-subunit) + 124 (α-subunit)	80 + 20	22 (β-subunit) + 5 (α-subunit)	4O2B

[1] Differences in the calculated ligand surface area are due to the PISA calculation algorithm, in which the result slightly depends on the orientation of the molecule as well as the model resolution.
[2] In case of more than one polypeptide chain in the asymmetric unit, the used chain is indicated in brackets.

As seen in Table 4.1 as well Figure 4.3A, all these Anticalins were selected against molecules of comparable size, with colchicine being the smallest with a mass of 399 Da and a surface area of around 618 Å^2. Nevertheless, this rather small molecule is contacted by 25 amino acids of D6.2(M69Q) – more than in any other Lcn2 variant or even the wild-type protein – which is reflected by a buried colchicine surface of 89 % (548 Å^2). From the 25 contacting amino acids, 11 residues that were randomized in the initial combinatorial library provide 55.3 % of the contact area, while a 12th residue (Gln69) was mutated during the affinity maturation. The other 13 residues are from the wild-type protein and provide 43 % of the contact area. The illustration in Figure 4.3D highlights the contribution of loop #2, which provides three ligand-interacting

amino acids amounting for 80.4 Å^2 or 23 % of the total contact surface from the protein side (346.4 Å^2). Interestingly, 64.7 Å^2 arise from the wild-type residue Phe71 building a vast π-stacking contact with the colchicine tropone ring and simultaneously forming a hydrogen bond with the acetamide group of colchicine via its peptide amide.

The unusual conformation of loop #2 in D6.2(M69Q) becomes immediately evident from the structural alignment of the three hapten-binding Anticalins (Figure 4.3A,B). In Lcn2, Petrocalin and CL31, β-strands C and D extend almost to the tip of loop #2, leaving only few amino acids uninvolved in the ladder of interstrand hydrogen bonds. In contrast, the flexible part of loop #2 in D6.2(M69Q) includes all residues from 70 to 77, which is comparable in length with the longest Lcn2 loop #1. Its structure is marked by a combination of interactions within the loop and with the neighboring structural elements. For instance, the peptide bond linking residues Pro72 and Phe71 acquires a *cis*-configuration, which is unusual compared with other Anticalins with crystal structure known up to date (see Figure 4.3B,D). The sharp inward turn of loop #2 begins at the position 69 (Gln69 in the crystallized protein or Met69 in the original variant D6.2), whose mutation from Val to Met/Gln was responsible for the affinity boost on the way from D6.1 to D6.2 (see Table 3.2). Formation of this turn appears even more unexpected given the fact that the flexibility of loop #2 is restricted by the disulfide bond connecting Cys76 to Cys175 near the C-terminus of the protein. Via this S-S bond, the C-terminus seems to be pulled inward into proximity of the hinge between loop #1 and β-strand B, thus favoring the formation of a peculiar pair of short parallel β-strands between the amino acid stretches Val170–Ile172 and Lys50–Ala52 (Figure 4.3C). The overall loop geometry is supported by a network of hydrogen bonds involving a water molecule positioned in the ‘loop hole’ and capable of building up to four H-bonds with the backbone nitrogen and oxygen atoms in residues 70 to 77 (Figure 4.3D). The influence of induced fit upon complexation of colchicine on the observed conformation of loop #2 remains an intriguing question.

Loops #3 and #4 also reveal structural changes unseen in the other three Anticalins. Loop #3 has lost the short α-helical span (positions 97-99), become longer and more flexible and also bent inward by up to 6.4 Å (see also Figure 3.32B), although it contributes only 2 Å^2 contact area with the ligand. In loop #4, the flexible region of the loop spread throughout the positions 126–132 and built 25 Å or 7 % of the contact area from the protein side, despite being bent slightly away from the ligand pocket compared with Lcn2, Petrocalin and CL31. Interestingly, the orientation of the longest and most flexible loop #1, whose conformational differences are responsible for a large portion of RMSD between the structures of Lcn2, Petrocalin and CL31, remains virtually unchanged from Lcn2 (Figure 4.3A,B).

It should be noted that the structure of D6.2(M69Q) has so far been considered to be representative for the structure of D6.2 itself, which carries Met at position 69. While this assumption can generally seem plausible given the similar length and shape of Met and Gln side chains as well as their comparable effect on the affinity of D6.1/D6.2, the substitution of Met69 to Gln might have introduced minor structural and energetic changes to loop #2 and its surroundings. As a most obvious example, the hydrogen bond between the side chain of Gln69 and the backbone amide of Ala52 would be impossible for the original variant D6.2, which carries Met69.

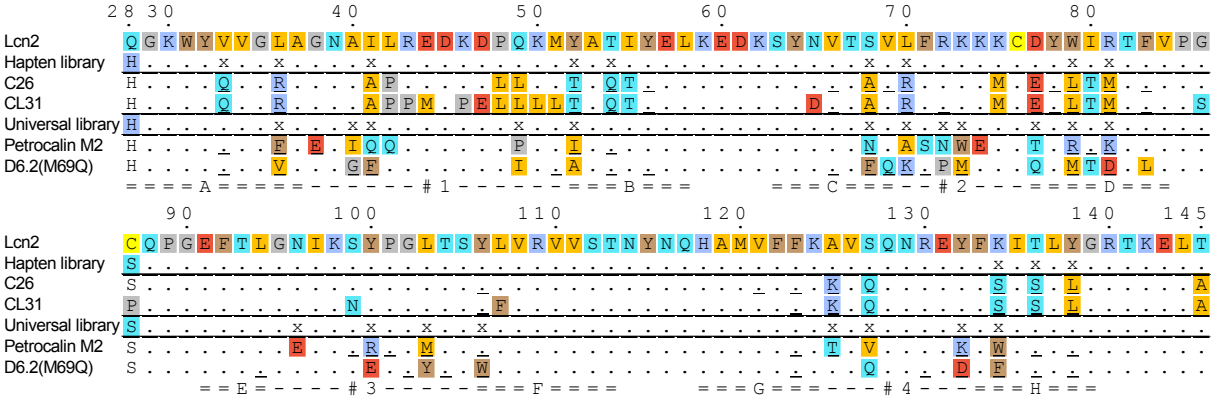

Figure 4.4. Amino acid sequence alignment of the central regions of several Anticalins selected against hapten-type ligands. The randomized positions in the combinatorial libraries used for the initial selection of the precursors of C26 and CL31 ('hapten' library) as well as of Petrocalin M2 and D6.2(M69Q) ('universal' library) are marked with an 'x' (CL31 originated from C26 via site-directed randomization as well as error-prone PCR; see Eggenstein *et al.*, 2014 for details). Amino acid residues building the interface with the ligand, as identified via PISA analysis of the crystal structures mentioned in Figure 4.3 (PDB:4IAW for C26), are underlined. Amino acids corresponding to the β-strands are marked with double lines, flexible loops – with single lines. For the coloring, cf. Figure 3.3.

Comparison of the amino acid sequences of the hapten-binding lipocalins (Figure 4.4) shows almost no matching residues at the mutagenized amino acid positions. On the contrary, it can be seen that amino acids of different size, hydrophobicity and charge are well tolerated by the scaffold. Together with the high shape complementarity to their ligands achieved in particular by the Colchicalin D6.2 and Petrocalin M2, this highlights the versatility of Lcn2 as a scaffold in general, as well as the suitability of the chosen randomization sites (Gebauer *et al.*, 2013). In earlier selection campaigns, two distinct libraries were used to select for protein-type and hapten-type ligands: for hapten-type ligands, residues in the central region of the binding pocket were chosen for randomization (Kim *et al.*, 2009) while for voluminous protein-type antigens, the more exposed parts of the flexible loops were randomized (Schönfeld *et al.*, 2009). However, the new 'universal' Lcn2-based library (Gebauer *et al.*, 2013) seems to be capable of delivering lipocalin variants with exquisite specificities towards small molecule haptens, peptides and protein epitopes. Via mutagenesis, the binding pocket can either

deepen to accommodate small ligands and allow them to enter the β-barrel, as in C26, CL31 and D6.2, or remain shallow, similar to the binding mode in the wild-type Lcn2 or Petrocalin. Of note, residues at four positions randomized in the 'hapten' library and omitted from the 'universal' library (Val33, Thr54, Thr136 and Tyr138) form contacts with the ligand in both Colchicalin and Petrocalin, making up for ~7 % of the interface area in both Anticalins; the substitution Thr136Val that was introduced into Colchicalin D6.4 via rational mutagenesis allowed to significantly increase the complex half-life (Table 3.5). This observation might be used in case other hapten-targeted Anticalin libraries are designed.

Table 4.2. Key biochemical characteristics of the hapten-binding Anticalins.

Protein	Melting point [°C]	Buried ligand surface [Å^2]	% Surface from library residues [a]	K_D [pM]	$t_{1/2}$ [min]
Lcn2	78.6 [b]	532	n.a.	410 [c]	n.a.
C26	69.9 [b]	533	74%	234 (7600) [b]	37 [b]
CL31	59.1 [b]	572	66%	273 [b]	138 [b]
Petrocalin M2	n.a.	557	78%	21 [d]	n.a.
D6.2	75.9	548 [e]	55%	120 [e]	90
D6.6	71.1	n.a.	n.a.	139	560

[a] Percentage of the buried ligand surface contributed by the residues randomized in the combinatorial library.
[b] Data from (Eggenstein *et al.*, 2014); K_D and $t_{1/2}$ values were measured via SPR analysis with Y^{III}•DPTA-RNAse conjugate, the K_D value in brackets was measured via fluorescence titration with free Y^{III}•DPTA.
[c] Data from (Goetz *et al.*, 2002; Abergel *et al.*, 2008), measured via fluorescence titration with Fe^{III}•enterobactin.
[d] Data from (Dauner *et al.*, 2018), measured via fluorescence titration with Fe^{III}•petrobactin at 10 nM protein.
[e] Buried ligand surface is shown for the M69Q mutant. The K_D value was measured via fluorescence titration with colchicine at 20 nM protein, $t_{1/2}$ was determined via real-time SPR with PEG_5-colchicine (see Figure 2.1).
PDB structures used for the calculations are the same as in Table 4.1.

Interestingly, the hapten-binding Anticalins with the cleft-like pocket resemble other members of the lipocalin family; the narrow entrance into the pocket is characteristic for this protein family, while Lcn2 with its wider funnel-like cavity is rather an exception (Breustedt *et al.*, 2006). Most members of the lipocalin family bind small hydrophobic ligands like retinol (Flower *et al.*, 2000; Breustedt *et al.*, 2006), which partially explains the tolerance of this scaffold to multiple mutations inside the β-barrel (Richter *et al.*, 2014). In the case of the Colchicalin D6.2, the Lcn2 scaffold 'offers' its inner space for ligand binding while maintaining the conformational stability of the wild-type protein, as shown by CD melting analysis: its melting temperature differs from that of Lcn2 by less than 3 °C (see Table 4.2). In agreement with the high thermal stability, in total 148 hydrogen bonds could be detected for D6.2(M69Q), compared with the 140 bonds calculated for Lcn2 using identical parameters (calculated via UCSF Chimera according to relaxed bonding criteria, as defined in Mills & Dean (1996) and Pettersen *et al.*

(2004)). One of these – the hydrogen bond between the side chains of Thr67 and Thr80 (Figure 4.3A,C,D) – became possible due to the mutation Ile80Thr, which occurred during the affinity maturation of the initial Colchicalin D6.1. Interestingly, the same bond-forming substitution Ile80Thr is also found in the DTPA-binding lipocalin variant Tb7.14 and its derivatives C26 and CL31; in that selection campaign, variants with Ile80Thr were identified several times independently after error-prone PCR as well as after site-specific saturation mutagenesis (Kim *et al.*, 2009). While at first glance this outer-shell substitution appears to be a 'junk' mutation without direct ligand contact, the repeated occurrence suggests that it might have been selected due to a stabilizing effect on the β-barrel with deeply buried haptens.

The high thermodynamic stability of the selected Colchicalins is accompanied by solid production yields as well as ease of downstream processing and biochemical handling. All analyzed Colchicalins behaved as strictly monomeric proteins with little to no tendency to aggregate or oligomerize as judged by SEC, whilst absence of chemical and/or post-translational modifications within the bacterial host or during the purification procedure was confirmed by ESI-MS for the most variants. Furthermore, during the protein crystallization trials, D6.2 and its derivatives could be concentrated to 50 mg/mL at low salt concentration (≤50 mM) and without use of surfactants or other stabilizers. All these are aspired in the target quality profiles of new biological entities, which will facilitate further development and manufacturing scale-up in the case of future industrial or clinical applications.

4.3 Anticalins against colchicine as antidotes

4.3.1 Design of animal experiments

For performing toxicity and pharmacokinetic studies with colchicine and its potential antidote Colchicalin, a *Rattus norvegicus* model was chosen. Despite physiological and metabolic differences from humans, *R. norvegicus* (the brown rat) has become a widely accepted model species for toxicity studies due to a convenient body size, low maintenance cost and thoroughly studied anatomy, metabolism and genetics (Oser, 1981). This animal model was also chosen here because an experimental design had been established and tested on rats in pre-clinical trials conducted for an Anticalin-based antidote against digoxigenin in cooperation with Abteilung für Klinische Toxikologie at the Klinikum rechs der Isar, Munich (Eyer *et al.*, 2012).

Colchicine intoxications result almost exclusively from oral administration. Hence, one could consider oral gavage to be the most appropriate way of testing colchicine poisoning. However, the highly variable individual profiles of colchicine adsorption, metabolism and excretion after oral administration often lead to unreliable pharmacokinetic and toxicological effects, as demonstrated in studies performed in rats or Göttingen minipigs (Peake *et al.*, 2015; Eddleston

et al., 2018). For instance, in a colchicine toxicity study carried out in a minipig model, Eddleston *et al.* (2018) failed to obtain interpretable pharmacokinetic data after oral colchicine gavage and had to switch to intravenous administration instead. After all, even though the latter administration route is not a perfect mimic of oral poisoning, its practical advantages, i.e. simplicity, comparability and reproducibility, might outweigh its disadvantages in case of colchicine poisoning. Bioavailability after i.v. administration was also reported to be similar to that after oral application (Putterman *et al.*, 1991).

The experiments carried out on the *Rattus norvegicus* model in this work had three major goals: (1) obtain data on the pharmacokinetics of colchicine in rat after i.v. administration, (2) determine optimal colchicine dosage for detecting its toxic effects within the time scale of the experiment and (3) measure the plasma pharmacokinetic profile of the Colchicalin D6.2 and its PASylated forms in order to choose the best candidate as antidote against colchicine.

For reaching the first goal, a set of experiments was designed during which the rats were put under deep narcosis, the necessary blood vessels were cannulated and the most important physiological parameters (body temperature, heart rate, blood pressure, etc.) were continuously monitored. Since narcosis can result in unstable breathing, artificial ventilation through a tracheal intubation was applied. This experimental setup was optimal for delivering reliable pharmacokinetic measurements, because colchicine injection as well as subsequent blood sampling could be performed in a fast and reproducible way, even though the general physiological influence of the narcosis and surgical intervention had to be tolerated. Resulting data on colchicine concentration in plasma showed little scattering and followed the expected biphasic exponential decay (see Chapter 3.5.1), thus confirming suitability of the chosen experimental setup for pharmacokinetic profiling.

The second purpose of the described set of experiments was the determination of the minimal colchicine dosage to achieve a poisoned state, which was necessary for later detecting the clinical improvement brought by application of the antidote. Ideally, the best experimental mimic of a real poisoning situation would involve lethal colchicine dosage on healthy conscious rats without surgical intervention, accompanied by an analogous experimental set including application of the antidote. However, treatment of awake rats with lethal doses of colchicine would be associated with severe and prolonged suffering of the animals (Ferguson, 1952; Sternberg *et al.*, 1954; Rosenbloom & Ferguson, 1968). The deep narcosis used in our experiments prevented this suffering. However, this anesthesia made surgical intervention necessary, which in turn limited the time scale of the experiment: since maintenance of the required physiological parameters under experimental conditions was challenging, the whole experiment had to be accomplished within 3–4 h.

There is anecdotal evidence that lethal colchicine toxicity in rats can develop already 1 h after *i.v.* injection (Chen *et al.*, 2008). In that study, all rats that received colchicine doses of at least 0.9 mg/[kg body mass] died within one hour after injection. In the design of our experiment with rats, an even higher colchicine dose (10 or 20 mg/kg) was chosen, assuming that the high colchicine concentration should suffice for the development of acute toxicity within the experimental time span.

However, administration of such a high colchicine dose raises a different problem as this necessitates injection of a large amount of protein in order to ensure complete stoichiometric complexing of colchicine within the body. Still, according to the literature, sequestration of 100 % of the colchicine dose may be not necessary. In the case described by Baud *et al.* (1995), the only example of reversal of colchicine intoxication by a Fab fragment in humans, the patient ingested 60 mg, or 0.96 mg/[kg body mass] colchicine. This lies above the dose of 0.8 mg/kg, for which 100 % mortality has been reported (see Table 4.3). The antidote applied in this case contained 7.5 % colchicine-specific Fab in 6.4 g of polyclonal Fab fragment preparation, i.e. in total 480 mg colchicine-binding Fab fragment. Assuming a molecular mass of 50 kDa for the Fab fragment, this amount should be capable of binding 3.8 mg colchicine, which is 6.4 % of the total ingested dose. The patient was brought to the hospital 27 h after the overdose and had a colchicine plasma level of 24 ng/mL; infusion of the Fab was started 9 h later (36 h after toxin ingestion). By the starting point of Fab infusion, colchicine concentration had further dropped to 12 ng/mL but rose abruptly to 70 ng/mL already 10 min after the onset of infusion. The first half of the Fab dose was given within 1 h while the second one was spread over the next 6 h, leading to a further increase of total plasma colchicine level to 100 ng/mL; at the same time, the concentration of unbound colchicine in plasma fell to undetectable levels, and urinary colchicine excretion increased 6-fold. These clinical findings suggest that complexation of only a minor portion of the ingested colchicine dose enabled efficient detoxification, which eventually led to full patient recovery.

Table 4.3. Toxicity (LD50) of colchicine in various species, grouped according to the administration route.

Administration route	Oral [mg/kg body mass]	Intravenous [mg/kg body mass]
Rattus norvegicus	26–51 (Wiesenfeld *et al.*, 2007)	1.6 (Rosenbloom & Ferguson, 1968)
Göttingen minipig	–	<0.25 (Eddleston *et al.*, 2018)
Human	0.5–0.8 (Stapczynski *et al.*, 1981)	presumably <0.2 (Jaeger *et al.*, 1980)

In a recent work by Peake *et al.* (2015), who studied reversal of colchicine toxicity after oral gavage upon administration of anti-colchicine Fab in rat, similar effects were observed: the injected 250 mg total Fab protein contained 12.5 mg toxin-specific Fab fragments capable of binding ~0.1 mg colchicine, which equaled 8 % of the applied colchicine dose (5 mg/kg, ~1.25 mg). Although this colchicine dose was sublethal and led only to gastrointestinal symptoms, the authors claimed that application of the Fab fragment led to an improvement of the rats' physiology as judged by the absence of diarrhea. Taken together, these evidences allow to assume that sequestration of the whole colchicine pool in the body is not necessary to achieve clinical recovery.

The efficacy of the reported sub-stoichiometric antidote treatment is difficult to explain. Theoretically, the colchicine trapping in plasma and the equilibrium-driven increase of the total colchicine plasma concentration could intensify colchicine renal elimination, which normally constitutes only 10–20 % of its excretion (Borron *et al.*, 1996). Even though upon antidote administration the plasma colchicine pool is mainly present in a Fab-bound state, a small portion of colchicine will always stay in its free form due to the Law of Mass Action. While the sizes of both the Fab fragment and colchicine lie below the glomerular cut-off of ~70 kDa, the Fab fragment has a hydrodynamic radius approaching the effective radius of the filtration pores (~3 nm vs ~3.7 nm; Lund *et al.*, 2003), and its filtration rate should lag far behind that of the small 400-Da colchicine molecule. Thus, the varying filtration rates of colchicine and the Fab fragment could at least partly account for the observed sub-stoichiometric detoxification.

4.3.2 Colchicine pharmacokinetics

Published data on colchicine pharmacokinetics in the rat is scarce: only two reports present data after intravenous administration (Hunter & Klaassen, 1975; Sabouraud *et al.*, 1992b). It is known that the toxicity (and probably also pharmacokinetics) of colchicine in rat is gender-dependent (Wiesenfeld *et al.*, 2007), but in both reports, male adult Sprague-Dawley rats were used, like in the current work.

In the first report on colchicine pharmacokinetics (Hunter & Klaassen, 1975), adult male Thorp Sprague-Dawley rats weighing 350–390 g were treated with doses of 0.2 and 2.0 mg/kg ^{3}H-colchicine in a volume of 2 mL/kg (i.e. ~0.7 mL) through the femoral vein. Blood samples of 0.5 mL were then collected in the course of two hours and the colchicine content in plasma was determined by quantifying the radioactivity. For the 2 mg/kg dose, the plasma concentration of colchicine fell from 4 to 0.3 µg/mL within the first 120 min after infusion. Qualitatively, the resulting colchicine PK profile has a similar shape to that obtained in the current work, but the $t_{1/2}$ values were not reported, which makes an exact comparison difficult.

In the second report (Sabouraud *et al.*, 1992b), in which anti-colchicine Fab fragments were tested in a rat model, the authors also analyzed the plasma pharmacokinetics of colchicine. Similar to the previous example, male Sprague-Dawley rats weighing 290±10 g were used. Infusion was performed via the femoral vein, and 0.4 mL blood samples were taken in the course of 150 min. However, in this case a lower ^{3}H-colchicine dose of only 0.015 mg/kg was administered. The reported $t_{1/2\alpha}$ and $t_{1/2\beta}$ values were 6 and 125 min, respectively, compared with ~1 and ~7 min observed in the current work.

The source of this large discrepancy is unclear but can be partly explained by the nearly 1000-fold difference between the administered colchicine doses. While lower doses would be fully absorbed by the overwhelming number of colchicine binding sites in the tissues, higher doses would saturate more tubulin units, thus reducing effective affinity within the tissues and promoting faster colchicine excretion. Furthermore, Sabouraud *et al.* (1992b) used a radioactivity-based colchicine assay, which does not discriminate between colchicine and its metabolites, at least if the radioactive atoms remain bound to the colchicine scaffold. In contrast, the HPLC method used in the current work was developed to specifically detect the native colchicine. Furthermore, the slower colchicine clearance reported by Sabouraud *et al.* could result from the different narcosis scheme used in that study (bolus of 60 mg/kg pentobarbitone sodium as well as additional doses of 5 mg/kg, as necessary), which influences the physiological condition of the rats.

As already mentioned in Chapter 3.5.1, curve fits of the plasma concentration profiles show above-zero asymptotes, which seems to result from an overlap with an additional peak of plasma concentration observed at 90 min or later (see Figure 3.36). This delayed peak was observed for all rats that received 10 mg/kg colchicine and survived until the end of the experiment (1.5 h). As a possible explanation, this peak could result from enterohepatic circulation – a well-known feature of colchicine intoxication in animal models as well as in clinical cases (Borron *et al.*, 1996; Chen *et al.*, 2008). For instance, a delayed plasma peak was observed within the first 6 h after oral gavage in human subjects (Ferron *et al.*, 1996). Due to the faster metabolism in rats, a corresponding peak would be expected at an earlier time point, in accordance with the described observations. The short time span of the experiment did not allow to observe the terminal elimination profile after the delayed colchicine peak. However, it is also possible that the observed increase in colchicine concentration after 90 min is linked to renal dysfunction due to the surgical intervention and narcosis.

4.3.3 Anticalin pharmacokinetics

The Colchicalin D6.2 was the first high-affinity (subnanomolar) colchicine binding protein selected in this work and had been chosen for the preclinical trials before the other variants (EI.3 to D6.6) were selected. However, this choice still appears reasonable since the variants selected afterwards possess similar equilibrium dissociation constants and slower binding kinetics (see Figure 3.34). Thus, D6.2 also offered the fastest colchicine-binding activity of all selected variants, combined with relatively fast colchicine release. Considering the possible detoxification mechanism that implies a role of the antidote as a blood-renal toxin transporter, faster binding and release kinetics should be favorable.

The small size of the lipocalin scaffold offer advantages for therapeutic applications such as good tissue penetration and fast renal elimination. The latter can also be considered a positive aspect for antidote applications in case of toxins with low tissue absorption. At the same time, the fast elimination is less suitable in case of colchicine with its high distribution volume and rather slow redistribution from tissue: an antidote bolus would be quickly eliminated and only deplete the plasma pool, thus missing the much larger tissue-bound portion of the toxin. While this caveat could be tackled by administering the antidote via prolonged antidote infusion rather than injection, a more elegant solution was used here by modifying the Anticalin by PASylation.

PASylation® technology developed at the Chair of Biological Chemistry and commercialized by XL-protein GmbH is one of the most advanced methods of extending the plasma half-life of proteins by increasing their hydrodynamic radius (Schlapschy *et al.*, 2013; Binder & Skerra, 2017). The technology is based on the N- or C-terminal genetic fusion of a proline/alanine/serine-rich polypeptide sequence, which occupies a large hydrodynamic volume due to its random coil structure. Since the attachment is performed on the genetic level, no additional purification (e.g., separation of the coupling reagent as in the case of PEGylation) is necessary. The capability of this technology to prolong or tune the plasma half-life of therapeutically relevant proteins, including Anticalins, has been demonstrated in various pre-clinical studies (Friedrich *et al.*, 2017; Pfeiffer, 2017; Xia *et al.*, 2019).

As only little data on the pharmacokinetics of PASylated proteins upon intravenous administration to rats was available by the time when the experiment was planned, the Colchicalin D6.2 was modified with two PAS versions of different lengths, i.e. 200 or 600 amino acid residues. Switching to an intracellular expression system based on the *E. coli* Origami B strain simplified the production of the PASylated Anticalin considerably, while requiring only minor changes to the purification strategy (see Chapter 3.5.2). Even though the production and purification of the PAS600-version was more challenging than the PAS200 fusion due to the

lower expression yield of the former, both versions could be prepared in amounts sufficient for the first preclinical experiments.

The time scheme for blood sampling (Table 3.6) was chosen in accordance with available pharmacokinetic data for PASylated leptin in a mouse model (Morath *et al.*, 2015). Remarkably, the half-lives determined for the PASylated versions of Colchicalin D6.2 differed from the non-PASylated protein by up to ~400-fold, from 2.7 min to 75 min for D6.2-PAS200 and to 17.6 h for D6.2-PAS600 (Figure 4.5).

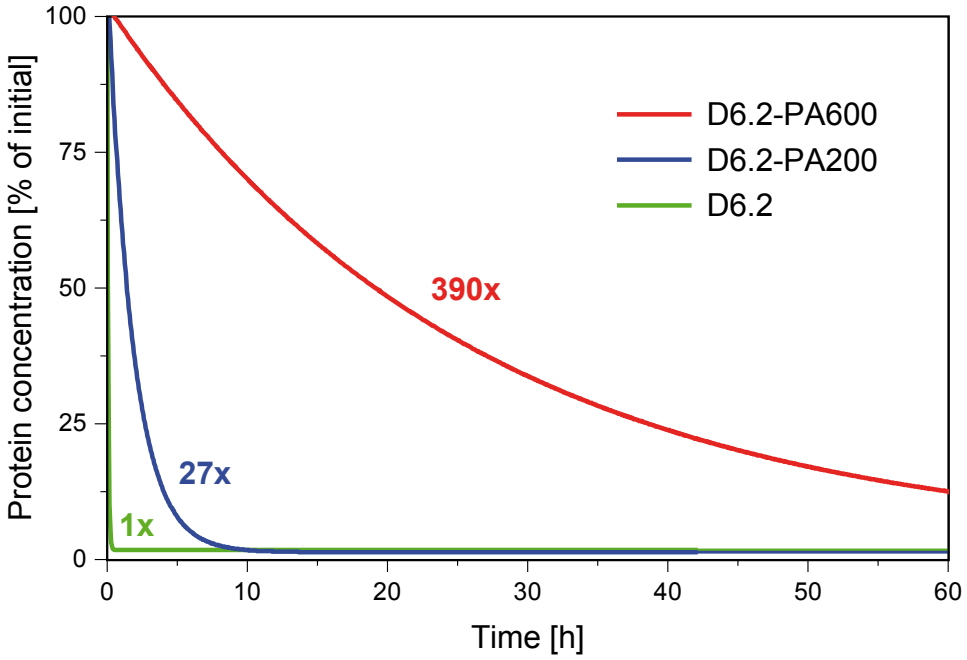

Figure 4.5. Pharmacokinetic profiles of the Colchicalin D6.2 and its PASylated versions in rat plasma. The gain in half-life factor compared with the non-PASylated D6.2 is indicated.

Pharmacokinetics of Anticalins in rats has not been extensively studied. The only case reported up to now describes PK profiling of Lcn2 modified with PAS100 or PAS200 upon intravenous administration in female Wistar rats (Skerra *et al.*, 2008). The attachment of PAS200 increased the half-life of Lcn2 from ~3 min to ~31 min, which is somewhat smaller than 75 min observed for D6.2-PA200 in this study. However, it should be considered that Skerra *et al.* used female animals and a different rat strain, which could influence the elimination behavior; furthermore, the first-generation PAS sequence consisting of proline, alanine and serine was employed, in contrast to the serine-free sequence used in the present work.

More PK studies were performed on mouse models. For instance, Schlapschy *et al.* (2013) investigated the pharmacokinetics of human interferon α2b as well as a therapeutically relevant Fab fragment – both modified with PAS200 or PAS600 – after intravenous application, whereas Morath *et al.* (2015) performed a study with the PASylated 'satiety hormone' leptin

applied peritoneally. In the first case, the terminal half-life increased from 0.54 h to 2.6 h (PAS200) and 15.9 h (PAS600) for the interferon and from 1.34 h to 5.2 h and 28.2 h, respectively, for the Fab fragment. Whereas the relative gains are much smaller than those achieved for the PASylated D6.2, the absolute values for both proteins are similar, especially for PAS600 (e.g. 15.9 h for IFN-PAS600 *vs* 17.6 h for D6.2-PAS600). The PAS200- and PAS600-modified leptin versions also demonstrated similar absolute half-live values (e.g., 19.6 h for leptin-PAS600), despite the longer half-life of the free leptin (26 min). Thus, the length of the fused PAS peptide was determinative for the plasma half-lives, the effect being more pronounced for small proteins and long PAS sequences.

Although the elimination half-life of the non-PASylated Colchicalin D6.2 is close to the calculated $t_{1/2}$ of its binding target colchicine, the true *in vivo* half-life of colchicine should be longer than the values calculated here due to the presence of a slower elimination phase that could not be characterized within the experimental time scope, as discussed above. On the other hand, the extremely slow elimination of D6.2-PA600 could turn into a disadvantage if the protein-toxin complex continues circulating in the blood after the toxin had been removed from the tissues. Thus, the Colchicalin D6.2-PA200 should be the most promising candidate for antidote applications as it represents a good compromise with regard to circulation half-life and also high production yield.

4.3.4 Potential problems for antidote applications

Insufficient affinity could theoretically impose a problem for gradient-driven detoxification according to the “peripheral sink” hypothesis (i.e. gradient-driven sequestration of the tubulin-bound colchicine from the tissues). Tubulins (first of all, α- and β-tubulin) are among the most abundant proteins in the mammalian cell (Geiger *et al.*, 2012). The great number of binding sites in the tissues means that a much higher affinity of the antidote towards colchicine is necessary in order to compete with its natural binding target. However, affinity of the Colchicalin D6.2 already lies in the same range as reported for the Fab fragment that was shown to be effective against colchicine intoxication both in animals and in one human case (Sabouraud *et al.*, 1991; Baud *et al.*, 1995). The affinity of D6.2 for colchicine is 4–5 orders of magnitude higher than that of colchicine to its natural ligand tubulin (Banerjee & Luduena, 1992), which should allow efficient detoxication. Nonetheless, it must be noted that the newly reported affinity of the anti-colchicine Fab from Micropharm Ltd. (ColchiBIND, see Table 1.2; Eddleston *et al.*, 2018) is one order of magnitude higher than that of the current Colchicalins. Whether the higher affinity brings a clinical benefit to the new anti-colchicine Fab is so far unclear. Another problem might arise from renal reabsorption of the Colchicalin•colchicine complex. Once the complex becomes reabsorbed after the primary filtration into the proximal

convoluted tubule, the kidney tissue itself may be damaged, which may hinder the detoxication efficiency.

Renal filtration of proteins and other large molecules depends on their hydrodynamic radius, structural rigidity and charge. The first two factors are determined by the pore size in the glomerular filtration slit. The apparent hydrodynamic radius (r_H) limit for proteins lies in the range of up to 37–38 Å (Lund *et al.*, 2003). The charge of the molecule also influences renal filtration because the filtration pores are negatively charged leading to lower filtration rates for anionic proteins due to electrostatic repulsion (Rennke *et al.*, 1978; Deen & Satvat, 1981). The renal clearance of globular proteins with molecular masses exceeding ~60 kDa (r_H = 37–38 Å), such as antibodies, is usually negligible (Strober & Waldmann, 1974; Lund *et al.*, 2003), resulting in plasma half-lives in the range of days to weeks (Dixon, 1952; Schaller *et al.*, 2008). Smaller proteins such as lipocalins cross the glomerular filtration barrier and appear in the primary urine formed in the glomerular lumen. However, only 1 % of these proteins can be found in the final excreted urine (Strober & Waldmann, 1974). This difference is explained by the active *reabsorption* of proteins in the proximal convoluted tubules (PCT).

Renal reabsorption of proteins filtered to the lumen correlates with their size, but is not exclusively determined by this parameter (Bernard *et al.*, 1987). In contrast to the diffusion-controlled glomerular filtration, reabsorption is based on endocytosis mediated by the receptors *megalin* and *cubilin* (Christensen & Birn, 2002; Nielsen *et al.*, 2016). Lcn2 is known to interact with megalin (dissociation constant measured by SPR, $K_D \approx 60$ nM) and is actively reabsorbed in the PCT (Hvidberg *et al.*, 2005), as are 99 % of the proteins filtered to the primary urine. Deletion of megalin in mice leads to the appearance of Lcn2 in the urine beside other proteins (proteinuria). Indeed, Lcn2 also serves as a protein marker of renal disfunction (Barasch *et al.*, 2016).

Of note, the interaction with megalin and, hence, tubular uptake is charge-dependent. The affinity of megalin to Lcn2 is higher than to most other lipocalins, which can be explained by its high net positive charge compared to other lipocalins (Åkerstrom *et al.*, 2000; Breustedt *et al.*, 2006). The Colchicalin D6.2 carries much fewer positive charges than the wild-type Lcn2 (p*I* 6.79 vs 9.24; see Table 4.4). However, the protein used for the PK experiments in rats carried a C-terminal His_6-tag, which increased its p*I* to the slightly basic value of 7.32. The pH in the proximal convoluted tubule is close to the plasma and usually drops to ~6.8 (DuBose Jr *et al.*, 1981; Hamm *et al.*, 2013). Thus, the Colchicalin D6.2 should retain positive charge and, hence, it is possible that the Colchicalin will be reabsorbed in the PCT.

Table 4.4. Overview of the Colchicalins and their calculated isoelectric points.

Variant	Mutations *	Calculated p*I*
wtLcn2	–	9.24
library Lcn2	Q28H/C87S	9.42
D6.1	see Figure 4.2	6.79
D6.2	V69M/I80T/F83L	6.79
EI.3	K30E/T93I	5.71
D6.4	K142I	5.26
D6.5	T136V	5.26
D6.6	Q77E	5.01

* Indicated are those mutations that are different from the variant in each line above. The p*I* was calculated from the primary sequence without affinity tags using Geneious.

The problem of proximal tubular reabsorption is well-known and typical for radionuclide-labeled Fab therapy. Several approaches have been proposed to cope with this problem (Akizawa *et al.*, 2008; Vegt *et al.*, 2010a). *Competitive inhibition* of the receptor-mediated tubular uptake with positively charged amino acids or their derivatives (Rolleman *et al.*, 2003), peptides and partially digested proteins (Vegt *et al.*, 2010b) was shown to be effective for reducing the uptake of positively-charged peptides. Analogously, competitive inhibition was achieved by co-administration of polyglutamic acid (Béhé *et al.*, 2005). *Inhibition of endocytosis* – the main mechanism of tubular protein uptake – also reduces protein reabsorption. For instance, nocodazole, an agent interfering with the formation of microtubules, was shown to decrease reabsorption of albumin by more than 50 % (Gekle *et al.*, 1997). Even more relevant for the current study, Rolleman *et al.* (2004) demonstrated a pronounced (>60 %) inhibitory effect on the tubular uptake of radioactively labeled octreotide (mimic of somatostatin) in rats if they were pre-treated with a 1 mg/kg intraperitoneal dose of colchicine 5 h prior to the administration of the peptide. Administration of 400 mg/kg lysine was similarly effective, while a combination of colchicine pre-treatment with lysine co-administration yielded >70 % inhibition.

This reabsorption-inhibiting effect of colchicine can be explained by the disruption of microtubular transport of the membrane vesicles in the tubular epithelial cells, preventing recycling of the membrane material with megalin (gp330) to the apical membrane. The latter leads to the disappearance of megalin from the apical membrane and its accumulation in the intracellular vesicles (Gutmann *et al.*, 1989; Elkjaer *et al.*, 1995; Mirela *et al.*, 2000). Thus, individuals poisoned with colchicine are likely to exhibit reduced tubular protein reabsorption *per se*. This is in line with the high occurrence of proteinuria as a clinical symptom of colchicine intoxication (Stapczynski *et al.*, 1981; Putterman *et al.*, 1991). This phenomenon becomes especially interesting in the context of the current work, meaning that the Colchicalin antidote

applied to a poisoned patient will act under conditions of colchicine-triggered reduction of renal protein reabsorption, which should boost its clearance via urinary secretion and prevent recycling of colchicine back into the blood circulation.

Alternatively to influencing the renal system, the problem of renal reabsorption can be solved by modifying the properties of the protein itself. For instance, Barasch *et al.* (2016) reported the engineering of wild-type lipocalin 2 for decreased reabsorption to be applied as a therapeutic iron chelator. Starting from the assumption that high renal reabsorption of Lcn2 is linked to its excessive positive surface charge, a collection of 47 lipocalin variants was prepared, in which Lys and Arg and His residues on the protein surface were exchanged to neutral or negatively charged amino acids. As a result, several variants were shown to evade tubular reabsorption, leading to urinal accumulation of up to 20 % of the administered protein dose. While such an extensive manipulation of the outer-shell residues might raise the chance of immunogenicity in case of repeated application, this should be of less importance for the treatment of acute colchicine poisoning considering that polyclonal animal sera are routinely used for this purpose. Thus, creation of analogous modifications of the Colchicalins that would lower tubular uptake and improve their detoxicating capability would be a logical step for the further development of lipocalin-based antidotes against colchicine.

4.4 Activity improvement of catalytic Anticalins

4.4.1 Selection and design of TSA-binding lipocalin variants

The Diels-Alder cycloaddition between TCTD and NEM represents one of the most well-studied reactions in connection with catalytic antibodies. The murine monoclonal antibody 1E9 was selected in 1989 at the beginning of the era of catalytic antibodies (Hilvert & Hill, 1989) and remains one of the most efficient artificial enzymes generated for a Diels-Alder transformation up to now. The success of 1E9 was possible due to the outstanding transition state-mimicking properties of the TSA (Figure 1.5, **9**), which was used as immunization hapten. This TSA constitutes a bulky ligand with an electron distribution pattern similar to the actual transition state, but at the same time structurally different from the final reaction product (see Figure 1.5), which reduces the chance of generating enzymes suffering from product inhibition (Tawfik *et al.*, 1994). The generation of catalytic proteins outside the antibody platform can open new possibilities since other proteins provide more sequence space and broadens the potential range of accessible reactions and catalytic modalities (Hilvert, 2000). The lipocalin 2 scaffold was shown in our laboratory to bind various ligands including small molecules (Gebauer & Skerra, 2012), making it a perspective candidate protein for the selection of novel catalysts.

Using the HPLC assay developed in this work, it was possible to quantify the rate difference between the uncatalyzed reaction and the reaction in the presence of the putative lipocalin-based Diels-Alderases C3A5 and E1G2. Somewhat unexpected, the lipocalin variant E1G2 possessing 1000-fold lower TSA affinity turned out to be the better catalyst, with higher turnover than C3A5. The introduction of mutations into E1G2 based on the observed sequence similarities with C3A5 using a semi-rational approach allowed the identification of the E1G2 triple mutant T79N/W81F/W134Y ('Catacalin NFY'), which showed 2-fold increased activity.

Unfortunately, the attempt to further boost the catalytic activity of the Catacalin NFY via affinity maturation against the TSA **9** yielded no improved variants. The failure to obtain better catalysts by merely selecting for improved affinity against the TSA is not surprising *per se*: numerous examples show that higher TSA affinity does not necessarily lead to higher catalytic efficiency (Piatesi & Hilvert, 2004; Siegel *et al.*, 2010). However, the absence of converging amino acid patterns among the ELISA hits, which would be expected in the case of a successful enrichment – and which was clearly seen during the affinity maturation of the Colchicalin D6.1 – may indicate that the phage display selection campaign suffered from a methodological problem. Thus, it is possible that application of an improved setup or a different selection strategy may deliver more active variants that could eventually make the reaction rate screenable, e.g. via the iodine-starch assay (Xu *et al.*, 1999).

It should be mentioned that an attempt to improve the catalytic activity of the Catacalin C3A5 via affinity maturation has been made by Johannes Krumm within his internship at the Chair of Biological Chemistry, TU Munich. The selection was based on the bacterial surface display setup used in the current work for the affinity maturation of the Colchicalin D6.1. As a result, multiple variants with improved TSA affinity and clear affinity-related sequence patterns could be identified after bacterial surface display. Nevertheless, none of the affinity-maturated versions acquired higher catalytic activity, suggesting that structure-guided rational design should be the method of choice for the further improvement of this Catacalin.

4.4.2 Comparison between the Catacalin C3A5 and the catalytic antibody 1E9

As described in Chapter 3.8, the Catacalin C3A5 was several times subjected to crystallization attempts within the current work, but all those crystals, albeit optically clear and homogeneous, contained layers of intergrown lattices that hindered evaluation of the dataset. Subsequently, another protein preparation of C3A5 was crystallized by Irmgard Neumaier and Dr. Andreas Eichinger (Chair of Biological Chemistry, TU Munich), yielding a sufficiently homogeneous crystal to enable the dataset solution via molecular replacement.

The availability of this crystal structure enables a comparison of the TSA-binding mode of C3A5 with the published catalytic antibody 1E9 and its derivatives (Xu *et al.*, 1999; Piatesi & Hilvert, 2004). The crystal structure of the 1E9 Fab fragment (PDB:1C1E; Xu *et al.*, 1999) was solved in complex with the TSA **9** (cf. Figure 1.5) – the same ligand as used for the selection of 1E9 as well as the Catacalins C3A5 and E1G2. Of note, further improved variants of 1E9 were subsequently published, but this discussion will concern the initial variant of 1E9 as the oldest and the most investigated one. For all kinetic experiments with 1E9 published after 2003, an expression- and stability-engineered Fab fragment of 1E9 carrying two mutations MetH87Thr and GlyL63Ser was used, which possesses TSA affinity of 100 pM and nearly identical catalytic parameters (Piatesi, 2003).

When analyzing the TSA binding modi for 1E9 and C3A5 and their possible influence on the catalysis, it must be kept in mind that the crystallization ligand **9** carries a caproic acid linker at the succinimide nitrogen, while the substrate NEM (**5**) as well as the actual transition state carries an ethyl group at the maleimide nitrogen (cf. Figure 1.5). One of the most striking features of the 1E9•TSA complex (Figure 4.6) is its nearly perfect shape complementarity. The highly hydrophobic binding pocket interacts with the TSA via a multitude of van der Waals contacts (see Table 4.5), with 86 % of the TSA surface buried upon binding. Notably, only an *N*-methyl substituent instead of the full *N*-caproyl group is defined in the TSA **9** in the published PDB structure 1C1E, which leaves the question open whether 86 % was calculated for the 'truncated' or the complete hapten.

In the C3A5•TSA complex, the ligand is bound less tightly, as reflected by two orders of magnitude lower affinity, but is immersed into a deeper binding pocket as typical for the lipocalin fold. The most notable difference between the binding modes of 1E9 and C3A5 is the ligand orientation: whereas the TSA is lying on the bottom of the binding pocket in C3A5 with its flat side, 1E9 complexes the TSA from the side (see Figure 4.6A). Covering almost 80 % of the hapten surface, 14 amino acid residues in C3A5 are involved in contacts. Notably, the caproyl side chain of the TSA is much better defined in C3A5 than in 1E9. Since Tyr100, which interacts almost exclusively with the caproyl tail, is responsible for 17.3% of the buried surface from the protein side, it is possible that the affinity of C3A5 towards the actual transition state carrying the short ethyl substituent from NEM may be significantly lower (Figure 4.6B). Quantum mechanical calculations performed for 1E9 showed that the free binding energy rises with increasing chain length of the TSA linker in the row from *N*-methyl to *N*-caproyl (Chen *et al.*, 2000), which supports its relevance for the TSA recognition by the antibody. Measurement of the affinities of C3A5 and 1E9 towards an ethyl version of the TSA would clarify this question.

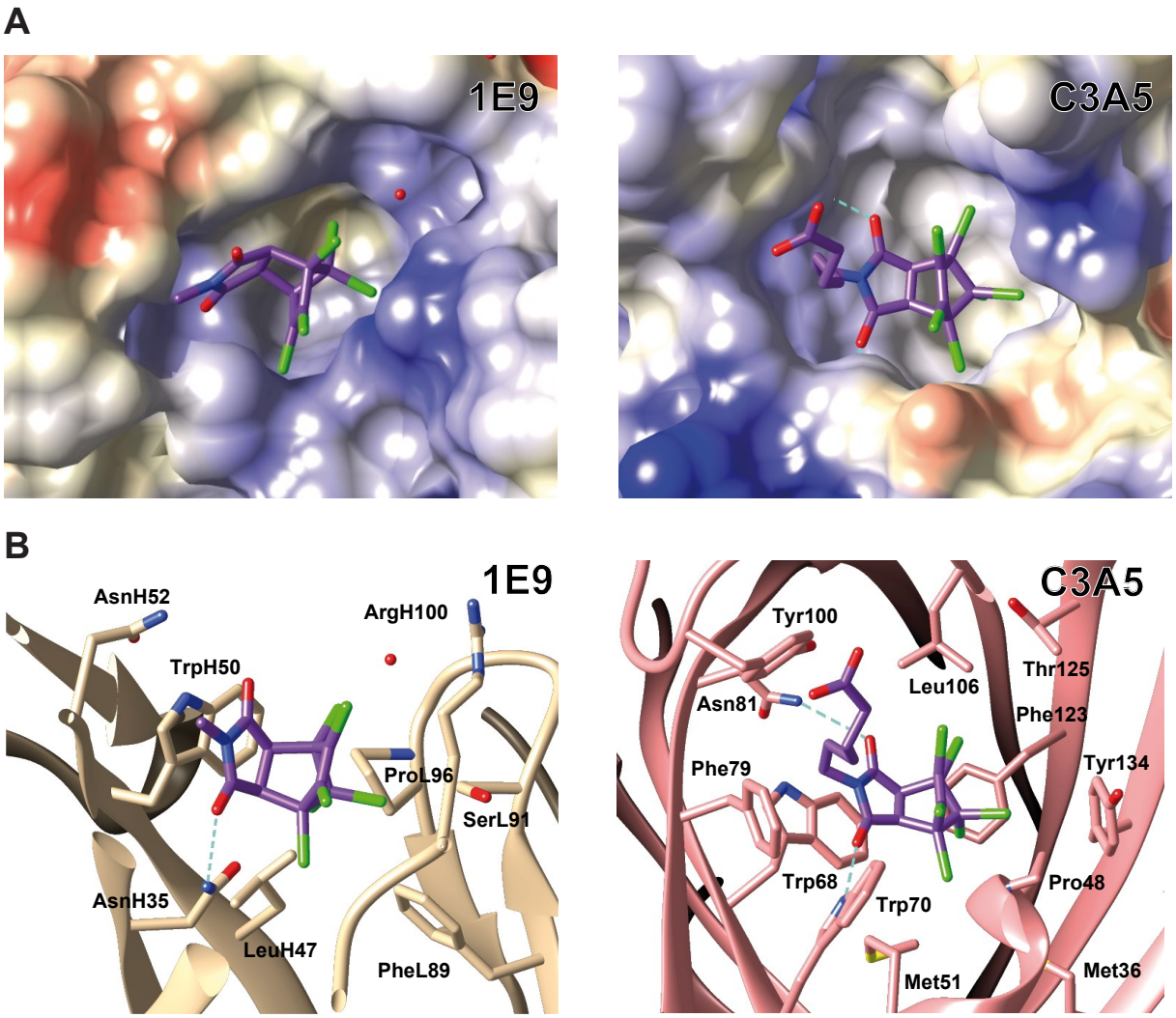

Figure 4.6. Comparison of the TSA binding modes between the catalytic antibody 1E9 (PDB:1C1E) and the Catacalin C3A5. **A:** The TSA in the binding cavity of 1E9 (left) and C3A5 (right). In the TSA (represented as stick model), carbon is colored violet, chlorine green, oxygen red, nitrogen blue. Accessible protein surface is colored according to the Coulombic potential (red for negative, blue for positive); visible hydrogen bonds are shown as dashed lines in cyan. Note the different orientation of the TSA in the ligand pockets of the two proteins. **B:** Amino acids responsible for the interaction with the TSA in 1E9 and C3A5 . Only the residues with a contact surface of at least 10 Å^2 are shown. For 1E9, light-chain residues are marked with 'L' and heavy-chain residues with 'H'. Both structures were clipped to improve visibility of the binding site.

The interactions of 1E9 with the TSA involve a notable π-stacking between the urea portion of the succinimide ring (corresponding to the maleimide ring of NEM) and the pyrrole ring of TrpH50. Interestingly, in the C3A5•TSA complex the same succinimide ring forms a π-stacking with the benzene ring of Trp68 (Figure 4.6B); these interactions are responsible for 18.5 % and 11.8 % of the contact area from the protein side, respectively. Furthermore, both proteins form hydrogen bonds with the carbonyl oxygens of the TSA. In 1E9, this involves AsnH35 and the more deeply buried carbonyl group of the TSA (Figure 4.6B), while in C3A5 hydrogen bonds

can be detected for both carbonyl groups with the indole nitrogen of Trp70 and the amide nitrogen of Asn81.

Table 4.5. Comparison of the ligand-binding parameters of antibody 1E9 and Catacalin C3A5.

Parameter	1E9	C3A5
Buried ligand surface *	86.3 %	79.6 %
Contacting amino acids *	16	14
Van der Waals contacts **	76	58
Hydrogen bonds **	1	2
π-stacking interactions	1	1
Affinity towards the TSA **9** ***	570 pM (full Ab) 50 pM (crystallized Fab) 100 pM ($M^{H87}T/G^{L63}S$ Fab)	3 nM

* Amino acids with a contact surface of at least 1 Å^2, analyzed via PDBe PISA (Krissinel & Henrick, 2007).
** Analysis performed using USCF Chimera (Pettersen *et al.*, 2004). Van der Waals contacts within 0.4 Å radius were counted.
*** Measured via fluorescence titration in solution at 15 °C for 1E9 (Piatesi, 2003) and at 25 °C for C3A5.

In the numerous publications devoted to 1E9, the H-bond between AsnH35 (the only polar residue in the binding pocket) and the TSA **9** was shown to be essential for the catalytic properties of 1E9. According to Xu *et al.* (1999), "*enthalpic stabilization of the actual transition state by an unusually close fit with the largely hydrophobic binding pocket of the antibody, punctuated by one strategically placed polar functionality,* […] *explains the catalytic efficiency of 1E9*". Indeed, substitution of AsnH35 by Ser or His led to a 10-fold or 6×10^5-fold loss of TSA affinity, respectively, accompanied by the complete loss of catalytic activity (Piatesi & Hilvert, 2004). However, the proposed explanation of how this H-bond contributes to the catalysis as well as the overall catalytic mechanism of 1E9 deserve a more detailed discussion.

As mentioned in Chapter 1.2.4, Diels-Alder reactions can be classified according to their electron demand (ED) character, which is explained by the frontier molecular orbital theory as illustrated in Figure 4.7. Standard-electron-demand reactions (Figure 4.7A) proceed through the interaction between the highest occupied molecular orbital (HOMO) of an electron-rich diene and the lowest unoccupied orbital (LUMO) of an electron-deficient alkene (dienophile), which is favored by the closer energy levels of these orbitals. In electron-deficient dienes, the HOMO energy is reduced, bringing it further away from the alkene LUMO. At the same time, the diene LUMO is lowered and becomes closer to the alkene HOMO. Thus, in this case the opposite interaction is favored, and the electron demand is inversed (Figure 4.7B).

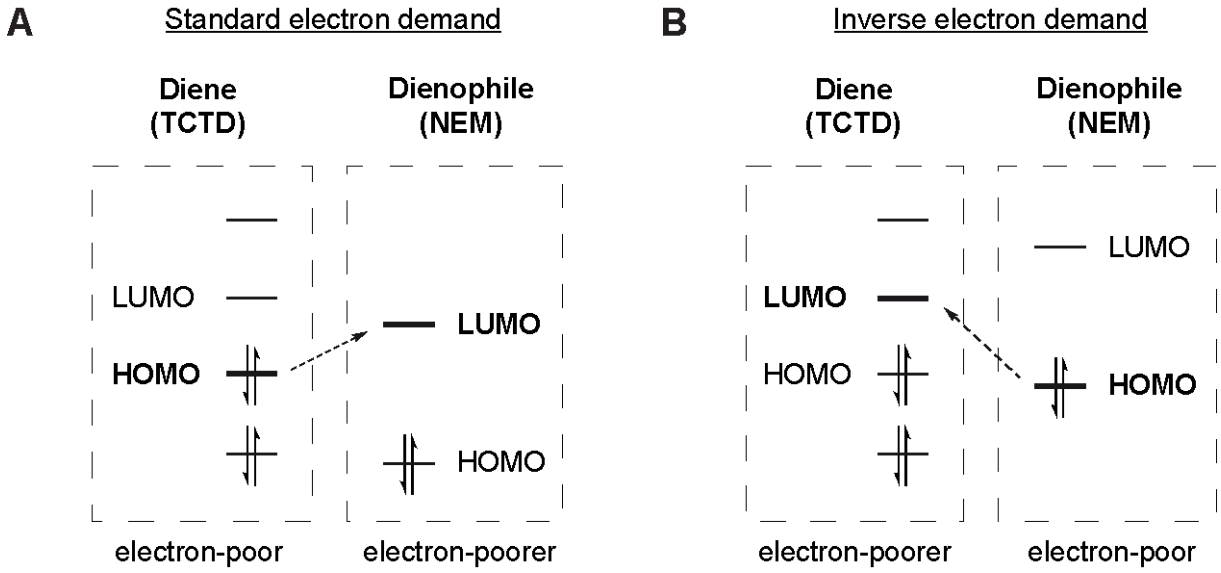

Figure 4.7. Possible electron demand preferences of the Diels-Alder reaction between TCTD and NEM explained by the frontier molecular orbital theory according to Carey & Sundberg (2007b). **A:** In standard electron demand reactions, typical for electron-rich dienes and electron-poor dienophiles, the interaction occurs between the highest occupied orbital (HOMO) of the diene and the lowest unoccupied orbital (LUMO) of the dienophile. **B:** For the inverse electron demand, the opposite interaction is favored. In the case of TCTD and NEM, both diene and dienophile are electron-deficient, making both interaction types possible, although some authors assume that the reaction catalyzed by 1E9 follows the inverse electron demand (Gozin & Hilvert, 2002).

A particular feature of the Diels-Alder cycloaddition between TCTD and NEM is that both the diene (with its many chloro-substituents) and the dienophile are electron-deficient; thus, the electron demand of this reaction cannot be classified unambiguously (see Figure 4.7). Generally, catalysis via standard ED should be favored by electron donation to TCTD (diene) and/or electron withdrawal from NEM (dienophile), and an inverse-ED route by the opposite effects. For instance, formation of the H-bond with the carbonyl oxygen of NEM in the activated complex reduces the electron density on the NEM (Walvoord *et al.*, 2014) and should favor standard ED. According to Chen *et al.* (2000), "*this hydrogen bond makes the dienophile component more electron-deficient and thus accelerates the Diels-Alder reaction*". However, Gozin & Hilvert (2002) assumed that the catalysis by 1E9 favors inverse electron demand, basing their judgement on the fact that 1E9 also accepts a bromine-substituted analog of TCTD but not a methyl-substituted one, which should react via standard ED. Furthermore, the π-stacking between NEM and the Trp side chain should also favor inverse electron demand, as it donates electron density to NEM.

Assuming that the reaction follows the inverse ED, an additional consideration concerns the symmetry of TSA binding, which could explain the poorer catalytic activity of C3A5. It is known that inverse-ED Diels-Alder reactions proceed through consecutive bond formation similar to Michael additions (Boger & Patel, 1989). From this perspective, the asymmetric TSA binding

mode and the one-side hydrogen bonding in 1E9 should favor the reaction, whereas the more symmetric NEM binding and the double H-bond in C3A5 should counteract this mechanism.

Furthermore, the poor activity of C3A5 may result from a low catalytic turnover involving an initial burst reaction followed by reversible or irreversible inactivation of the active site such as chemical modification of the protein with one of the reactants or reaction products. Such an initial burst was especially apparent for the Catacalin C3A5: as seen in Figure 3.42, the difference from the background rate for C3A5 was the highest within the first hour of the reaction, after which the reaction slowed down to the rate of the uncatalyzed reaction. As an argument in favor of irreversible inactivation, the activity of C3A5 was much more sensitive to exhaustive methylation of amino groups than E1G2 (data not shown), implying presence of a catalytically relevant amino group in the active site that might react with NEM in a Michael addition and thus lose its function. Furthermore, the low turnover number might also be linked to the deep binding pocket, which could hinder the product release from the active site.

Even though the TSA **9** constitutes a very good mimic of the putative transition state, the Diels-Alder reaction between NEM and TCTD is a difficult model system due to the poor detectability of the reaction products, especially if the initial activity level and the turnover are low. In fact, Xu *et al.* (1999) managed to quantify the reaction rate via a photometric assay based on the reaction of SO_2 that is released in a following reaction, with starch-bound iodine, leading to reaction-dependent loss of color. However, the same assay was not applicable for C3A5 and even for NFY due to its sensitivity only for higher educt concentrations ([NEM]×[TCTD] >1 mM) at which the rate enhancement achieved by C3A5 or NFY was barely detectable. Using higher Catacalin concentrations led to strong signal drift, making this assay unsuitable for these low-activity catalysts.

Inaccessibility of a high-throughput activity assay imposes an obstacle for the development of catalysts via directed evolution. Nevertheless, although orders-of-magnitude activity improvement would be difficult to achieve via rational mutagenesis, an activity boost that would make the activity level accessible for a high-throughput assay (such as the iodine-starch assay) might be sufficient to increase the chances of selecting more active Catacalin variants that could rival the catalytic efficiency of 1E9 and possibly reveal new catalytic modalities for the Diels-Alder cycloaddition. The Catacalin NFY would be the better candidate for such an endeavour because of the higher activity and apparently larger catalytic turnover; however, its crystal structure remains to be solved. Furthermore, the evolving powerful computational methods, which have already been successfully applied for creating *de novo* Diels-Alderases (Siegel *et al.*, 2010; Eiben *et al.*, 2012), could provide a valuable complementary approach for further engineering of catalytic Anticalins.

5. Summary

Protein engineering of lipocalins has led to a well-established class of alternative scaffold proteins known as Anticalins®. In particular, the human lipocalin 2 (Lcn2) has served as a basis for the creation of binding proteins against a variety of small-molecule, peptide and protein targets. In the present work, Lcn2 was employed as a scaffold for the development of high-affinity binding proteins against two haptens of different biological or chemical relevance by means of directed evolution and rational protein design: (i) selection of lipocalin variants that bind colchicine ('Colchicalins') and (ii) development of lipocalin-based catalysts for a Diels-Alder cycloaddition ('Catacalins').

The plant alkaloid colchicine is one of the oldest pharmaceutical compounds with acknowledged medicinal action; its use in the treatment of gout can be traced back to Ancient Egypt. However, due to its narrow therapeutic window, colchicine intoxications are common and include occasional, suicidal and even homicidal cases. Furthermore, *Colchicum autumnale*, the main natural source of colchicine, is often confused with bear's garlic, which is traditionally collected in Central Europe for gastronomic purpose, also leading to lethal poisoning. Here, a lipocalin variant with nanomolar affinity towards colchicine was selected from a Lcn2-based random library via combination of phage display and bacterial surface display. The binding strength of the initial variant ('Colchicalin D6.1') was improved via affinity maturation using bacterial surface display, yielding the variant 'D6.2' with a K_D of ~120 pM and a complex half-life of 1.5 h. This variant was modified using the PASylation® technology in order to extend its plasma half-life, and the pharmacokinetics of the original and the PASylated versions of the Colchicalin was investigated in a *Rattus norvegicus* model – along with the pharmacokinetics of colchicine itself – upon intravenous application. Based on the Colchicalin D6.2, a competitive ELISA for the detection of colchicine in biological fluids was developed, which provided sensitivity down to the single-digit nanomolar concentration range. Also, a high-resolution crystal structure of the Colchicalin D6.2 in complex with colchicine was obtained, unraveling unique features of the ligand-binding modus unseen in other lipocalin-based binding proteins that were published so far. Eventually, via a combination of affinity maturation and structure-guided mutagenesis, the Colchicalin variant D6.6 with an exceptional complex half-life of more than 9 h was obtained, which opens applications as a general-purpose biochemical affinity pair as an alternative to the biotin- or digoxigenin-based systems.

Another interesting application of the lipocalin scaffold is the development of lipocalin-based catalysts for a Diels-Alder cycloaddition between the model compounds tetrachlorothiophene dioxide (TCTD, diene) and N-ethylmaleimide (NEM, dienophile). The generation of a first catalyst was accomplished in previous work via selection of lipocalin variants with affinity to a

transition state analog (TSA) for this reaction. In this work, two promising variants, C3A5 and E1G2, were functionally characterized and further improved. After development of an HPLC-based analytical method with short run time, a rate enhancement of the Diels-Alder reaction by both lipocalin variants, C3A5 and E1G2 (‘Catacalins’), was detected for the first time. Interestingly, E1G2 was catalytically more active despite its lower TSA affinity than for C3A5. Optimization of the reaction parameters such as buffer pH, content of organic co-solvent and substrate-to-protein ratio, further increased the rate-enhancing effect of the Catacalins. Subsequently, based on the sequence similarities between the two Catacalins, the catalytic activity of E1G2 was improved two-fold via semi-rational mutagenesis, yielding the Catacalin ‘NFY’. Affinity maturation of the Catacalins C3A5 and NFY towards the TSA yielded no variants with higher activity. Attempts to crystallize the Catacalin NFY were not fruitful; however, it was possible to obtain crystals of the Catacalin C3A5 in complex with the TSA, which provided structural insights into the mechanism of transition state recognition and should enable structure-guided improvement of its catalytic activity in future work.

The high-affinity colchicine-binding lipocalin variants obtained in this work, the Colchicalins, offer potential as antidotes for the treatment of acute colchicine intoxication as well as biochemical affinity reagents, thanks to the exceptional complex stability. Furthermore, the catalytic lipocalin variants, the Catacalins, open a novel area for the development of artificial biocatalysts and may shed light on new catalytic modalities for Diels-Alder cycloadditions.

6. List of abbreviations

ABTS	2,2'-azino-*bis*(3-ethylbenzothiazoline-6-sulphonic acid)
ADEPT	antibody-dependent enzyme prodrug therapy
AEX	anion exchange chromatography
AP	alkaline phosphatase
APS	ammonium persulfate
BBP	bilin binding protein
BBS	borate buffered saline
BBS-E	BBS with 1 mM EDTA
Bis-Tris	2-[*bis*(2-hydroxyethyl)amino]-2-(hydroxymethyl)propane-1,3-diol
BCCP	biotin carboxyl carrier protein
BCIP	5-bromo-4-chloro-3-indolyl phosphate
BSA	bovine serum albumin
CAPS	*N*-cyclohexyl-3-aminopropanesulfonic acid
CCF	crystal-induced chemotactic factor
CD	cluster of differentiation
CDR	complementarity-determining region
CF	centrifuge
cfu	colony-forming unit
CEX	cation exchange chromatography
DA	Diels-Alder
ddH_2O	double-distilled water
DMAB	dimethylaminoborane
DMC	demethylcolchicine
DMF	dimethylformamide
DTPA	diethylenetriaminepentaacetic acid
DTT	1,4-dithio-DL-threitol
ECG	electrocardiogram

EDC	1-ethyl-3-(3-dimethylaminopropyl)carbodiimide
EDTA	ethylenediamine tetraacetic acid
ELISA	enzyme-linked immunosorbent assay
ESI-MS	electrospray ionization mass spectrometry
Fab	antigen-binding fragment
FACS	fluorescence-activated cell sorting
FMF	familial Mediterranean fever
FPLC	fast protein liquid chromatography
GDP / GTP	guanosine [di/tri]phosphate
HEPES	4-(2-hydroxyethyl)-1-piperazineethanesulfonic acid
HPLC	high-performance liquid chromatography
HRP	horse radish peroxidase
HSA	human serum albumin
IEX	ion exchange chromatography
IL	interleukin
IMAC	immobilized metal affinity chromatography
Lcn2	human lipocalin 2
MACS	magnetic-assisted cell sorting
MAP	microtubule-associated protein
MES	2-(*N*-morpholino)ethanesulfonic acid
MPD	2-methyl-2,4-pentanediol
MWCO	molecular weight cut-off
NaP_i	sodium phosphate buffer
NATA	*N*-acetyltryptophanamide
NBT	nitro blue tetrazolium
NHS	*N*-hydroxysuccinimide
NEM	*N*-ethylmaleimide
NGAL	neutrophil gelatinase-associated lipocalin

4-NPP	(4-nitrophenyl) dihydrogen phosphate
NTA	nitrilotriacetic acid
OD_{550}	optical density at 550 nm wavelength
PAGE	polyacrylamide gel electrophoresis
PCT	proximal convoluted tubule
PE	phycoerythrin
PEG	polyethylene glycol
PBS (/$T_{0.1}$)	phosphate buffered saline (with 0.1 % (v/v) Tween 20)
PGE2	prostaglandin E2
P-gp	glycoprotein P
PK	pharmacokinetics
PP	polypropylene
PVDF	polyvinylidene fluoride
RBS	ribosome-binding site
RMSD	root mean square deviation
RP-HPLC	reverse phase HPLC
SAC	*Strep*-Tactin affinity chromatography
SDS	sodium dodecyl sulfate
SEC	size-exclusion chromatography
SPR	surface plasmon resonance
SUMO	small ubiquitin-like modifier
TCTD	tetrachlorothiophene dioxide
TFA	trifluoroacetic acid
TNF	tumor necrosis factor
Tris	*tris*(hydroxymethyl)aminomethane
TSA	transition state analog
VIP	vasoactive intestinal peptide
wt	wild type

7. References

Abe E., Lemaire-Hurtel A.-S., Duverneuil C., Etting I., Guillot E., de Mazancourt P. & Alvarez J.-C. 2006. A novel LC-ESI-MS-MS method for sensitive quantification of colchicine in human plasma: application to two case reports. *J. Anal. Toxicol.* 30, 210-5.

Abergel R. J., Clifton M. C., Pizarro J. C., Warner J. A., Shuh D. K., Strong R. K. & Raymond K. N. 2008. The Siderocalin/Enterobactin Interaction: A Link between Mammalian Immunity and Bacterial Iron Transport. *J. Am. Chem. Soc.* 130, 11524-11534.

Abergel R. J., Wilson M. K., Arceneaux J. E., Hoette T. M., Strong R. K., Byers B. R. & Raymond K. N. 2006. Anthrax pathogen evades the mammalian immune system through stealth siderophore production. *Proc. Natl. Acad. Sci. USA* 103, 18499-18503.

Adler Y., Zandman-Goddard G., Ravid M., Avidan B., Zemer D., Ehrenfeld M., Shemesh J., Tomer Y. & Shoenfeld Y. 1994. Usefulness of colchicine in preventing recurrences of pericarditis. *Am. J. Cardiol.* 73, 916-7.

Agudelo C. A. & Schumacher H. R. 1973. The synovitis of acute gouty arthritis. A light and electron microscopic study. *Hum. Pathol.* 4, 265-79.

Åkerstrom B., Flower D. R. & Salier J.-P. 2000. Lipocalins: unity in diversity. *Biochim. Biophys. Acta Protein Struct. Mol. Enzymol.* 1482, 1-8.

Akizawa H., Uehara T. & Arano Y. 2008. Renal uptake and metabolism of radiopharmaceuticals derived from peptides and proteins. *Adv. Drug Del. Rev.* 60, 1319-1328.

Aller S. G., Yu J., Ward A., Weng Y., Chittaboina S., Zhuo R., Harrell P. M., Trinh Y. T., Zhang Q. & Urbatsch I. L. 2009. Structure of P-glycoprotein reveals a molecular basis for poly-specific drug binding. *Science* 323, 1718-1722.

Amoura Z., Schermann J. M., Zerah X., Wechsler B. & Godeau P. 1993. Première mise en évidence du passage transplacentaire de la colchicine au cours de la maladie périodique. *La Revue de Médecine Interne* 14, 593.

Amrollahi-Sharifabadi M., Seghatoleslami A., Amrollahi-Sharifabadi M., Bayani F. & Mirjalili M. 2013. Fatal colchicine poisoning by accidental ingestion of Colchicum persicum: a case report. *Am. J. Forensic Med. Pathol.* 34, 295-8.

Arevalo J. H., Stura E. A., Taussig M. J. & Wilson I. A. 1993. Three-dimensional structure of an anti-steroid Fab′ and progesterone-Fab′ complex. *J. Mol. Biol.* 231, 103-118.

Atas B., Caksen H., Tuncer O., Kirimi E., Akgun C. & Odabas D. 2004. Four children with colchicine poisoning. *Hum. Exp. Toxicol.* 23, 353-6.

Atwell S. & Wells J. a. 1999. Selection for improved subtiligases by phage display. *Proc. Natl. Acad. Sci. USA* 96, 9497-502.

Bachmann B. J. 1972. Pedigrees of some mutant strains of Escherichia coli K-12. *Bacteriol. Rev.* 36, 525-57.

Banerjee A. & Luduena R. F. 1992. Kinetics of colchicine binding to purified beta-tubulin isotypes from bovine brain. *J. Biol. Chem.* 267, 13335-9.

Barabe F., Gilbert C., Liao N., Bourgoin S. G. & Naccache P. H. 1998. Crystal-induced neutrophil activation VI. Involvment of FcgammaRIIIB (CD16) and CD11b in response to inflammatory microcrystals. *FASEB J.* 12, 209-20.

Barasch J., Hollmen M., Deng R., Hod E. A., Rupert P. B., Abergel R. J., Allred B. E., Xu K., Darrah S. F. & Tekabe Y. 2016. Disposal of iron by a mutant form of lipocalin 2. *Nature Commun.* 7, 12973.

Barkovskiy M., Ilyukhina E., Dauner M., Eichinger A. & Skerra A. 2018. An engineered lipocalin that tightly complexes the plant poison colchicine for use as antidote and in bioanalytical applications. *Biol. Chem.* 400, 351-366.

Baud F. J., Sabouraud a., Vicaut E., Taboulet P., Lang J., Bismuth C., Rouzioux J. M. & Scherrmann J. M. 1995. Brief report: treatment of severe colchicine overdose with colchicine-specific Fab fragments. *N. Engl. J. Med.* 332, 642-645.

Béhé M., Kluge G., Becker W., Gotthardt M. & Behr T. M. 2005. Use of polyglutamic acids to reduce uptake of radiometal-labeled minigastrin in the kidneys. *J. Nucl. Med.* 46, 1012-1015.

Ben-Chetrit E., Ben-Chetrit A., Berkun Y. & Ben-Chetrit E. 2010. Pregnancy outcomes in women with familial Mediterranean fever receiving colchicine: is amniocentesis justified? *Arthritis Care Res. (Hoboken)* 62, 143-8.

Bennett E. L., Alberti M. H. & Flood J. F. 1981. Uptake of [3 H] colchicine into brain and liver of mouse, rat, and chick. *Pharmacol. Biochem. Behav.* 14, 863-869.

Bensel N., Bahr N., Reymond M. T., Schenkels C. & Reymond J. L. 1999. Catalytic antibodies by fluorescence screening. *Helv. Chim. Acta* 82, 44-52.

Bensel N., Reymond M. T. & Reymond J. L. 2001. Pivalase catalytic antibodies: towards abzymatic activation of prodrugs. *Chem. Eur. J.* 7, 4604-4612.

Bernard A., Viau C., Ouled A. & Lauwerys R. 1987. Competition between Low- and High-Molecular-Weight Proteins for Renal Tubular Uptake. *Nephron* 45, 115-118.

Bhattacharyya B., Panda D., Gupta S. & Banerjee M. 2008. Anti-mitotic activity of colchicine and the structural basis for its interaction with tubulin. *Med. Res. Rev.* 28, 155-183.

Binder U., Matschiner G., Theobald I. & Skerra A. 2010. High-throughput sorting of an Anticalin library via EspP-mediated functional display on the Escherichia coli cell surface. *J. Mol. Biol.* 400, 783-802.

Binder U. & Skerra A. 2017. PASylation®: a versatile technology to extend drug delivery. *Curr. Opin. Colloid Interface Sci.* 31, 10-17.

Bismuth C., Gaultier M. & Conso F. 1977. Aplasie médullaire après intoxication aiguë à la colchicine. *Nouv. Presse Med.* 6, 1625-1629.

Boger D. L. & Patel M. 1989. Recent Applications of the Inverse Electron Demand Diels-Alder Reaction. *In:* H, S. & Fv, S. E. (eds.) *Progress in Heterocyclic Chemistry.*

Borisy G. G. & Taylor E. W. 1966. The Mechanism of Action of Colchicine: Binding of Colchincine-3H to Cellular Protein. *The Journal of Cell Biology* 34, 525-533.

Borron S. W., Scherrmann J. M. & Baud F. J. 1996. Markedly altered colchicine kinetics in a fatal intoxication: Examination of contributing factors. *Hum. Exp. Toxicol.* 15, 885-890.

Bosley A. D. & Ostermeier M. 2005. Mathematical expressions useful in the construction, description and evaluation of protein libraries. *Biomol. Eng.* 22, 57-61.

Braisted A. C. & Schultz P. G. 1990. An antibody-catalyzed bimolecular Diels-Alder reaction. *J. Am. Chem. Soc.* 112, 7430-7431.

Breustedt D. A., Schönfeld D. L. & Skerra A. 2006. Comparative ligand-binding analysis of ten human lipocalins. *Biochim. Biophys. Acta, Proteins Proteomics* 1764, 161-173.

Brncić N., Visković I., Perić R., Dirlić A., Vitezić D. & Cuculić D. 2001. Accidental plant poisoning with Colchicum autumnale: report of two cases. *Croat. Med. J.* 42, 673-5.

Brunger A. T. 1997. Free R value: cross-validation in crystallography. *Methods Enzymol.* 277, 366–396.

Brvar M., Kozelj G., Mozina M. & Bunc M. 2004a. Acute poisoning with autumn crocus (Colchicum autumnale L.). *Wiener klinische Wochenschrift* 116, 205-208.

Brvar M., Ploj T., Kozelj G., Mozina M., Noc M. & Bunc M. 2004b. Case report: fatal poisoning with Colchicum autumnale. *Crit. Care* 8, R56-R59.

Bullock W. O., Fernandez J. M. & Short J. M. 1987. XL1-Blue - a high efficiency plasmid transforming recA Escherichia coli strain with beta-galactosidase selection. *BioTechniques* 5, 376-379.

Byrne M. J., Lees N. R., Han L. C., van der Kamp M. W., Mulholland A. J., Stach J. E., Willis C. L. & Race P. R. 2016. The Catalytic Mechanism of a Natural Diels-Alderase Revealed in Molecular Detail. *J. Am. Chem. Soc.* 138, 6095-8.

Caner J. E. 1965. Colchicine inhibition of chemotaxis. *Arthritis Rheum.* 8, 757-64.

Carey F. A. & Sundberg R. J. 2007a. *Advanced Organic Chemistry: Part A: Structure and Mechanisms*, Springer Science & Business Media.

Carey F. A. & Sundberg R. J. 2007b. *Advanced Organic Chemistry: Part B: Reaction and Synthesis*, Springer Science & Business Media.

Caviston J. P. & Holzbaur E. L. F. 2006. Microtubule motors at the intersection of trafficking and transport. *Trends Cell Biol.* 16, 530-537.

CCP4 1994. The CCP4 suite: programs for protein crystallography. *Acta Crystallogr. D* 50, 760–763.

Cerquaglia C., Diaco M., Nucera G., La Regina M., Montalto M. & Manna R. 2005. Pharmacological and clinical basis of treatment of Familial Mediterranean Fever (FMF) with colchicine or analogues: an update. *Curr. Drug Targets Inflamm. Allergy* 4, 117-124.

Chapman P. T., Yarwood H., Harrison A. A., Stocker C. J., Jamar F., Gundel R. H., Peters A. M. & Haskard D. O. 1997. Endothelial activation in monosodium urate monohydrate crystal-induced inflammation: in vitro and in vivo studies on the roles of tumor necrosis factor alpha and interleukin-1. *Arthritis Rheum.* 40, 955-65.

Chappey O., Niel E., Dervichian M., Wautier J. L., Scherrmann J. M. & Cattan D. 1994. Colchicine concentration in leukocytes of patients with familial Mediterranean fever. *Br. J. Clin. Pharmacol.* 38, 87-9.

Chappey O. N., Niel E., Wautier J. L., Hung P. P., Dervichian M., Cattan D. & Scherrmann J. M. 1993. Colchicine disposition in human leukocytes after single and multiple oral administration. *Clin. Pharmacol. Ther.* 54, 360-7.

Chen J., Deng Q., Wang R., Houk K. N. & Hilvert D. 2000. Shape Complementarity, Binding-Site Dynamics, and Transition State Stabilization: A Theoretical Study of Diels–Alder Catalysis by Antibody 1E9. *ChemBioChem* 1, 255-261.

Chen V. B., Arendall W. B., 3rd, Headd J. J., Keedy D. A., Immormino R. M., Kapral G. J., Murray L. W., Richardson J. S. & Richardson D. C. 2010. MolProbity: all-atom structure validation for macromolecular crystallography. *Acta Crystallogr. D* 66, 12–21.

Chen Y. J., Huang S. M., Liu C. Y., Yeh P. H. & Tsai T. H. 2008. Hepatobiliary excretion and enterohepatic circulation of colchicine in rats. *Int. J. Pharm.* 350, 230-239.

Chia E. W., Grainger R. & Harper J. L. 2008. Colchicine suppresses neutrophil superoxide production in a murine model of gouty arthritis: a rationale for use of low-dose colchicine. *Br. J. Pharmacol.* 153, 1288-95.

Christensen E. I. & Birn H. 2002. Megalin and cubilin: multifunctional endocytic receptors. *Nat. Rev. Mol. Cell Biol.* 3, 258-267.

Chuang S. E., Chen A. L. & Chao C. C. 1995. Growth of E. coli at low temperature dramatically increases the transformation frequency by electroporation. *Nucleic Acids Res.* 23, 1641.

Cohen S. N., Chang A. C. & Hsu L. 1972. Nonchromosomal antibiotic resistance in bacteria: genetic transformation of Escherichia coli by R-factor DNA. *Proc. Natl. Acad. Sci. USA* 69, 2110-4.

Colovos C. & Yeates T. O. 1993. Verification of protein structures: patterns of nonbonded atomic interactions. *Protein Sci.* 2, 1511–1519.

Conde C. & Caceres A. 2009. Microtubule assembly, organization and dynamics in axons and dendrites. *Nat. Rev. Neurosci.* 10, 319-32.

Copeman W. S. C. 1964. *A short history of the gout and the rheumatic diseases,* Berkeley,, University of California Press.

Court L. s. C. C. 1862. Trial of CATHERINE WILSON (40) (t18620922-996). *Old Bailey Proceedings Online.* London, UK: London's Central Criminal Court.

Cronstein B. N., Molad Y., Reibman J., Balakhane E., Levin R. I. & Weissmann G. 1995. Colchicine alters the quantitative and qualitative display of selectins on endothelial cells and neutrophils. *J. Clin. Invest.* 96, 994-1002.

Danel V. C., Wiart J. F., Hardy G. A., Vincent F. H. & Houdret N. M. 2001. Self-poisoning with Colchicum autumnale L. flowers. *J. Toxicol. Clin. Toxicol.* 39, 409-411.

Dauner M., Eichinger A., Lücking G., Scherer S. & Skerra A. 2018. Reprogramming Human Siderocalin To Neutralize Petrobactin, the Essential Iron Scavenger of Anthrax Bacillus. *Angew. Chem. Int. Ed.* 57, 14619-14623.

de Lannoy I. A., Mandin R. S. & Silverman M. 1994. Renal secretion of vinblastine, vincristine and colchicine in vivo. *J. Pharmacol. Exp. Ther.* 268, 388-95.
Deen W. M. & Satvat B. 1981. Determinants of the glomerular filtration of proteins. *Am. J. Physiol. Renal Physiol.* 241, F162-F170.
Deveaux M., Hubert N. & Demarly C. 2004. Colchicine poisoning: case report of two suicides. *Forensic Sci. Int.* 143, 219-22.
Dewar M. 1945. Structure of colchicine. *Nature* 155, 141-142.
Dewar M. J., Olivella S. & Stewart J. J. 1986. Mechanism of the Diels-Alder reaction: reactions of butadiene with ethylene and cyanoethylenes. *J. Am. Chem. Soc.* 108, 5771-9.
Dickgießer S. 2011. *Versuche zur Selektion eines katalytisch wirksamen Anticalins.* MSc Thesis, Technische Universität München.
Dixon F. J. 1952. The Half-Life of Homologous Gamma Globulin (Antibody) in Several Species. *J. Exp. Med.* 96, 313-318.
Doerner A., Rhiel L., Zielonka S. & Kolmar H. 2014. Therapeutic antibody engineering by high efficiency cell screening. *FEBS Lett.* 588, 278-87.
Donovan J. 2007. Colchicine. *In:* Shannon, M. W., Borron, S. & Burns, M. (eds.) *Haddad and Winchester's clinical management of poisoning and drug overdose.* Philadelphia: Saunders/Elsevier.
Drion N., Lemaire M., Lefauconnier J. M. & Scherrmann J. M. 1996. Role of P-glycoprotein in the blood-brain transport of colchicine and vinblastine. *J. Neurochem.* 67, 1688-93.
DuBose Jr T. D., Pucacco L. R. & Carter N. W. 1981. Determination of disequilibrium pH in the rat kidney in vivo: evidence of hydrogen secretion. *Am. J. Physiol. Renal Physiol.* 240, F138-F146.
Eddleston M., Fabresse N., Thompson A., Al Abdulla I., Gregson R., King T., Astier A., Baud F. J., Clutton R. E. & Alvarez J.-C. 2018. Anti-colchicine Fab fragments prevent lethal colchicine toxicity in a porcine model: a pharmacokinetic and clinical study. *Clin. Toxicol.* 56, 1-9.
Eddleston M. & Persson H. 2003. Acute plant poisoning and antitoxin antibodies. *J. Toxicol. Clin. Toxicol.* 41, 309-315.
Eggenstein E., Eichinger a., Kim H.-J. J. & Skerra a. 2014. Structure-guided engineering of Anticalins with improved binding behavior and biochemical characteristics for application in radio-immuno imaging and/or therapy. *J. Struct. Biol.* 185, 203-214.
Ehrenfeld M., Levy M., Sharon P., Rachmilewitz D. & Eliakim M. 1982. Gastrointestinal effects of long-term colchicine therapy in patients with recurrent polyserositis (familial mediterranean fever). *Dig. Dis. Sci.* 27, 723-7.
Eiben C. B., Siegel J. B., Bale J. B., Cooper S., Khatib F., Shen B. W., Players F., Stoddard B. L., Popovic Z. & Baker D. 2012. Increased Diels-Alderase activity through backbone remodeling guided by Foldit players. *Nat. Biotechnol.* 30, 190-2.
Eigsti O. J. & Dustin P. J. 1955. *Colchicine in agriculture, medicine, biology, and chemistry.*, Iowa State College Press.
Elkjaer M., Birn H., Agre P., Christensen E. I. & Nielsen S. 1995. Effects of microtubule disruption on endocytosis, membrane recycling and polarized distribution of Aquaporin-1 and gp330 in proximal tubule cells. *Eur. J. Cell Biol.* 67, 57-72.
Ellwood M. G. & Robb G. H. 1971. Self-poisoning with colchicine. *Postgrad. Med. J.* 47, 129-31.
Emsley P. & Cowtan K. 2004. Coot: model-building tools for molecular graphics. *Acta Crystallogr. D Biol. Crystallogr.* 60, 2126–2132.
Engelborghs Y. 1998. General features of the recognition by tubulin of colchicine and related compounds. *Eur. Biophys. J.* 27, 437-445.
Eren M. I., Bebber M. R., Norris J. D., Perrone A., Rutkoski A., Wilson M. & Raghanti M. A. 2019. Experimental replication shows knives manufactured from frozen human feces do not work. *J. Archaeol. Sci. Rep.* 27, 102002.
European Medicines Agency E. 2010. Public summary of opinion on orphan designation. *In:* Products, C. F. O. M. (ed.). London, United Kingdom: European Medicines Agency.

Eyer F., Steimer W., Nitzsche T., Jung N., Neuberger H., Müller C., Schlapschy M., Zilker T. & Skerra A. 2012. Intravenous application of an anticalin dramatically lowers plasma digoxin levels and reduces its toxic effects in rats. *Toxicol. Appl. Pharmacol.* 263, 352-9.

Fage C. D., Isiorho E. A., Liu Y., Wagner D. T., Liu H. W. & Keatinge-Clay A. T. 2015. The structure of SpnF, a standalone enzyme that catalyzes [4 + 2] cycloaddition. *Nat. Chem. Biol.* 11, 256-8.

Farrell K. W. & Wilson L. 1984. Tubulin-colchicine complexes differentially poison opposite microtubule ends. *Biochemistry* 23, 3741-3748.

Ferguson F. C. 1952. Colchicine. I. General pharmacology. *J. Pharmacol. Exp. Ther.* 106, 261-270.

Fernando Diaz J. & Andreu J. M. 1991. Kinetics of dissociation of the tubulin-colchicine complex. Complete reaction scheme and comparison to thermodynamic measurements. *J. Biol. Chem.* 266, 2890-6.

Fernando R. & Fernando D. N. 1990. Poisoning with plants and mushrooms in Sri Lanka: a retrospective hospital based study. *Vet. Hum. Toxicol.* 32, 579-81.

Fernando R. & Widyaratna D. 1997. Poisons Information Monograph 245 - Gloriosa superba L. *International Programme on Chemical Safety (IPCS).*

Ferrige A., Seddon M., Jarvis S., Skilling J. & Aplin R. 1991. Maximum entropy deconvolution in electrospray mass spectrometry. *Rapid Commun. Mass Spectrom.* 5, 374-377.

Ferron G. M., Rochdi M., Jusko W. J. & Scherrmann J.-M. 1996. Oral Absorption Pharmacokinetics Volunteers after Characteristics and of Coichicine in Healthy Single and Multiple Doses. *J. Clin. Pharmacol.*, 874-883.

Finkelstein Y., Aks S. E., Hutson J. R., Juurlink D. N., Nguyen P., Dubnov-Raz G., Pollak U., Koren G. & Bentur Y. 2010. Colchicine poisoning: the dark side of an ancient drug. *Clin. Toxicol. (Phila.)* 48, 407-14.

Flesch F., Krencker E., Mootien Y., Kintz P., Ihadade`ne N. & Jaeger A. Diagnosis Wandering in a Case of Accidental Poisoning by Colchicum Autumnale. *In:* Committee, E. S., ed. European Association of Poisons Centres and Clinical Toxicologists XXII International Congress, 2002. 241-399.

Fling S. P. & Gregerson D. S. 1986. Peptide and protein molecular weight determination by electrophoresis using a high-molarity tris buffer system without urea. *Anal. Biochem.* 155, 83-8.

Flower D. R., North A. C. & Sansom C. E. 2000. The lipocalin protein family: structural and sequence overview. *Biochim. Biophys. Acta Protein Struct. Mol. Enzymol.* 1482, 9-24.

Folpini A. & Furfori P. 1995. Colchicine toxicity - clinical features and treatment. Massive overdose case report. *J. Toxicol. Clin. Toxicol.* 33, 71-7.

Friedrich L., Kornberger P., Mendler C. T., Multhoff G., Schwaiger M. & Skerra A. 2017. Selection of an Anticalin® against the membrane form of Hsp70 via bacterial surface display and its theranostic application in tumour models. *Biol. Chem.* 399, 235-252.

Galland-Decker C., Charmoy A., Jolliet P., Spertini O., Hugli O. & Pantet O. 2016. Progressive Organ Failure After Ingestion of Wild Garlic Juice. *J. Emerg. Med.* 50, 55-60.

Ganguly A., Yang H., Sharma R., Patel K. D. & Cabral F. 2012. The Role of Microtubules and Their Dynamics in Cell Migration. *J. Biol. Chem.* 287, 43359-43369.

Gao C., Lavey B. J., Lo C.-H. L., Datta A., Wentworth P. & Janda K. D. 1998. Direct selection for catalysis from combinatorial antibody libraries using a boronic acid probe: primary amide bond hydrolysis. *J. Am. Chem. Soc.* 120, 2211-2217.

Gao C., Lin C. H., Lo C. H., Mao S., Wirsching P., Lerner R. a. & Janda K. D. 1997. Making chemistry selectable by linking it to infectivity. *Proc. Natl. Acad. Sci. USA* 94, 11777-82.

Garrod A. B. S. 1859. *The nature and treatment of gout, and rheumatic gout,* London, Walton and Maberly.

Gebauer M., Schiefner A., Matschiner G. & Skerra A. 2013. Combinatorial design of an Anticalin directed against the extra-domain B for the specific targeting of oncofetal fibronectin. *J. Mol. Biol.* 425, 780-802.

Gebauer M. & Skerra A. 2009. Engineered protein scaffolds as next-generation antibody therapeutics. *Curr. Opin. Chem. Biol.* 13, 245-55.

Gebauer M. & Skerra A. 2012. Anticalins: small engineered binding proteins based on the lipocalin scaffold. *Methods Enzymol.* 503, 157-88.

Geiger T., Wehner A., Schaab C., Cox J. & Mann M. 2012. Comparative proteomic analysis of eleven common cell lines reveals ubiquitous but varying expression of most proteins. *Mol. Cell. Proteomics* 11, M111. 014050.

Gekle M., Mildenberger S., Freudinger R., Schwerdt G. & Silbernagl S. 1997. Albumin endocytosis in OK cells: dependence on actin and microtubules and regulation by protein kinases. *Am. J. Physiol. Renal Physiol.* 272, F668-F677.

Gibson T. J. 1984. *Studies on the Epstein-Barr virus genome.* PhD Thesis, University of Cambridge.

Goetz D. H., Holmes M. A., Borregaard N., Bluhm M. E., Raymond K. N. & Strong R. K. 2002. The neutrophil lipocalin NGAL is a bacteriostatic agent that interferes with siderophore-mediated iron acquisition. *Mol. Cell* 10, 1033-1043.

Goldfinger S. E. 1972. Colchicine for familial Mediterranean fever. *N. Engl. J. Med.* 287, 1302.

Gooneratne B. W. 1966. Massive generalized alopecia after poisoning by Gloriosa superba. *Br. Med. J.* 1, 1023-4.

Goud G. N., Artsaenko O., Bols M. & Sierks M. 2001. Specific glycosidase activity isolated from a random phage display antibody library. *Biotechnol. Prog.* 17, 197-202.

Gozin Y. & Hilvert D. 2002. Steric and Electronic Effects on an Antibody-Catalyzed Diels ± Alder Reaction. *Helv. Chim. Acta* 85, 4328-4336.

Graening T. & Schmalz H.-G. 2004. Total Syntheses of Colchicine in Comparison: A Journey through 50 Years of Synthetic Organic Chemistry. *Angew. Chem. Int. Ed.* 43, 3230-3256.

Gründemann D. & Schömig E. 1996. Protection of DNA during preparative agarose gel electrophoresis against damage induced by ultraviolet light. *BioTechniques* 21, 898-903.

Gumm B., Wilkinson J., Aldridge M., Landon J. & Al Abdulla I. 2016. Cell-Based Cytotoxicity and Immunocytotoxicity Assays for Colchicine and Ovine Anti-Colchicine Sera and Fab Fragments. *J. Clin. Toxicol.* 06.

Gutmann E., Niles J., McCluskey R. & Brown D. 1989. Colchicine-induced redistribution of an apical membrane glycoprotein (gp330) in proximal tubules. *Am. J. Physiol. Cell Physiol.* 257, C397-C407.

Güven A. G., Bahat E., Akman S., Artan R. & Erol M. 2002. Late diagnosis of severe colchicine intoxication. *Pediatrics* 109, 971-973.

Hamm L. L., Alpern R. J. & Preisig P. A. 2013. Cellular mechanisms of renal tubular acidification. *In: Seldin and Giebisch's The Kidney (Fifth Edition).* Elsevier.

Harris R., Marx G., Gillett M., Kark A. & Arunanthy S. 2000. Colchicine-induced bone marrow suppression: treatment with granulocyte colony-stimulating factor. *J. Emerg. Med.* 18, 435-40.

Hartung E. F. 1954. History of the Use of Colchicum and related Medicaments in Gout. *Ann. Rheum. Dis.* 13, 190-200.

Hashimoto T., Hashimoto J., Teruya K., Hirano T., Shin-ya K., Ikeda H., Liu H. W., Nishiyama M. & Kuzuyama T. 2015. Biosynthesis of versipelostatin: identification of an enzyme-catalyzed [4+2]-cycloaddition required for macrocyclization of spirotetronate-containing polyketides. *J. Am. Chem. Soc.* 137, 572-5.

Hilvert D. 2000. Critical analysis of antibody catalysis. *Annu. Rev. Biochem.* 69, 751-793.

Hilvert D. & Hill K. 1989. Antibody catalysis of the Diels-Alder reaction. *J. Am. Chem. Soc.* 111, 9261-9262.

Holmes M. A., Paulsene W., Jide X., Ratledge C. & Strong R. K. 2005. Siderocalin (Lcn 2) also binds carboxymycobactins, potentially defending against mycobacterial infections through iron sequestration. *Structure* 13, 29-41.

Hood R. L. 1994. Colchicine poisoning. *J. Emerg. Med.* 12, 171-177.

Hooft R. W., Vriend G., Sander C. & Abola E. E. 1996. Errors in protein structures. *Nature* 381, 272.

Hu Y.-J., Liu Y., Zhang L.-X., Zhao R.-M. & Qu S.-S. 2005. Studies of interaction between colchicine and bovine serum albumin by fluorescence quenching method. *J. Mol. Struct.* 750, 174-178.

Hunter A. L. & Klaassen C. D. 1975. Biliary excretion of colchicine. *J. Pharmacol. Exp. Ther.* 192, 605-17.

Hvidberg V., Jacobsen C., Strong R. K., Cowland J. B., Moestrup S. K. & Borregaard N. 2005. The endocytic receptor megalin binds the iron transporting neutrophil-gelatinase-associated lipocalin with high affinity and mediates its cellular uptake. *FEBS Lett.* 579, 773-777.

Inoue S. 1967. Cell Motility by Labile Association of Molecules: The nature of mitotic spindle fibers and their role in chromosome movement. *J. Gen. Physiol.* 50, 259-292.

Iwanaga S. 2007. Biochemical principle of Limulus test for detecting bacterial endotoxins. *Proc. Jpn. Acad. Ser. B Phys. Biol. Sci.* 83, 110-9.

Jäckel C., Kast P. & Hilvert D. 2008. Protein design by directed evolution. *Annu. Rev. Biophys.* 37, 153-73.

Jaeger A. & Flesch F. 1990. Poisons Information Monograph 142 - Colchicum autumnale L. *International Programme on Chemical Safety (IPCS).*

Jaeger A., Flesch F., Sauder P. & Kopferschmitt J. 1989. Poisons Information Monograph 141 - Colchicine. *International Programme on Chemical Safety (IPCS).*

Jaeger A., Simon C., Tempe J., Mantz J., Bismuth C., Conso F., Mathiot C., Baumelou A., Bavoux F. & Jouanjean X. 1980. Lethal reactions to intravenous colchicine. *La Nouvelle presse medicale* 9, 1586.

Janda K. D., Lo L. C., Lo C. H., Sim M. M., Wang R., Wong C. H. & Lerner R. A. 1997. Chemical selection for catalysis in combinatorial antibody libraries. *Science* 275, 945-8.

Jaspersen-Schib R., Theus L., Guirguis-Oeschger M., Gossweiler B. & Meier-Abt P. J. 1996. [Serious plant poisonings in Switzerland 1966-1994. Case analysis from the Swiss Toxicology Information Center]. *Schweiz. Med. Wochenschr.* 126, 1085-98.

Jencks W. P. 1969. *Catalysis in chemistry and enzymology,* New York ; London, McGraw-Hill.

Jones E. G. 1810. *An account of the remarkable effects of the Eau Médicinale d'Husson in the Gout*, London.

Joosten R. P., Long F., Murshudov G. N. & Perrakis A. 2014. The PDB_REDO server for macromolecular structure model optimization. *IUCrJ* 1, 213–220.

Jordan K. M., Cameron J. S., Snaith M., Zhang W., Doherty M., Seckl J., Hingorani A., Jaques R. & Nuki G. 2007. British Society for Rheumatology and British Health Professionals in Rheumatology Guideline for the Management of Gout. *Rheumatology* 46, 1372-1374.

Jose J., Krämer J., Klauser T., Pohlner J. & Meyer T. F. 1996. Absence of periplasmic DsbA oxidoreductase facilitates export of cysteine-containing passenger proteins to the Escherichia coli cell surface via the Igaβ autotransporter pathway. *Gene* 178, 107-110.

Kabsch W. & Sander C. 1983. Dictionary of protein secondary structure: pattern recognition of hydrogen-bonded and geometrical features. *Biopolymers* 22, 2577–2637.

Kande Vidanalage C. J., Ekanayeka R. & Wijewardane D. K. 2016. Case report: a rare case of attempted homicide with Gloriosa superba seeds. *BMC Pharmacol Toxicol* 17, 26.

Kaplan M. M., Schmid C., Provenzale D., Sharma a., Dickstein G. & McKusick a. 1999. A prospective trial of colchicine and methotrexate in the treatment of primary biliary cirrhosis. *Gastroenterology* 117, 1173-80.

Karlsson R., Michaelsson A. & Mattsson L. 1991. Kinetic analysis of monoclonal antibody-antigen interactions with a new biosensor based analytical system. *J. Immunol. Methods* 145, 229-240.

Katz E. Z., Ehrenfeld M., Levy M. & Eliakim M. 1982. Plasma colchicine concentration in patients with recurrent polyserositis (familial Mediterranean fever) on long-term prophylaxis. *Arthritis Rheum.* 25, 227-31.

Kershenobich D., Vargas F., Garcia-Tsao G., Tamayo R. P., Gent M. & Rojkind M. 1988. Colchicine in the Treatment of Cirrhosis of the Liver. *N. Engl. J. Med.* 318, 1709-1713.

Kim H. J., Eichinger A. & Skerra A. 2009. High-affinity recognition of lanthanide(III) chelate complexes by a reprogrammed human lipocalin 2. *J. Am. Chem. Soc.* 131, 3565-76.

Kim H. J., Ruszczycky M. W., Choi S.-h., Liu Y.-n. & Liu H.-w. 2011. Enzyme-catalysed [4+ 2] cycloaddition is a key step in the biosynthesis of spinosyn A. *Nature* 473, 109-112.

King M. V., De Vries J. & Pepinsky R. 1952. An x-ray diffraction determination of the chemical structure of colchicine. *Acta Crystallogr.* 5, 437-440.

Kintz P., Jamey C., Tracqui a. & Mangin P. 1997. Colchicine poisoning: report of a fatal case and presentation of an HPLC procedure for body fluid and tissue analyses. *J. Anal. Toxicol.* 21, 70-72.

Klas K., Tsukamoto S., Sherman D. H. & Williams R. M. 2015. Natural Diels-Alderases: Elusive and Irresistable. *J. Org. Chem.* 80, 11672-85.

Klintschar M., Beham-Schmidt C., Radner H., Henning G. & Roll P. 1999. Colchicine poisoning by accidental ingestion of meadow saffron (Colchicum autumnale): pathological and medicolegal aspects. *Forensic Sci. Int.* 106, 191-200.

Kreutzberg G. W. 1969. Neuronal dynamics and axonal flow. IV. Blockage of intra-axonal enzyme transport by colchicine. *Proc. Natl. Acad. Sci. USA* 62, 722-8.

Krissinel E. & Henrick K. 2007. Inference of macromolecular assemblies from crystalline state. *J. Mol. Biol.* 372, 774-97.

Kurz J. L. 1963. Transition State Characterization for Catalyzed Reactions. *J. Am. Chem. Soc.* 85, 987-991.

Laemmli U. K. 1970. Cleavage of structural proteins during the assembly of the head of bacteriophage T4. *Nature* 227, 680-5.

Lamzin V. S., Perrakis A. & Wilson K. S. 2012. ARP/wARP – automated model building and refinement. *In:* E, A., Dm, H. & Mg, R. (eds.) *International tables for crystallography.* Dordrecht ; London : D. Reidel Pub. Co., 1983-.

Langreth R. & Koons C. 2015. 2,000% Drug Price Surge Is a Side Effect of FDA Safety Program. *Bloomberg* [Online]. Available: https://www.bloomberg.com/news/articles/2015-10-06/2-000-drug-price-surge-is-a-side-effect-of-fda-safety-program [Accessed 01 March 2017].

Laskowski R. A., MacArthur M. W., Mos D. S. & Thornton J. M. 1993. PROCHECK: a program to check the stereochemical quality of protein structures. *J. Appl. Crystallogr.* 26, 283–291.

Leete E. 1963. The biosynthesis of the alkaloids of Colchicum. III. The incorporation of phenylalanine-2-C14 into colchicine and demecolcine. *J. Am. Chem. Soc.* 85, 3666-3669.

Leighton J. A., Bay M. K., Maldonado A. L., Johnson R. F., Schenker S. & Speeg K. V. 1990. The effect of liver dysfunction on colchicine pharmacokinetics in the rat. *Hepatology* 11, 210-5.

Leighton J. A., Bay M. K., Maldonado A. L., Schenker S. & Speeg K. V. 1991. Colchicine clearance is impaired in alcoholic cirrhosis. *Hepatology* 14, 1013-1015.

Lesley S. A., Patten P. A. & Schultz P. G. 1993. A genetic approach to the generation of antibodies with enhanced catalytic activities. *Proc. Natl. Acad. Sci. USA* 90, 1160-5.

Lev S., Snyder D., Azran C., Zolotarsky V. & Dahan A. 2017. Severe hypertriglyceridemia and colchicine intoxication following suicide attempt. *Drug Des. Devel. Ther.* 11, 3321-3324.

Link L. H., Bindels A. J. G. H., Brassé B. P., Intven F. A., Grouls R. J. E. & Roos A. N. 2014. Severe colchicine intoxication; always lethal ?!? *Neth. J. Crit. Care* 18, 20-22.

Liu-Bryan R., Scott P., Sydlaske A., Rose D. M. & Terkeltaub R. 2005. Innate immunity conferred by Toll-like receptors 2 and 4 and myeloid differentiation factor 88 expression is pivotal to monosodium urate monohydrate crystal-induced inflammation. *Arthritis Rheum.* 52, 2936-46.

Lo C.-H. L., Wentworth P., Jung K. W., Yoon J., Ashley J. A. & Janda K. D. 1997. Reactive Immunization Strategy Generates Antibodies with High Catalytic Proficiencies. *J. Am. Chem. Soc.* 119, 10251-10252.

Lund U., Rippe A., Venturoli D., Tenstad O., Grubb A. & Rippe B. 2003. Glomerular filtration rate dependence of sieving of albumin and some neutral proteins in rat kidneys. *Am. J. Physiol. Renal Physiol.* 284, F1226-F1234.

Luthy R., Bowie J. U. & Eisenberg D. 1992. Assessment of protein models with three-dimensional profiles. *Nature* 356, 83–85.

Macleod J. G. & Phillips L. 1947. Hypersensitivity to colchicine. *Ann. Rheum. Dis.* 6, 224-229.

Maier U. H. & Zenk M. H. 1997. Colchicine is formed by para-para phenol coupling from autumnaline. *Tetrahedron Lett.* 38, 7357-7360.

Malakhov M. P., Mattern M. R., Malakhova O. A., Drinker M., Weeks S. D. & Butt T. R. 2004. SUMO fusions and SUMO-specific protease for efficient expression and purification of proteins. *J. Struct. Funct. Genomics* 5, 75-86.

Mandel N. S. 1976. The structural basis of crystal-induced membranolysis. *Arthritis Rheum.* 19 Suppl 3, 439-45.

Manske R. H. F., Holmes H. L. & Rodrigo R. G. A. 1950. The Alkaloids. Chemistry and physiology. New York: Academic Press.

Margolis R. L. & Wilson L. 1977. Addition of colchicine-tubulin complex to microtubule ends: the mechanism of substoichiometric colchicine poisoning. *Proc. Natl. Acad. Sci. USA* 74, 3466-3470.

Martinon F., Burns K. & Tschopp J. 2002. The inflammasome: a molecular platform triggering activation of inflammatory caspases and processing of proIL-beta. *Mol. Cell* 10, 417-26.

Martinon F., Petrilli V., Mayor A., Tardivel A. & Tschopp J. 2006. Gout-associated uric acid crystals activate the NALP3 inflammasome. *Nature* 440, 237-41.

Mayer J.-P. A. 2013. *Rationales und kombinatorisches Protein-Engineering mit Lipocalinen.* Technische Universität München.

McCarty D. J. 2008. Urate crystals, inflammation, and colchicine. *Arthritis Rheum.* 58, S20-4.

Meng H., Tonnesen M. G., Marchese M. J., Clark R. A., Bahou W. F. & Gruber B. L. 1995. Mast cells are potent regulators of endothelial cell adhesion molecule ICAM-1 and VCAM-1 expression. *J. Cell. Physiol.* 165, 40-53.

Micropharm. 2019. *Micropharm Ltd. - Product Pipeline* [Online]. Available: https://micropharm.co.uk/products/product_pipeline/ [Accessed 30 September 2019].

Mills J. & Dean P. M. 1996. Three-dimensional hydrogen-bond geometry and probability information from a crystal survey. *J. Comput. Aided Mol. Des.* 10, 607-622.

Mirela B., Mila M.-P., Brown D. & Ivan S. 2000. In colchicine-treated rats, cellular distribution of AQP-1 in convoluted and straight proximal tubule segments is differently affected. *Pflügers Archiv* 439, 321-330.

Miyachi Y., Taniguchi S., Ozaki M. & Horio T. 1981. Colchicine in the treatment of the cutaneous manifestations of Behcet's disease. *Br. J. Dermatol.* 104, 67-70.

Moore J. C. 1811. *Two Letters to Dr. Jones on the composition of the Eau médicinale d'Husson ... Second edition, corrected,* London, Printed for J. Johnson & Co.

Morath V., Bolze F., Schlapschy M., Schneider S., Sedlmayer F., Seyfarth K., Klingenspor M. & Skerra A. 2015. PASylation of Murine Leptin Leads to Extended Plasma Half-Life and Enhanced in Vivo Efficacy. *Mol. Pharm.* 12, 1431-42.

Moree W. J., van der Marel G. A. & Liskamp R. M. J. 1991. Peptides containing a sulfinamide or a sulfonamide moiety: New transition-state analogues. *Tetrahedron Lett.* 32, 409-412.

Nagesh K. R., Menezes R. G., Rastogi P., Naik N. R., Rasquinha J. M., Senthilkumaran S. & Fazil A. 2011. Suicidal plant poisoning with Colchicum autumnale. *J. Forensic Leg. Med.* 18, 285-7.

Neuwinger H. D. 1996. *African ethnobotany : poisons and drugs : chemistry, pharmacology, toxicology,* London ; New York, Chapman & Hall.

Niel E. & Scherrmann J.-M. 2006. Colchicine today. *Joint, bone, spine : revue du rhumatisme* 73, 672-8.

Nielsen R., Christensen E. I. & Birn H. 2016. Megalin and cubilin in proximal tubule protein reabsorption: from experimental models to human disease. *Kidney Int.* 89, 58-67.

Nuki G. 2008. Colchicine: Its mechanism of action and efficacy in crystal-induced inflammation. *Curr. Rheumatol. Rep.* 10, 218-227.

Olins P. O., Devine C. S., Rangwala S. H. & Kavka K. S. 1988. The T7 phage gene 10 leader RNA, a ribosome-binding site that dramatically enhances the expression of foreign genes in Escherichia coli. *Gene* 73, 227-35.

Oser B. L. 1981. The rat as a model for human toxicological evaluation. *J. Toxicol. Environ. Health, A: Curr. Iss.* 8, 521-542.

Packer M. S. & Liu D. R. 2015. Methods for the directed evolution of proteins. *Nat. Rev. Genet.* 16, 379-394.

Panda D., Daijo J. E., Jordan M. a. & Wilson L. 1995. Kinetic stabilization of microtubule dynamics at steady state in vitro by substoichiometric concentrations of tubulin-colchicine complex. *Biochemistry* 34, 9921-9929.

Paschke M. 2006. Phage display systems and their applications. *Appl. Microbiol. Biotechnol.* 70, 2-11.

Pauling L. 1948. Chemical achievement and hope for the future. *Am. Sci.* 36, 51-8.

Peake P. W., Pianta T. J., Succar L., Fernando M., Buckley N. A. & Endre Z. H. 2015. Fab fragments of ovine antibody to colchicine enhance its clearance in the rat. *Clin. Toxicol.* 53, 1-6.

Peat T. S., Christopher J. A. & Newman J. 2005. Tapping the Protein Data Bank for crystallization information. *Acta Crystallogr. D Biol. Crystallogr.* 61, 1662-1669.

Pelletier P. J., Caventou J.-B. & Gilbert. 1820. Chemische Untersuchung mehrerer Pflanzenkörper aus der Familie des Colchicum, (Sabadill, weisse Niesswurz der Officinen, Herbst-Zeitlose) und ihres wirksamen Princips (des Veratrin) Annalen der Physik Volume 65, Issue 8. *Annalen der Physik* [Online], 65.

Peters E. A., Schatz P. J., Johnson S. S. & Dower W. J. 1994. Membrane insertion defects caused by positive charges in the early mature region of protein pIII of filamentous phage fd can be corrected by prlA suppressors. *J. Bacteriol.* 176, 4296-4305.

Pettersen E. F., Goddard T. D., Huang C. C., Couch G. S., Greenblatt D. M., Meng E. C. & Ferrin T. E. 2004. UCSF Chimera - a visualization system for exploratory research and analysis. *J. Comput. Chem.* 25, 1605-12.

Pfeiffer S. K. 2017. *Biologische Evaluierung radioaktiv markierter Bindeproteine für die nuklearmedizinische Bildgebung der Glioblastom-Vaskulatur.* lmu.

Piatesi A. 2003. *Binding properties and Diels-Alder activity of an efficient antibody catalyst.* ETH Zurich.

Piatesi A. & Hilvert D. 2004. Immunological optimization of a generic hydrophobic pocket for high affinity hapten binding and Diels-Alder activity. *ChemBioChem* 5, 460-6.

Pollack S. J., Jacobs J. W. & Schultz P. G. 1986. Selective chemical catalysis by an antibody. *Science* 234, 1570-3.

Pontius J., Richelle J. & Wodak S. J. 1996. Deviations from standard atomic volumes as a quality measure for protein crystal structures. *J. Mol. Biol.* 264, 121–136.

Prinz W. A., Aslund F., Holmgren A. & Beckwith J. 1997. The role of the thioredoxin and glutaredoxin pathways in reducing protein disulfide bonds in the Escherichia coli cytoplasm. *J. Biol. Chem.* 272, 15661-7.

Proft T. 2009. *Microbial toxins : current research and future trends,* Norfolk, Caister Academic Press.

Putterman C., Ben-Chetrit E., Levy M., Putterman C., Ben-Chetrit E. & Levy M. 1991. Colchicine intoxication: clinical pharmacology, risk factors, features, and management. *Semin. Arthritis Rheum.* 21, 143-155.

Rabhi-Essafi I., Sadok A., Khalaf N. & Fathallah D. M. 2007. A strategy for high-level expression of soluble and functional human interferon alpha as a GST-fusion protein in E. coli. *Protein Eng. Des. Sel.* 20, 201-9.

Rabinovitch O., Zemer D., Kukia E., Sohar E. & Mashiach S. 1992. Colchicine treatment in conception and pregnancy: two hundred thirty-one pregnancies in patients with familial Mediterranean fever. *Am. J. Reprod. Immunol.* 28, 245-6.

Radzicka A. & Wolfenden R. 1995. A proficient enzyme. *Science* 267, 90.

Rakonjac J., Bennett N. J., Spagnuolo J., Gagic D. & Russel M. 2011. Filamentous bacteriophage: biology, phage display and nanotechnology applications. *Curr. Issues Mol. Biol.* 13, 51-76.

Ravelli R. B. G., Gigant B., Curmi P. A., Jourdain I., Lachkar S., Sobel A. & Knossow M. 2004. Insight into tubulin regulation from a complex with colchicine and a stathmin-like domain. *Nature* 428, 198-202.

Rennke H. G., Patel Y. & Venkatachalam M. A. 1978. Glomerular filtration of proteins: clearance of anionic, neutral, and cationic horseradish peroxidase in the rat. *Kidney Int.* 13, 278-88.

Richette P. & Bardin T. 2010. Gout. *Lancet* 375, 318-28.

Richter A. 2018. *Entwicklung, Evaluierung und Optimierung von Anticalinen gegen den tumorassoziierten VEGF-Rezeptor 3.* Dissertation, Technische Universität München.

Richter A., Eggenstein E. & Skerra A. 2014. Anticalins: exploiting a non-Ig scaffold with hypervariable loops for the engineering of binding proteins. *FEBS Lett.* 588, 213-8.

Roberge C. J., Gaudry M., de Medicis R., Lussier A., Poubelle P. E. & Naccache P. H. 1993. Crystal-induced neutrophil activation. IV. Specific inhibition of tyrosine phosphorylation by colchicine. *J. Clin. Invest.* 92, 1722-9.

Rochdi M., Sabouraud A., Girre C., Venet R. & Scherrmann J. M. 1994. Pharmacokinetics and absolute bioavailability of colchicine after i.v. and oral administration in healthy human volunteers and elderly subjects. *Eur. J. Clin. Pharmacol.* 46, 351-354.

Rodi D. J., Soares A. S. & Makowski L. 2002. Quantitative assessment of peptide sequence diversity in M13 combinatorial peptide phage display libraries. *J. Mol. Biol.* 322, 1039-1052.

Rolleman E. J., Krenning E. P., van Gameren A., Bernard B. F. & de Jong M. 2004. Uptake of [111In-DTPA0] octreotide in the rat kidney is inhibited by colchicine and not by fructose. *J. Nucl. Med.* 45, 709-713.

Rolleman E. J., Valkema R., de Jong M., Kooij P. P. & Krenning E. P. 2003. Safe and effective inhibition of renal uptake of radiolabelled octreotide by a combination of lysine and arginine. *Eur. J. Nucl. Med. Mol. Imag.* 30, 9-15.

Romesberg F. E., Spiller B., Schultz P. G. & Stevens R. C. 1998. Immunological origins of binding and catalysis in a Diels-Alderase antibody. *Science* 279, 1929-1933.

Rosenbloom S. J. & Ferguson F. 1968. Fatty change in organs of the rat treated with colchicine. *Toxicol. Appl. Pharmacol.* 13, 50-61.

Rouan S. E., Otterness I., Cunningham A. & Rhodes C. 1989. Specific, high affinity colchicine binding monoclonal antibodies: development and characterization of the antibodies. *Hybridoma* 8, 435-448.

Rouan S. K., Otterness I. G., Cunningham a. C., Holden H. E. & Rhodes C. T. 1990. Reversal of colchicine-induced mitotic arrest in Chinese hamster cells with a colchicine-specific monoclonal antibody. *Am. J. Pathol.* 137, 779-787.

Ryckman C., McColl S. R., Vandal K., de Medicis R., Lussier A., Poubelle P. E. & Tessier P. A. 2003. Role of S100A8 and S100A9 in neutrophil recruitment in response to monosodium urate monohydrate crystals in the air-pouch model of acute gouty arthritis. *Arthritis Rheum.* 48, 2310-20.

Sabouraud A., Cano N. & Scherrmann J. M. 1994a. Radioimmunoassay of colchicine with antisera exhibiting variable cross-reactivity. *Ther. Drug Monit.* 16, 179-85.

Sabouraud A., Chappey O., Dupin T. & Scherrmann J. M. 1994b. Binding of colchicine and thiocolchicoside to human serum proteins and blood cells. *Int. J. Clin. Pharmacol. Ther.* 32, 429-32.

Sabouraud A., Rochdi M., Urtizberea M., Christen M. O., Achtert G. & Scherrmann J. M. 1992a. Pharmacokinetics of colchicine: a review of experimental and clinical data. *Z. Gastroenterol.* 30 Suppl 1, 35-9.

Sabouraud a., Urtizberea M., Grandgeorge M., Gattel P., Makula M. E. & Scherrmann J. M. 1991. Dose-dependent reversal of acute murine colchicine poisoning by goat colchicine-specific Fab fragments. *Toxicology* 68, 121-132.

Sabouraud A. E., Urtizberea M., Benmoussa K., Cano N. J. & Scherrmann J. M. G. 1992b. Fab-bound Colchicine Appears to Adopt Fab Fragment Disposition in Rats. *J. Pharm. Pharmacol.* 44, 1015-1019.

Sabouraud A. E., Urtizberea M., Cano N. J., Grandgeorge M., Rouzioux J. M. & Scherrmann J. M. 1992c. Colchicine-specific Fab fragments alter colchicine disposition in rabbits. *J. Pharmacol. Exp. Ther.* 260, 1214-9.

Sambrook J. & Russell D. W. 2001. *Molecular cloning: a laboratory manual,* Cold Spring Harbor, N.Y., Cold Spring Harbor Laboratory Press.

Sanner M. F., Olson A. J. & Spehner J. C. 1996. Reduced surface: an efficient way to compute molecular surfaces. *Biopolymers* 38, 305-20.

Sannohe S., Makino Y., Kita T., Kuroda N. & Shinozuka T. 2002. Colchicine poisoning resulting from accidental ingestion of meadow saffron (Colchicum autumnale). *J. Forensic Sci.* 47, 1391-6.

Sato M., Yagishita F., Mino T., Uchiyama N., Patel A., Chooi Y.-H., Goda Y., Xu W., Noguchi H., Yamamoto T., Hotta K., Houk K. N., Tang Y. & Watanabe K. 2015. Involvement of Lipocalin-like CghA in Decalin-Forming Stereoselective Intramolecular [4+2] Cycloaddition. *ChemBioChem* 16, 2294-2298.

Schaller J., Gerber S., Kämpfer U., Lejon S. & Trachsel C. 2008. The Immune System. *In: Human Blood Plasma Proteins: Structure and Function.*

Scherrmann J. M., Urtizberea M., Pierson P. & Terrien N. 1989. The effect of colchicine-specific active immunization on colchicine toxicity and disposition in the rabbit. *Toxicology* 56, 213-222.

Schiefner A., Gebauer M., Richter A. & Skerra A. 2018. Anticalins reveal high plasticity in the mode of complex formation with a common tumor antigen. *Structure* 26, 649-656. e3.

Schinkel A. H. 1999. P-Glycoprotein, a gatekeeper in the blood–brain barrier. *Adv. Drug Del. Rev.* 36, 179-194.

Schiweck W. & Skerra A. 1995. Fermenter production of an artificial fab fragment, rationally designed for the antigen cystatin, and its optimized crystallization through constant domain shuffling. *Proteins: Struct. Funct. Bioinform.* 23, 561-565.

Schlapschy M., Binder U., Börger C., Theobald I., Wachinger K., Kisling S., Haller D. & Skerra A. 2013. PASylation: a biological alternative to PEGylation for extending the plasma half-life of pharmaceutically active proteins. *Protein Eng. Des. Sel.* 26, 489–501.

Schlehuber S. 2001. *Evolutives Protein-Design eines „Anticalins" mit Bindungsspezifität für Digoxigenin.* PhD Dissertation, Technische Universtität München.

Schlehuber S., Beste G. & Skerra A. 2000. A Novel Type of Receptor Protein, Based on the Lipocalin Scaffold, with Specificity for Digoxigenin. *J. Mol. Biol.* 297, 1105-1120.

Schlehuber S. & Skerra A. 2005. Lipocalins in drug discovery: from natural ligand-binding proteins to "anticalins". *Drug Discov. Today* 10, 23-33.

Schmidt T. G. M. & Skerra A. 2007. The Strep-tag system for one-step purification and high-affinity detection or capturing of proteins. *Nat. Protoc.* 2, 1528-35.

Schönfeld D., Matschiner G., Chatwell L., Trentmann S., Gille H., Hülsmeyer M., Brown N., Kaye P. M., Schlehuber S., Hohlbaum A. M. & Skerra A. 2009. An engineered lipocalin

specific for CTLA-4 reveals a combining site with structural and conformational features similar to antibodies. *Proc. Natl. Acad. Sci. USA* 106, 8198-8203.

Schuenemann T. A., Delgado-Nixon V. M. & Dalbey R. E. 1999. Direct evidence that the proton motive force inhibits membrane translocation of positively charged residues within membrane proteins. *J. Biol. Chem.* 274, 6855-6864.

Serafimov J. M., Gillingham D., Kuster S. & Hilvert D. 2008. The putative Diels-Alderase macrophomate synthase is an efficient aldolase. *J. Am. Chem. Soc.* 130, 7798-9.

Sergeeva A., Kolonin M. G., Molldrem J. J., Pasqualini R. & Arap W. 2006. Display technologies: application for the discovery of drug and gene delivery agents. *Adv. Drug Del. Rev.* 58, 1622-54.

Siegel J. B. J., Zanghellini A., Lovick H. H. M., Kiss G., Lambert A. R., St Clair J. L., Gallaher J. L., Hilvert D., Gelb M. H., Stoddard B. L., Houk K. N., Michael F. E. & Baker D. 2010. Computational design of an enzyme catalyst for a stereoselective bimolecular Diels-Alder reaction. *Science* 329, 309-13.

Skerra A. 2000. Lipocalins as a scaffold. *Biochim. Biophys. Acta Protein Struct. Mol. Enzymol.* 1482, 337-350.

Skerra A. 2001. 'Anticalins': a new class of engineered ligand-binding proteins with antibody-like properties. *J. Biotechnol.* 74, 257-75.

Skerra A. 2007. Alternative non-antibody scaffolds for molecular recognition. *Curr. Opin. Biotechnol.* 18, 295-304.

Skerra A. 2008. Alternative binding proteins: anticalins - harnessing the structural plasticity of the lipocalin ligand pocket to engineer novel binding activities. *FEBS J.* 275, 2677-83.

Skerra A., Dreher M. L. & Winter G. 1991a. Filter screening of antibody Fab fragments secreted from individual bacterial colonies: Specific detection of antigen binding with a two-membrane system. *Anal. Biochem.* 196, 151-155.

Skerra A., Pfitzinger I. & Pluckthun A. 1991b. The functional expression of antibody Fv fragments in Escherichia coli: improved vectors and a generally applicable purification technique. *Biotechnology. (N. Y.)* 9, 273-8.

Skerra A., Theobald I. & Schlapschy M. 2008. *Biological active proteins having increased in vivo and/or vitro stability*. PCT IEP2008/005020.

Smiley J. A. & Benkovic S. J. 1994. Selection of catalytic antibodies for a biosynthetic reaction from a combinatorial cDNA library by complementation of an auxotrophic Escherichia coli: antibodies for orotate decarboxylation. *Proc. Natl. Acad. Sci. USA* 91, 8319-23.

Smith G. 1985. Filamentous fusion phage: novel expression vectors that display cloned antigens on the virion surface. *Science* 228, 1315-1317.

Smith G. P. 1993. Preface. Surface display and peptide libraries. *Gene* 128, 1 - 2.

Speeg K. V., Maldonado A. L., Liaci J. & Muirhead D. 1992a. Effect of cyclosporine on colchicine secretion by a liver canalicular transporter studied in vivo. *Hepatology* 15, 899-903.

Speeg K. V., Maldonado A. L., Liaci J. & Muirhead D. 1992b. Effect of cyclosporine on colchicine secretion by the kidney multidrug transporter studied in vivo. *J. Pharmacol. Exp. Ther.* 261, 50-5.

Stapczynski J. S., Rothstein R. J., Gaye W. a. & Niemann J. T. 1981. Colchicine overdose: report of two cases and review of the literature. *Ann. Emerg. Med.* 10, 364-9.

Sternberg S. S., Ferguson F. C. & Theodore P. S. 1954. Colchicine. III. Pathology and hematology in cats and rats. *Cancer* 7, 607-616.

Stevenson J. D. & Thomas N. R. 2000. Catalytic antibodies and other biomimetic catalysts. *Nat. Prod. Rep.* 17, 535-577.

Stewart J. D. & Benkovic S. J. 1995. Transition-state stabilization as a measure of the efficiency of antibody catalysis. *Nature* 375, 388.

Strauch K. L. & Beckwith J. 1988. An Escherichia coli mutation preventing degradation of abnormal periplasmic proteins. *Proc. Natl. Acad. Sci. USA* 85, 1576-80.

Strober W. & Waldmann T. A. 1974. The Role of the Kidney in the Metabolism of Plasma Proteins. *Nephron* 13, 35-66.

Studier F. W. & Moffatt B. A. 1986. Use of bacteriophage T7 RNA polymerase to direct selective high-level expression of cloned genes. *J. Mol. Biol.* 189, 113-130.

Suga H. & Tanimoto N. 1994. Glycosidase antibodies induced to a half-chair transition-state analog. *J. Am. Chem. Soc.*, 11197-11198.

Sullivan T. P., King L. E., Jr. & Boyd A. S. 1998. Colchicine in dermatology. *J. Am. Acad. Dermatol.* 39, 993-9.

Sundov Z., Nincevic Z., Definis-Gojanovic M., Glavina-Durdov M., Jukic I., Hulina N. & Tonkic A. 2005. Fatal colchicine poisoning by accidental ingestion of meadow saffron-case report. *Forensic Sci. Int.* 149, 253-6.

Sutton T. 1814. On Mr. Want's Discovery of the Mode of preparing the Eau Medicinale. *Med. Phys. J.* 32, 198-207.

Szostková M., Horáková D. & Němec M. 1999. The influence of the growth phase of enteric bacteria on electrotransformation with plasmid DNA. *Folia Microbiol.* 44, 177-180.

Tanaka F. 2002. Catalytic antibodies as designer proteases and esterases. *Chem. Rev.* 102, 4885-906.

Tanaka F. & Barbas C. F., 3rd 2002. Reactive immunization: a unique approach to catalytic antibodies. *J. Immunol. Methods* 269, 67-79.

Tang Y., Hicks J. B. & Hilvert D. 1991. In vivo catalysis of a metabolically essential reaction by an antibody. *Proc. Natl. Acad. Sci. USA* 88, 8784-6.

Tateishi T., Soucek P., Caraco Y., Guengerich F. P. & Wood A. J. 1997. Colchicine biotransformation by human liver microsomes. Identification of CYP3A4 as the major isoform responsible for colchicine demethylation. *Biochem. Pharmacol.* 53, 111-6.

Tawfik D., Eshhar Z. & Green B. 1994. Catalytic antibodies: a critical assessment. *Mol. Biotechnol.* 1, 87-103.

Terkeltaub R., Tenner A. J., Kozin F. & Ginsberg M. H. 1983. Plasma protein binding by monosodium urate crystals. Analysis by two-dimensional gel electrophoresis. *Arthritis Rheum.* 26, 775-83.

Terrien N., Urtizberea M. & Scherrmann J. M. 1990. Reversal of advanced colchicine toxicity in mice with goat colchicine-specific antibodies. *Toxicol. Appl. Pharmacol.* 104, 504-510.

Thiebaut F., Tsuruo T., Hamada H., Gottesman M. M., Pastan I. & Willingham M. C. 1987. Cellular localization of the multidrug-resistance gene product P-glycoprotein in normal human tissues. *Proc. Natl. Acad. Sci. USA* 84, 7735-7738.

Thomas N. R. 1996. Catalytic antibodies–reaching adolescence? *Nat. Prod. Rep.* 13, 479-511.

Tramontano A., Janda K. D. & Lerner R. A. 1986. Catalytic antibodies. *Science* 234, 1566-70.

Troger U., Lins H., Scherrmann J. M., Wallesch C. W. & Bode-Boger S. M. 2005. Tetraparesis associated with colchicine is probably due to inhibition by verapamil of the P-glycoprotein efflux pump in the blood-brain barrier. *BMJ* 331, 613.

Tung W. L. & Chow K.-C. 1995. A modified medium for efficient electrotransformation of E. coli. *Trends Genet.* 11, 128-129.

Ueda K., Cardarelli C., Gottesman M. M. & Pastan I. 1987. Expression of a full-length cDNA for the human "MDR1" gene confers resistance to colchicine, doxorubicin, and vinblastine. *Proc. Natl. Acad. Sci. USA* 84, 3004-8.

van den Brulle J., Fischer M., Langmann T., Horn G., Waldmann T., Arnold S., Fuhrmann M., Schatz O., O'Connell T., O'Connell D., Auckenthaler A. & Schwer H. 2008. A novel solid phase technology for high-throughput gene synthesis. *BioTechniques* 45, 340-3.

van Zoelen G., de Vries I. & Meulenbelt J. 2002. Colchicine Poisoning: Ingestion of Colchicumautumnale Flowers. *In:* Committee, E. S. (ed.) *European Association of Poisons Centres and Clinical Toxicologists XXII International Congress.*

Vegt E., de Jong M., Wetzels J. F. M., Masereeuw R., Melis M., Oyen W. J. G., Gotthardt M. & Boerman O. C. 2010a. Renal Toxicity of Radiolabeled Peptides and Antibody Fragments: Mechanisms, Impact on Radionuclide Therapy, and Strategies for Prevention. *J. Nucl. Med.* 51, 1049-1058.

Vegt E., Eek A., Oyen W. J., de Jong M., Gotthardt M. & Boerman O. C. 2010b. Albumin-derived peptides efficiently reduce renal uptake of radiolabelled peptides. *Eur. J. Nucl. Med. Mol. Imag.* 37, 226-234.

Vehier-Mounier C., Saulnier F., Durocher A., Houdret N., Lhermitte M., Lefebvre M. C. & Wattel F. 1989. [Acute colchicine poisoning. Value of intra-erythrocyte assay]. *Presse Med.* 18, 1755.

Vermette P., Gengenbach T., Divisekera U., Kambouris P. A., Griesser H. J. & Meagher L. 2003. Immobilization and surface characterization of NeutrAvidin biotin-binding protein on different hydrogel interlayers. *J. Colloid Interface Sci.* 259, 13-26.

Vogt M. & Skerra A. 2001. Bacterially produced apolipoprotein D binds progesterone and arachidonic acid, but not bilirubin or E-3M2H. *J. Mol. Recognit.* 14, 79-86.

von Richter O., Burk O., Fromm M. F., Thon K. P., Eichelbaum M. & Kivisto K. T. 2004. Cytochrome P450 3A4 and P-glycoprotein expression in human small intestinal enterocytes and hepatocytes: a comparative analysis in paired tissue specimens. *Clin. Pharmacol. Ther.* 75, 172-83.

von Störck A. B. 1763. *Libellus, quo demonstratur: colchici autumnalis radicem,* Vindobonae, Typis Joannis Thomae Trattner.

von Störck A. B. 1764. *An essay on the use and effects of the root of the Colchicum autumnale, or meadow-saffron,* London, T. Becket, P.A. de Hondt.

Vopel S. C. 2016. *Konstruktion und Charakterisierung von Anticalinen mit Spezifität für chromophore Liganden.* PhD Dissertation, Technische Universität München.

Wagner J., Lerner R. A. & Barbas III C. F. 1995. Efficient aldolase catalytic antibodies that use the enamine mechanism of natural enzymes. *Science* 270, 1797.

Wallace L. & Ertel H. 1970. Colchicine Plasma Levels. *Am. J. Med.* 48, 443-448.

Wallace S. L., Singer J. Z., Duncan G. J., Wigley F. M. & Kuncl R. W. 1991. Renal function predicts colchicine toxicity: guidelines for the prophylactic use of colchicine in gout. *J. Rheumatol.* 18, 264-269.

Walter T. S., Meier C., Assenberg R., Au K.-F., Ren J., Verma A., Nettleship Joanne E., Owens R. J., Stuart David I. & Grimes J. M. 2006. Lysine Methylation as a Routine Rescue Strategy for Protein Crystallization. *Structure* 14, 1617-1622.

Walvoord R. R., Huynh P. N. & Kozlowski M. C. 2014. Quantification of electrophilic activation by hydrogen-bonding organocatalysts. *J. Am. Chem. Soc.* 136, 16055-16065.

Wang S., Luo Y., Yi X., Yu W., Xu Z., Ma X., He J. & Liu Q. 2007. A highly efficient and highly reliable protocol for transformation of Escherichia coli by electroporation. *J. Rapid Methods Automat. Micro.* 15, 253-258.

Want J. 1811. On the treatment of gout. *Med. Phys. J.* 26, 188-203.

Wassermann A. 1965. *Diels-Alder Reactions. Organic Background and Physico-chemical Aspects*, Elsevier Publishing Company.

Watanabe K., Mie T., Ichihara A., Oikawa H. & Honma M. 2000. Detailed reaction mechanism of macrophomate synthase. Extraordinary enzyme catalyzing five-step transformation from 2-pyrones to benzoates. *J. Biol. Chem.* 275, 38393-401.

Weakley-Jones B., Gerber J. E. & Biggs G. 2001. Colchicine poisoning: case report of two homicides. *Am. J. Forensic Med. Pathol.* 22, 203-6.

Wehner F., Musshoff F., Schulz M., Martin D. & Wehner H.-D. 2006. Detection of colchicine by means of LC-MS/MS after mistaking meadow saffron for bear's garlic. *Forensic Sci. Med. Pathol.* 2, 193-197.

Weichenberger C. X. & Sippl M. J. 2007. NQ-Flipper: recognition and correction of erroneous asparagine and glutamine side-chain rotamers in protein structures. *Nucleic Acids Res.* 35, W403-6.

Weiner D. P., Wiemann T., Wolfe M. M., Wentworth P. & Janda K. D. 1997. A pentacoordinate oxorhenium (V) metallochelate elicits antibody catalysts for phosphodiester cleavage. *J. Am. Chem. Soc.* 119, 4088-4089.

Wentworth P., Datta A., Smith S., Marshall A., Partridge L. J., Blackburn G. M., Uni V., Kingdom U., May R. V. & Alder D. 1997. Antibody Catalysis of BAc2 Aryl Carbamate

Ester Hydrolysis: A Highly Disfavored Chemical Process. *J. Am. Chem. Soc.* 7863, 2315-2316.

Wentworth P., Liu Y., Wentworth A. D., Fan P., Foley M. J. & Janda K. D. 1998. A bait and switch hapten strategy generates catalytic antibodies for phosphodiester hydrolysis. *Proc. Natl. Acad. Sci. USA* 95, 5971-5975.

Wiesenfeld P. L., Garthoff L. H., Sobotka T. J., Suagee J. K. & Barton C. N. 2007. Acute oral toxicity of colchicine in rats: effects of gender, vehicle matrix and pre-exposure to lipopolysaccharide. *J. Appl. Toxicol.* 27, 421-33.

Wilson D. R. & Finlay B. B. 1998. Phage display: applications, innovations, and issues in phage and host biology. *Can. J. Microbiol.* 44, 313-329.

Wilson L. & Meza I. 1973. The mechanism of action of colchicine. Colchicine binding properties of sea urchin sperm tail outer doublet tubulin. *J. Cell Biol.* 58, 709-719.

Wirsching P., Ashley J. A., Lo C.-H. L., Janda K. D. & Lerner R. A. 1995. Reactive immunization. *Science* 270, 1775.

Wolfenden R. 1969. Transition state analogues for enzyme catalysis. *Nature* 223, 704-705.

Wright D. G. & Malawista S. E. 1973. Mobilization and extracellular release of granular enzymes from human leukocytes during phagocytosis: inhibition by colchicine and cortisol but not by salicylate. *Arthritis Rheum.* 16, 749-58.

Xia Y., Schlapschy M., Morath V., Roeder N., Vogt E. I., Stadler D., Cheng X., Dittmer U., Sutter K. & Heikenwalder M. 2019. PASylated interferon α efficiently suppresses hepatitis B virus and induces anti-HBs seroconversion in HBV-transgenic mice. *Antiviral Res.* 161, 134-143.

Xu J., Deng Q., Chen J., Houk K. N., Bartek J., Hilvert D. & Wilson I. a. 1999. Evolution of shape complementarity and catalytic efficiency from a primordial antibody template. *Science* 286, 2345-2348.

Xu L., Adams B., Jeliazkova-Mecheva V. V., Trimble L., Kwei G. & Harsch A. 2008. Identification of novel metabolites of colchicine in rat bile facilitated by enhanced online radiometric detection. *Drug Metab. Disposition* 36, 731-739.

Yanisch-Perron C., Vieira J. & Messing J. 1985. Improved M13 phage cloning vectors and host strains: nucleotide sequences of the M13mp18 and pUC19 vectors. *Gene* 33, 103-19.

Yim H. H. & Villarejo M. 1992. osmY, a new hyperosmotically inducible gene, encodes a periplasmic protein in Escherichia coli. *J. Bacteriol.* 174, 3637-44.

Yu J., Choi S. Y., Moon K. D., Chung H. H., Youn H. J., Jeong S., Park H. & Schultz P. G. 1998. A glycosidase antibody elicited against a chair-like transition state analog by in vitro immunization. *Proc. Natl. Acad. Sci. USA* 95, 2880-4.

Yurdakul S., Mat C., Tuzun Y., Ozyazgan Y., Hamuryudan V., Uysal O., Enocak M. & Yazici H. 2001. A double-blind trial of colchicine in Behçet's syndrome. *Arthritis Rheum.* 44, 2686-2692.

Zheng Q., Guo Y., Yang L., Zhao Z., Wu Z., Zhang H., Liu J., Cheng X., Wu J., Yang H., Jiang H., Pan L. & Liu W. 2016. Enzyme-Dependent [4+2] Cycloaddition Depends on Lid-like Interaction of the N-Terminal Sequence with the Catalytic Core in PyrI4. *Cell Chem. Biol.* 23, 352-60.

8. Appendix

Figure 8.1. Nucleotide and amino acid sequences of lipocalin 2 and Colchicalin D6.1 (cf. Figure 3.18) – after processing of the signal peptide and without an affinity tag.

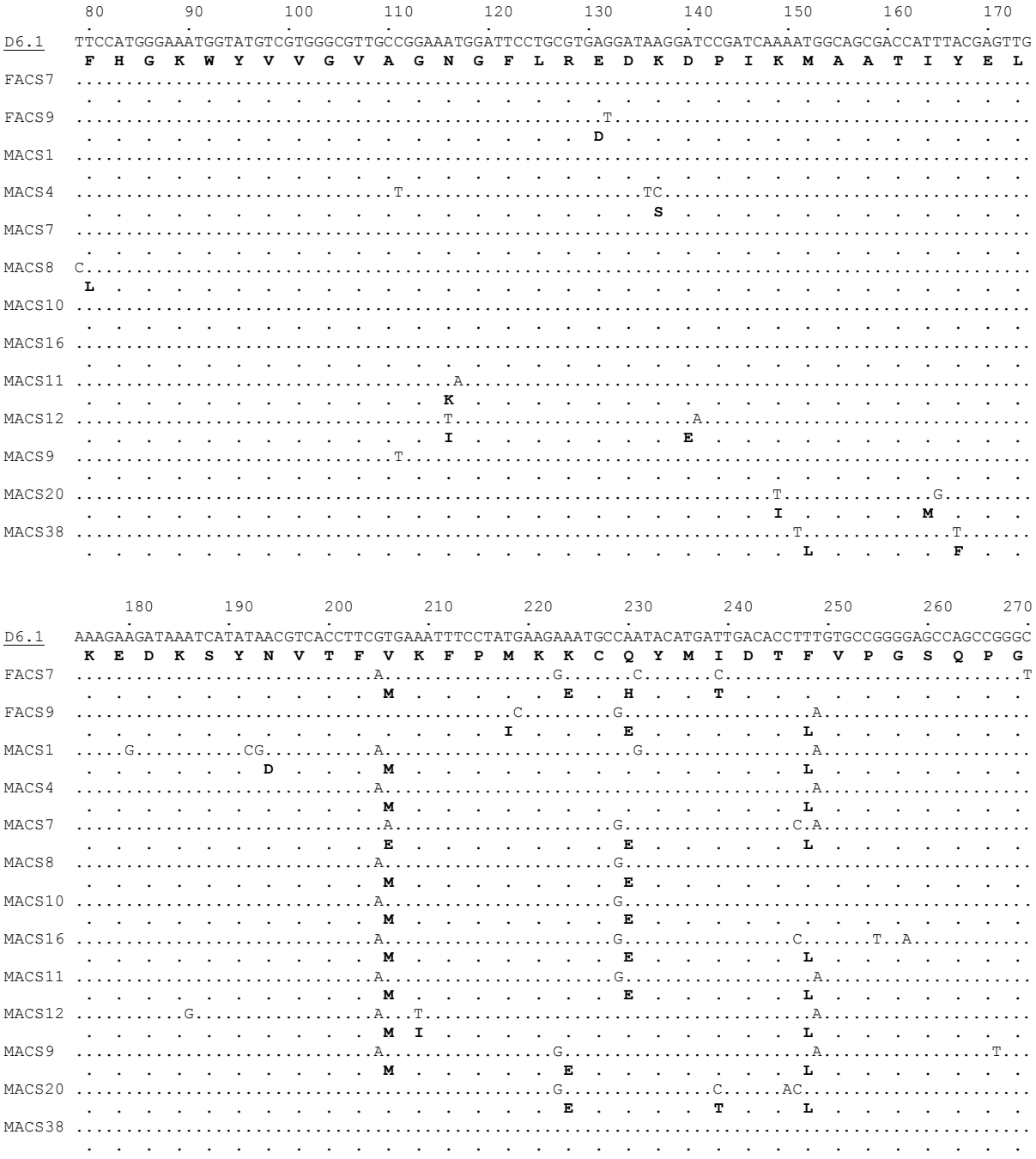

Figure 8.2. Nucleotide and amino acid sequences of the central coding regions of the most promising clones identified in the single-clone analysis via FACS during the affinity maturation of Colchicalin D6.1 (cf. Figure 3.22).

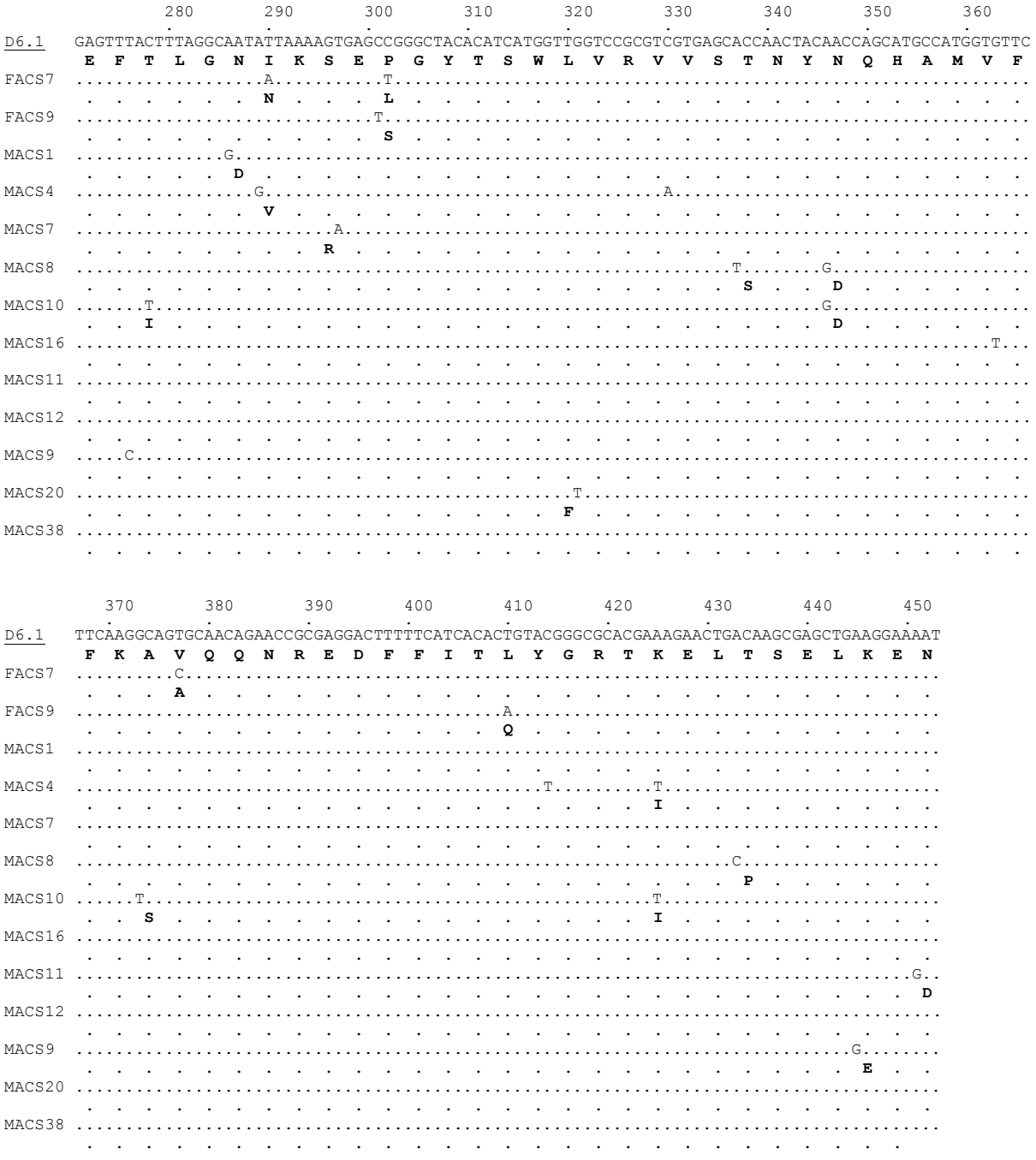

Figure 8.2 (continued from previous page).

Table 8.1. Crystallographic analysis and refinement statistics for the Colchicalin D6.2(M69Q) in complex with colchicine.

Parameter	Value
Crystal Data:	
Space group	$P4_122$
Unit cell dimensions a, b, c [Å], α=β=γ=90°	46.68, 46.68, 136.85
Molecules per asymmetric unit	1
Data Collection:	
Wavelength [Å]	0.89429
Resolution range [Å][a]	46.68–2.20 (2.32–2.20)
I/σ [I][a]	6.3 (1.9)
R_{merge} [%][a, b]	9.4 (41.0)
Unique reflections	8323
Multiplicity[a]	10.3 (9.0)
Completeness[a]	99.9 (99.4)
Refinement:	
R_{cryst} / R_{free}[c]	19.7/26.6
Protein atoms	1394
Ligand atoms	29
Solvent atoms	36
Average B-factor [Å^2]	
Protein	36.92
Ligand	25.34
Water	28.06
Geometry:	
R.m.s.d. bond lengths, angles [Å, °]	0.011, 1.634
Ramachandran analysis[d]: core, allowed, generously allowed, disallowed [%]	91.2, 8.1, 0.0, 0.7

[a] Values in parentheses are for the highest resolution shell

[b] $R_{merge} = \sum_h \sum_i |I_i(h) - \langle I(h)\rangle| / \sum_h \sum_i I_i(h)$ $\quad R_{cryst} = \sum_h \big||F_0(h)| - |F_c(h)|\big| / \sum_h |F_0(h)|$

[c] R_{free} is R_{cryst} with 5 % of the reflections that were randomly selected and excluded from the refinement (Brunger, 1997)

[d] Calculated with PROCHECK

Table 8.2. Crystallographic analysis and preliminary refinement statistics for the Catacalin C3A5 in complex with the TSA.

Parameter	Value
Crystal	
Space group	P2
Molecules per asymmetric unit	3
Cell constants:	
a, b, c [Å]	96.4, 39.0, 96.4
α, β, γ [°]	90.0, 120.0, 90.0
Resolution [Å]	1.7
Refinement	
R factor [%] (in prog.)	14.9
R free [%] (in prog.)	18.9

Table 8.3. Buffer/precipitant conditions of the in-house crystallization screen ('vector screen').

No.	Well	Precipitants	Conc.	Stock	Buffer	pH	Conc.	Stock	Additive	Conc.	Stock
1	1A1	PEG 4000	12 % w/v	50							
2	1A2	PEG 8000	18 % w/v	50	MES	6.5	0.1 M	1			
3	1A3	Na K phosphate	3 M	4		7					
4	1A4	PEG 3350	20 % w/v	50					Na_3 citrate	0.1 M	1.6
5	1A5	PEG 4000	15 % w/v	50	HEPES	7	0.1 M	1			
6	1A6	$(NH_4)_2SO_4$	1.1 M	3.7							
7	1A7	PEG 4000	16 % w/v	50	Na_3 citrate	5.6	0.1 M	1.6			
		Isopropanol	10 % v/v	100							
8	1A8	PEG 2000	15 % w/v	60							
9	1A9	$(NH_4)_2SO_4$	1 M	3.7							
10	1A10	$(NH_4)_2SO_4$	3.2 M	3.7	HEPES	7	0.1 M	1			
11	1A11	PEG MME 2000	20 % w/v	40	Tris-HCl	8.5	0.1 M	1	$NiCl_2$	0.01 M	1
12	1A12	PEG 8000	10 % w/v	50	Tris-HCl	7	0.1 M	1	$MgCl_2$	0.2 M	3
13	1B1	PEG 4000	20 % w/v	50	HEPES	7.5	0.1 M	1			
		Isopropanol	7 % v/v	100							
14	1B2	PEG 4000	30 % w/v	50	Tris-HCl	8.5	0.1 M	1	Li_2SO_4	0.2 M	2.5
15	1B3	PEG 400	50 % v/v	100	MES	6	0.1 M	1			
16	1B4	PEG 400	42.7 % v/v	100	HEPES	7.5	0.1 M	1	$CaCl_2$	0.2 M	1
17	1B5	PEG 10000	20 % w/v	50	MES	6.5	0.1 M	1			
18	1B6	PEG 1000	20 % w/v	50	Tris-HCl	7	0.1 M	1			
19	1B7	Na_3 citrate	1.6 M	1.6							
20	1B8	PEG 8000	18 % w/v	50					$(NH_4)_2SO_4$	0.2 M	3.7
21	1B9	PEG 3350	10 % w/v	50							
22	1B10	Na_3 citrate	0.8 M	1.6							
23	1B11	PEG 3350	20 % w/v	50					Na formate	0.2 M	5
24	1B12	Na_3 citrate	1.6 M	1.6							
25	1C1	$(NH_4)_2SO_4$	2.7 M	3.7							
26	1C2	PEG 4000	16 % w/v	50	Tris-HCl	8.5	0.1 M	1			
27	1C3	PEG 8000	18 % w/v	50	Tris-HCl	8.5	0.1 M	1	Li_2SO_4	0.2 M	2.5
28	1C4	Li_2SO_4	1.05 M	2.5	HEPES	7.5	0.1 M	1	$CaCl_2$	0.2 M	1
29	1C5	PEG 3350	20 % w/v	50							
30	1C6	PEG 3350	20 % w/v	50					NH_4Cl	0.2 M	4
31	1C7	PEG 4000	19 % w/v	50	Na_3 citrate	5.6	0.095 M	1.6	Glycerol	5 % v/v	60
		Isopropanol	19 % v/v	100							
32	1C8	NaCl	4.3 M	5							
33	1C9	PEG 4000	17 % w/v	50	HEPES	7.5	0.085 M	1	Glycerol	15 % v/v	60
		Isopropanol	8.5 % v/v	100							
34	1C10	PEG 6000	15 % w/v	50	Tris-HCl	7.5	0.1 M	1			
35	1C11	PEG 8000	18 % w/v	50	Tris-HCl	8.5	0.1 M	1			
36	1C12	Ethanol	20 % v/v	100	Tris-HCl	8.5	0.1 M	1			

37	1D1	$(NH_4)_2SO_4$	2 M	3.7							
38	1D2	PEG MME 2000	25 % w/v	40	Na cacodylate	6.5	0.1 M	1	$MgCl_2$	0.2 M	3
39	1D3	$(NH_4)_2SO_4$	1.6 M	3.7	HEPES	7	0.1 M	1			
40	1D4	PEG 6000	20 % w/v	50	Tris-HCl	8	0.1 M	1	$MgCl_2$	0.2 M	3
41	1D5	Na K phosphate	1.8 M	4		7					
42	1D6	PEG 10000	20 % w/v	50	HEPES	7.5	0.1 M	1			
43	1D7	PEG 3350	25 % w/v	50	Tris-HCl	8.5	0.1 M	1			
44	1D8	MPD	65 % v/v	100							
45	1D9	PEG 3350	25 % w/v	50	Tris-HCl	8.5	0.1 M	1	NaCl	0.2 M	5
46	1D10	PEG 400	30 % v/v	100	CAPS	10.5	0.1 M	1			
47	1D11	PEG 6000	20 % w/v	50	Na_3 citrate	5	0.1 M	1.6			
48	1D12	PEG 400	30 % v/v	100	Na acetate	4.5	0.1 M	4	$CdCl_2$	0.1 M	1
49	1E1	PEG 4000	8 % w/v	50	Na acetate	4.5	0.1 M	4			
50	1E2	PEG 8000	20 % w/v	50	HEPES	7.5	0.1 M	1			
51	1E3	PEG 4000	25 % w/v	50	Na cacodylate	6.5	0.1 M	1			
52	1E4	Isopropanol	5 % v/v	100					$(NH_4)_2SO_4$	2 M	3.7
53	1E5	PEG 8000	8 % w/v	50	Tris-HCl	8.5	0.1 M	1			
54	1E6	PEG 3350	20 % w/v	50					NaCl	0.2 M	5
55	1E7	PEG 3350	18 % w/v	50	Na_3 citrate	5.6	0.1 M	1.6			
56	1E8	PEG 3000	20 % w/v	50	Na acetate	4.5	0.1 M	4			
57	1E9	Li_2SO_4	0.8 M	2.5	Tris-HCl	8.5	0.1 M	1			
58	1E10	PEG MME 2000	20 % w/v	40	Tris-HCl	7	0.1 M	1			
59	1E11	PEG 8000	20 % w/v	50	Tris-HCl	8	0.1 M	1			
60	1E12	NaCl	4.3 M	5	HEPES	7.5	0.1 M	1			
61	1F1	PEG MME 550	12.5 % v/v	100	MES	6.5	0.1 M	1	$ZnSO_4$	0.01 M	0.05
62	1F2	PEG 4000	20 % w/v	50	Na_3 citrate	5.6	0.1 M	1.6			
		Isopropanol	18 % v/v	100							
63	1F3	PEG 4000	36 % w/v	50					$(NH_4)_2SO_4$	0.2 M	3.7
64	1F4	PEG 3350	25 % w/v	50	Tris-HCl	8.5	0.1 M	1	$MgCl_2$	0.2 M	3
65	1F5	PEG 1500	15 % w/v	50							
66	1F6	PEG 8000	20 % w/v	50					KH_2PO_4	0.05 M	1.5
67	1F7	PEG 4000	18 % w/v	50	Na acetate	4.5	0.1 M	4			
68	1F8	NaCl	2.5 M	5	Na acetate	4.5	0.1 M	4	Li_2SO_4	0.2 M	2.5
69	1F9	PEG 4000	30 % w/v	50	Na acetate	4.5	0.1 M	4			
70	1F10	PEG 3000	20 % w/v	50	HEPES	7.5	0.1 M	1	NaCl	0.2 M	5
71	1F11	PEG 6000	8.8 % w/v	50	Na acetate	6.8	0.2 M	4			
72	1F12	PEG 4000	4 % w/v	50	Na acetate	4.5	0.1 M	4			
73	1G1	PEG 6000	10 % w/v	50					NaCl	2 M	5
74	1G2	MPD	38 % v/v	100							
75	1G3	PEG 1500	30 % w/v	50							
76	1G4	PEG 3350	20 % w/v	50					$MgCl_2$	0.2 M	3
77	1G5	Na_3 citrate	0.1 M	1.6		5					
78	1G6	PEG 6000	10 % w/v	50	HEPES	7.5	0.1 M	1	MPD	4 % v/v	100

79	1G7	PEG 4000	35 % w/v	50							
80	1G8	PEG 3350	20 % w/v	50					KNO_3	0.2 M	1
81	1G9	PEG 4000	12 % w/v	50	HEPES	7.5	0.1 M	1	NaCl	0.1 M	5
82	1G10	PEG 8000	10 % w/v	50	HEPES	7.5	0.1 M	1	Ethylene glycol	8 % v/v	80
83	1G11	Na malonate	3.4 M	4		7					
84	1G12	PEG MME 550	30 % v/v	100	HEPES	7.5	0.1 M	1			
85	1H1	PEG 4000	30 % w/v	50	Tris-HCl	8.5	0.1 M	1			
86	1H2	PEG 6000	20 % w/v	50	MES	6	0.1 M	1			
87	1H3	PEG 4000	8 % w/v	50							
88	1H4	PEG 4000	12 % w/v	50	Na phosphate	7	0.05 M	1			
89	1H5	PEG 3350	20 % w/v	50							
90	1H6	PEG 400	30 % v/v	100	HEPES	7.5	0.1 M	1	$MgCl_2$	0.1 M	3
91	1H7	PEG 6000	12 % w/v	50							
		NaCl	2 M	5							
92	1H8	$MgSO_4$	1.6 M	2	MES	6.5	0.1 M	1			
93	1H9	PEG 6000	20 % w/v	50	HEPES	7	0.1 M	1	NaCl	0.2 M	5
94	1H10	MPD	70 % v/v	100	HEPES	7.5	0.1 M	1			
95	1H11	1,4-butanediol	20 % v/v	100	Na acetate	4.5	0.1 M	4			
96	1H12	PEG 3350	25 % w/v	50	Bis-Tris	5.5	0.1 M	1	$MgCl_2$	0.2 M	3
97	2A1	PEG 3350	20 % w/v	50					$LiNO_3$	0.2 M	1
98	2A2	NaCl	1.5 M	5	Na acetate	4.5	0.1 M	4			
99	2A3	PEG 20000	6 % w/v	50	MES	6.5	0.1 M	1			
100	2A4	Dioxane	35 % v/v	100							
101	2A5	PEG 4000	22 % w/v	50					Na acetate	0.1 M	4
		$(NH_4)_2SO_4$	0.2 M	3.7							
102	2A6	MPD	30 % v/v	100	Na acetate	4.5	0.1 M	4	$CaCl_2$	0.02 M	1
103	2A7	PEG 400	12 % v/v	100	Na K phosphate	6.2	0.1 M	4			
104	2A8	MPD	35 % v/v	100							
105	2A9	PEG 3350	25 % w/v	50	Bis-Tris	5.5	0.1 M	1	Li_2SO_4	0.2 M	2.5
106	2A10	PEG 3350	20 % w/v	50					$(NH_4)_2$ tartrate	0.2 M	2
107	2A11	MPD	40 % v/v	100	MES	6.5	0.1 M	1			
108	2A12	PEG 3350	15 % w/v	50					K thiocyanate	0.1 M	2
109	2B1	PEG 400	30 % v/v	100	Tris-HCl	8	0.1 M	1			
110	2B2	PEG 4000	15 % w/v	50	Tris-HCl	7.5	0.1 M	1	Li_2SO_4	0.2 M	2.5
111	2B3	MPD	40 % v/v	100	HEPES	7	0.1 M	1			
112	2B4	PEG 4000	10 % w/v	50	HEPES	7.5	0.1 M	1			
		Isopropanol	5 % v/v	100							
113	2B5	PEG 8000	25 % w/v	50					LiCl	0.2 M	5
114	2B6	$(NH_4)_2SO_4$	2.2 M	3.7					Na_2HPO_4	0.2 M	4
115	2B7	Na K phosphate	1.3 M	4							
116	2B8	PEG 3000	20 % w/v	50	Tris-HCl	7	0.1 M	1	Ca diacetate	0.2 M	1
117	2B9	PEG 3350	25 % w/v	50	Bis-Tris	6.5	0.1 M	1	Li_2SO_4	0.2 M	2.5
118	2B10	PEG 3350	20 % w/v	50					Li_3 citrate	0.2 M	1

119	2B11	PEG 3350	20 % w/v	50					$(NH_4)_2H$ citrate	0.2 M	2
120	2B12	PEG 1000	33 % w/v	50	Glycine	10	0.02 M	2			
121	2C1	PEG 3350	12 % w/v	50	HEPES	7.5	0.1 M	1			
122	2C2	PEG 8000	8 % w/v	50	Tris-HCl	8	0.1 M	1			
123	2C3	Na_3 citrate	0.6 M	1.6							
124	2C4	PEG 3350	25 % w/v	50	Bis-Tris	5.5	0.1 M	1			
125	2C5	$NH_4H_2PO_4$	0.4 M	3							
126	2C6	MPD	65 % v/v	100	Tris-HCl	8	0.1 M	1			
127	2C7	PEG 400	40 % v/v	100	Na_2H citrate	5.6	0.1 M	1	$MgCl_2$	0.2 M	3
128	2C8	PEG 3350	20 % w/v	50					K formate	0.2 M	1
129	2C9	PEG 3350	25 % w/v	50	HEPES	7.5	0.1 M	1	Li_2SO_4	0.2 M	2.5
130	2C10	PEG 1500	30 % w/v	50	Na acetate	4.5	0.1 M	4			
131	2C11	PEG 3350	20 % w/v	50					Mg diformate	0.2 M	1
132	2C12	PEG MME 550	15 % v/v	100	MES	6.5	0.1 M	1			
133	2D1	PEG 8000	16 % w/v	50	Na_3 citrate	5.6	0.1 M	1.6			
134	2D2	PEG 3350	16 % w/v	50	Tris-HCl	8.5	0.1 M	1	Li_2SO_4	0.2 M	2.5
135	2D3	NaCl	1.5 M	5							
136	2D4	PEG 3350	25 % w/v	50	Bis-Tris	5.5	0.1 M	1	NaCl	0.2 M	5
137	2D5	PEG MME 5000	20 % w/v	40					Na_3 citrate	0.2 M	1.6
138	2D6	Na_3 citrate	1.2 M	1.6							
139	2D7	PEG 600	30 % v/v	80	MES	6	0.1 M	1	Glycerol	10 % v/v	60
		PEG 1000	5 % w/v	50							
140	2D8	PEG 3350	20 % w/v	50					Na thiocyanate	0.2 M	5
141	2D9	PEG 3350	20 % w/v	50					Na malonate	0.2 M	4
142	2D10	PEG 4000	10 % w/v	50	Na acetate	4	0.1 M	4			
143	2D11	PEG 4000	35 % w/v	50	MES	6	0.1 M	1			
144	2D12	PEG 4000	15 % w/v	50	Na cacodylate	6	0.1 M	1			
145	2E1	$(NH_4)_2SO_4$	2 M	3.7					Glycerol	20 % v/v	60
146	2E2	PEG 4000	20 % w/v	50					$(NH_4)_2SO_4$	0.3 M	3.7
147	2E3	PEG 300	20 % v/v	100	Tris-HCl	8.5	0.1 M	1	Glycerol	10 % v/v	60
		PEG 8000	5 % w/v	50							
148	2E4	PEG 3350	25 % w/v	50	HEPES	7.5	0.1 M	1	$MgCl_2$	0.2 M	3
149	2E5	PEG MME 550	25 % v/v	100	HEPES	7	0.05 M	1	$MgCl_2$	0.01 M	3
150	2E6	PEG 200	40 % v/v	100	HEPES	7.5	0.1 M	1			
151	2E7	PEG 400	40 % v/v	100	MES	6	0.1 M	1			
		PEG 3000	5 % w/v	50							
152	2E8	Ethylene glycol	27 % v/v	80							
153	2E9	PEG 3350	20 % w/v	50					NH_4F	0.2 M	1
154	2E10	PEG 4000	32 % w/v	50	Tris-HCl	8.5	0.1 M	1	LiCl	0.8 M	5
155	2E11	MPD	20 % v/v	100	MES	6.5	0.1 M	1			
156	2E12	PEG 10000	18 % w/v	50	HEPES	7	0.1 M	1			
157	2F1	PEG 4000	10 % w/v	50	Na_3 citrate	5.6	0.1 M	1.6			
		Isopropanol	12.7 % v/v	100							

158	2F2	$(NH_4)_2SO_4$	2.2 M	3.7					Na acetate	0.2 M	4
159	2F3	PEG 8000	20 % w/v	50	CHES	9.5	0.1 M	1			
160	2F4	PEG 3350	20 % w/v	50					NaF	0.2 M	1
161	2F5	PEG 4000	15 % w/v	50	Tris-HCl	7.5	0.1 M	1	$MgCl_2$	0.2 M	3
162	2F6	Na malonate	1.9 M	4		7					
163	2F7	PEG 200	50 % v/v	100	Tris-HCl	7	0.1 M	1			
164	2F8	PEG 8000	4 % w/v	50	Tris-HCl	8.5	0.1 M	1			
165	2F9	PEG 3350	20 % w/v	50					Mg diacetate	0.2 M	1
166	2F10	PEG 8000	2 % w/v	50							
		Li_2SO_4	1 M	2.5							
167	2F11	PEG 2000	15 % w/v	60					LiCl	0.1 M	5
168	2F12	PEG MME 5000	18 % w/v	40	Na acetate	5.5	0.1 M	4			
169	2G1	Isopropanol	20 % v/v	100	Na acetate	4.5	0.1 M	4	$CaCl_2$	0.2 M	1
170	2G2	NaCl	1.6 M	5	Na acetate	4.5	0.1 M	4			
171	2G3	NaCl	2.5 M	5	Tris-HCl	7	0.1 M	1	$MgCl_2$	0.2 M	3
172	2G4	PEG 3350	20 % w/v	50					$NaNO_3$	0.2 M	6
173	2G5	PEG 8000	0 % w/v	50					KH_2PO_4	0.05 M	1.5
174	2G6	NaCl	4 M	5	HEPES	7	0.1 M	1			
175	2G7	Ethanol	15 % v/v	100	Imidazole	8	0.1 M	2	$MgCl_2$	0.2 M	3
176	2G8	PEG MME 5000	20 % w/v	40	Bis-Tris	6.5	0.1 M	1			
177	2G9	PEG 3350	20 % w/v	50					KSO_4	0.2 M	1
178	2G10	PEG 8000	15 % w/v	50							
		Li_2SO_4	0.5 M	2.5							
179	2G11	PEG 6000	20 % w/v	50	HEPES	7	0.1 M	1	NH_4Cl	0.2 M	4
180	2G12	MPD	20 % v/v	100	Na acetate	4.5	0.1 M	4	$CaCl_2$	0.02 M	1
181	2H1	PEG 6000	32 % w/v	50	MES	6.5	0.1 M	1			
182	2H2	Ethylene glycol	12.5 % v/v	80							
183	2H3	PEG 400	44.4 % v/v	100							
184	2H4	PEG 3350	20 % w/v	50					$MgSO_4$	0.2 M	2
185	2H5	$(NH_4)_2SO_4$	1.5 M	3.7	HEPES	7	0.1 M	1			
186	2H6	PEG 6000	30 % w/v	50	HEPES	7	0.1 M	1			
187	2H7	PEG 400	30 % v/v	100	Tris-HCl	8.5	0.1 M	1	$MgCl_2$	0.2 M	3
188	2H8	PEG MME 5000	10 % w/v	40	HEPES	7	0.1 M	1	Tacsimate	5 % v/v	100
189	2H9	PEG 3350	20 % w/v	50					Na_2 tartrate	0.2 M	2
190	2H10	PEG 10000	16 % w/v	50	Tris-HCl	8.5	0.1 M	1			
191	2H11	PEG 6000	20 % w/v	50	Tris-HCl	8	0.1 M	1	$CaCl_2$	0.2 M	1
192	2H12	PEG 4000	24 % w/v	50	Tris-HCl	8.5	0.08 M	1	$MgCl_2$	0.16 M	3
		Glycerol	20 % v/v	60							
193	3A1	PEG 1500	24 % w/v	50					Glycerol	15.86 % v/v	60
194	3A2	PEG 8000	30 % w/v	50	Na acetate	4.5	0.1 M	4	Li_2SO_4	0.2 M	2.5
195	3A3	PEG 8000	20 % w/v	50	CAPS	10.5	0.1 M	1	NaCl	0.2 M	5
196	3A4	Ethanol	10 % v/v	100					NaCl	1.5 M	5
197	3A5	NaCl	3 M	5	Na acetate	4.5	0.1 M	4			

198	3A6	PEG 400	18 % v/v	100	Na acetate	4.5	0.1 M	4	$MgCl_2$	0.1 M	3
199	3A7	PEG 3350	20 % w/v	50					K acetate	0.2 M	1
200	3A8	PEG 3000	30 % w/v	50	Tris-HCl	8.5	0.1 M	1	Li_2SO_4	0.2 M	2.5
201	3A9	PEG 3350	20 % w/v	50					NH_4NO_3	0.2 M	8
202	3A10	PEG 6000	20 % w/v	50	Na_3 citrate	4	0.1 M	1.6	LiCl	1 M	5
203	3A11	PEG 4000	8 % w/v	50	Imidazole-malate	6	0.2 M	1			
204	3A12	MPD	40 % v/v	100	Na acetate	5	0.1 M	4			
205	3B1	PEG 1000	25 % w/v	50	MES	6.5	0.1 M	1			
206	3B2	MPD	35 % v/v	100	Tris-HCl	7	0.1 M	1	NaCl	0.2 M	5
207	3B3	PEG 1000	20 % w/v	50	Na cacodylate	6.5	0.1 M	1	$MgCl_2$	0.2 M	3
208	3B4	MPD	30 % v/v	100	Na acetate	4.5	0.1 M	4	NaCl	0.2 M	5
209	3B5	NaCl	3 M	5	Bis-Tris	6.5	0.1 M	1			
210	3B6	PEG 4000	12 % w/v	50	Na_3 citrate	5.6	0.1 M	1.6	Li_2SO_4	0.1 M	2.5
211	3B7	PEG 3350	20 % w/v	50					Na_2SO_4	0.2 M	1
212	3B8	PEG 6000	15 % w/v	50					Glycerol	3.965 % v/v	60
213	3B9	PEG 6000	20 % w/v	50	MES	6	0.1 M	1	$CaCl_2$	0.2 M	1
214	3B10	PEG 400	17 % v/v	100	Na acetate	4.5	0.1 M	4			
215	3B11	PEG 4000	15 % w/v	50	Imidazole-malate	6	0.2 M	1			
216	3B12	MPD	20 % v/v	100	MES	6	0.1 M	1			
217	3C1	Na K phosphate	0.8 M	4							
218	3C2	NaCl	2.5 M	5	Imidazole	8	0.1 M	2			
219	3C3	PEG 3350	20 % w/v	50					NH_4NO_3	0.2 M	8
220	3C4	1,6-Hexanediol	1 M	5	Na acetate	4.5	0.1 M	4	$CoCl_2 \cdot 6H_2O$	0.01 M	0.5
221	3C5	$(NH_4)_3$ citrate	1.8 M	3							
222	3C6	PEG 3350	20 % w/v	50					KF	0.2 M	1
223	3C7	PEG 3350	20 % w/v	50					$(NH_4)_2SO_4$	0.2 M	3.7
224	3C8	PEG 10000	30 % w/v	50	Tris-HCl	8.5	0.1 M	1			
225	3C9	PEG 6000	10 % w/v	50	MES	6.5	0.1 M	1			
226	3C10	PEG 400	33 % v/v	100	HEPES	7	0.1 M	1	$CaCl_2$	0.2 M	1
227	3C11	PEG 400	15 % v/v	100	HEPES	7	0.1 M	1	$CaCl_2$	0.2 M	1
228	3C12	MPD	20 % v/v	100	HEPES	7	0.1 M	1			
229	3D1	PEG 6000	10 % w/v	50	MES	6	0.1 M	1			
230	3D2	PEG 3000	30 % w/v	50	CHES	9.5	0.1 M	1			
231	3D3	PEG 20000	10 % w/v	50	Bicine	9	0.1 M	1	Dioxane	2 % v/v	100
232	3D4	Li_2SO_4	1 M	2.5	Tris-HCl	8.5	0.1 M	1	$NiCl_2$	0.01 M	1
233	3D5	Tacsimate	35 % v/v	100		7					
234	3D6	PEG 3350	20 % w/v	50					KCl	0.2 M	3.5
235	3D7	PEG 3350	20 % w/v	50					NaH_2PO_4	0.2 M	4
236	3D8	PEG 20000	20 % w/v	50							
237	3D9	PEG 8000	18 % w/v	50					Li_2SO_4	0.2 M	2.5
238	3D10	PEG 8000	8 % w/v	50	Na_3 citrate	5	0.1 M	1.6			
239	3D11	$(NH_4)_2SO_4$	2.2 M	3.7					KH_2PO_4	0.2 M	1.5
240	3D12	MPD	65 % v/v	100	Bicine	9	0.1 M	1			

241	3E1	MPD	40 % v/v	100	Imidazole	8	0.1 M	2	$MgCl_2$	0.2 M	3
242	3E2	Ethanol	15 % v/v	100	Tris-HCl	7	0.1 M	1			
243	3E3	PEG 8000	10 % w/v	50							
		PEG 1000	10 % w/v	50							
244	3E4	PEG 400	26.6 % v/v	100	HEPES	7.5	0.095 M	1	Glycerol	5 % v/v	60
		$CaCl_2$	0.19 M	1							
245	3E5	PEG 3350	25 % w/v	50	Bis-Tris	6.5	0.1 M	1			
246	3E6	PEG 3350	20 % w/v	50					NaI	0.2 M	2
247	3E7	PEG 3350	20 % w/v	50					$NH_4H_2PO_4$	0.2 M	3
248	3E8	$(NH_4)_2SO_4$	2.4 M	3.7					Na_3 citrate	0.1 M	1.6
249	3E9	PEG 6000	18 % w/v	50	Na acetate	5	0.05 M	4			
250	3E10	PEG 8000	8 % w/v	50	HEPES	7	0.1 M	1			
251	3E11	Jeffamine ED 2001	31.7 % w/v	50	HEPES	7	0.1 M	1			
252	3E12	Na malonate	1.2 M	4							
253	3F1	PEG 300	40 % v/v	100	Tris-HCl	7	0.1 M	1	PEG 1000	5 % w/v	50
254	3F2	MPD	35 % v/v	100	Na acetate	4.5	0.1 M	4			
255	3F3	LiCl	1 M	5							
256	3F4	PEG 8000	25.5 % w/v	50					$(NH_4)_2SO_4$	0.17 M	3.7
		Glycerol	15 % v/v	60							
257	3F5	PEG MME 550	30 % v/v	100	Bis-Tris	6.5	0.1 M	1	$CaCl_2$	0.05 M	1
258	3F6	PEG 3350	20 % w/v	50					KI	0.2 M	1
259	3F7	Li_2SO_4	1.5 M	2.5	Tris-HCl	8.5	0.1 M	1			
260	3F8	$(NH_4)_2SO_4$	3 M	3.7					MPD	1.087 % v/v	100
261	3F9	Isopropanol	38.2 % v/v	100	Na acetate	4.5	0.1 M	4	$CaCl_2$	0.2 M	1
		Glycerol	15.9 % v/v	60							
262	3F10	Na_3 citrate	1 M	1.6	HEPES	7	0.1 M	1			
263	3F11	NaCl	1 M	5	Na acetate	4.5	0.1 M	4			
264	3F12	KCl	2.2 M	3.5							
265	3G1	PEG 400	40 % v/v	100	Na acetate	4.5	0.1 M	4			
266	3G2	Isopropanol	10 % v/v	100	Imidazole	8	0.1 M	2			
267	3G3	Glycerol	23.8 % v/v	60							
268	3G4	PEG 8000	12 % w/v	50					Li_2SO_4	0.4 M	2.5
		Glycerol	20 % v/v	60							
269	3G5	PEG 3350	25 % w/v	50	Bis-Tris	6.5	0.1 M	1	$MgCl_2$	0.2 M	3
270	3G6	PEG 3350	20 % w/v	50					Na acetate	0.2 M	4
271	3G7	PEG 400	13.3 % v/v	100	MES	6.5	0.1 M	1			
272	3G8	PEG 4000	20 % w/v	50	HEPES	7.5	0.1 M	1	$MgCl_2$	0.2 M	3
273	3G9	PEG 4000	15 % w/v	50	Na cacodylate	6.5	0.1 M	1	Li_2SO_4	0.2 M	2.5
274	3G10	PEG 4000	15 % w/v	50	Imidazole-malate	7	0.2 M	1			
275	3G11	PEG 6000	20 % w/v	50	Bicine	8.5	0.1 M	1			
276	3G12	PEG 1000	25 % w/v	50	Na acetate	4.5	0.1 M	4			
277	3H1	Ethanol	15 % v/v	100	CHES	9.5	0.1 M	1			

278	3H2	MPD	35 % v/v	100	HEPES	7.5	0.1 M	1	NaCl	0.2 M	5
279	3H3	Imidazole	1 M	2							
280	3H4	Li_2SO_4	0.75 M	2.5	HEPES	7.5	0.1 M	1			
281	3H5	PEG MME 2000	30 % w/v	40					K thiocyanate	0.1 M	2
282	3H6	PEG 3350	20 % w/v	50					Ca diacetate	0.2 M	1
283	3H7	PEG MME 2000	25 % w/v	40							
284	3H8	PEG 3350	20 % w/v	50					K_3 citrate	0.2 M	1
285	3H9	PEG 4000	15 % w/v	50	Na cacodylate	6.5	0.1 M	1	$MgCl_2$	0.2 M	3
286	3H10	PEG 600	36 % v/v	80	HEPES	7.5	0.1 M	1			
287	3H11	PEG 6000	20 % w/v	50	MES	6	0.1 M	1	LiCl	1 M	5
288	3H12	PEG 6000	30 % w/v	50	HEPES	7	0.1 M	1	LiCl	1 M	5
289	4A1	Na K phosphate	1.4 M	4		7.5					
290	4A2	Isopropanol	35 % v/v	100	Na_2H citrate	5.6	0.1 M	1			
		PEG 1000	5 % w/v	50							
291	4A3	Isopropanol	35 % v/v	100	Na acetate	4.5	0.1 M	4			
292	4A4	Ethanol	15 % v/v	100	HEPES	7.5	0.1 M	1	$MgCl_2$	0.2 M	3
293	4A5	PEG 400	28 % v/v	100	HEPES	7.5	0.1 M	1	$CaCl_2$	0.2 M	1
294	4A6	$(NH_4)_2SO_4$	1.5 M	3.7					Glycerol	25 % v/v	60
295	4A7	MPD	45 % v/v	100	Bis-Tris	6.5	0.1 M	1	$CaCl_2$	0.2 M	1
296	4A8	PEG 4000	10 % w/v	50	HEPES	7.5	0.1 M	1	NaCl	0.1 M	5
297	4A9	1,6-Hexanediol	2.96 M	5	Tris-HCl	8.5	0.05 M	1	$MgSO_4$	0.005 M	2
298	4A10	PEG 20000	12 % w/v	50	Imidazole	7	0.1 M	2			
299	4A11	Tacsimate	60 % v/v	100	Bis-Tris-Propane	7	0.1 M	1			
300	4A12	PEG 6000	10 % w/v	50					$MgCl_2$	0.01 M	3
301	4B1	Na malonate	3.4 M	4		6					
302	4B2	PEG 200	50 % v/v	100	Tris-HCl	7	0.1 M	1	Li_2SO_4	0.05 M	2.5
303	4B3	PEG 200	30 % v/v	100	Na acetate	4.5	0.1 M	4	NaCl	0.1 M	5
304	4B4	PEG 400	30 % v/v	100	CHES	9.5	0.1 M	1			
305	4B5	PEG 4000	30 % w/v	50	Tris-HCl	8.5	0.1 M	1	Li_2SO_4	0.2 M	2.5
306	4B6	Na formate	3.6 M	5					Glycerol	10 % v/v	60
307	4B7	PEG MME 2000	20 % w/v	40	Tris-HCl	8.5	0.1 M	1	Trimethylamine N-oxide	0.2 M	5
308	4B8	PEG 400	18 % v/v	100	HEPES	7.5	0.1 M	1	$MgCl_2$	0.1 M	3
309	4B9	PEG 3350	20 % w/v	50					NH_4I	0.2 M	1
310	4B10	Na acetate	1.8 M	4	Bis-Tris-Propane	7	0.1 M	1			
311	4B11	PEG 8000	7 % w/v	50	MES	6.5	0.1 M	1	Glycerol	20 % v/v	60
312	4B12	PEG 6000	16 % w/v	50					Na_3 citrate	0.01 M	1.6
313	4C1	Isopropanol	15 % v/v	100							
314	4C2	PEG 400	40 % v/v	100	Tris-HCl	8.5	0.1 M	1	Li_2SO_4	0.2 M	2.5
315	4C3	PEG 400	40 % v/v	100	Imidazole	8	0.1 M	2			
316	4C4	Na_3 citrate	1 M	1.6	Tris-HCl	7	0.1 M	1	NaCl	0.2 M	5
317	4C5	PEG 4000	20 % w/v	50	Na_3 citrate	5.6	0.1 M	1.6			
		Isopropanol	20 % v/v	100							

318	4C6	PEG 8000	5.2 % w/v	50	Tris-HCl	8.5	0.065 M	1	Glycerol	35 % v/v	60
319	4C7	PEG 3350	25 % w/v	50	Bis-Tris	6.5	0.1 M	1	NaCl	0.2 M	5
320	4C8	Li_2SO_4	2 M	2.5	MES	5.6	0.05 M	1	$MgCl_2$	0.01 M	3
321	4C9	PEG 3350	20 % w/v	50					$Mg(NO_3)_2$	0.2 M	1
322	4C10	Na acetate	2.8 M	4	Bis-Tris-Propane	7	0.1 M	1			
323	4C11	MPD	25 % v/v	100	HEPES	7.5	0.1 M	1			
		PEG 4000	2 % w/v	50							
324	4C12	PEG 6000	20 % w/v	50	Imidazole	8	0.05 M	2			
325	4D1	MPD	23 % v/v	100							
326	4D2	MPD	40 % v/v	100	Na cacodylate	6.5	0.1 M	1	PEG 8000	5 % w/v	50
327	4D3	PEG 3000	10 % w/v	50	CHES	9.5	0.1 M	1			
328	4D4	Na K tartrate	1 M	2	Tris-HCl	7	0.1 M	1	Li_2SO_4	0.2 M	2.5
329	4D5	1,6-Hexanediol	3.4 M	5	Tris-HCl	8.5	0.1 M	1	$MgCl_2$	0.2 M	3
330	4D6	PEG 4000	5.6 % w/v	50	Na acetate	4.5	0.07 M	4	Glycerol	30 % v/v	60
331	4D7	PEG 3350	15 % w/v	50					Mg diformate	0.1 M	1
332	4D8	PEG 400	10 % v/v	100	MES	6	0.05 M	1	$MgCl_2$	0.01 M	3.5
		KCl	0.1 M	3							
333	4D9	PEG 3350	20 % w/v	50					Zn diacetate	0.2 M	1
334	4D10	NaCl	3.2 M	5	Bis-Tris-Propane	7	0.1 M	1			
335	4D11	PEG 1500	20 % w/v	50	HEPES	7.5	0.1 M	1			
336	4D12	PEG 8000	10 % w/v	50					Mg diacetate	0.2 M	1
337	4E1	Ethylene glycol	40 % v/v	80	Na acetate	4.5	0.1 M	4			
338	4E2	2-Ethoxyethanol	35 % v/v	100	Na K phosphate	6.2	0.1 M	4	NaCl	0.2 M	5
339	4E3	PEG 8000	10 % w/v	50	CHES	9.5	0.1 M	1	NaCl	0.2 M	5
340	4E4	$(NH_4)_2SO_4$	2 M	3.7	Tris-HCl	7	0.1 M	1	Li_2SO_4	0.2 M	2.5
341	4E5	PEG MME 550	20 % v/v	100	Bicine	9	0.1 M	1	NaCl	0.1 M	5
342	4E6	PEG 4000	10 % w/v	50	Na_3 citrate	5.6	0.1 M	1.6			
		Isopropanol	10 % v/v	100							
343	4E7	MPD	12 % v/v	100	Na acetate	4.5	0.1 M	4	NaCl	0.1 M	5
344	4E8	Li_2SO_4	1 M	2.5	Na cacodylate	6	0.05 M	1	$MgCl_2$	0.01 M	3
345	4E9	PEG 3350	20 % w/v	50					NH_4 acetate	0.2 M	5
346	4E10	Na formate	2 M	5	Bis-Tris-Propane	7	0.1 M	1			
347	4E11	PEG 4000	20 % w/v	50	Tris-HCl	8.5	0.1 M	1	$CaCl_2$	0.2 M	1
348	4E12	$(NH_4)_2SO_4$	1.2 M	3.7					Na_3 citrate	0.05 M	1.6
		Isopropanol	3.82 % v/v	100							
349	4F1	2-Ethoxyethanol	35 % v/v	100	Na cacodylate	6.5	0.1 M	1			
350	4F2	1,2-Propanediol	30 % w/v	100	HEPES	7.5	0.1 M	1	PEG 400	20 % v/v	100
351	4F3	MPD	35 % v/v	100	MES	6	0.1 M	1	Li_2SO_4	0.2 M	2.5
352	4F4	Isopropanol	14 % v/v	100	Na acetate	4.5	0.07 M	4	$CaCl_2$	0.14 M	1
		Glycerol	30 % v/v	60							
353	4F5	$MgCl_2$	2 M	3	Bicine	9	0.1 M	1			
354	4F6	PEG 8000	7.5 % w/v	50					Li_2SO_4	0.5 M	2.5
355	4F7	PEG 6000	12 % w/v	50	Na acetate	4.5	0.1 M	4	NaCl	0.1 M	5

356	4F8	Li_2SO_4	1.8 M	2.5	Na cacodylate	6	0.05 M	1	$MgSO_4$	0.01 M	2
357	4F9	PEG 3350	20 % w/v	50					Li_2SO_4	0.2 M	2.5
358	4F10	$NaNO_3$	4 M	6	Bis-Tris-Propane	7	0.1 M	1			
359	4F11	PEG 4000	30 % w/v	50	HEPES	7.5	0.1 M	1	$CaCl_2$	0.2 M	1
360	4F12	MPD	76.1 % v/v	100	Tris-HCl	8.5	0.1 M	1			
361	4G1	PEG 300	40 % v/v	100	CHES	9.5	0.1 M	1	NaCl	0.2 M	5
362	4G2	PEG 400	30 % v/v	100	HEPES	7.5	0.1 M	1	Glycerol	10 % v/v	60
		PEG 3000	5 % w/v	50							
363	4G3	PEG 8000	10 % w/v	50	Na K phosphate	6.2	0.1 M	4	NaCl	0.2 M	5
364	4G4	PEG 8000	16 % w/v	50					KH_2PO_4	0.04 M	1.5
		Glycerol	20 % v/v	60							
365	4G5	$NH_4H_2PO_4$	0.26 M	3					Glycerol	35 % v/v	60
366	4G6	NaCl	3 M	5	Bis-Tris	5.5	0.1 M	1			
367	4G7	PEG 6000	12 % w/v	50	Na acetate	4.5	0.1 M	4	$MgCl_2$	0.1 M	3
368	4G8	PEG 4000	10 % w/v	50	Na cacodylate	6	0.05 M	1	$CaCl_2$	0.01 M	1
		KCl	0.2 M	3.5							
369	4G9	PEG 400	22 % v/v	100	MES	6	0.1 M	1			
370	4G10	Na K phosphate	1.8 M	4		5					
371	4G11	PEG 4000	10 % w/v	50	HEPES	7.5	0.1 M	1			
		Isopropanol	6.37 % v/v	100							
372	4G12	Ethanol	57 % v/v	100							
373	4H1	2-Ethoxyethanol	35 % v/v	100	Na_2H citrate	5.6	0.1 M	1			
374	4H2	PEG 600	40 % v/v	80	CHES	9.5	0.1 M	1			
375	4H3	Ethanol	15 % v/v	100	Na_2H citrate	5.6	0.1 M	1	Li_2SO_4	0.2 M	2.5
376	4H4	Na malonate	1 M	4		7					
377	4H5	PEG 4000	25.5 % w/v	50	Tris-HCl	8.5	0.085 M	1	Li_2SO_4	0.17 M	2.5
		Glycerol	15 % v/v	60							
378	4H6	Tacsimate	60 % v/v	100		7					
379	4H7	Isopropanol	10 % v/v	100	Na_3 citrate	5.6	0.1 M	1.6	Na_3 citrate	0.1 M	1.6
380	4H8	PEG 4000	10 % w/v	50	Tris-HCl	7.5	0.05 M	1	$MgCl_2$	0.05 M	3
		KCl	0.2 M	3.5							
381	4H9	PEG 10000	16 % w/v	50	Bis-Tris	6.5	0.1 M	1			
382	4H10	Na K phosphate	1.8 M	4		8.2					
383	4H11	PEG 4000	20 % w/v	50					Na_3 citrate	0.1 M	1.6
		Isopropanol	6.37 % v/v	100							
384	4H12	Isopropanol	31.9 % v/v	100	HEPES	7.5	0.1 M	1	$MgCl_2$	0.1 M	3
385	5A1	t-Butanol	32.1 % v/v	100	Tris-HCl	8.5	0.1 M	1	$CaCl_2$	0.1 M	1
386	5A2	PEG 3350	20 % w/v	50					NH_4 formate	0.2 M	4
387	5A3	PEG 3350	20 % w/v	50	Bis-Tris-Propane	8.5	0.1 M	1	Na_2SO_4	0.2 M	1
388	5A4	Ethanol	10 % v/v	100							
389	5A5	MPD	40 % v/v	100	Tris-HCl	7.5	0.1 M	1			
390	5A6	PEG 6000	6.6 % w/v	50	MES	6.6	0.225 M	1			
391	5A7	PEG 600	33 % v/v	80	Imidazole-malate	5.5	0.2 M	1			

392	5A8	PEG 300	30 % v/v	100	Na acetate	5	0.1 M	4			
393	5A9	Isopropanol	2.5 % v/v	100							
		$(NH_4)_2SO_4$	1 M	3.7							
394	5A10	PEG 6000	10 % w/v	50	HEPES	7	0.1 M	1	LiCl	1 M	5
395	5A11	MPD	65 % v/v	100	HEPES	7	0.1 M	1			
396	5A12	Na K phosphate	1.4 M	4		8.2					
397	5B1	PEG 3350	12 % w/v	50	MES	6.5	0.1 M	1	NaCl	0.5 M	5
398	5B2	PEG 3350	20 % w/v	50					NH_4Cl	0.2 M	4
399	5B3	PEG 4000	22 % w/v	50	Tris-HCl	8.5	0.1 M	1	Li_2SO_4	0.2 M	2.5
		Isopropanol	10 % v/v	100					2-thioethanol	0.5 % v/v	5
400	5B4	PEG MME 2000	25 % w/v	40	Na acetate	5.5	0.1 M	4	Li_2SO_4	0.2 M	2.5
401	5B5	PEG 400	30 % v/v	100	Na_3 citrate	5.6	0.1 M	1.6	Li_2SO_4	0.1 M	2.5
		NaCl	0.1 M	5							
402	5B6	PEG 4000	19 % w/v	50	Tris-HCl	8	0.03 M	1	$MgCl_2$	0.1 M	3
403	5B7	PEG 10000	17.5 % w/v	50	Imidazole-malate	8.5	0.2 M	1			
404	5B8	PEG 400	30 % v/v	100	Glycine	9	0.05 M	2	$CaCl_2$	0.2 M	1
405	5B9	Ethanol	10 % v/v	100	Tris-HCl	8.5	0.1 M	1			
406	5B10	MPD	40 % v/v	100	HEPES	6.5	0.1 M	1			
407	5B11	NaCl	1.6 M	5							
408	5B12	Na K phosphate	1.8 M	4		5.6			NH_4 formate	0.1 M	4
409	5C1	PEG 3350	22 % w/v	50							
410	5C2	PEG 3350	20 % w/v	50					K formate	0.2 M	1
411	5C3	PEG 4000	30 % w/v	50	Tris-HCl	7.5	0.1 M	1	CsCl	0.1 M	2
		Li_2SO_4	0.25 M	2.5							
412	5C4	PEG MME 2000	25 % w/v	40	Na acetate	5.5	0.1 M	4	KBr	0.2 M	3.5
413	5C5	PEG 400	30 % v/v	100	MOPS	7	0.1 M	1	NaCl	0.1 M	5
414	5C6	PEG 400	44 % v/v	100	Tris-HCl	8	0.1 M	1	$CaCl_2$	0.2 M	1
415	5C7	PEG MME 2000	18 % w/v	40	Na cacodylate	6.5	0.1 M	1			
416	5C8	PEG 2000	12 % w/v	60	Na cacodylate	6.5	0.1 M	1			
417	5C9	MPD	35 % v/v	100	HEPES	7.5	0.1 M	1			
418	5C10	PEG 4000	25 % w/v	50					$(NH_4)_2SO_4$	0.17 M	3.7
		Glycerol	15 % v/v	60							
419	5C11	LiCl	4 M	5							
420	5C12	Na K phosphate	1.8 M	4		7.5					
421	5D1	PEG 3350	32.5 % w/v	50	Tris-HCl	8.5	0.1 M	1	$MgCl_2$	0.2 M	3
		NaCl	0.5 M	5							
422	5D2	MPD	20 % v/v	100	Tris-HCl	8	0.1 M	1			
423	5D3	PEG 8000	10 % w/v	50	Tris-HCl	8.5	0.1 M	1	NaCl	0.05 M	5
424	5D4	PEG 4000	15 % w/v	50	Na acetate	5.5	0.1 M	4	Na acetate	0.3 M	4
425	5D5	PEG 4000	12 % w/v	50	Na_3 citrate	3.5	0.1 M	1.6	$MgCl_2$	0.1 M	3
		NaCl	0.1 M	5							
426	5D6	PEG 2000	31 % w/v	60	Bicine	9	0.1 M	1			
427	5D7	PEG MME 2000	36 % w/v	40	Na cacodylate	6.5	0.1 M	1			

428	5D8	MPD	35 % v/v	100	HEPES	7	0.1 M	1	NaCl	0.2 M	5
429	5D9	t-Butanol	12.5 % v/v	100	Tris-HCl	8.5	0.1 M	1			
430	5D10	$NH_4H_2PO_4$	1 M	3							
431	5D11	PEG MME 2000	25 % w/v	40	Na acetate	4.5	0.1 M	4			
432	5D12	Na malonate	1.5 M	4		5					
433	5E1	PEG 4000	10 % w/v	50	HEPES	7.5	0.1 M	1			
434	5E2	PEG 6000	20 % w/v	50	MES	6	0.1 M	1	NaCl	0.2 M	5
435	5E3	PEG 10000	10 % w/v	50	HEPES	7.5	0.1 M	1			
436	5E4	PEG 20000	8 % w/v	50	Na acetate	5.5	0.1 M	4	Na acetate	0.3 M	4
		PEG MME 550	8 % v/v	100							
437	5E5	PEG 4000	12 % w/v	50	Na_3 citrate	5.6	0.1 M	1.6	NaCl	0.1 M	5
438	5E6	PEG 2000	23 % w/v	60	Tris-HCl	8	0.1 M	1	$Mg(NO_3)_2$	0.3 M	1
439	5E7	PEG 4000	30 % w/v	50	Imidazole-malate	6	0.2 M	1			
440	5E8	$(NH_4)_2SO_4$	2.2 M	3.7					Na malonate	0.2 M	4
441	5E9	PEG 400	15 % v/v	100	Na acetate	4.5	0.1 M	4	$CdCl_2$	0.1 M	1
442	5E10	MPD	40 % v/v	100					$NaNO_3$	0.2 M	6
443	5E11	LiCl	1 M	5	Tris-HCl	8	0.1 M	1			
444	5E12	Na malonate	1.9 M	4		6					
445	5F1	PEG 10000	15 % w/v	50	HEPES	7.5	0.1 M	1	DTT	0.005 M	1
446	5F2	PEG 6000	20 % w/v	50	MES	6	0.1 M	1	$MgCl_2$	0.2 M	3
447	5F3	PEG 6000	10 % w/v	50	HEPES	7	0.05 M	1	Mg diacetate	0.15 M	1
		NH_4 acetate	0.2 M	5							
448	5F4	PEG MME 2000	25 % w/v	40	Tris-HCl	7.5	0.1 M	1	$MgCl_2$	0.2 M	3
449	5F5	PEG 4000	12 % w/v	50	Tris-HCl	8.5	0.1 M	1	NaCl	0.1 M	5
450	5F6	PEG 4000	15 % w/v	50	HEPES	7	0.1 M	1	$MgCl_2$	0.1 M	3
451	5F7	PEG 3350	36 % w/v	50	HEPES	7.5	0.1 M	1	$MgCl_2$	0.2 M	3
452	5F8	NaF	0.6 M	1	Na acetate	4.5	0.1 M	4			
453	5F9	PEG 8000	8.5 % w/v	50	HEPES	7.5	0.085 M	1	Glycerol	15 % v/v	60
454	5F10	MPD	40 % v/v	100					KH_2PO_4	0.2 M	4
455	5F11	PEG 6000	10 % w/v	50	Tris-HCl	8	0.1 M	1	LiCl	1 M	5
456	5F12	NaCl	4 M	5	Tris-HCl	8	0.1 M	1			
457	5G1	PEG MME 5000	20 % w/v	40					$MgCl_2$	0.2 M	3
458	5G2	PEG 3350	20 % w/v	50	Bis-Tris-Propane	7.5	0.1 M	1	Na_2SO_4	0.2 M	1
459	5G3	PEG 8000	15 % w/v	50	Bis-Tris-Propane	7	0.05 M	1	$(NH_4)_2SO_4$	0.1 M	3.7
		Glycerol	10 % v/v	60							
460	5G4	PEG MME 2000	25 % w/v	40	Tris-HCl	8.5	0.1 M	1	$MgCl_2$	0.2 M	3
461	5G5	PEG 400	19.6 % v/v	100	HEPES	7.5	0.1 M	1	$CaCl_2$	0.2 M	1
462	5G6	PEG 4000	20 % w/v	50	Na_3 citrate	4.5	0.1 M	1.6			
463	5G7	PEG 8000	25 % w/v	50	Tris-HCl	8.5	0.1 M	1	Li_2SO_4	0.5 M	2.5
464	5G8	NaCl	1.6 M	5	Tris-HCl	8.5	0.1 M	1			
465	5G9	PEG 400	27 % v/v	100	HEPES	7.5	0.09 M	1	$MgCl_2$	0.18 M	3
		Glycerol	10 % v/v	60							
466	5G10	MPD	40 % v/v	100	MES	6	0.1 M	1			

467	5G11	PEG 6000	20 % w/v	50	Tris-HCl	8	0.1 M	1	LiCl	1 M	5
468	5G12	PEG 6000	30 % w/v	50	Tris-HCl	8	0.1 M	1			
469	5H1	PEG MME 5000	20 % w/v	40					Na_2 tartrate	0.2 M	2
470	5H2	PEG 3350	20 % w/v	50	Bis-Tris-Propane	8.5	0.1 M	1	NaI	0.2 M	2
471	5H3	KH_2PO_4	1.5 M	1.5							
472	5H4	Li_2SO_4	1.8 M	2.5	Tris-HCl	7.5	0.1 M	1			
473	5H5	PEG 400	30 % v/v	100	Na acetate	4.5	0.1 M	4	Li_2SO_4	0.2 M	2.5
474	5H6	PEG 6000	8 % w/v	50	MES	6	0.1 M	1	$MgCl_2$	0.1 M	3
475	5H7	PEG 4000	12 % w/v	50	Na_3 citrate	5.6	0.1 M	1.6	Isopropanol	5 % v/v	100
476	5H8	Jeffamine ED 2001	0.53 % w/v	50	HEPES	7	0.1 M	1	Na malonate	1.1 M	4
477	5H9	PEG 6000	20 % w/v	50	HEPES	6.5	0.1 M	1			
478	5H10	MPD	65 % v/v	100	MES	6	0.1 M	1			
479	5H11	Na K phosphate	0.8 M	4		8.2					
480	5H12	PEG 6000	30 % w/v	50	Bicine	9	0.1 M	1			

The first digit of the well ID is the plate number, followed by the coordinates on the 96-well plate. Concentrations of the stock solutions ('Stock') are given in the same unit as the respective final concentration ('Conc.'). Most aqueous stock solutions were supplied with 0.02 % (w/v) NaN_3 as preservative.